



HAL
open science

Electrochemical advanced oxidation processes for emerging organic contaminants removal with graphene-based modified carbon felt electrode

Weilu Yang

► **To cite this version:**

Weilu Yang. Electrochemical advanced oxidation processes for emerging organic contaminants removal with graphene-based modified carbon felt electrode. Organic chemistry. Université Paris-Est; Nankai da xue – Zhongguo Tianjin, 2019. English. NNT : 2019PESC2025 . tel-02482626

HAL Id: tel-02482626

<https://theses.hal.science/tel-02482626>

Submitted on 18 Feb 2020

HAL is a multi-disciplinary open access archive for the deposit and dissemination of scientific research documents, whether they are published or not. The documents may come from teaching and research institutions in France or abroad, or from public or private research centers.

L'archive ouverte pluridisciplinaire **HAL**, est destinée au dépôt et à la diffusion de documents scientifiques de niveau recherche, publiés ou non, émanant des établissements d'enseignement et de recherche français ou étrangers, des laboratoires publics ou privés.

Joint PhD degree in Environmental Science and Engineering



Docteur de l'Université Paris-Est

PhD degree of Nankai University

Spécialité Science et Technologie de l'Environnement

Specialty: Environmental Science and Technology

Thèse de doctorat d'université - PhD thesis

Weilu YANG

**Electrochemical advanced oxidation processes for emerging organic
contaminants removal with graphene-based modified carbon felt electrode**

**Procédés électrochimiques d'oxydation avancée pour l'élimination de contaminants
organiques émergents avec l'électrode en feutre de carbone modifiée à base de
graphène**

To be defended on June 17, 2019

In front of the PhD committee

Prof. Ignacio SIRES SADORNIL	Reviewer	Barcelona University - Spain
Prof. Xinhua QI	Reviewer	Agro-Environmental Protection Institute
Prof. Mehmet A. OTURAN	Promotor	Université Paris-Est - France
Prof. Minghua ZHOU	Co-promotor	Nankai University - China
Dr. Nihal OTURAN	Examiner	Université Paris-Est - France
Prof. Can WANG	Examiner	Tianjin University - China

ACKNOWLEDGEMENTS

I would like to thank my supervisors Prof. Mehmet A. OTURAN and Prof. Minghua ZHOU sincerely for giving me the chance to carry out this thesis work. It is my precious experience and memory to work with Prof. Mehmet A. Oturan and Prof. Minghua ZHOU, I have learned a lot from them. Also, I would like to thank gratefully to Dr. Nihal Oturan for giving me many useful suggestions and technical supports during conducting experiments.

I wish to express my gratitude to Prof. Ignacio Sir és (Barcelona University, Spain) and Prof. Xinhua Qi (Agro-Environmental Protection Institute, China) for reading and evaluating my thesis. Express my thanks to Dr Nihal Oturan (Université Paris-Est , France) and Prof. Can WANG (Tianjin University, China) for their precious time to be part of thesis jury.

I also wish to thank Dr Ying ZHANG for her suggestions and help, and thank all of my colleges in my group for their company, and thank Helene in LGE Université Paris-Est for her kindness and help. Thank Fuzhen LIU very much for her companionship and help.

Thank for the fund supported by China Scholarship Council (CSC) affiliated with the Ministry of Education of P.R. China. Thanks to the National Key Research and Development Program (2016YFC0400706), the National Natural Science Foundation of China (No. 21773129, 21811530274) and the Tianjin Natural Science Foundation (No. 16JCZDJC39300) for their financial support for this paper.

Finally, I would especially like to thank my family members for their understanding and encouragement. And, also I want to say thanks to myself, for the persistence and endeavor.

ABSTRACT

In recent years, the emerging organic contaminants have attracted wide attention. Among them, pharmaceuticals and personal care products (PPCPs) have become international research hotspots. Compared with the traditional pollutants, generally, the emerging contaminants are difficult to be analyzed due to the limitation of analytical technologies and their low concentration in water. The traditional sewage treatment plants can not achieve efficient degradation and removal effects. Advanced oxidation processes (AOPs), as efficient pollutant treatment technology, have been widely used in the treatment of refractory organic pollutants such as emerging organic contaminants in water because of their strong oxidation ability, which can effectively degrade and mineralize pollutants in water. Electro-Fenton (EF) is one of the advanced electrochemical oxidation processes (EAOPs), where hydrogen peroxide (H_2O_2) is in situ generated via Fenton reaction under electric field, thus decreasing the cost and avoiding the risks during the process of H_2O_2 preparation, storage and transportation. However, the traditional EF has two key bottlenecks: narrow pH applicability and low treatment efficiency. Graphene, as a new type of carbon material, has great potential for wastewater treatment due to its excellent conductivity and high specific surface area. Based on this, this paper prepared graphene via electrochemical exfoliation method and synthesized graphene-based modified carbon felt electrode as EF cathode, significantly improving the yield of H_2O_2 and efficiency of organics degradation in EF. In order to extend the application range of pH and avoid potential pollution caused by leaching metals with EF, in-situ iron-free EAOPs with cathodes modified with nitrogen-doped graphene were constructed for emerging organic contaminants removal. The mechanism of catalysis with nitrogen-doped graphene and cathode micro-interface process have been explored, illustrating the high efficient in-situ catalysis mechanism and providing references for the development of EAOPs. The main research contents and conclusions are as follows:

(1) In this work, a novel graphite felt cathode modified with electrochemically exfoliated graphene (EEGr) and carbon black was developed, presenting a very high H_2O_2 generation rate of $7.7 \text{ mg h}^{-1} \text{ cm}^{-2}$ with relatively low energy consumption (9.7 kWh kg^{-1}). Characterized by SEM, TEM, AFM, Raman, XRD and XPS, the synthesized EEGr was proved to be the 3-4 layers thin sheet with low defects. Important manufacture parameters including the ratio and loading of EEGr were optimized, and

the effect of pH and cathode potential on H₂O₂ generation as well as the stability performance of cathodes were investigated. At optimized cathode potential of -0.9 V and pH 7, the modified cathode with EEGr kept stable performance for H₂O₂ generation, which was 2 times of the cathode without EEGr. Further explored by CV, rotating disk electrode (RDE) and contact angles, the presence of EEGr was found to accelerate the electrons transfer rate, benefit oxygen surface reaction without changing the mechanism of two-electrons ORR, which contributed to the enhanced performance of H₂O₂ production and the possible mechanism was suggested. Finally, such graphene modified cathode demonstrated the effective performance of the degradation of four kinds of representative pollutants (Orange II, methylene blue, phenol and sulfadiazine) by EF process, proving great potential of practical application for wastewater treatment.

(2) The oxidative degradation and mineralization of imatinib (IMA), an antineoplastic drug for cancer treatment, were investigated by EF process using a graphene modified carbon felt cathode (EEGr-CF) comparatively with raw carbon felt (CF) cathode. For the first time the removal of IMA from water and the determination of absolute rate constant ($4.56 \times 10^9 \text{ M}^{-1} \text{ s}^{-1}$) for IMA oxidation by $\cdot\text{OH}$ were investigated by EF process. The effects of operating parameters including catalyst concentration and applied current on the process efficiency were considered. Complete mineralization of 34.5 mg L⁻¹ IMA was obtained at 8 h treatment with EEGr-CF cathode while only 75% TOC removal was attained with raw CF cathode under same operating conditions. Also, the formation and evolution of the carboxylic acids during oxidation process provided better performances with EEGr-CF cathode. N atoms presented in IMA were finally released to the solution as NH₄⁺ and NO₃⁻ ions. Besides, toxicity assessment with Microtox[®] method proved the formation of intermediates more toxic than IMA during mineralization process. However, solution toxicity was totally removed at the end of treatment with EEGr-CF cathode. These results showed that the EEGr-CF cathode was great potential for new emerging contaminants removal and the development of EF process for wastewater treatment.

(3) EF process can be regarded as the coupling of anodic oxidation process and homogeneous EF process. Thus, the effect of anode materials on the mineralization and electrochemical oxidation of pharmaceutical imatinib (IMA) was explored by EF and anodic oxidation (AO) processes using four kinds of anode material: Pt, DSA (Ti/RuO₂-IrO₂), BDD and sub-stoichiometric titanium oxide (Ti₄O₇). A series of

comparison experiments including oxidative degradation kinetics of IMA, total organic carbon (TOC) decay and mineralization efficiency were conducted at pH 3 and ambient temperature. In both cases, DSA and Pt was less effective anode for the anodic oxidation and mineralization of IMA solution compared with Ti_4O_7 and BDD anodes. Complete mineralization of 0.1 mM (corresponding to 34.8 mg L^{-1} initial TOC) IMA solution was obtained both in EF and AO processes with BDD anode at 300 mA. The Ti_4O_7 anode exhibited better performances than DSA and Pt anode, reaching 84% TOC removal efficiency in EF and 73% in AO processes at 8 h electrolysis, providing much potent cathode material as the cost-effective candidate for wastewater treatment. Besides, the formation and evolution of five short-chain carboxylic acids (oxalic, pyruvic, oxamic, formic and acetic) and inorganic ions (NH_4^+ , NO_3^-) during mineralization of IMA solution were identified and followed by ion exclusion HPLC and ion chromatography, respectively. Finally, a plausible degradation pathway of IMA by $\cdot\text{OH}$ was proposed according to the intermediates detected by HPLC and GC-MS. What is important is that the relative contribution of homogeneous (generated in the bulk) and heterogeneous (formed at anode surface) hydroxyl radicals on the kinetic decay and mineralization of IMA by EF process with different anodes was explored firstly. The analysis of $\alpha ((k_{EF}-k_{AO})/k_{AO})$ value indicated that Ti_4O_7 is a potential anode for generating heterogeneous $\text{Ti}_4\text{O}_7(\cdot\text{OH})$ in AO process under low current and homogeneous $\cdot\text{OH}$ plays the major role for TOC degradation with Pt anode.

(4) To extend the optimal pH range for EF process and avoid the addition of catalysts, synthesized N-EEGr via calcination at low temperature with NH_4NO_3 as nitrogen resource. The prepared N-EEGr demonstrated as a highly efficient carbon based catalyst for electrochemical advanced oxidation processes (EAOPs) application to environmental remediation, which contributes superior catalytic activity for activation of H_2O_2 to $\cdot\text{OH}$ for organics degradation. Herein, for the first time, the in-situ metal-free EAOP with carbon felt cathode modified by N-EEGr was established. The N-EEGr-GF cathode was systematically characterized, and its electrocatalytic behavior for oxygen reduction reaction as well as the degradation performance were investigated. N-doping was found increasing the catalytic decomposition rate of organics but not changing the electrochemical generation of H_2O_2 . ESR spectra, methanol and benzoquinone capture confirmed the existence of $\cdot\text{OH}$ and $\cdot\text{O}_2$ in EAOPs, while the former played the dominant role. Compared with traditional EF process, this in-situ metal-free EAOP

demonstrated 4-times higher efficiencies with a more broad suitability upon pH. In view of its competitive advantage in reusability and environmental friendliness without catalysts addition and second pollution, this process can be regarded as the competent substitution of traditional EF process for wastewater treatment.

(5) To further optimize the performances of in-situ metal-free EAOPs for organics degradation, the herbicide 2,4-dichlorophenoxyacetic acid (2,4-D) in aqueous solutions has been studied as target pollutants in the in-situ metal-free EAOPs using N-EEGr-GF cathode with ammonium nitrate as nitrogen source. Different ratios of EEGr / ammonium nitrate (1:0, 1:1, 1:3, 1:7) modified cathodes (N0-EEGr-GF, N1-EEGr-GF, N3-EEGr-GF, N7-EEGr-GF) were explored with electrochemical characterizations, and it was verified that N1-EEGr had the most significant catalytic performance for accelerating the activation of in-situ generated H_2O_2 into hydroxyl radicals. The effects of operating parameters such as applied potential, solution pH and initial concentration of 2,4-D on the degradation efficiency with N1-EEGr-GF were investigated. High mineralization rate (88%) of 20 mg L^{-1} 2,4-D solution was attained at pH 7 after 480 min. The N-doped graphene as catalyst was found to be more efficient in degradation performance compared with the unmodified graphite felt cathode. This in-situ metal-free EAOP using N-EEGr-GF cathode allowed extension of working pH range compared to optimal pH 3 in EF process. Finally, a plausible pathway for 2,4-D mineralization was proposed according to the identified intermediated products.

Key words: Graphene; Electro-Fenton; Nitrogen-doping; In-situ metal-free electrochemical advanced oxidation; Emerging organic contaminants; Mineralization; Cost effectiveness

TABLE OF CONTENTS

ABSTRACT	3
LIST OF TABLES	12
LIST OF FIGURES	14
Chapter 1 Introduction	20
1.1 Research background.....	20
1.1.1 New emerging organic contaminants	20
1.1.2 Treatment methods for new emerging organic contaminants.....	22
1.2 Developments of cathode materials of electro-Fenton process	25
1.2.1 Electro-Fenton technology	25
1.2.2 The development of anodes in EF process	29
1.2.3 The development of cathodes in EF process	30
1.3 The development of graphene-based electro-Fenton cathodes.....	33
1.3.1 Description of graphene	33
1.3.2 Traditional methods for preparation of graphene	33
1.3.3 Electrochemical exfoliation for graphene preparation	35
1.3.4 Application of electro-Fenton with graphene-based cathode	37
1.4 Contents and structure of the research.....	38
1.4.1 Purpose and significance of thesis research	38
1.4.2 Contents of the research	39
Chapter 2 Ultrahigh yield of hydrogen peroxide on graphite felt cathode modified with electrochemically exfoliated graphene	47
2.1 Introductionl	48
2.2 Experimental.....	50
2.2.1 EEGr synthesis	50

Table of content

2.2.2 Cathode modification with EEGr and carbon black.....	50
2.2.3 Characterization and analytical methods.....	51
2.2.4 Pollutants degradation by electro-Fenton.....	53
2.3 Results and discussion.....	54
2.3.1 Optimizing the ratio and loading of EEGr on modified graphite felt cathode.....	57
2.3.2 Performance and stability of the modified cathode for H ₂ O ₂ production	58
2.3.3 Possible mechanism for the high yield of H ₂ O ₂ production.....	61
2.3.4 The performance of pollutants degradation.....	67
2.4 Conclusions.....	68
Chapter 3 Electrocatalytic destruction of pharmaceutical imatinib by electro-Fenton process with graphene-based cathode.....	73
3.1 Introduction.....	74
3.2 Materials and methods.....	76
3.2.1 Chemicals.....	76
3.2.2 Electrochemical cell.....	77
3.2.3. Preparation and characterization of EEGr-CF cathode.....	77
3.2.4 Instruments and analytical procedures.....	77
3.3 Results and discussion.....	80
3.3.1 Effect of Fe ²⁺ concentration and current on IMA oxidative degradation kinetics.....	80
3.3.2 Comparative performance of raw CF and EEGr-CF cathodes in IMA degradation.....	82
3.3.3 Comparison of the mineralization efficiency by EF process with raw CF and EEGr-CF cathode.....	85
3.3.4 Identification and evolution of carboxylic acids during EF treatment of	

Table of content

IMA	88
3.3.5 Evolution of inorganic ions during electro-oxidation of IMA	89
3.3.6 Assessment of toxicity during degradation of IMA with raw CF and EEGr-CF cathodes	91
3.4 Conclusions	92
Chapter 4 Effect of anode materials on the performance of Electrocatalytic generation of homogeneous and heterogeneous hydroxyl radicals for cold mineralization of anti-cancer drug imatinib	98
4.1 Introduction	99
4.2 Materials and methods.....	102
4.2.1 Chemicals	102
4.2.2 Electrolytic system	102
4.2.3 Electrochemical measurements and analysis.....	103
4.3 Results and discussion.....	104
4.3.1 Kinetic decay of IMA	104
4.3.2 Comparison of the mineralization power of different anodes	108
4.3.3 Identification and evolution of inorganic ions and carboxylic acids during EF degradation of IMA	117
4.3.4. Identification of aromatic intermediates and proposed reaction pathway	120
4.3.5 Assessment of acute toxicity during EF degradation of IMA solution..	122
4.4 Conclusions	123
Chapter 5 Highly efficient in-situ metal-free electrochemical advanced oxidation process using graphite felt modified with N-doped graphene	130
5.1 Introduction	131
5.2 Experimental.....	132

Table of content

5.2.1 Synthesis of N-EEGr	132
5.2.2 Physical Characterization	133
5.2.3 Electrochemical Measurements	133
5.2.4 Catalytic Activity Measurements.....	133
5.3 Results and discussion	134
5.3.1. Material characterization	134
5.3.2. Activity towards ORR	135
5.3.3. Characterization of modified electrode	135
5.3.4. Catalytic performances of in-situ metal-free EAOPs with modified electrode.....	139
5.3.5. Possible mechanism of in-situ metal-free EAOPs with N-doped graphene	140
5.3.6. Performance comparison with traditional EF process.....	142
5.4 Conclusions	144
Chapter 6 Enhanced activation of hydrogen peroxide using nitrogen doped graphene for effective removal of herbicide 2,4-D from water by iron-free electrochemical advanced oxidation	149
6.1 Introduction	150
6.2 Materials and methods.....	152
6.2.1 Chemical reagents.....	152
6.2.2 Preparation of N-EEGr and N-EEGr-GF.....	153
6.2.3 Characterizations and electrochemical measurements	153
6.2.4 Degradation of 2,4-D with in-situ EAOP	153
6.3 Results and discussion	155
6.3.1 Characterization of different N-EEGr	155
6.3.2 Electrocatalytic activity of N-EEGr by CV	155

Table of content

6.3.3 Mineralization of 2,4-D using N-EEGr-GF cathode in EAOP.....	160
Fig. 5 Evolution of TOC and MCE during EAOP with N0-EEGr-GF and N1-EEGr-GF cathodes. [2,4-D]: 20 mg L ⁻¹ , volume: 100 mL, pH 7, applied voltage : 4 V, [Na ₂ SO ₄]: 50 mM.	162
6.3.4 Performances of the iron-free EAOP compared with literatures.....	162
6.3.5 Identification of aromatic intermediates and carboxylic acids.....	164
6.4 Conclusions	169
Chapter 7 Conclusions and Prospects	174
7.1 Main conclusions.....	174
7.2 Prospects and suggestions	177
Publications	178

LIST OF TABLES

Chapter 1 Introduction

Table 1. Common pharmaceuticals in the environment.

Table 2. Comparison of anodes used in electro-Fenton process.

Chapter 2 Ultrahigh yield of hydrogen peroxide on graphite felt cathode modified with electrochemically exfoliated graphene

Table 1. Atomic percentage in the samples.

Table 2. Performance comparison with literatures.

Table 3. Degradation of pollutants with different cathodes

Chapter 3 Electrocatalytic destruction of pharmaceutical imatinib by electro-Fenton process with graphene-based cathode

Table 1. Some physico-chemicals properties of IMA.

Table 2. Values of the apparent rate constant (k_{app}) for the oxidation of IMA by $\bullet\text{OH}$ generated in EF process.

Chapter 4 Effect of anode materials on the performance of Electrocatalytic generation of homogeneous and heterogeneous hydroxyl radicals for cold mineralization of anti-cancer drug imatinib

Table 1. Apparent rate constants (k_{app}) as a function of anode materials and current applied for kinetics decay of IMA in EF and AO processes with CF cathode.

Table 2. Apparent rate constants (k_{app}) as a function of anode materials and current applied for TOC degradation in EF and AO processes with CF cathode.

Table3: Intermediate products identified using HPLC and GC-MS during the mineralization of IMA with BDD anode in EF process.

Chapter 5 Highly efficient in-situ metal-free electrochemical advanced oxidation process using graphite felt modified with N-doped graphene

Chapter 6 Enhanced activation of hydrogen peroxide using nitrogen doped graphene for effective removal of herbicide 2,4-D from water by iron-free electrochemical advanced oxidation

Table 1. Atomic percentage in the samples.

Table 2. The values of k_{app} of 2,4-D degradation with in-situ EAOPs.

Table 3. Performances of 2,4-D degradation comparison with literature.

Table 4. Intermediate products detected by HPLC and GC-MS.

Chapter 7 Conclusions and Prospects

LIST OF FIGURES

Chapter 1 Introduction

Figure 1. The mechanism of electro-Fenton process.

Figure 2. Comparison of anodes used in electro-Fenton process.

Figure 3. Preparation process for graphene.

Figure 4. Electrochemical exfoliation process for preparation of graphene.

Chapter 2 Ultrahigh yield of hydrogen peroxide on graphite felt cathode modified with electrochemically exfoliated graphene

Figure 1. SEM (a), TEM (b, c) and AFM (d) of the EEGr from the graphite foil and Raman spectrum of graphite foil and EEGr (e).

Figure 2. XRD patterns of the graphite foil and EEGr (a); XPS survey spectra of graphite foil and EEGr (b); high-resolution C 1s spectrum of EEGr (c) and graphite foil (d).

Figure 3. The performances of modified graphite felts with different ratio (a) and loading of EEGr (b) for H₂O₂ generation.

Figure 4. The performance of H₂O₂ generation with different potentials (a) and pH (b); Stability of modified cathode with EEGr-20 over 10 cycles of the rate of H₂O₂ generation and EEC (c). Conditions: V=100 mL, pH=7, Potential: -0.9 V.

Figure 5. N₂ adsorption/desorption isotherms of EEGr-20 and unmodified graphite felt electrodes (a); Nyquist plot of EEGr-20 and unmodified graphite felt electrodes (b); Cyclic voltammograms of three different modified cathodes (modified graphite felt with EEGr, EEGr-0, EEGr-20) (c); The Linear sweep voltammetry of modified electrode with EEGr-0 (d) and EEGr-20 (e) in O₂ saturated Na₂SO₄ solution at a scan rate of 50 mV s⁻¹ with RDE. Inset: K-L

plots at different potentials; electrocatalytic activity towards Fe(III)/Fe(II) redox couple detected with CV techniques (f); Contact angles of unmodified graphite felt (g), modified graphite felt with EEGr-0 (h) and with EEGr-20 (i).

Figure 6. The schematic diagram of the ORR process.

Figure 7. The degradation of orange II, methylene blue, sulfadiazine and phenol. Conditions: Pt anode; V=100 mL; pH=3; $[\text{Fe}^{2+}]$ =0.4 mM; Na_2SO_4 : 50 mM; Potential: -0.9 V.

Chapter 3 Electrocatalytic destruction of pharmaceutical imatinib by electro-Fenton process with graphene-based cathode

Figure 1. Optimization of operating parameters for IMA degradation with raw CF cathode in EF process. Effect of catalyst $[\text{Fe}^{2+}]$ concentration at I : 16.66 mA cm^{-2} (a), and effect of current at 0.1 mM $[\text{Fe}^{2+}]$ (b) on IMA decay kinetics. $[\text{IMA}]$: 0.07 mM (34.5 mg L^{-1}), V: 150 mL, pH 3, $[\text{Na}_2\text{SO}_4]$: 50 mM.

Figure 2. Comparison of performance of raw CF and EEGr-CF cathodes in IMA degradation (a) and H_2O_2 generation (b). pH 3, 200 mA. $[\text{IMA}]$: 0.07 mM, $[\text{Fe}^{2+}]$: 0.1 mM, V: 150 mL, $[\text{Na}_2\text{SO}_4]$: 50 mM.

Figure 3. Determination of absolute rate constant for IMA oxidation (k_{IMA}) by competition kinetics method using EEGr-CF cathode (a); Kinetic analysis for determination of k_{IMA} (b). $[\text{IMA}]$: 0.07 mM, $[\text{4-HBA}]$: 0.07 mM, V: 150 mL, pH: 3, $[\text{Fe}^{2+}]$: 0.1 mM, I: 60 mA, $[\text{Na}_2\text{SO}_4]$: 50 mM.

Figure 4. Effect of current on TOC removal (a, b) and MCE (c, d) during mineralization of 0.07 mM (34.5 mg L^{-1}) IMA solution with raw CF (a, c) and EEGr-CF (b, d) cathodes V: 150 mL, pH: 3, $[\text{Fe}^{2+}]$: 0.1 mM, $[\text{Na}_2\text{SO}_4]$: 50 mM.

Figure 5. Effect of applied current on EC evolution during IMA degradation by EF process with raw CF (a) and EEGr-CF (b) cathodes. V: 150 mL, pH: 3, $[\text{Fe}^{2+}]$: 0.1 mM, $[\text{Na}_2\text{SO}_4]$: 50 mM.

Figure 6. Time-course of identified short-chain carboxylic acids during the electrooxidation of 0.07 mM (34.5 mg L⁻¹) IMA in EF process with raw CF (a) and EEGr-CF cathodes (b). V: 150 mL, pH: 3, [Fe²⁺]: 0.1 mM, *I*: 200 mA, [Na₂SO₄]: 50 mM.

Figure 7. Time-course of identified inorganic ions (NH₄⁺ and NO₃⁻) during electrooxidation of 0.07 mM (34.5 mg L⁻¹) IMA in EF process with raw CF (a) and EEGr-CF cathodes (b). V: 150 mL, pH: 3, [Fe²⁺]: 0.1 mM, *I*: 200 mA, [Na₂SO₄]: 50 mM (for NO₃⁻), [K₂SO₄]: 50 mM (for NH₄⁺ since the presence of Na⁺ ion hinders the detection of NH₄⁺ in ion chromatography).

Figure 8. Evolution of acute toxicity during EF treatment of 0.07 mM (34.5 mg L⁻¹) IMA solution with raw CF (a) and EEGr-CF cathode (b) at 200 mA. The toxicity is expressed as the inhibition of the luminescence of *V. fischeri* bacteria after 5 min and 15 min exposure time. V: 150 mL, pH: 3, [Fe²⁺]: 0.1 mM, [Na₂SO₄]: 50 mM.

Chapter 4 Effect of anode materials on the performance of Electrocatalytic generation of homogeneous and heterogeneous hydroxyl radicals for cold mineralization of anti-cancer drug imatinib

Figure 1. Effect of applied current on the kinetics degradation of IMA in DSA/CF cell (a, b), Pt/CF cell (c, d), Ti₄O₇/CF cell (e, f) and BDD/CF cell (g, h): (a, c, e, g) EF, (b, d, f, h) AO process. [IMA]: 34.5 mg L⁻¹, V: 230 mL, [Fe²⁺]: 0.1 mM (only in EF process), pH 3, [Na₂SO₄]: 50 mM.

Figure 2. Effect of current on the TOC removal of 0.07 mM IMA solution (corresponding to 24.1 mg L⁻¹ initial TOC) in EF (a, c, e, h) and AO (b, d, f, g) with DSA/CF (a, b), Pt/CF (c, d), Ti₄O₇/CF (e, f) and BDD/CF (g, h) cells. V: 230 mL, [Fe²⁺]: 0.1 mM (only in EF process), pH 3, [Na₂SO₄]: 50 mM.

Figure 3. Effect of applied current on the evolution of MCE with different anodes in EF

List of figures

(a, c, e, h) and AO (b, d, f, g) with DSA/CF (a, b), Pt/CF (c, d), Ti₄O₇/CF (e, f) and BDD/CF (g, h) cells [IMA]₀: 0.07 mM (34.5 mg L⁻¹), V: 230 mL, [Fe²⁺]: 0.1 mM (only in EF process), pH 3, [Na₂SO₄]: 50 mM.

Figure 4. The function ($\alpha: (k_{EF}-k_{AO})/k_{AO}$) of homogeneous $\cdot\text{OH}$ and heterogeneous $\cdot\text{OH}$ with current applied for kinetics decay of IMA (a, b) and TOC degradation (c, d) with different anodes.

Figure 5. Effect of applied current on the EC of IMA degradation in EF process with DSA (a), Pt (b), Ti₄O₇ (c) and BDD (d) anode. [IMA]: 0.1 mM, V: 230 mL, [Fe²⁺]: 0.1 mM, pH 3, [Na₂SO₄]: 50 mM

Figure 6. Time-course of identified inorganic ions (NH₄⁺ and NO₃⁻) during electrooxidation of 0.1 mM IMA in EF process with BDD anode. V: 230 mL, [Fe²⁺]: 0.1 mM, pH 3, I: 300 mA, [Na₂SO₄]: 50 mM (for NO₃⁻), [K₂SO₄]: 50 mM (for NH₄⁺ since the presence of Na⁺ ion hinders the detection of NH₄⁺ in ion chromatography).

Figure 7. Identification and evolution of carboxylic acids generated during the process of IMA degradation in EF system with BDD anode. [IMA]: 0.1 mM, V: 230 mL, [Fe²⁺]: 0.1 mM, pH 3, I: 300 mA, [Na₂SO₄]: 50 mM.

Figure 8. Proposed degradation pathway for IMA degradation by $\cdot\text{OH}$ radicals generated in EF process with BDD anode.

Figure 9. Evolution of acute toxicity of IMA solution during EF treatment with BDD anode at 300 mA. The toxicity is expressed as the inhibition of luminescence of *V. fischeri* bacteria after 5 min and 15 min exposure time. V: 230 mL, [Fe²⁺]: 0.1 mM, pH 7, I: 300 mA, [Na₂SO₄]: 50 mM.

Chapter 5 Highly efficient in-situ metal-free electrochemical advanced oxidation process using graphite felt modified with N-doped graphene

Figure 1. SEM images of N-EEGr, EEGr (inset) (a); XRD of EEGr, N-EEGr (b); Raman

spectrum of EEGr, N-EEGr (c); XPS spectra of EEGr and N-EEGr (d); high-resolution N 1s spectrum of EEGr (e) and N-EEGr (f).

Figure 2. Cyclic voltammograms of EEGr and N-EEGr (a); The Linear sweep voltammetry of EEGr (b) and N-EEGr (c) in O₂ saturated Na₂SO₄ solution at a scan rate of 20 mV s⁻¹ with RDE. Inset: K-L plots at different potentials.

Figure 3. SEM images of EEGr-GF (a) and N-EEGr-GF (b); N₂ adsorption/desorption isotherms of the EEGr-GF and N-EEGr-GF electrodes (c); Electroactive surface area of EEGr-GF and N-EEGr-GF detection (d); Nyquist plot of the two electrodes (EEGr-GF and N-EEGr-GF) (e).

Figure 4. The degradation of phenol in the EAOPs at different experiment conditions, methanol 20 mL and benzoquinone 5 mM; V=100 mL; pH=3; Na₂SO₄: 50 mM; Potential: -0.9 V (a); The performance of H₂O₂ generation with EEGr-GF and N-EEGr-GF (b); ESR spectrum in EAOPs with two different modified cathode electrodes (c); The concentration of [•]OH on the two electrodes in EAOPs (d).

Figure 5. Schematic illustration of the in-situ metal-free EAOPs with EEGr-GF and N-EEGr-GF electrode.

Figure 6. Comparison with traditional EF process and in-situ metal-free EAOPs (a); The stability of N-EEGr-GF electrode in EAOPs (b).

Chapter 6 Enhanced activation of hydrogen peroxide using nitrogen doped graphene for effective removal of herbicide 2,4-D from water by iron-free electrochemical advanced oxidation

Figure 1. XPS spectra of N-EEGr (N0, N1, N3, N7) (a); high-resolution N 1s spectrum of N3-EEGr (b) and three kinds of N content in N-EEGr (N0, N1, N3, N7) (c).

Figure 2. Cyclic voltammetry of N-EEGr (N0, N1, N3, N7) (a); The relationship between graphite N and H₂O₂ generation rate (b).

Figure 3. Relationship between the content of pyridinic N and catalytic performance of EAOP.

Figure 4. Effect of initial concentration of 2,4-D, pH 3, applied voltage: 4 V (a), pH (b) and applied voltage (c) on the degradation of 2,4-D and stability of N1-EEGr-GF cathode for 2,4-D degradation (d). [2,4-D]: 20 mg L⁻¹ (for Figures 4b-4c), pH 7, applied voltage: 4 V, volume: 100 mL, [Na₂SO₄]: 50 mM.

Figure 5. Evolution of TOC and MCE during EAOP with N0-EEGr-GF and N1-EEGr-GF cathodes. [2,4-D]: 20 mg L⁻¹, volume: 100 mL, pH 7, applied voltage : 4 V, [Na₂SO₄]: 50 mM.

Figure 6. The degradation of 2,4-D with scavengers of [•]OH (methanol) in the EAOP (a); Time-course of the identified short-chain carboxylic acids with N1-EEGr-GF electrode in EAOP (b). [2,4-D]: 20 mg L⁻¹, volume : 100 mL, pH: 7, applied voltage : 4 V, [Na₂SO₄]: 50 mM.

Figure 7. Reaction pathway proposed for degradation of 2,4-D by the EAOP.

Chapter 7 Conclusions and Prospects

Chapter 1 Introduction

1.1 Research background

1.1.1 New emerging organic contaminants

In the nature environment, organic matters are degraded by microorganisms and converted into inorganic matters. Then, the inorganic matters are synthesized through various living activities to synthesize organic matters. This material cycle belongs to the basic cycle of biogeochemistry in environment. However, some compounds such as polychlorinated biphenyls, fluorochemicals, synthetic detergents are difficult to be biodegraded in water during the recirculation. These refractory organic pollutants are difficult to be decomposed by biological metabolism under natural conditions^[1, 2]. These compounds have certain toxicity, persistence and wide distribution, and will be gradually concentrated through the food chain, which will cause certain harm to the natural ecological environment and human health.

The reason why refractory organic pollutants are difficult to be degraded by microorganisms is that the external conditions such as temperature, humidity, acidity and alkalinity beyond optimal conditions for biological treatment, and the most important reason is because of the chemical composition and structure of these organic pollutants. There are no enzymes for these compounds in the microbial community, making them resistant to degradation^[3-5]. In addition, some refractory organic pollutants have certain toxicity, such as pesticides, printing and dyeing wastewater, etc. These toxicities can inhibit the growth of microorganisms and cannot be rapidly degraded. Refractory organic pollutants are generally classified into the following categories: polycyclic aromatic hydrocarbon compounds, heterocyclic compounds, organochlorine compounds, synthetic detergents, polychlorinated biphenyls, pesticides, and dyes. In recent years, the concept of new emerging organic contaminants has further attracted people's attention^[6]. New emerging organic pollutants, including persistent organic pollutants (POPs), pharmaceutical and personal care products (PPCPs), and disinfectant by-products (DBPs), are usually present in the environment at lower concentration, but

have greater threat on health and ecological environments^[7-9].

The concept of pharmaceuticals and personal care products (PPCPs) was firstly proposed by Daughton in 1999. It refers to all pharmaceutical products (including prescription and over-the-counter drugs and biological agents), diagnostics, health products, cosmetics, disinfectants and catalysts, preservatives added during the manufacture of PPCPs^[10-12]. At present, there are about 4,500 kinds of pharmaceuticals widely used in the field of disease prevention and treatment in human activities, such as antibiotics, analgesics, and anticancer drugs (Table 1-1). With the development of modern medical technology, the sales and use of pharmaceuticals are also increasing year by year. Taking antibiotics with serious effects on residual drugs in the environment as an example, the problem of increasingly serious drug-resistant pathogens caused by it has been widely concerned. If no effective measures are taken, it is estimated that by 2050, the problem of drug resistance will possibly lead to 10 million premature deaths a year^[13].

Table1-1 Common pharmaceuticals in the environment

Name	No. CAS	Molecular formula	Application
Ibuprofen	15687-27-1	C ₁₃ H ₁₈ O ₂	Relieve pain and inflammation
Naproxen	22204-53-1	C ₁₄ H ₁₄ O ₃	Relieve pain and inflammation
diclofenac sodium	15307-79-6	C ₁₄ H ₁₀ C ₁₂ NNaO ₂	Relieve pain and inflammation
fentanyl	437-38-7	C ₂₂ H ₂₈ N ₂ O	analgesic
aspirin	50-78-2	C ₉ H ₈ O ₄	analgesic
imatinib	152459-95-5	C ₂₉ H ₃₁ N ₇ O	anti-cancer drug
docetaxel	114977-28-5	C ₄₃ H ₅₃ NO ₁₄	anti-cancer drug
ultravist solution	73334-07-3	C ₁₈ H ₂₄ I ₃ N ₃ O ₈	developer X-ray
roxithromycin	80214-83-1	C ₄₁ H ₇₆ N ₂ O ₁₅	antibiotics
ciprofloxacin	85721-33-1	C ₁₇ H ₁₈ FN ₃ O ₃	antibiotics
norfloxacin	70458-96-7	C ₁₆ H ₁₈ O ₃ N ₃ F	antibiotics

Human and animal medical products are the main sources of PPCPs. After

ingestion by human or animal, only a few of the medicines have been metabolized, most of which are eventually discharged into the sewage through urine or feces in their original form; personal care products such as cosmetics are brought into the sewage pipe after bathing, swimming and other activities; in addition, some unused and expired medicines are eventually brought into urban life sewage through waste disposal and other ways^[14, 15]. On the other hand, in the process of manufacturing PPCPs, a large number of pollutants will be released. Because of the lack of timely and effective detection methods and strict discharge standards, a large number of wastewater and waste residues with PPCPs will be discharged into the water environment. As a developing country, China undertakes a lot of processing and production of PPCPs and related raw materials, so the pollution of PPCPs can not be underestimated.

Unlike traditional POPs, PPCPs are mostly polar, soluble in water and weak in volatility. Therefore, they do not have the characteristics of "global cycle", mainly pass through water phase transmission and food chain diffusion. Although the concentration of PPCPs in water is generally very low and exists only in microgram liters, the continuous output caused by human activities and the inefficiency of traditional treatment methods result in a large amount of PPCPs in water, which is called "pseudo persistent chemicals"^[16].

1.1.2 Treatment methods for new emerging organic contaminants

At present, the treatment methods for emerging organic pollutants at home and abroad can be divided into physical and chemical methods, biological methods and so on.

1.1.2.1 Physicochemical treatment

Physicochemical treatment of refractory organic pollutants mainly includes adsorption, coagulation, extraction and membrane separation.

1.1.2.2 Biological method

Biological method is the process of degrading organic matters into inorganic matters by microbial metabolisms. It can be divided into aerobic method, anaerobic

method and enzymatic method. It has the advantages of no secondary pollutions, high treatment capacity and low operation cost. However, it is often necessary to provide a suitable environment for microorganisms to survive and reproduce in order to increase the efficiency of their oxidation and decomposition of organic matters. According to the characteristics of new emerging organic pollutants, there are several biological methods used at present:

Biological enhancement technology:

The biodegradability of the existing biological treatment system was improved by introducing microorganisms that can degrade refractory organic pollutants through inoculation technology. The cultivation and source of these efficient microbial strains are mainly from natural screening, construction of genetic engineering bacteria and horizontal gene transfer technology.

Anoxic denitrification technique:

In anoxic environment, denitrifying bacteria can use organic carbon as an electron donor for denitrification process, and nitrate nitrogen or nitrite nitrogen as an electron acceptor for anaerobic respiration to achieve simultaneous denitrification and organic carbon removal.

Anaerobic hydrolysis acidification pretreatment technology:

Anaerobic hydrolysis acidification pretreatment technology includes two stages: hydrolysis and acidification. For refractory organic pollutants, it can catalyze hydrolysis of macromolecule organic substances or insoluble substances into small molecules or soluble substances such as glucose and amino acids through hydrolysis stage. In the acidification stage, small molecules of carboxylic acids were formed under anaerobic conditions, which created conditions for further degradation with aerobic biochemistry.

1.1.2.3 Oxidation

Oxidation is a process of decomposing pollutants by using strong oxidants. It can be divided into chemical oxidation methods and advanced oxidation processes.

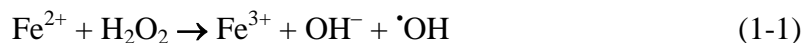
Chemical oxidation methods:

A method of oxidizing target pollutants by the loss of electrons is an oxidation. The commonly used oxidants are active manganese dioxide and hydrogen peroxide.

Advanced oxidation processes (AOPs):

Advanced oxidation processes refer to the production of hydroxyl radicals with strong oxidation ability, which is far superior to ordinary chemical oxidants. It is the strongest inorganic oxidant besides fluorine^[17], and has a very strong oxidation electrode potential (2.8 V), with directly mineralizing almost all refractory and macromolecular substances or improving the biodegradability of pollutants by peroxidation. It has a very high reaction rate constant^[18], and has certain advantages in the treatment of trace harmful pollutants in the environment. The AOPs have been successfully applied to sludge treatment^[19], coking wastewater, papermaking wastewater and other refractory industrial wastewater degradation^[20] and landfill leachate treatment^[21]. According to the different ways and reaction conditions of free radicals, AOPs can be divided into ultraviolet photocatalytic oxidation, electrochemical oxidation, ultrasonic oxidation, Fenton oxidation and so on^[22, 23]. In recent years, new types of advanced oxidation, such as persulfate oxidation and electrochemical oxidation, have attracted more and more attention.

Fenton's method was discovered in 1894. In acidic environment, Fenton reagent reaction (hydrogen peroxide and iron salt) is used to produce hydroxyl radicals with high activity and high oxidation potential to degrade organic matters. The reaction is as follows:



At the same time, Fe^{3+} can be reduced to Fe^{2+} by reacting with hydrogen peroxide, which ensures the continuity of the reaction through the regeneration of ferrous ions.



Fenton technology has been well studied and developed for its high efficiency in the treatment of refractory organic pollutants^[24-26]. Traditional Fenton technology has some limitations in improving the mineralization efficiency of pollutants, mainly in three aspects: firstly, Fenton reaction can produce highly active hydroxyl radicals only under acidic conditions (pH 2.8-3); secondly, it can produce a lot of iron mud pollution; thirdly, the utilization rate of hydrogen peroxide is low^[27, 28]. In order to avoid the above

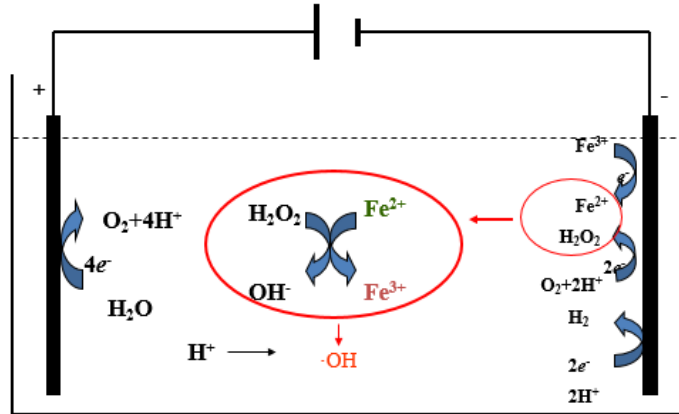
shortcomings of traditional Fenton reaction, the combined treatment processes such as light Fenton, electro-Fenton and micro-electrolysis Fenton effectively improve the efficiency and application range of Fenton method for pollutants degradation ^[29-34].

1.2 Developments of cathode materials for electro-Fenton process

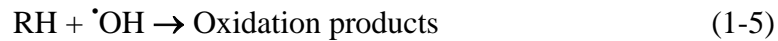
1.2.1 Electro-Fenton technology

Electrochemical advanced oxidation processes (EAOPs) are environmental friendly technologies, and their applications in wastewater treatment have attracted wide attention in recent years. Among them, electro-Fenton (EF) technology is the most widely used advanced electrochemical oxidation technology, which is equivalent to the coupling of electrochemical action and Fenton method. Divalent iron ions can be produced on the anode by the action of applied electricity such as reactions (1-3). At the same time, under acidic conditions, the surface of the cathode electrode will undergo a redox reaction of two electrons, thus the dissolved oxygen in the system can be converted into hydrogen peroxide under aeration, such as reactions (1-4). The formation of ferrous ions and hydrogen peroxide can be controlled by the applied electricity and the rate of formation of hydroxyl radicals is controlled by the Fenton reaction as in reaction (1-1). Compared with the traditional Fenton method, the EF technology can better control the process of reaction, effectively avoid the storage and transportation of hydrogen peroxide and reduce costs and risks. In addition, the electricity used in the process of EF is a clean and pollution-free energy, so the whole process will not produce secondary pollution, and can be used as an environmental friendly technology for water and wastewater treatment. The reaction mechanism diagram is shown in Figure 1.1^[35].



Fig. 1.1 The mechanism of electro-Fenton process^[35]

The reactions for the degradation of pollutants by EF technology are as follows:



Hydroxyl radicals are very active and decompose quickly; they can not be stored in the solution for a long time and accumulated continuously, so the hydroxyl radicals in the final reaction system will reach an equilibrium state.

Usually, the experimental parameters affecting the degradation efficiency of EF technology including pH, temperature, dissolved oxygen, catalyst concentration, current density, electrode spacing and hydrogen peroxide concentration.

As Fenton reaction, the optimum pH range of the EF technology is about 3. Therefore, the solution pH has a great influence on the efficiency of EF process. In the traditional Fenton process, when the solution pH is high, iron ions will form iron hydroxide precipitation. At low pH, iron ions and hydrogen peroxide form a stable complex, which leads to the passivation of the catalyst, thus greatly reducing the oxidation efficiency. As shown in reaction (1-4), acidic solutions are more conducive to the formation of hydrogen peroxide. However, when the pH is too low, the enhancement of side reaction will also consume the hydrogen peroxide (1-6). In addition, when the pH of the solution is less than 3, hydrogen peroxide tends to remain stable by combining with hydrogen ions to form hydrated hydrogen ions (1-7). Because the regeneration of ferrous ions is produced via the reaction of ferric iron ions with

hydrogen peroxide (1-2), too low pH is not conducive to the effective operation of EF. Since hydrogen peroxide is very unstable in alkaline environment, when the pH is greater than 5, the EF efficiency will decrease sharply. Under neutral or high pH conditions, hydrogen peroxide can rapidly decompose into oxygen and water. The reaction rate constants are $2.3 \times 10^{-2} \text{ min}^{-1}$ and $7.4 \times 10^{-2} \text{ min}^{-1}$ at pH 7 and 10.5, respectively.



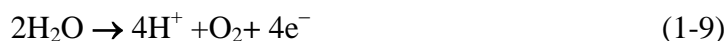
For this reason, the heterogeneous EF technology, which uses solid catalysts to decompose hydrogen peroxide to produce hydroxyl radicals, has attracted great attention of researchers because it can overcome the shortcomings of traditional homogeneous EF technology which must optimize the amount of catalyst used and broaden the scope of application of solution pH. Initially, natural iron ores such as goethite and magnetite were selected as heterogeneous catalysts for wastewater treatment^[36, 37]. It was found that the added iron ores had the function of adjusting the solution pH, which provided the possibility for the effective treatment of neutral or acidic solutions by EF technology. Pyrite and chalcopyrite have also been successfully used to degrade drugs under neutral pH conditions and obtain high removal and mineralization rates^[38-40]. At the same time, various iron-containing or transition metal oxides have also become a research hotspot, which have been synthesized as heterogeneous catalysts alone or effectively combined with microporous and mesoporous support materials to prepare composite electrodes of heterogeneous EF process for the degradation of pollutants^[41-43]. Professor Qiu Jianrong of Huazhong University of Science and Technology treated Rhodamine B wastewater with gas diffusion electrode composed of nanometer iron oxide ($\text{Fe}@\text{Fe}_2\text{O}_3$) and carbon nanotube materials. The removal efficiency reached 91.5% in 120 minutes at medium pH condition^[44]. Professor Zhu Yihua of East China University of Science and Technology prepared a heterogeneous electrical Fenton cathode material (Fe-GMCA) for the degradation of dye wastewater by using carbon aerogels prepared from iron oxide (Fe_3O_4) and graphene carbon nanotubes. The removal rate of 99% can be obtained

at 60 min^[45].

The applied current drives the cathodic oxygen reduction reaction to produce hydrogen peroxide. Higher applied current can increase the yield of hydrogen peroxide, thereby improving the efficiency of pollutants degradation in EF process. At the same time, high current density can also promote the regeneration of ferrous ions.



Usually, when the current density increases to a certain value, the efficiency of EF process decreases with the further increase of the current density, which is due to the enhancement of side reactions in the electrolytic system. Anodic oxygen evolution (1-9) and cathodic hydrogen evolution (1-10) reactions occur at high current densities. These side effects limit the progress of reactions (1-5) and (1-8), leading to the reduction of the EF efficiency.



An appropriate concentration of ferrous ions is a necessary condition for the EF process. The efficiency of EF process increases with the higher ferrous ion concentration (1-1), which enhances the degradation efficiency of pollutants. It is reported that the degradation rate of TOC in the EF process increases when the concentration of ferrous ions enhances from 0 to 1 mM. The effect of ferrous ion concentration on the degradation of 2,6-dimethylaniline in the EF process shows that the kinetic rate constant accelerates with the ferrous ion concentration increase from 1.0 mM to 1.5 mM, but when the ferrous ion concentration increases from 1.5 mM to 2.0 mM, the degradation rate does not increase significantly^[46].

The concentration of hydrogen peroxide is very important to the efficiency of EF technology. The removal rate of pollutants increases with the increasing hydrogen peroxide concentration, which is due to the higher amounts of hydroxyl radical generated (1-1). Similarly, when the concentration of hydrogen peroxide reaches a certain limit, the removal rate of pollutants will decrease due to hydroxyl radicals consuming hydrogen peroxide and other side reactions (1-11, 1-12, 1-13).



1.2.2 The development of anodes in EF process

Anode material is very important for EF technology. Selection of unstable anode will lead to electrode loss in electrolyte, while high oxygen evolution potential anode can produce heterogeneous hydroxyl radicals (1-14) through oxidation of water during the EF process for organics degradation:



Thus, the whole process can be called "paired electrocatalysis" because oxidant hydroxyl radicals can be formed in both anodic and cathodic reactions. Therefore, high oxygen evolution potential electrode materials with strong oxidation ability are often used as EF anodes.

Platinum electrode (Pt) is often selected as an anode material for the degradation of organic compounds due to its good electrical conductivity and high chemical stability (Fig. 1.2) ^[35]. But because of its high cost, it is seldom used in practical application. In addition to Pt electrodes, Fig. 1.2 shows several other commonly used anode materials for EF. Sopaj et al. ^[47] degraded sulfamethazine (0.2 mM) with boron-doped diamond (BDD) anode. At current intensity of 29.16 mA cm⁻² for 4 hours, 100% TOC degradation rate was obtained. Zcan et al. ^[48], Sir s et al. ^[49] also used EF technology with BDD anode for wastewater treatment. Prabhakaran et al. ^[50] and Huang et al. ^[51] tried to use Ti-IrO₂-RuO₂ as anode. Stable anode DSA is also one of the commonly used anodes in recent years. Chmayssem et al. ^[52] used DSA (Ti/RuO₂) anode in EF technology for degradation of bisphenol A (150 mg L⁻¹), achieving 89% removal rate at pH 3, 0.2 A for 90 minutes. The penetrating EF technology with DSA anode was used to degrade methylene blue, orange II, acetylsalicylic acid, tetracycline and 2,4-D. Under the optimum conditions, removal rates of 91%, 67%, 64%, 73% and 92% were obtained respectively ^[53]. In addition, in the past two years, the French Paris-Est University

Oturan's group has attempted to use the sub-stoichiometric titanium oxide electrode (Ti_4O_7) as anode in EF process for pollutants degradation. The antibiotic amoxicillin (0.1 mM) can be completely degraded at 120 mA current, and the titanium oxide electrode is proved to be an efficient and stable anode material. It was found that the degradation efficiency of amoxicillin by titanium oxide electrode was similar to that of BDD electrode, but the cost was greatly reduced. It could be used as an alternative of BDD electrode with high efficiency^[54, 55].

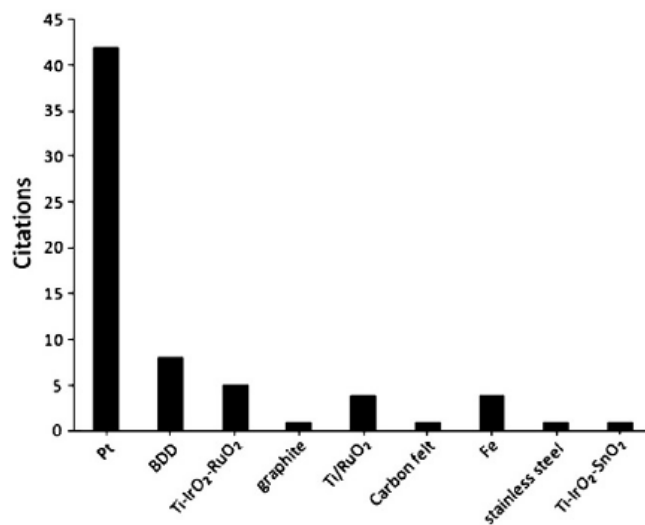


Fig. 1.2 Comparison of anodes used in electro-Fenton process^[35]

1.2.3 The development of cathodes in EF process

For the EF technology, efficient hydrogen peroxide yield is a necessary condition for high efficiency. Hydrogen peroxide is produced by cathodic reduction of dissolved oxygen or air (reaction 1-5). Cathode materials such as graphite, carbon-PTFE gas diffusion electrode, activated carbon, carbon fibers, graphite felt^[30, 56, 57], carbon black^[58], carbon nanotubes^[59], graphite carbon, graphene^[60, 61] have been reported to be used to increase the yield of hydrogen peroxide.

Although it is known that carbon electrodes can produce hydrogen peroxide by oxygen reduction reaction, Oloman and Watkinson^[62] have been systematically studied in this field since 1970 through a liquid trickle bed or a packed bed electrochemical

reactor filled with graphite particles. Carbon materials are non-toxic, non-polluting, with high hydrogen evolution potential and low catalytic activity for the decomposition of hydrogen peroxide, and have good conductivity and stability. Due to the low solubility of oxygen in aqueous solution (about 40 or 8 mg L⁻¹ for pure oxygen and air at 1 atm, 25°C respectively), gas diffusion electrodes and three-dimensional electrodes with high specific surface area are very suitable for providing a certain current intensity in practical applications.

Gas diffusion electrodes make the solution immersed on the carbon surface contact with the gas through the pore structure. The electrodes are divided into diffusion layer and catalytic layer. The diffusion layer is beneficial to the diffusion of oxygen, while the catalytic layer has a large number of active sites on its surface, which can lead to rapid oxygen reduction reaction for the generation of hydrogen peroxide. The solution is separated from the gas by conductive materials (stainless steel or nickel mesh, etc.) as the support of the substrate, thus forming a gas, liquid and solid three-phase reaction zone with a certain catalytic activity to improve the yield of hydrogen peroxide. Zhang et al. [63] enhanced cathodic hydrogen peroxide production and pollutant degradation by using gas diffusion electrode (G-GDE) based on graphene@graphite. Compared with the traditional GDE electrode, G-GDE has better oxygen reduction performance by increasing the conductivity of the electrode and the active sites of surface catalysis, doubling the production of hydrogen peroxide and increasing the degradation rate of pollutants. Carbon nanotubes (CNTs) based gas diffusion electrodes prepared by rolling process were used for the degradation of acetylsalicylic acid (ASA) in EF process. The results show that hydrogen peroxide of 805 mg L⁻¹ can be produced at 100 mA current for 180 minutes. Under the optimum conditions, ASA can be completely removed within 10 minutes, and the TOC removal rate of solution reaches 62% [64] at 1 hour. Microporous gas diffusion electrodes have been reported to increase cathodic hydrogen peroxide production to 0.8 mmol L⁻¹ h⁻¹[65]. It is proved that the gas diffusion electrode can be used as an efficient EF cathode.

Three-dimensional electrode materials exhibit a high surface area to volume ratio, which is conducive to mass transfer and diffusion of dissolved oxygen. At the same time, the cost is low and easy to be controlled. They are often used as EF cathode materials.

For example, ACF is a three-dimensional electrode material with large adsorption capacity and good conductivity. It has high mechanical integrity and can accumulate a large amount of hydrogen peroxide. Wang et al. ^[66] used activated carbon fiber as cathode and Ti/RuO₂ as anode, 0.6 mmol L⁻¹ hydrogen peroxide can be produced by 180 min reaction at 360 mA current. Compared with graphite as cathode system under the same conditions, the production of hydrogen peroxide has increased about 10 times. The EF system was used to degrade acid red 14 dyes at 0.36 A current and pH 3. After 6 hours, the TOC removal rate reached 70%. ACFs have a certain adsorption capacity, so they often interact with the EF process to improve the degradation rate of pollutants. Zhao et al. ^[67] showed that ACFs could greatly promote the removal efficiency of nitrobenzene by UV/EF system. 98% of nitrobenzene can be removed in 20 minutes, and 90% of TOC can be removed in 5 hours.

Graphite felt electrode is one of the most widely used three-dimensional electrode materials because of its huge three-dimensional active area and excellent mechanical strength. It has great advantages in practical application and regeneration of ferrous ions. The untreated graphite felt electrode has good conductivity, but its specific surface area and electrochemical activity are not very high, so the production of hydrogen peroxide will be limited when it is used as cathode. Therefore, the study of improving the electrocatalytic activity of graphite felt electrodes by modifying graphite felt electrodes has been reported extensively. Carbon black, carbon nanotubes, acetylene black and metal oxides have been reported to be used for modification of graphite felt. Wang et al. ^[68] increased the specific surface area and hydrophilicity of graphite felt cathode by calcining potassium hydroxide at high temperature. The results showed that the reaction rate (0.198 min⁻¹) of using the AGF-900 electrode calcined at 900°C as the EF cathode for the degradation of dimethyl phthalate (DMP) was about 10 times of the unmodified graphite felt cathode (0.020 min⁻¹). Graphite felt can also increase its catalytic activity by high temperature activation with gaseous acetic acid ^[69]. Under the conditions of -0.7 V and pH 1, the cathode AGF1100 can produce 500 mgL⁻¹ hydrogen peroxide in 60 minutes.

In addition, in recent years, a large number of new (modified) cathode electrodes have been reported to effectively increase the production of hydrogen peroxide and thus

improve the effect of pollutants degradation by EF, especially composite cathode materials have become a research hotspot. Van et al.^[70] used Fe-CHI/Ni|ACF|Fe-CHI/Ni as composite cathode to remove Rhodamine B. Composite electrodes such as Fe@Fe₂O₃/ACF^[71], Cu₂O/CNTs/PTFE^[72] and Fe@Fe₂O₃/CNT^[44] were also used to degrade pollutants by EF cathode. Zhu et al.^[73] used impregnation method and modified chitosan iron as EF cathode material. The optimum parameters for decolorization of Rhodamine B were studied.

1.3 The development of graphene-based electro-Fenton cathodes

1.3.1 Description of graphene

Graphene is a monolayer lamellar structure material composed of carbon atoms. It is a hexagonal honeycomb lattice planar film composed of carbon atoms and sp² hybrid orbitals, as a two-dimensional material with only one carbon atom thickness. Graphene, which exists in nature, has always been difficult to peel out of single-layer structure. In 2004, Andre Geim and Konstantin Novoselov, two scientists from the University of Manchester, UK, obtained graphene sheets^[74] consisting of only one layer of carbon atoms by micromechanical peeling, breaking the decades-old theory that thermodynamic fluctuations do not allow two-dimensional crystals to exist freely at finite temperatures^[75].

1.3.2 Traditional methods for preparation of graphene

1.3.2.1 Solid phase method

Graphite can be seen as a monolayer of graphene composed of numerous layers, which is bound by van der Waals force. The bonding energy between layers is about 2 eV/nm². In theory, the external force required for graphite peeling is about 300 nN/um²^[76]. Graphite can be peeled by ordinary tape. In 2004, Andre Geim and Konstantin Novoselov obtained single-layer graphene sheets^[74] by repeatedly peeling high-directional pyrolytic graphite. Later, Schleberger et al. prepared graphene sheets^[77] by replacing SiO₂ substrates with insulating crystal substrates such as Al₂O and TiO₂. In

order to further improve the yield of graphene prepared by stripping method, Kim et al. used atomic force microscopy probe instead of traditional tape to strip high directional pyrolysis graphite, and obtained a single layer of graphene^[78]. This micromechanical force stripping method is theoretically the best way to obtain graphene with good structure and properties. However, this method has low yield, poor repeatability and high time cost, which can not meet the needs of industrialization and large-scale production.

1.3.2.2 Liquid phase method

Redox method is a liquid phase method widely used at present. Graphite oxide is produced by the reaction of natural graphite with strong oxidizing substances. Graphite oxide is dispersed into graphene oxide by ultrasonic wave. At last, oxygen-containing groups on the surface of graphene oxide are removed by adding reductant, and graphene is reduced. Hummers and Offeman, for example, react graphite with potassium permanganate in concentrated sulphuric acid to produce graphene oxide^[79] with a carbon-oxygen ratio of about 2:1.

1.3.2.3 Gas phase method

Chemical vapor deposition (CVD) is the representative of the gas phase method. It refers to the process of graphene formation on the surface of the matrix by the chemical reaction of the reactant under the gaseous condition by energy excitation. In 2008, Kong et al. used polycrystalline Ni as the substrate and chemical vapor deposition (CVD) to introduce highly diluted carbon-containing gases, which were decomposed into carbon atoms at high temperature and deposited on the surface of Ni plate to form graphene^[80]. The graphene film obtained by this method has a large surface area (depending on the area of the substrate) and can be directly used without post-treatment. It has excellent transparency and conductivity. High quality graphene can be obtained by this method, but the process is complex and the cost is high.

In addition to the above typical graphene preparation methods, there are ultrasonic dispersion method, organic synthesis method, plasma enhanced method and arc discharge method, each has its own advantages. The preparation of graphene, the

optimization of its structure and properties, large-scale production and cost control are still the research hotspots in this field in the future.

In addition, Chinese researchers have also made great contributions to the preparation and practical application of graphene. In 2008, Bai Xuedong, National Laboratory of Condensate Physics of Chinese Academy of Sciences, and Wang Eng'e's team successfully explored the preparation of high quality graphene by stripping, embedding and expanding graphite (Fig. 1.3). The prepared graphene was characterized and analyzed by transmission electron microscopy (TEM). The results show that the graphene prepared by them has two orders of magnitude higher conductivity than that prepared by conventional redox graphite method, and has higher conductivity at room temperature and low temperature^[81]. Although graphene has some applications in new energy, new materials and other fields, its application in large high-end optoelectronic devices is still not ideal. The key bottleneck is that the growth rate of large single-crystal graphene is usually less than 0.4 micron/s, which makes it difficult to obtain larger graphene single crystals.

In 2017, Liu Kaihui, a researcher at Peking University and other researchers, together with the National Institute of Science and Technology of Yushan, Korea, published a paper. By transforming industrial polycrystalline copper foil into single crystal copper foil and using epitaxy growth technology and ultrafast growth technology, the world's largest ($5 \times 50 \text{ cm}^2$) epitaxy single crystal graphene material^[82] was successfully obtained in 20 minutes, which was extracted for fast growth of meter-grade single crystal graphene. It provides the necessary scientific basis and lays a foundation for the industrial application of graphene single crystal quantum technology.

1.3.3 Electrochemical exfoliation for graphene preparation

Electrochemical method means that in a certain electrolyte solution, the graphite material is used as the electrode. By applying a certain voltage to the electrode material, under the action of electric field, the ions in the electrolyte will enter into the graphite interlayer and make it expand continuously, so that graphene can be peeled off slowly.

The electrochemical preparation of graphene has obvious advantages over solid phase method, liquid phase method and gas phase method. Firstly, the electrochemical method mainly uses electricity without additional organic reagents, which is environmentally friendly. In addition, the electrochemical method can peel the graphite electrode by applying voltage to expand it. It has the advantages of high speed and low cost, and can be widely used. Graphene was prepared by electrochemical stripping with graphite as anode and platinum as cathode. After dissolving and dispersing in dimethylformamide solution (Fig. 1.4), the tablet has very high transparency (about 96%). After simple nitric acid treatment, the resistance is less than $1 \text{ k}\Omega \text{ sq}^{-1}$ ^[83]. Mir et al.^[84] prepared three-layer graphene sheets by electrochemical stripping of graphite, and investigated the influence parameters in the process of electrochemical stripping. Nickel atom doped graphene has been reported to promote the reduction of carbon dioxide. Porous carbon materials prepared by electrochemical stripping of graphene adhering to zinc oxide particles can be used as anodes in lithium batteries^[85].

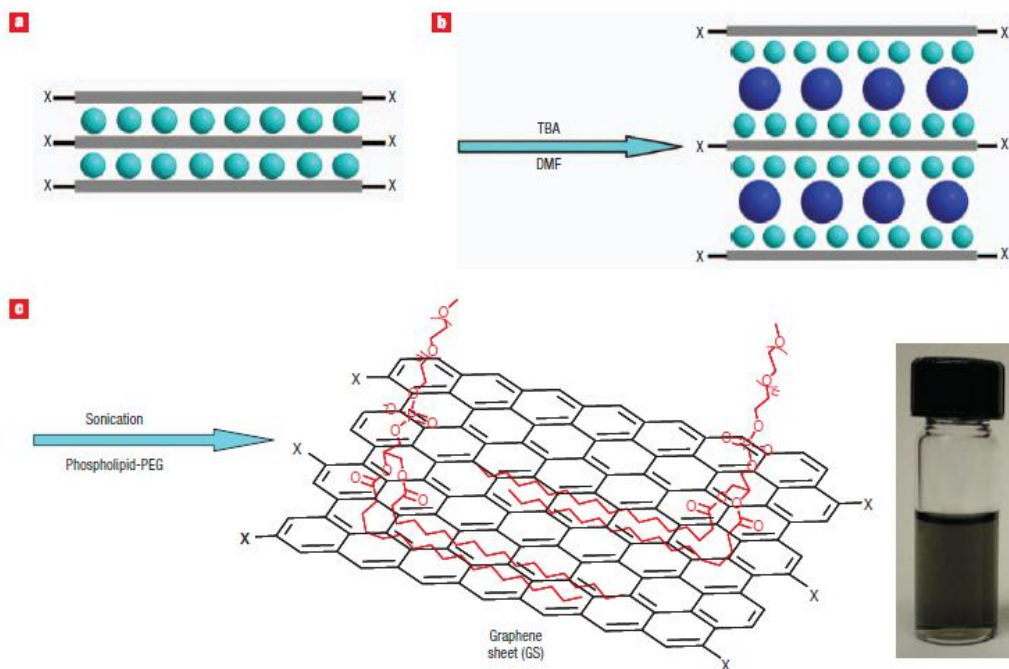


Fig. 1.3 Preparation process for graphene^[81]

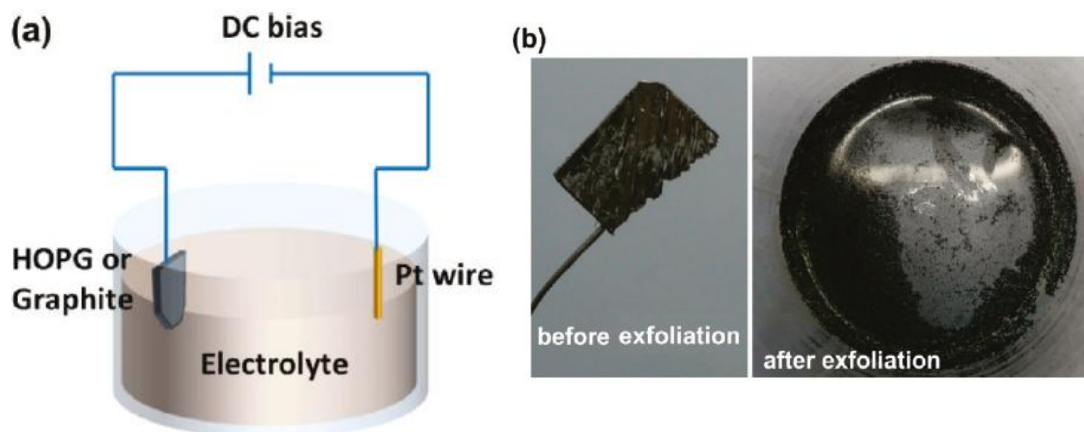


Fig. 1.4 Electrochemical exfoliation process for preparation of graphene^[83]

1.3.4 Application of electro-Fenton with graphene-based cathode

The cathode is the working electrode of the electric Fenton process. In situ hydrogen peroxide production and the rate of hydroxyl radical production by reaction with catalyst depend mainly on the cathode material and its properties. Since graphene-based electrode materials have been proved to have similar properties to the above gas diffusion electrodes, graphene has been used as an electro-Fenton cathode material to produce hydrogen peroxide and degrade pollutants. Jiang et al.^[86] used the catalytic membrane EF system prepared by graphene was used to degrade florfenicol, a low concentration antibiotic, with a removal rate of 90%, much better than the single electrochemical filtration process (50%) and the filtration process (27%). Graphene modified carbon felt electrode can be used as EF cathode to degrade dyes. The dyes can be completely removed within 5 minutes. Under the optimum current condition, it can be mineralized completely (94.3%) in 8 hours. The electrode has good stability and operates 10 times. The mineralization rate remains above 64.3%^[87]. Mousset uses graphene-based carbon cloth as the electro-Fenton cathode. Under the same conditions, the removal rate of organic TOC is increased by about 1.7 times compared with that of

unmodified carbon cloth^[88]. Zhang et al. ^[89]used graphene-based heterogeneous electro-Fenton system to degrade rhodamine B, FeOOH/ γ -Al₂O₃ as catalyst, sodium sulfate and magnesium sulfate as electrolyte solution respectively, and discussed the change trend of pH and degradation mechanism under different conditions. Divyapriya^[90] degraded bisphenol A with graphene and iron oxide composite electrode (QEEG/Fe₃O₄) by electro-Fenton system. At pH 3, 100% removal rate could be obtained in 90 minutes, 98% removal rate could be obtained under neutral conditions, and the iron leaching rate of the composite electrode was less than 1%. Graphene composite electrode Ce-Fe-graphene (CeO/FeO-RGO) Fenton-like system has 99% removal rate of antibiotic sulfamethazine (20 mg L⁻¹) and 73%^[91]degradation rate of TOC under the condition of 8 mM hydrogen peroxide and 7 pH.

Because graphene itself has high specific surface area and excellent conductivity, the electro-Fenton cathode based on graphene has great advantages in increasing the rate of electron transfer and hydrogen peroxide produced by cathodic oxygen reduction reaction. It can be used as a kind of electrode material with high activity and stability for the treatment of actual wastewater.

1.4 Contents and structure of the research

1.4.1 Purpose and significance of thesis research

The emergences of a large number of new organic pollutants at low concentrations in aquatic environment and their refractory character have attracted wide attention. Electro-Fenton belongs to advanced oxidation technology, which has a good effect on the degradation of refractory organic pollutants. However, the traditional electric Fenton technology has two bottlenecks: narrow pH range and limited efficiency. This research mainly focuses on how to effectively solve these two problems and improve the performance of traditional electric Fenton. Firstly, high quality graphene was prepared by electrochemical stripping method and used to modify carbon felt electrode, which greatly improved the performance of traditional EF. Furthermore, we construct in-situ

advanced oxidation technology of non-metal by using graphene modified carbon felt electrode doped with nitrogen, which can effectively expand the scope of application of pH, and do not need additional catalysts to achieve the goal of high efficiency and low consumption of pollutants treatment.

1.4.2 Contents of the research

In view of the above problems, this paper is divided into seven chapters, the specific structure is as follows:

The first chapter is an introduction. This paper mainly describes the research background and significance, research progress, and clarifies the main research content and organizational structure of the paper.

In the second chapter, the preparation and characterization of graphene-based modified carbon felt electrode were introduced. Graphene was prepared by electrochemical stripping method and its properties were determined by a series of characterizations. Then the carbon felt electrode was modified and optimized by the prepared graphene. The oxygen reduction reaction mechanism of the modified electrode was explored and explained by means of material characterization and electrochemical performance test.

In the third chapter, the effect of graphene modified carbon felt cathode electro-Fenton technology on the degradation of imatinib was studied. The mineralization properties of graphene modified carbon felt cathode and unmodified carbon felt cathode were compared. The effects of current intensity and iron ion concentration were investigated. The ability of graphene-based carbon felt cathode electro-Fenton technology to degrade pollutants was verified by the determination of carboxylic acid, inorganic ion and the monitoring of solution toxicity.

In the fourth chapter, the heterogeneous free radicals produced by anodic oxidation, the coupling effect between cathodic hydrogen peroxide and homogeneous free radicals produced by iron ion reaction and the comparison of degradation performance of organic compounds were studied. We degraded imatinib (IMA) in electrochemical advanced oxidation systems of four anode materials (DSA, Pt, Ti4O7,

BDD). The degradation of imatinib by EF system with different anodes and the comparison of the effects of homogeneous and heterogeneous free radicals in the degradation process were investigated. The degradation pathway of imatinib was predicted by the detection of inorganic ions and carboxylic acids, ion chromatography and GC-MS.

In the fifth chapter, nitrogen-doped graphene was prepared by using ammonium nitrate as nitrogen source, and the material was characterized and its electrochemical properties were tested. Carbon felt electrode was modified by N-doped graphene and its electrochemical properties were tested. Nitrogen-doped graphene modified carbon felt cathode electro-Fenton system was used to degrade pollutants and the catalytic mechanism of the electrode was explored.

In Chapter 6, nitrogen-doped graphene was used to construct in-situ advanced oxidation system. The degradation performance and energy consumption of the system were compared with those of the traditional EF system. The system was used to degrade 2,4-D, and the in-situ advanced oxidation pathway of nonmetal was deduced by the determination of carboxylic acid, inorganic ions and intermediate products.

Chapter 7 summarizes the whole paper and puts forward feasible suggestions for future research.

References

- [1] Kim K-H, Ihm S-K, et al. Heterogeneous catalytic wet air oxidation of refractory organic pollutants in industrial wastewaters: a review[J]. *Journal of Hazardous Materials*, 2011, 186: 16-34.
- [2] Chiang L-C, Chang J-E, Tseng S-C, et al. Electrochemical oxidation pretreatment of refractory organic pollutants[J]. *Water Science and Technology*, 1997, 36: 123-130.
- [3] Ma J, Sui M-H, Chen Z-L, et al. Degradation of refractory organic pollutants by catalytic ozonation—activated carbon and Mn-loaded activated carbon as catalysts[J]. *Ozone: Science and Engineering*, 2004, 26: 3-10.
- [4] Bowers A, Gaddipati P, Eckenfelder Jr W, et al., *Treatment of toxic or refractory wastewaters with hydrogen peroxide*, *Water Pollution Research and Control Brighton*, Elsevier 1988, pp. 477-486.
- [5] Martínez-Huitle C A, Ferro S, et al. Electrochemical oxidation of organic pollutants for the wastewater treatment: direct and indirect processes[J]. *Chemical Society Reviews*, 2006, 35: 1324-1340.

- [6] Richardson S D, et al. Water analysis: emerging contaminants and current issues[J]. Analytical chemistry, 2009, 81: 4645-4677.
- [7] Sharma B M, Bharat G K, Tayal S, et al. Environment and human exposure to persistent organic pollutants (POPs) in India: A systematic review of recent and historical data[J]. Environment international, 2014, 66: 48-64.
- [8] Liu J-L, Wong M-H, et al. Pharmaceuticals and personal care products (PPCPs): a review on environmental contamination in China[J]. Environment international, 2013, 59: 208-224.
- [9] López-Serna R, Posadas E, García-Encina P A, et al. Removal of contaminants of emerging concern from urban wastewater in novel algal-bacterial photobioreactors[J]. Science of The Total Environment, 2019, 662: 32-40.
- [10] Esplugas S, Bila D M, Krause L G T, et al. Ozonation and advanced oxidation technologies to remove endocrine disrupting chemicals (EDCs) and pharmaceuticals and personal care products (PPCPs) in water effluents[J]. Journal of hazardous materials, 2007, 149: 631-642.
- [11] Wang J, Chu L, et al. Irradiation treatment of pharmaceutical and personal care products (PPCPs) in water and wastewater: an overview[J]. Radiation Physics and Chemistry, 2016, 125: 56-64.
- [12] Yang Y, Ok Y S, Kim K-H, et al., et al. Occurrences and removal of pharmaceuticals and personal care products (PPCPs) in drinking water and water/sewage treatment plants: A review[J]. Science of the Total Environment, 2017, 596: 303-320.
- [13] O’neill J, et al. Tackling a global health crisis: initial steps[J]. The Review on Antimicrobial Resistance Chaired by Jim O’Neill, 2015,
- [14] Barceló D, Petrovic M, Pharmaceuticals and personal care products (PPCPs) in the environment, [J]. Springer, 2007.
- [15] Pojana G, Fantinati A, Marcomini A, et al. Occurrence of environmentally relevant pharmaceuticals in Italian drinking water treatment plants[J]. International journal of environmental analytical chemistry, 2011, 91: 537-552.
- [16] Kasprzyk-Hordern B, Dinsdale R M, Guwy A J, et al. The removal of pharmaceuticals, personal care products, endocrine disruptors and illicit drugs during wastewater treatment and its impact on the quality of receiving waters[J]. Water research, 2009, 43: 363-380.
- [17] Liu J-L, Wong M-H, et al. Pharmaceuticals and personal care products (PPCPs): a review on environmental contamination in China[J]. Environment international, 2013, 59: 208-224..
- [18] Sánchez-Sánchez C M, Exposito E, Casado J, et al. Goethite as a more effective iron dosage source for mineralization of organic pollutants by electro-Fenton process[J]. Electrochemistry communications, 2007, 9: 19-24.
- [19] Novoselov K S, Geim A K, Morozov S V, et al. Electric field effect in atomically thin carbon films[J]. science, 2004, 306: 666-669.
- [20] Zhou Y, Bao Q, Tang L a L, et al. Hydrothermal Dehydration for the “Green” Reduction of Exfoliated Graphene Oxide to Graphene and Demonstration of Tunable Optical Limiting Properties[J]. Chemistry of Materials, 2009, 21: 2950-2956.
- [21] Divyapriya G, Nambi I M, Senthilnathan J, et al. An innate quinone functionalized

electrochemically exfoliated graphene/Fe₃O₄ composite electrode for the continuous generation of reactive oxygen species[J]. *Chemical Engineering Journal*, 2017, 316: 964-977.

[22] Szpyrkowicz L, Juzzolino C, Kaul S N, et al. A comparative study on oxidation of disperse dyes by electrochemical process, ozone, hypochlorite and Fenton reagent[J]. *Water Research*, 2001, 35: 2129-2136.

[23] Soon A N, Hameed B, et al. Heterogeneous catalytic treatment of synthetic dyes in aqueous media using Fenton and photo-assisted Fenton process[J]. *Desalination*, 2011, 269: 1-16.

[24] Brillas E, Sirés I, Oturan M A, et al. Electro-Fenton process and related electrochemical technologies based on Fenton's reaction chemistry[J]. *Chemical reviews*, 2009, 109: 6570-6631.

[25] Lin S H, Lo C C, et al. Fenton process for treatment of desizing wastewater[J]. *Water research*, 1997, 31: 2050-2056.

[26] Deng Y, Englehardt J D, et al. Treatment of landfill leachate by the Fenton process[J]. *Water research*, 2006, 40: 3683-3694.

[27] Kang Y W, Hwang K-Y, et al. Effects of reaction conditions on the oxidation efficiency in the Fenton process[J]. *Water research*, 2000, 34: 2786-2790.

[28] Zhang H, Choi H J, Huang C-P, et al. Optimization of Fenton process for the treatment of landfill leachate[J]. *Journal of Hazardous materials*, 2005, 125: 166-174.

[29] Guivarch E, Trevin S, Lahitte C, et al. Degradation of azo dyes in water by electro-Fenton process[J]. *Environmental Chemistry Letters*, 2003, 1: 38-44.

[30] Pimentel M, Oturan N, Dezotti M, et al. Phenol degradation by advanced electrochemical oxidation process electro-Fenton using a carbon felt cathode[J]. *Applied Catalysis B: Environmental*, 2008, 83: 140-149.

[31] Devi L G, Kumar S G, Reddy K M, et al. Photo degradation of Methyl Orange an azo dye by Advanced Fenton Process using zero valent metallic iron: Influence of various reaction parameters and its degradation mechanism[J]. *Journal of hazardous materials*, 2009, 164: 459-467.

[32] Bautitz I R, Nogueira R F P, et al. Degradation of tetracycline by photo-Fenton process—Solar irradiation and matrix effects[J]. *Journal of Photochemistry and Photobiology A: Chemistry*, 2007, 187: 33-39.

[33] Neppolian B, Jung H, Choi H, et al. Sonolytic degradation of methyl tert-butyl ether: the role of coupled fenton process and persulphate ion[J]. *Water Research*, 2002, 36: 4699-4708.

[34] Soon A N, Hameed B, et al. Heterogeneous catalytic treatment of synthetic dyes in aqueous media using Fenton and photo-assisted Fenton process[J]. *Desalination*, 2011, 269: 1-16.

[35] Nidheesh P, Gandhimathi R, et al. Trends in electro-Fenton process for water and wastewater treatment: an overview[J]. *Desalination*, 2012, 299: 1-15.

[36] Sánchez-Sánchez C M, Exposito E, Casado J, et al. Goethite as a more effective iron dosage source for mineralization of organic pollutants by electro-Fenton process[J]. *Electrochemistry communications*, 2007, 9: 19-24.

[37] Expósito E, Sánchez-Sánchez C M, Montiel V, et al. Mineral iron oxides as iron source in electro-Fenton and photoelectro-Fenton mineralization processes[J]. *Journal of the electrochemical*

society, 2007, 154: E116-E122.

[38] Labiadh L, Oturan M A, Panizza M, et al. Complete removal of AHPS synthetic dye from water using new electro-fenton oxidation catalyzed by natural pyrite as heterogeneous catalyst[J]. Journal of hazardous materials, 2015, 297: 34-41.

[39] Barhoumi N, Oturan N, Olvera-Vargas H, et al. Pyrite as a sustainable catalyst in electro-Fenton process for improving oxidation of sulfamethazine. Kinetics, mechanism and toxicity assessment[J]. Water research, 2016, 94: 52-61.

[40] Barhoumi N, Labiadh L, Oturan M A, et al. Electrochemical mineralization of the antibiotic levofloxacin by electro-Fenton-pyrite process[J]. Chemosphere, 2015, 141: 250-257.

[41] Hou B, Han H, Jia S, et al., et al. Heterogeneous electro-Fenton oxidation of catechol catalyzed by nano-Fe₃O₄: kinetics with the Fermi's equation[J]. Journal of the Taiwan Institute of Chemical Engineers, 2015, 56: 138-147.

[42] Zhang G, Zhou Y, Yang F, et al. FeOOH-catalyzed heterogeneous electro-Fenton system upon anthraquinone@ graphene nanohybrid cathode in a divided electrolytic cell: catholyte-regulated catalytic oxidation performance and mechanism[J]. Journal of The Electrochemical Society, 2015, 162: H357-H365.

[43] Hammouda S B, Fourcade F, Assadi A, et al. Effective heterogeneous electro-Fenton process for the degradation of a malodorous compound, indole, using iron loaded alginate beads as a reusable catalyst[J]. Applied Catalysis B: Environmental, 2016, 182: 47-58.

[44] Ai Z, Mei T, Liu J, et al. Fe@ Fe₂O₃ core-shell nanowires as an iron reagent. 3. Their combination with CNTs as an effective oxygen-fed gas diffusion electrode in a neutral electro-Fenton system[J]. The Journal of Physical Chemistry C, 2007, 111: 14799-14803.

[45] Chen W, Yang X, Huang J, et al. Iron oxide containing graphene/carbon nanotube based carbon aerogel as an efficient E-Fenton cathode for the degradation of methyl blue[J]. Electrochimica Acta, 2016, 200: 75-83.

[46] Ting W P, Lu M C, Huang Y H, et al. Kinetics of 2,6-dimethylaniline degradation by electro-Fenton process[J]. Journal of Hazardous Materials, 2009, 161: 1484-1490.

[47] Sopaj F, Oturan N, Pinson J, et al. Effect of the anode materials on the efficiency of the electro-Fenton process for the mineralization of the antibiotic sulfamethazine[J]. Applied Catalysis B: Environmental, 2016, 199: 331-341.

[48] Özcan A, Şahin Y, Koparal A S, et al. A comparative study on the efficiency of electro-Fenton process in the removal of protham from water[J]. Applied Catalysis B: Environmental, 2009, 89: 620-626.

[49] Sires I, Garrido J A, Rodriguez R M, et al. Catalytic behavior of the Fe³⁺/Fe²⁺ system in the electro-Fenton degradation of the antimicrobial chlorophene[J]. Applied Catalysis B: Environmental, 2007, 72: 382-394.

[50] Prabhakaran D, Kannadasan T, Basha C A, et al. Treatability of resin effluents by electrochemical oxidation using batch recirculation reactor[J]. International Journal of Environmental Science & Technology, 2009, 6: 491-498.

- [51] Huang Y-H, Huang Y-F, Chang P-S, et al. Comparative study of oxidation of dye-Reactive Black B by different advanced oxidation processes: Fenton, electro-Fenton and photo-Fenton[J]. *Journal of hazardous materials*, 2008, 154: 655-662.
- [52] Chmayssem A, Taha S, Hauchard D, et al. Scaled-up electrochemical reactor with a fixed bed three-dimensional cathode for electro-Fenton process: Application to the treatment of bisphenol A[J]. *Electrochimica Acta*, 2017, 225: 435-442.
- [53] Ma L, Zhou M, Ren G, et al. A highly energy-efficient flow-through electro-Fenton process for organic pollutants degradation[J]. *Electrochimica Acta*, 2016, 200: 222-230.
- [54] Oturan N, Ganiyu S O, Raffy S, et al. Sub-stoichiometric titanium oxide as a new anode material for electro-Fenton process: application to electrocatalytic destruction of antibiotic amoxicillin[J]. *Applied Catalysis B: Environmental*, 2017, 217: 214-223.
- [55] Ganiyu S O, Oturan N, Raffy S, et al. Sub-stoichiometric titanium oxide (Ti₄O₇) as a suitable ceramic anode for electrooxidation of organic pollutants: A case study of kinetics, mineralization and toxicity assessment of amoxicillin[J]. *Water research*, 2016, 106: 171-182.
- [56] Özcan A., Şahin Y, Koparal A S, et al. Degradation of picloram by the electro-Fenton process[J]. *Journal of Hazardous Materials*, 2008, 153: 718-727.
- [57] Panizza M, Oturan M A, et al. Degradation of Alizarin Red by electro-Fenton process using a graphite-felt cathode[J]. *Electrochimica Acta*, 2011, 56: 7084-7087.
- [58] Liu J, Sun X, Song P, et al. High-performance oxygen reduction electrocatalysts based on cheap carbon black, nitrogen, and trace iron[J]. *Advanced materials*, 2013, 25: 6879-6883.
- [59] Thiam A, Zhou M, Brillas E, et al. Two-step mineralization of Tartrazine solutions: study of parameters and by-products during the coupling of electrocoagulation with electrochemical advanced oxidation processes[J]. *Applied Catalysis B: Environmental*, 2014, 150: 116-125.
- [60] Liu T, Wang K, Song S, et al. New electro-Fenton gas diffusion cathode based on nitrogen-doped graphene@ carbon nanotube composite materials[J]. *Electrochimica Acta*, 2016, 194: 228-238.
- [61] Carneiro J F, Paulo M J, Siaj M, et al. Nb₂O₅ nanoparticles supported on reduced graphene oxide sheets as electrocatalyst for the H₂O₂ electrogeneration[J]. *Journal of catalysis*, 2015, 332: 51-61.
- [62] Oloman C, Watkinson A P, et al. The electroreduction of oxygen to hydrogen peroxide on fluidized cathodes[J]. *The Canadian journal of chemical engineering*, 1975, 53: 268-273.
- [63] Zhang Z, Meng H, Wang Y, et al. Fabrication of graphene@ graphite-based gas diffusion electrode for improving H₂O₂ generation in Electro-Fenton process[J]. *Electrochimica Acta*, 2018, 260: 112-120.
- [64] Yang H, Zhou M, Yang W, et al. Rolling-made gas diffusion electrode with carbon nanotube for electro-Fenton degradation of acetylsalicylic acid[J]. *Chemosphere*, 2018, 206: 439-446.
- [65] Qiao L, Bai J, Luo T, et al. High yield of H₂O₂ and efficient S recovery from toxic H₂S splitting through a self-driven photoelectrocatalytic system with a microporous GDE cathode[J]. *Applied Catalysis B: Environmental*, 2018, 238: 491-497.

- [66] Wang A, Qu J, Ru J, et al. Mineralization of an azo dye Acid Red 14 by electro-Fenton's reagent using an activated carbon fiber cathode[J]. *Dyes and Pigments*, 2005, 65: 227-233.
- [67] Zhao C, Si B, Mirza Z A, et al. Activated carbon fiber (ACF) enhances the UV/EF system to remove nitrobenzene in water[J]. *Separation and Purification Technology*, 2017, 187: 397-406.
- [68] Wang Y, Liu Y, Wang K, et al. Preparation and characterization of a novel KOH activated graphite felt cathode for the electro-Fenton process[J]. *Applied Catalysis B: Environmental*, 2015, 165: 360-368.
- [69] Pan Z, Wang K, Wang Y, et al. In-situ electrosynthesis of hydrogen peroxide and wastewater treatment application: A novel strategy for graphite felt activation[J]. *Applied Catalysis B: Environmental*, 2018, 237: 392-400.
- [70] Fan Y, Ai Z, Zhang L, et al. Design of an electro-Fenton system with a novel sandwich film cathode for wastewater treatment[J]. *Journal of hazardous materials*, 2010, 176: 678-684.
- [71] Li J, Ai Z, Zhang L, et al. Design of a neutral electro-Fenton system with Fe@ Fe₂O₃/ACF composite cathode for wastewater treatment[J]. *Journal of hazardous materials*, 2009, 164: 18-25.
- [72] Ai Z, Xiao H, Mei T, et al. Electro-Fenton degradation of rhodamine B based on a composite cathode of Cu₂O nanocubes and carbon nanotubes[J]. *The Journal of Physical Chemistry C*, 2008, 112: 11929-11935.
- [73] Hernando M, Mezcuca M, Fernández-Alba A, et al. Environmental risk assessment of pharmaceutical residues in wastewater effluents, surface waters and sediments[J]. *Talanta*, 2006, 69: 334-342.
- [74] Novoselov K S, Geim A K, Morozov S V, et al. Electric field effect in atomically thin carbon films[J]. *science*, 2004, 306: 666-669.
- [75] Mermin N D, et al. Crystalline order in two dimensions[J]. *Physical Review*, 1968, 176: 250.
- [76] Soldano C, Mahmood A, Dujardin E, et al. Production, properties and potential of graphene[J]. *Carbon*, 2010, 48: 2127-2150.
- [77] Akċdtekin S, El Kharrazi M, K̇hler B, et al. Graphene on insulating crystalline substrates[J]. *Nanotechnology*, 2009, 20: 155601.
- [78] Zhang Y, Small J P, Pontius W V, et al. Fabrication and electric-field-dependent transport measurements of mesoscopic graphite devices[J]. *Applied Physics Letters*, 2005, 86: 073104.
- [79] Hummers Jr W S, Offeman R E, et al. Preparation of graphitic oxide[J]. *Journal of the american chemical society*, 1958, 80: 1339-1339.
- [80] Reina A, Jia X, Ho J, et al. Large area, few-layer graphene films on arbitrary substrates by chemical vapor deposition[J]. *Nano letters*, 2008, 9: 30-35.
- [81] Li X, Zhang G, Bai X, et al. Highly conducting graphene sheets and Langmuir–Blodgett films[J]. *Nature nanotechnology*, 2008, 3: 538.
- [82] Xu X, Zhang Z, Dong J, et al. Ultrafast epitaxial growth of metre-sized single-crystal graphene on industrial Cu foil[J]. *Science Bulletin*, 2017, 62: 1074-1080.
- [83] Ching-Yuan S, Ang-Yu L, Yanping X, et al. High-quality thin graphene films from fast electrochemical exfoliation[J]. *ACS Nano*, 2011, 5: 2332-2339.

- [84] Afkham M, Singh D K, Anupam S, et al. Size distribution of trilayer graphene flakes obtained by electrochemical exfoliation of graphite: Effect of the synthesis parameters[J]. *Materials Chemistry and Physics*,
- [85] Ma Z, Tao L, Liu D, et al. Ultrafine nano-sulfur particles anchored on: In situ exfoliated graphene for lithium-sulfur batteries[J]. *Journal of Materials Chemistry A*, 2017, 5: 9412-9417.
- [86] Jiang W L, Xia X, Han J L, et al., et al. Graphene Modified Electro-Fenton Catalytic Membrane for in Situ Degradation of Antibiotic Florfenicol[J]. *Environmental Science & Technology*, 2018, 52: acs.est.8b01894-.
- [87] Le T X H, Bechelany M, Lacour S, et al. High removal efficiency of dye pollutants by electron-Fenton process using a graphene based cathode[J]. *Carbon*, 2015, 94: 1003-1011.
- [88] Mousset E, Zheng T K, Syafiq M, et al. Electrocatalytic activity enhancement of a graphene ink-coated carbon cloth cathode for oxidative treatment[J]. *Electrochimica Acta*, 2016, 222: 1628-1641.
- [89] Zhang G, Zhou Y, Yang F, et al. FeOOH-Catalyzed Heterogeneous Electro-Fenton System upon Anthraquinone@Graphene Nanohybrid Cathode in a Divided Electrolytic Cell: Catholyte-Regulated Catalytic Oxidation Performance and Mechanism[J]. *Journal of the Electrochemical Society*, 2015, 162: H357-H365.
- [90] Divyapriya G, Nambi I M, Senthilnathan J, et al. An innate quinone functionalized electrochemically exfoliated graphene/Fe₃O₄ composite electrode for the continuous generation of reactive oxygen species[J]. *Chemical Engineering Journal*, 2017, 316: 964-977.
- [91] Zhong W, Hu J, Wang J, et al. Removal of sulfamethazine antibiotics using Ce Fe-graphene nanocomposite as catalyst by Fenton-like process[J]. *Journal of Environmental Management*, 2016, 182: 284-291.

Chapter 2. Ultrahigh yield of hydrogen peroxide on graphite felt cathode modified with electrochemically exfoliated graphene

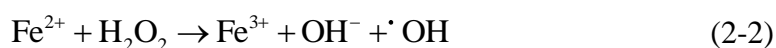
Abstract:

The development of efficient oxygen reduction reaction (ORR) cathode for hydrogen peroxide production represents an important challenge in the field of electrochemical processes and is highly demanded for chemical industries and environmental remediation application. In this work, a novel graphite felt cathode modified with electrochemically exfoliated graphene (EEGr) and carbon black was developed, presenting a very high H_2O_2 generation rate of $7.7 \text{ mg h}^{-1} \text{ cm}^{-2}$ with relatively low energy consumption (9.7 kWh kg^{-1}). Characterized by SEM, TEM, AFM, Raman, XRD and XPS, the synthesized EEGr was proved to be the 3-4 layers thin sheet with low defects. Important cathode manufacture parameters including the ratio and loading of EEGr were optimized; and the dependence of H_2O_2 generation with pH and cathode potential as well as performance stability were investigated. At optimized cathode potential -0.9 V and pH 7, the modified cathode kept stable performance for H_2O_2 generation during 10 cycles, which was 2 times of the cathode without EEGr. Further explored by CV, rotating disk electrode (RDE) and contact angles analysis, the presence of EEGr was found to accelerate electrons transfer rate, benefit oxygen surface reaction, but not change two-electron ORR number, which contributed to the enhanced performance for H_2O_2 production and possible mechanism was suggested. Finally, such graphene modified cathode demonstrated effectiveness for the degradation of four kinds of representative pollutants (Orange II, methylene blue, phenol and sulfadiazine) by electro-Fenton process, proving great potential practical application for organic wastewater treatment.

2.1 Introduction

Hydrogen peroxide is highly desirable and important for many manufacturing industries such as chemicals and paper-making as well as environmental remediation since it is a versatile and environmentally friendly oxidizing agent without generation of hazardous residues upon decomposition, only oxygen and water. However, the traditional process of anthraquinone oxidation, which is a multistep process to extract H_2O_2 from organic agents, is not regarded as a green method^[1]. Thus the development of efficient method represents an important challenge, and significant efforts have been made either to reduce its synthesis cost^[2, 3], or expand its application fields including environmental remediation^[4].

In the latter field, recent years, electro-Fenton, which combines with ferrous ion addition and the in-situ electrochemically generated H_2O_2 (eq.1) has attracted much concern for its advantages such as easy-controlling, high efficiency and environmental compatibility due to the formation of highly powerful hydroxyl radicals ($\cdot\text{OH}$) (eq.2).



A high yield of H_2O_2 was prerequisite for the high efficiency of electro-Fenton. Various cathode materials have been widely attempted such as active carbon, carbon fiber^[5], graphite felt^[6-8], carbon black^[9], carbon nanotubes^[10], graphite carbon and graphene^[11, 12]. As a commercially available material, graphite felt is regarded as one of the most widely used cathodes due to its large active surface and mechanical integrity, but still the yield of H_2O_2 production is not satisfying, and extensive efforts via chemical, electrochemical oxidation or acidic treatment have been made^[8]. Particularly, in our previous work, the graphite felt modified with carbon black could dramatically improve the H_2O_2 generation rate up to 10 times (about $2.2 \text{ mg h}^{-1} \text{ cm}^{-2}$) when comparing with the pristine one^[13].

Recent years, as a new carbonaceous material, graphene, which is a

two-dimensional, one atom thick sheet composed of sp^2 carbon atoms arranged in a honeycomb structure, has been used as an efficient adsorbent or catalyst for environmental application due to its outstanding electrical conductivity and high specific surface area, which have become a very hot research area^[14-16]. However, very few applications using it as cathode for H_2O_2 generation have been reported^[17, 18], and what's more, the yield of H_2O_2 is still limited and the role of graphene has not been well elucidated though these cathodes modified with graphene are supposed to improve H_2O_2 electro-generation^[18, 19]. For example, Xu et al. reported an average H_2O_2 generation rate of $1.03 \text{ mg h}^{-1} \text{ cm}^{-2}$ on a graphene doped gas diffusion cathode, while Mousset et al. showed that it was $0.64 \text{ mg h}^{-1} \text{ cm}^{-2}$ on the 3D graphene foam^[18].

These facts indicated that graphene based cathodes for H_2O_2 production need more extensive and comprehensive studies since the synthesis of graphene and its assembly on the cathode would significantly determine the cathode characteristics. Firstly, traditional graphene synthetic methods, e.g., Hummers's method, was conventionally used for graphene synthesis, however, there are some disadvantages including extreme experimental conditions^[20], high cost^[21] and possible environmental pollution, while electrochemical exfoliation of graphite (EEGr) has been reported to be a efficient method for a high production of graphene in several hours^[20, 22]. It would be easier to synthesize low defect graphene, expecting better cathode characteristics for H_2O_2 generation. Secondly, the manufacture of graphene-based electrodes either with pristine graphene or use of graphene coatings over some flat substrates, till now, no attempt on three dimensional material substrates, e.g., graphite felt, has been tested. As demonstrated in our previous work^[13], it would be reasonable that a small graphene loading instead of carbon black on graphite felt would enhance the specific surface area and the conductivity of the cathode, which would further improve the performance of hydrogen peroxide production.

In this context, this work reported a novel graphene-based cathode assembly strategy for high yield of H_2O_2 using graphite felt cathode modified with carbon black and graphene derived by a fast electrochemical exfoliation from graphite foil with an expansion time dramatically reduced to 1 min. The objectives of this study were: 1)

synthesis of graphene by a fast electrochemical exfoliation and its characterization, 2) assembly of graphene-based cathode and optimization of important manufacture process, 3) assessment and comparison of its properties with unmodified electrode, and to elucidate possible enhancement mechanism for H₂O₂ production, and 4) to evaluate the degradation and mineralization efficiency of four kinds of model pollutants by electro-Fenton. This modified cathode exhibited a very high H₂O₂ generation rate with relatively low energy consumption, opening up a new avenue for developing efficient graphene-based cathode for electro-Fenton.

2.2 Experimental

2.2.1 EEGr synthesis

Before electrochemical exfoliation, the graphite foils were soaked in ethanol with ultrasonic treatment for 30 min, then they were dried 24 h for ready. EEGr was electrochemically exfoliated in a beaker system with aqueous electrolyte containing 2 mL concentrated H₂SO₄, 10 mL KOH and 100 mL deionized water, using platinum foil sheet (1×1 cm²) and graphite foil (2×4 cm²) as the cathode and anode, respectively. Firstly, a bias potential of 2.5 V was applied for 1 min of expansion time, and then, the applied bias potential was increased to 10 V for about 3-5 mins. Subsequently, the exfoliated graphene sheets were filtered with 0.22 μm membrane, and then these collected graphene flakes were dispersed into N,N-Dimethylformamide (DMF) solution with 5 min sonication. Finally, after vacuum filtration with deionized water to remove DMF, they were put into a vacuum dryer for 1 day.

2.2.2 Cathode modification with EEGr and carbon black

Graphite felt (2×2.5 cm²) was used as the base cathode, carbon black and EEGr were used to modify it. With the addition of 0.14 mL PTFE, 3 mL ethanol and 2 mL deionized water, after quick shake for 15 s, a kind of seriflux was formed, which was coated onto the two sides of the graphite felt, after drying in the room temperature, the

modified graphite felt electrode was annealed for 30 min at 360 °C.

The performance of the modified electrode was evaluated by the yield of H₂O₂ production and compared to the one without EEGr. The H₂O₂ electrochemical generation experiments were operated in an undivided cell in 0.05 M Na₂SO₄ (0.1 L) and with 0.7 L min⁻¹ air aeration at room temperature. The modified graphite felt was selected as the cathode, and DSA (2×4 cm²) was employed as the anode. The distance between the anode and cathode was 1 cm. At every 10 min intervals, 0.5 mL sample was taken for analyzing the concentration of H₂O₂.

The concentration of H₂O₂ was measured by the potassium titanium (IV) oxalate method at λ=400 nm with a UV-Vis spectrophotometer (UV759, Shanghai Instrument Analysis Instrument C0., Ltd). The current efficiency (CE) for the production of H₂O₂ was calculated with the following formula (3)^[23]:

$$CE = \frac{nFCV}{\int_0^t Idt} \times 100\% \quad (2-3)$$

Where n is the number of electrons transferred for oxygen reduction for H₂O₂, F is the Faraday constant (96,485 C mol⁻¹), C is the concentration of H₂O₂ production (mol L⁻¹), V is the bulk volume (L), I is the current (A), and t is the time of electrochemical process (s).

The electric energy consumption (EEC, kWh kg⁻¹) was measured by formula (4)

$$EEC = \frac{1000UIt}{CV_s} \quad (2-4)$$

Where U is the applied voltage (V), I is the current (A), t is the time of electrochemical process (h), C is the concentration of the H₂O₂ generated (mg L⁻¹), and V_s is the solution volume (L).

2.2.3 Characterization and analytical methods

The morphology of EEGr was determined using scanning electron microscopy

(SEM) (LEO-1530VP, Germany), transmission electron microscopy (TEM) (TitanTM G2 60-300, Japan) and atomic force microscopy (AFM) (JPK NanoWizard, Germany). The Raman spectra were recorded with a Renish Modular Raman spectrometer equipped with a Stellar Pro Argon-ion laser at 514 nm (50 mW). The crystalline structure was determined by X ray diffraction (XRD) (XRD-7000, Shimadzu) and the surface elemental composition by X-ray photoelectron spectroscopy (XPS) (Kratos-ultra DLD, Shimadzu) using Mono Al K α radiation ($h\nu = 1486.7$ eV). The contact angle of water on the material surface was examined by a contact angle meter (JC2000D, China) with a water drop volume of 0.2 μ L.

Linear sweep voltammetry (LSV) was carried out to compare the electrochemical behavior during H₂O₂ generation which was recorded by the CHI660D workstation at a scan rate of 50 mV s⁻¹ in a three-electrode cell system. The modified cathode was used as the working electrode, a platinum sheet as the counter electrode and a saturated calomel electrode (SCE) as the reference electrode at ambient temperature. Electrochemical impedance spectroscopy (EIS) was performed in the frequency range of 0.1-10⁵ Hz. The specific surface area of the electrodes was determined by nitrogen adsorption in a constant volume adsorption apparatus (BET, Autosorb-UQ-MP, America). What's more, cyclic voltammetry was used to explore the ORR activity for H₂O₂ generation on the modified and unmodified graphite felt cathodes. And the active surface area of the electrodes, rotating disk electrode (RDE) was used to investigate the oxygen reduction activity of modified electrode in saturated O₂ solution at a scan rate of 50 mV s⁻¹.

Different kinds of cathodes with or without EEGr were made for the RDE study, respectively. For the carbon black electrode, 7 mg carbon black with 0.9 mL ethanol and 0.1 mL PTFE was mixed, and to prepare for another working electrode, 2 mg EEGr and 8 mg carbon black powder was suspended in a mixture containing 0.9 mL ethanol and 0.1 mL PTFE, after the quick shock for 10 s, 0.01 mL of the mixture was dropped onto a glass carbon electrode (0.196 cm²) and then dried at room temperature.

The selectivity for H₂O₂ production was evaluated by the calculation of the electron transfer numbers according to the slopes of the Koutecky-Levich plots by the

following two equations:

$$\frac{1}{J} = \frac{1}{J_k} + \frac{1}{Bw^{\frac{1}{2}}} \quad (2-5)$$

$$B = 0.62nFA\nu^{\frac{1}{6}}C_{O_2}D_{O_2}^{\frac{2}{3}} \quad (2-6)$$

Where J and J_k are the detected current density and kinetic current density, respectively (mA cm^{-2}), w is the angular velocity (rad s^{-1}), F is the Faraday constant (C mol^{-1}), n is the electron transfer numbers, C_{O_2} is the bulk concentration of O_2 (mol cm^{-3}), ν is the kinematic viscosity ($\text{cm}^2 \text{s}^{-1}$), and D_{O_2} is the diffusion coefficient of O_2 in the electrolyte solution ($\text{cm}^2 \text{s}^{-1}$).

In order to ensure the electroactive surface area of the modified graphite felts, the Randles-Sevcik equation was used as follows:

$$I_p = 2.69 \times 10^5 \times AD^{\frac{1}{2}}n^{\frac{1}{2}}\nu^{\frac{1}{2}}C \quad (2-7)$$

Where I_p is the peak current (A), n is the number of electrons involving in the redox reaction ($n=1$), A is the area of the electrode (cm^2), D is the diffusion coefficient of the molecule in solution ($7.6 \times 10^{-6} \text{ cm}^2 \text{ s}^{-1}$), C is the concentration of the probe molecule in the bulk solution ($1 \times 10^{-5} \text{ cm}^3$) and ν is the scan rate of the CV (0.01 V s^{-1}).

2.2.4 Pollutants degradation by electro-Fenton

In order to verify the performance of cathodes, the graphite felts modified with or without EEGr were used as the cathode for pollutants degradation by electro-Fenton. The electrolyte solution was same as the one for H_2O_2 generation except the addition of 0.04 mM FeSO_4 .

Antibiotics are widely used in humans and animals to prevent and treat infection diseases, dyes and phenols are widely presented in many industries wastewater^[24, 25], thus Orange II (50 mg L^{-1}), methylene blue (50 mg L^{-1}), phenol (50 mg L^{-1}) and sulfadiazine (20 mg L^{-1}) were chosen as the representative pollutants. The concentration and Total organic carbon (TOC) removal efficiency of each pollutant were detected

every 10 min intervals and the results with the two cathodes were compared with each other.

TOC was monitored by a TOC analyzer (Analytikjena multi N/C 3100, Germany) to qualify the degree of mineralization in the electro-Fenton treatment of pollutants. The concentration removal efficiency (R%) and TOC removal efficiency (TOC%) of the pollutants were calculated according to the following equations, respectively:

$$R(\%) = \frac{c_0 - c_t}{c_0} \times 100\% \quad (2-8)$$

$$TOC\% = \frac{TOC_0 - TOC_t}{TOC_0} \times 100\% \quad (2-9)$$

Where c_0 , TOC_0 , c_t , TOC_t was the initial and final value of pollutants concentration and TOC, respectively.

2.3 Results and discussion

The SEM image (Fig. 1a) revealed that the EEGr flakes were thin sheets, and all of them were laminar arrangement. The TEM image reconfirmed they were 3-4 thin laminar layers (Fig. 1b and 1c). The typical AFM image (Fig. 1d) showed that, the statistical thickness of the EEGr flakes were within 3 nm. As we know, the single sheet graphene was 0.7-1.0 nm^[26], so it could be concluded that the synthesized graphene was 3-4 layers, which was consistent with TEM observation.

Fig. 1e shows Raman spectrum of EEGr and the original graphite foil. The bands of 1350 and 1582 cm⁻¹ represented the D and G bands, respectively. Obviously the EEGr exhibited an intense D band, where graphite foil did not have. It was reported that D band had relation with the disorder or defect in the structure because of the disorderliness in the graphene sheets. Besides, the D/G value was 0.52, which was similar to the result of 0.54 reported by Chen et al.^[27], and was much smaller than the reduced graphene oxide (1.0-1.5)^[28], suggesting that a low defect density of EEGr was obtained. What's more, the EEGr had an intense 2D bond at around 2720 cm⁻¹, which

was the evidence of sp^2 carbon materials, and 2D/G ratio was assigned to a second order two phonon process and usually used to determine the layers of graphene^[28]. The 2D/G ratio of 0.76 showed that the 4 layer numbers of EEGr had low defects and few layer numbers.

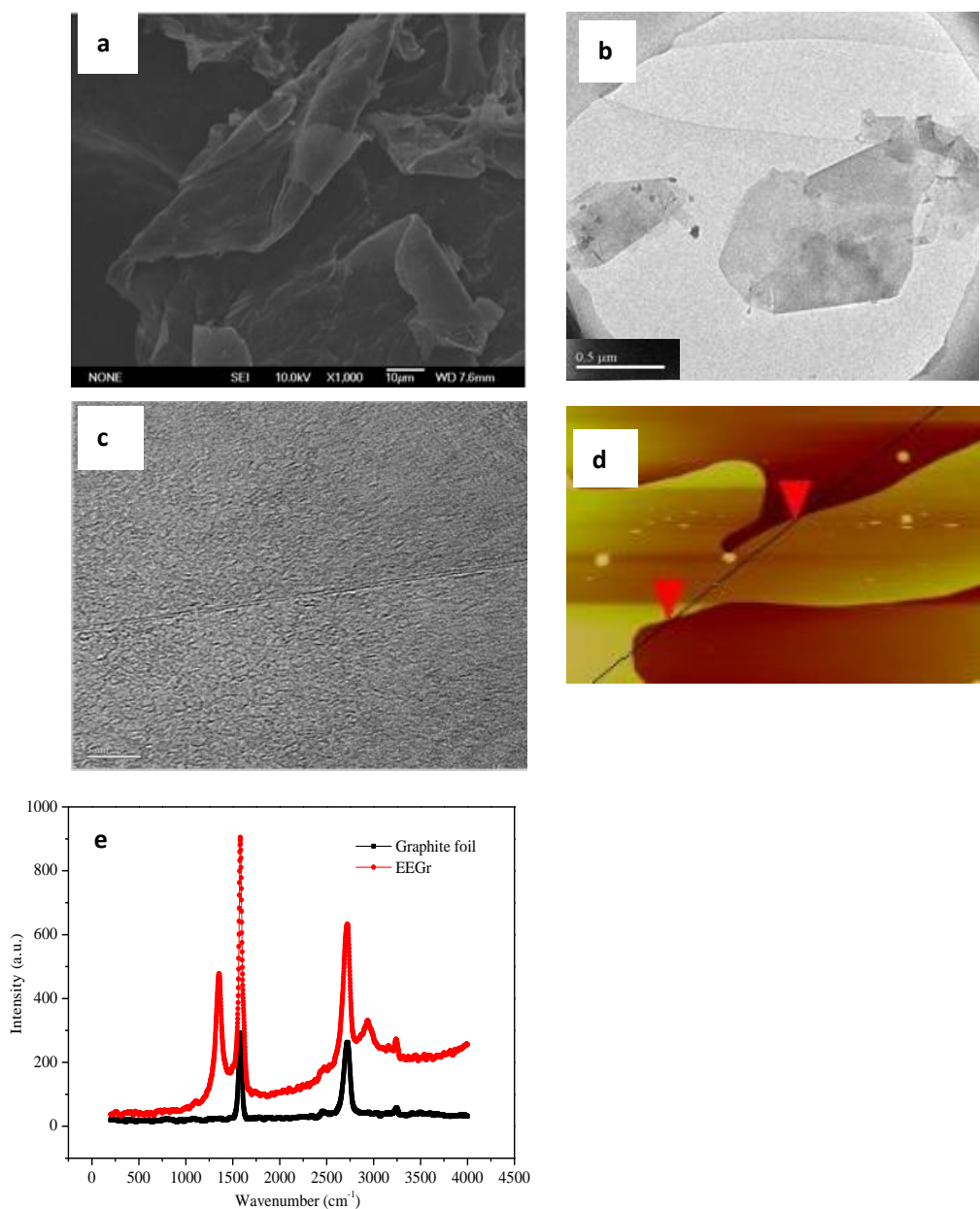


Fig. 1 SEM (a) , TEM (b, c) and AFM (d) of the EEGr from the graphite foil and Raman spectrum of

graphite foil and EEGr (e).

The XRD pattern of graphite foil and EEGr (Fig. 2a) displayed that the two materials had a strong sharp diffraction peak (002) and a weaker sharp peak (004), which were attributed to the crystalline graphitic structure^[29]. It should be noted that the highest intensity peak (002) for EEGr was found to be shifted toward the lower diffraction angles (26.42 °), which was 26.76 ° for graphite foil. The results proved that the lattice was expanded during electrochemical exfoliation^[28].

XPS presented the chemical composition of the EEGr and graphite foil (Fig. 2b): the atomic oxygen content detected in EEGr and graphite foil was 12.88% and 8.52%, and the atomic carbon content was 81.69% and 89.49%, respectively (Table 1). The measured O/C atomic ratios thus increased from 0.095 (graphite foil) to 0.157 (EEGr), which were higher than others,^{34,38} but still lower than 0.18 derived from anodic exfoliation^[30]. According to the high-resolution spectrum of C 1s (Fig. 2c and Fig. 2d), a sharp peak existed at a binding energy (BE) of 284.8 eV corresponding to the sp² carbon (graphitic C=C species), and the other peaks at 285 eV, 286.3 eV and 287.2 eV are assigned to the sp³ carbons (C-OH), and the carbon-oxygen groups (C-O-C, C=O), respectively^[31]. Compared to graphite foil, the intensity of C-OH peak of EEGr increased a little and the C=O peak was detected in EEGr while not in graphite foil, which confirmed that part of the graphite foil was oxidized in the process of synthesis graphene.

Table 1 Atomic percentage in the sample

Name		C1s	O1s	N1s	S2p	O/C
Graphite foil	At %	89.49	8.52	1.27	0.73	0.095
EEGr	At %	81.69	12.88	4.54	0.88	0.157

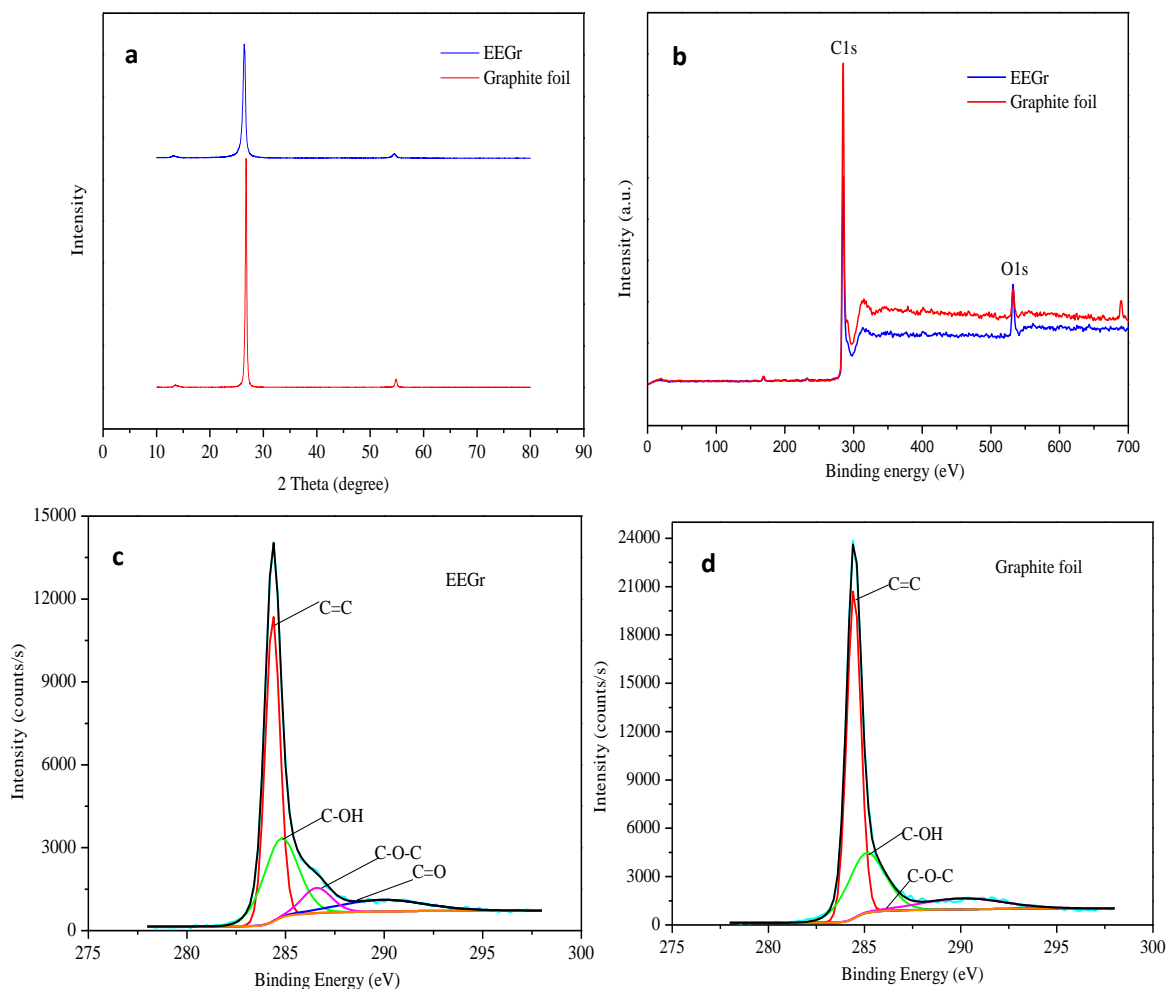


Fig. 2 XRD patterns of the graphite foil and EEGr (a); XPS survey spectra of graphite foil and EEGr (b); high-resolution C 1s spectrum of EEGr (c) and graphite foil (d).

2.3.1 Optimizing the ratio and loading of EEGr on modified graphite felt cathode

The ratio and loading of EEGr on graphite felt would significantly affect the cathode characteristics and its performance for hydrogen peroxide production, thus they were optimized as two important factors in cathode manufacture. Fig. 3a shows the yield of H_2O_2 on the cathodes modified with different ratio of EEGr to carbon black (0,

10, 20, 30, 40%). It was observed that the concentration of H_2O_2 after 60 min electrolysis increased with the increase of EEGr ratio until 20%, but further increase the ratio led to the decrease of H_2O_2 . For cathode modified with 20% EEGr (for simplification, we called it EEGr-20), the concentration of H_2O_2 reached near 100 mg L^{-1} , which was much higher than the unmodified (EEGr-0). Accordingly, EEGr-20 obtained the highest H_2O_2 production rate with the lowest EEC of 5.2 kWh kg^{-1} .

The EEGr synthesis process was further optimized with different loadings of EEGr when all ratios held on 20%. As shown in Fig.3b, a higher EEGr loading enhanced the H_2O_2 production, and the highest H_2O_2 production was obtained with EEGr loading of 0.056 g, which was almost no difference with that of EEGr loading of 0.072g and more than 1.5 times of the unmodified one. According to these experimental results, the EEGr ratio of 20% with loading of 0.056 g (i.e., 11.2 mg cm^{-2}) was chosen as the proper condition.

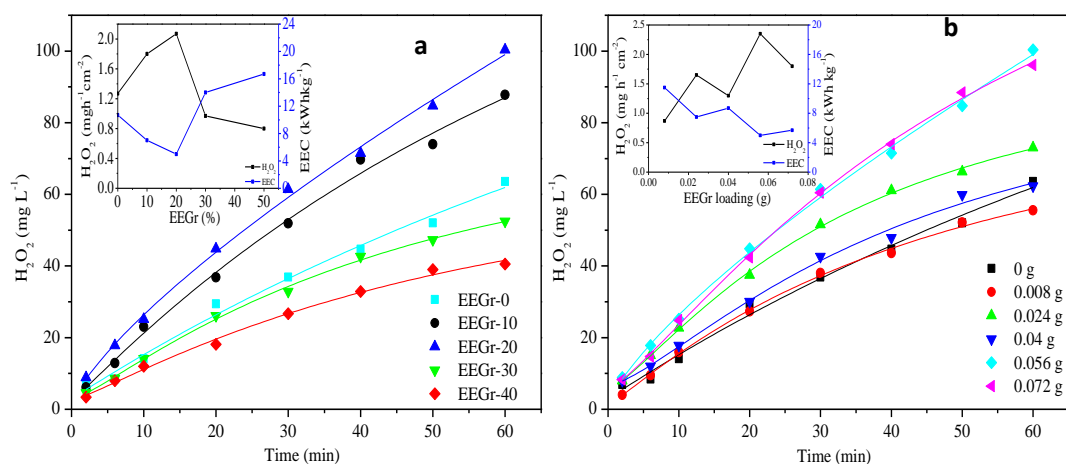


Fig. 3 The performances of modified graphite felts with different ratio (a) and loading of EEGr (b) for H_2O_2 generation.

2.3.2 Performance and stability of the modified cathode for H_2O_2 production

To explore the proper cathode potential, the yield of H_2O_2 at -0.5, -0.7, -0.9 and -1.1 V were investigated. As shown in Fig. 4a, it increased with the improvement of cathode potential, reaching 426 mg L^{-1} (- 1.1 V) at 120 min. The CE followed the same tendency with cathode potential (insert Fig. 4a), which was in agreement with literature^[32]. However, EEC was found significantly increased with cathode potential. Taking these factors into consideration, it could be concluded that -0.9 V was the optimized condition, in which the average H_2O_2 generation rate was $3.7 \text{ mg h}^{-1} \text{ cm}^{-2}$, which was more than 3 times of the one in a graphene doped gas diffusion electrode (GDE).

H_2O_2 generation is dependent on pH value due to the participation of proton in H_2O_2 electro-generation process^[33]. The results in Fig. 4b showed that the yield of H_2O_2 was the highest at pH 7, and then decreased as pH continued to increase, which was 366 mg L^{-1} at pH 9 and 336 mg L^{-1} at pH 11 with average H_2O_2 generation rate of 7.5 and $7.2 \text{ mg h}^{-1} \text{ cm}^{-2}$. These facts proved that pH 7 was the proper condition for H_2O_2 generation, which was accordant with literature. One possible reason was that the residual H^+ reduced at the cathode with H_2 generation might be a competing reaction that decreased H_2O_2 generation^[34-36]. Since the conversion of dissolved oxygen to H_2O_2 consumes protons in acidic solution,⁴³ according to eq. 1. The decrease of H_2O_2 at high pH condition was because that the H^+ existed in the solution may be not enough for the generation of H_2O_2 , leading to a lower yield of H_2O_2 at pH 9 and 11. Additionally, the inset Fig. 4b also proved that the highest yield of H_2O_2 was obtained at pH 7 with the highest current efficiency and the lowest energy consumption.

Fig. 4c shows the repeated experiments operated over 10 consecutive batches using the same modified cathode under the same conditions. After 10 cycles, the average rate of H_2O_2 generation slightly fluctuated around $7.2 \text{ mg h}^{-1} \text{ cm}^{-2}$, and all of the EEC were around 9.7 kWh kg^{-1} , indicating that the modified graphite felt cathode with EEGr was pretty stable and reusable for the production of H_2O_2 with a low energy consumption.

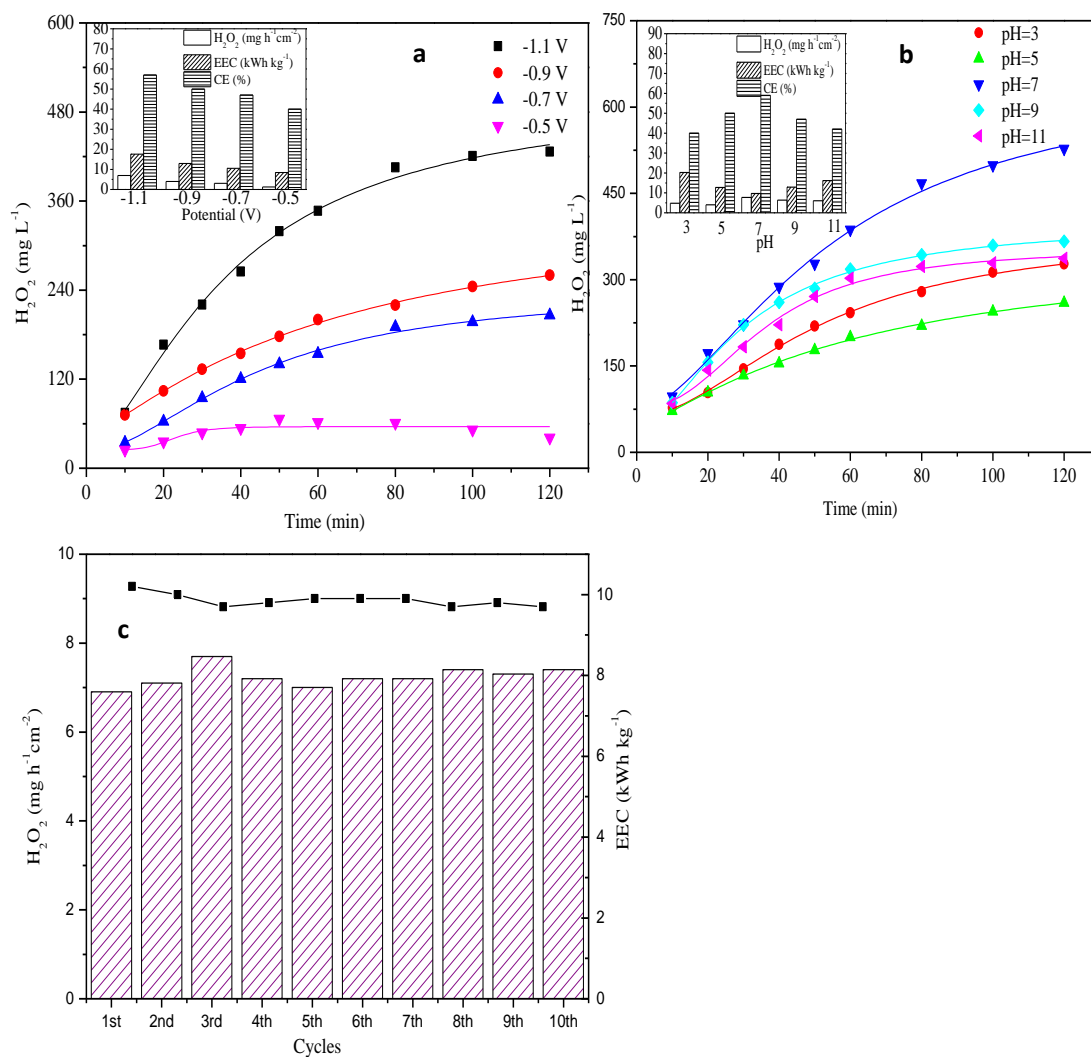


Fig.4 The performance of H₂O₂ generation with different potentials (a) and pH (b); Stability of modified cathode with EEGr-20 over 10 cycles of the rate of H₂O₂ generation and EEC (c).

Conditions: V=100 mL, pH=7, Potential: -0.9 V.

The performances (H₂O₂ production rate, EEC and CE) of the modified graphite felt cathodes in this study were compared with literature that using graphene, or the most common graphite felt and GDE as the cathode (Table 2). Compared with all the

reported cathode using graphene or graphene coating/doping, the H₂O₂ production rate in the present work was the highest, though some EEC and EC data were not available. For example, Xu et al. used graphene doped GDE for the degradation of brilliant blue with a H₂O₂ generation rate of 1.03 mg h⁻¹ cm⁻², and Mousset et al. reported that 0.0048, 0.0072 and 0.64 mg h⁻¹ cm⁻² were obtained with graphene coated on quartz, graphene sheet, and 3D graphene foam cathode. In the present work, even at low bias potential of -0.5 V, the H₂O₂ generation rate could reach 1.3 mg h⁻¹ cm⁻².

Compared with the modified cathodes using graphite felt as the base, the modification with graphene in the present work also possessed the best performance. For example, H₂O₂ generation rate of 0.44 and 1.4 mg h⁻¹ cm⁻² was obtained with the modification of carbon-PTFE and anodization, respectively^[37, 38]. In our previous work, the H₂O₂ generation rate on the graphite felt modified with carbon black increased to 2.2 mg h⁻¹ cm⁻², but the energy consumption (7.5 kWh kg⁻¹) was much higher than that in the present work (4.9 kWh kg⁻¹).

Generally, GDE is regarded as one of the best type of cathode for H₂O₂ production, which is also verified in Table 2, in which the H₂O₂ generation rate advantage over graphite felt based electrodes. However, this high H₂O₂ generation rates are usually accompanied by high EEC. For example, Reis et al. obtained a generation rate of 11 mg h⁻¹ cm⁻² H₂O₂ with a high EEC of 22.1 kWh kg⁻¹ due to the high potential of -1.75 V. Therefore, if taken account for the same EEC, this result was still worse than the result the present work (7.7 mg h⁻¹ cm⁻² H₂O₂ generation rate with an EEC of 9.7 kWh kg⁻¹).

In summary, the results proved that modified graphite felt cathode with EEGr in this study was outstanding for the ultrahigh generation rate of H₂O₂ with relatively low EEC at the same time, which would be more promising for practical application.

2.3.3 Possible mechanism for the high yield of H₂O₂ production

To discover why this modified cathode has a very high yield of hydrogen peroxide production, many characterizations were carried out. Fig. 5a shows the

Chapter 2 Ultrahigh yield of hydrogen peroxide on graphite felt cathode modified with electrochemically exfoliated graphene

nitrogen adsorption isotherms of EEGr-20 and unmodified graphite felt cathode.

Cathode material	Experimental conditions	H ₂ O ₂ generation rate (mg h ⁻¹ cm ⁻²)	EEC (kWh kg ⁻¹)	CE (%)	Reference
Graphite felt modified	Cathode area 3.5 cm ² , V 100 mL, pH 3, O ₂ flow rate 0.13 L min ⁻¹	1.4	-	35-65	[38]
Graphite felt modified	Cathode area 10 cm ² , V 130 mL, pH 6.4, air flow rate 0.4 L min ⁻¹	0.44	-	87	[37]
Graphite felt modified	Cathode area 20 cm ² , V 100 mL, pH 7	2.2	7.5	68-98	[6]
GDE	Cathode area 20 cm ² , V 400 mL, potential – 1.0 V, O ₂ 0.02 MPa	4.6	6	-	[39]
GDE	Cathode area 20 cm ² , V 200 mL, potential – 1.75 V, pH 1, air flow rate 5 L min ⁻¹	11	22.1	-	[35]
GDE	Cathode area 14 cm ² , V 200 mL, pH 7, air flow rate 0.5 L min ⁻¹	12.16	15.9	51-88	[40]
Hierarchically Porous Carbon	Cathode area 10 cm ² , pH 6, bias potential – 0.4 V	/	/	70-90.7	[33]
Graphite-Graphene	Cathode area 12 cm ² , V 200 mL, pH 3, O ₂ flow rate 0.33 L min ⁻¹	1.03	6.7	42-68	[2]
Graphene sheet	Cathode area 20 cm ² , V 150 mL, pH 3, bias potential -0.60 V	0.0072	/	/	[5]
3D Graphene foam	Cathode area 20 cm ² , V 150 mL, pH 3, bias potential -0.61 V	0.64	/	/	
Carbon cloth-Gr (m _{Gr} : 0.27 mg cm ⁻²)	Cathode area 24 cm ² , V 80 mL, pH 3, air flow rate 0.2 L min ⁻¹	0.225	/	/	[6]
Monolayer graphene	V 150 mL, pH 3, bias potential -0.58 V	0.0048	/	/	[18]
Graphite felt-EEGr (m _{EEGr} : 11.2 mg cm ⁻²)	Cathode area 5 cm ² , V 100 mL, pH 7, bias potential -0.9 V	7.7	9.7	42-92	

Table 2 Performance comparison with literatures

The BET surface area and pore volume of unmodified graphite felt were $3.92 \text{ m}^2 \text{ g}^{-1}$ and $0.0026 \text{ cm}^3 \text{ g}^{-1}$, while $9.83 \text{ m}^2 \text{ g}^{-1}$ and $0.029 \text{ cm}^3 \text{ g}^{-1}$ for EEGr-20 cathode. The results suggested that EEGr-20 cathode reached about 2.5 times and 11.2 times of BET and pore volume of the unmodified graphite felt cathode, respectively. Such significant improvement would be of great advantage to enhance the yield of H_2O_2 .

The conductivity of EEGr-20 and unmodified graphite felt electrodes can be confirmed by EIS. Fig. 5b shows that each Nyquist plot includes a semicircle part and a liner part. The semicircle is an indication of the charge transfer resistance during the electrochemical reaction and the line can be attributed to the diffusion controlled Warburg impedance^[41]. The results showed that EIS of unmodified graphite felt electrode has a larger semicircle and tilted vertical line in low frequency region. By contrast, the EEGr-20 electrode consists of a slightly depressed semicircle in high frequency and more vertical line in the range of low frequency, indicating that EEGr-20 electrode has lower charge transfer resistance and faster ion diffusion compared with unmodified graphite felt electrode. Thus it can be concluded that the EEGr has contributed to the high electrochemical performance of EEGr-20 electrode.

Fig. 5c shows CV of the three different cathodes (EEGr-0, EEGr-20 and unmodified graphite felt cathode), confirming EEGr-20 had the highest peak current density. It was observed that EEGr-20 had a strong reduction peak at -0.4 V vs SCE, proving a fast reduction rate for H_2O_2 production on the cathode^[32].

RDE was further used to investigate the ORR activity of the modified cathode, as shown in Fig. 5d and Fig. 5e, the current density increased with rotation rate because of the shortened diffusion layer^[42], which was consistent with literature.²⁷ The curves of steady-state diffusion plateau currents analyzed through Koutecky-Levich plots (inset in Fig. 5d and Fig. 5e) proved the electron number during the electrochemical processes, which was 2.25 (EEGr-0) and 2.43 (EEGr-20), showing both processes with the two electrodes were two-electron ORR processes. Therefore, EEGr introduction simply accelerated the rate of the electron transfer rather than changing the ORR mechanism,

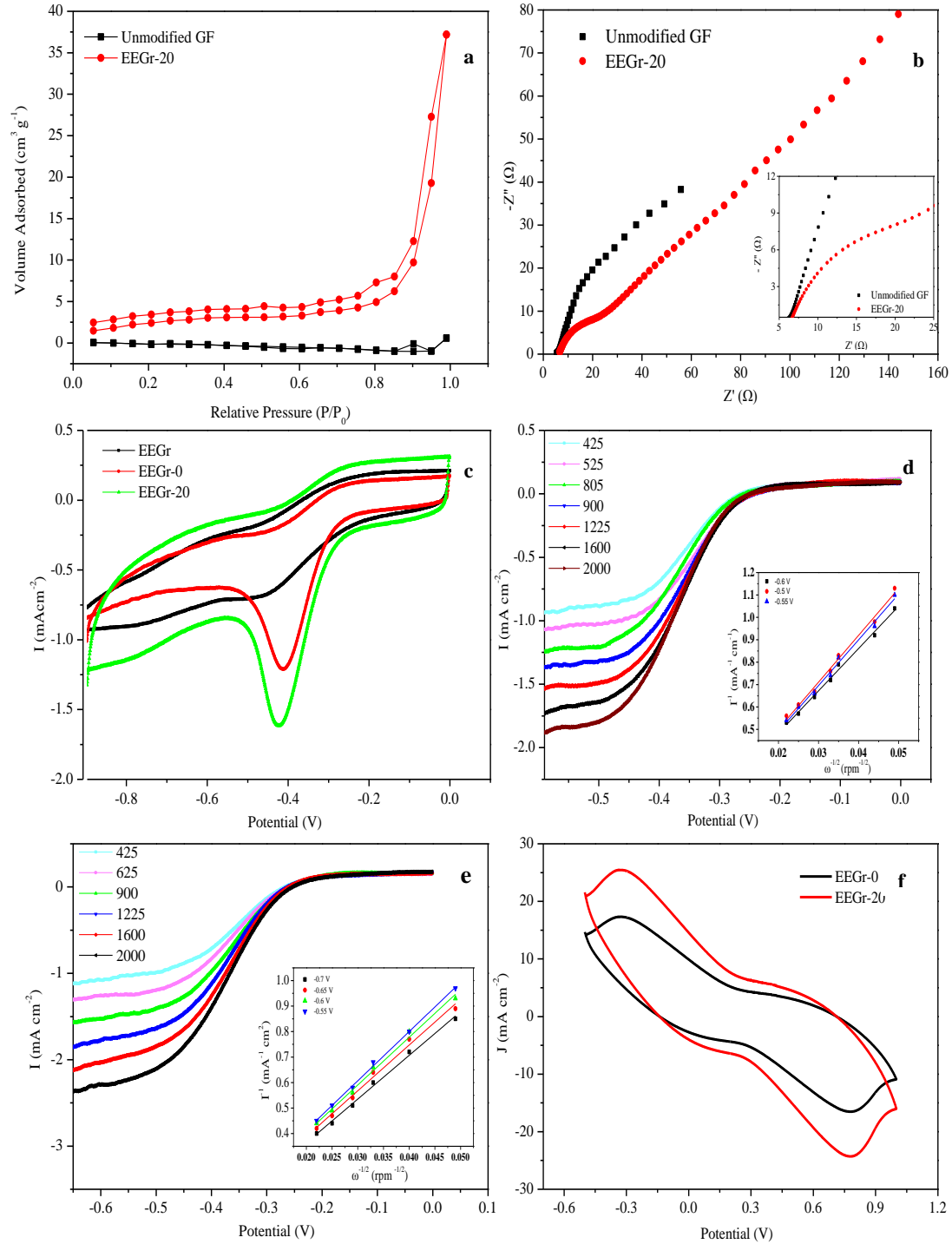
which was consistent with the results of H_2O_2 production in Fig. 3a and Fig.3b.

Additionally, CV of the modified graphite felts were operated in solution of $[\text{Fe}(\text{CN})_6]^{3-}/[\text{Fe}(\text{CN})_6]^{4-}$ (Fig. 5f), and a 1.5-fold increase of the peak current was observed on EEGr-20, proving that the introduction of EEGr could improve the active surface of the modified electrode. According to eq. 7, the electroactive surfaces were calculated to be 171 cm^2 (EEGr-20) and 116 cm^2 (EEGr-0). The 1.5-fold improvement of the surface area should lead to a higher rate of electrochemical reactions on the cathode, which was consistent with the results in Fig. 5c.

The contact angles were commonly used to measure the hydrophilicity of carbon materials. Hydrophilicity is a critical feature for H_2O_2 generation, generally, the higher hydrophilicity, the faster diffusion of O_2 , and thus result in a higher H_2O_2 generation.²⁸ From Fig. 5g to Fig. 5i, the contact angles of three different cathodes were presented, which were 123° (unmodified graphite felt), 112° (modified graphite felt with EEGr-0) and 100° (modified graphite felt with EEGr-20), respectively. It can be seen that the hydrophilicity of modified cathode with EEGr-20 was highest, providing helpfulness to O_2 diffusion and high yield of H_2O_2 production.

Based on the characterizations above, a possible mechanism for this ultrahigh production of hydrogen peroxide is suggested. Fig. 6 shows the schematic diagram of the ORR on the modified graphite felts with/without EEGr. The introduction of EEGr on the cathode not only accelerated the rates of electrons transfer without changing the mechanism of ORR, but also increased the cathode surface hydrophilicity to promote oxygen diffusion. What's more, the electroactive surface of cathode was also improved, which increased active site on the cathode for ORR. These factors contributed to a higher H_2O_2 production with a lower EEC.

Chapter 2 Ultrahigh yield of hydrogen peroxide on graphite felt cathode modified with electrochemically exfoliated graphene



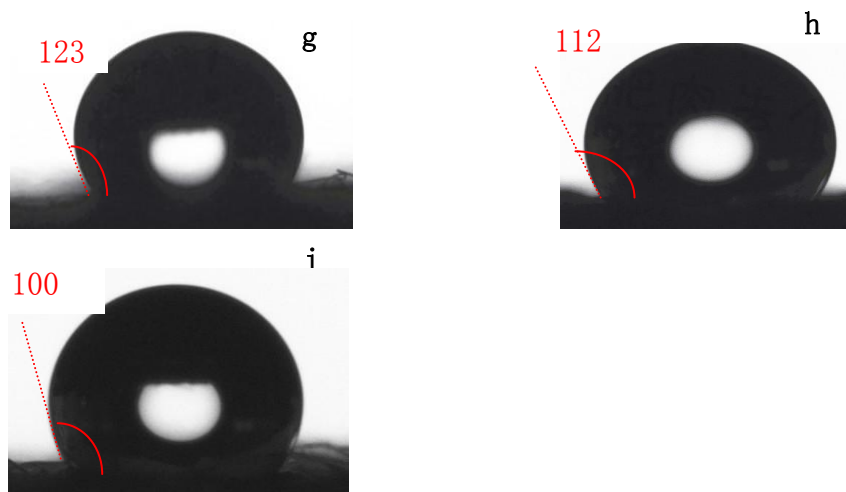


Fig.5 N_2 adsorption/desorption isotherms of EEGr-20 and unmodified graphite felt electrodes (a); Nyquist plot of EEGr-20 and unmodified graphite felt electrodes (b); Cyclic voltammograms of three different modified cathodes (modified graphite felt with EEGr, EEGr-0, EEGr-20) (c); The Linear sweep voltammetry of modified electrode with EEGr-0 (d) and EEGr-20 (e) in O_2 saturated Na_2SO_4 solution at a scan rate of 50 mV s^{-1} with RDE. Inset: K-L plots at different potentials; electrocatalytic activity towards Fe(III)/Fe(II) redox couple detected with CV techniques (f); Contact angles of unmodified graphite felt (g), modified graphite felt with EEGr-0 (h) and with EEGr-20 (i).

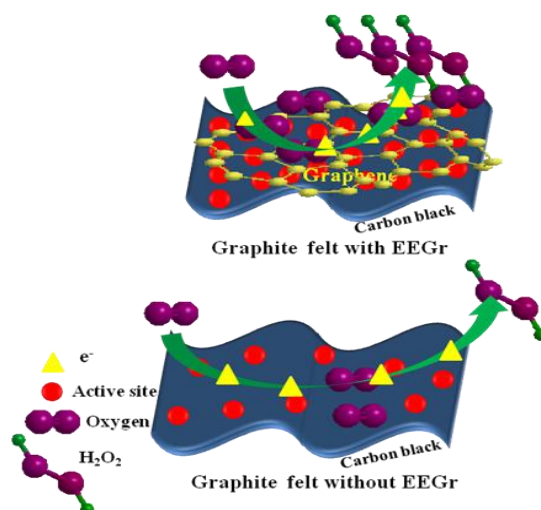


Fig. 6 The schematic diagram of the ORR process.

2.3.4 The performance of pollutants degradation

In order to evaluate the effectiveness of the modified cathode with EEGr-20 for electro-Fenton, the degradation of a series of model organic pollutants including orange II, methylene blue, sulfadiazine and phenol were conducted. As shown in Fig. 7, almost all of the pollutants could be completely removed within 1 h, and the removal efficiencies on EEGr-20 were much better than that on EEGr-0. Their difference on TOC removal was more significant (insert Fig. 7), for example, the TOC removal efficiency of sulfadiazine was about 100% on EEGr-20, while only about 69% for EEGr-0. Table 3 lists the comparison of pollutant and TOC removal efficiency, as well as the pseudo-first order kinetic constant (k). The results proved that about 1.95-2.47 fold of the k value were obtained with EEGr-20 compared with the ones with EEGr-0. This phenomenon was not surprised since it was consistent with the results of H₂O₂ production, proving that the modified cathode with EEGr-20 was potent for organic wastewater treatment by EF.

Table 3 Degradation of pollutants with different cathodes.

Pollutants	Cathode	Removal efficiency (%)	TOC (%)	k (min ⁻¹)	R ²
Orange II	EEGr-20	100	79	0.52	0.98
	EEGr-0	89.8	70	0.22	0.96
Methylene blue	EEGr-20	98.2	52	0.37	0.96
	EEGr-0	88	24	0.19	0.94
Sulfadiazine	EEGr-20	100	100	0.62	0.94
	EEGr-0	87	69	0.27	0.9
Phenol	EEGr-20	95	46	0.37	0.95
	EEGr-0	82	27	0.15	0.90

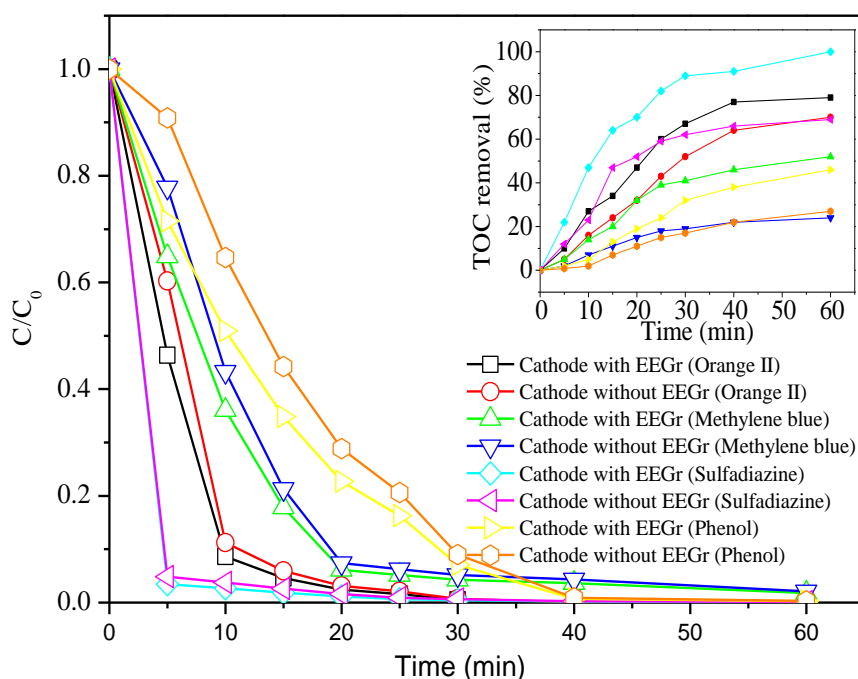


Fig. 7 The degradation of orange II, methylene blue, sulfadiazine and phenol. Conditions: Pt anode; $V=100$ mL; $\text{pH}=3$; $[\text{Fe}^{2+}]=0.4$ mM; Na_2SO_4 : 50 mM; Potential: -0.9 V.

2.4 Conclusions

A novel modified graphite felt cathode with graphene by electrochemical exfoliation method was developed, which presented an ultrahigh yield of H_2O_2 production. The EEGr was proved to be 3-4 layers with low level defects. Optimized ratio of EEGr and loading on the modified graphite felts were explored, and EEGr-20 with a loading of 11.2 mg cm^{-2} was the best for H_2O_2 production. By optimizing cathode potential and pH, a significant improvement of H_2O_2 yield of $7.7 \text{ mg h}^{-1} \text{ cm}^{-2}$ was obtained at pH 7 and -0.9 V potential. In addition, this performance kept stable after 10 cycles reuse. Possible mechanism for this high performance was suggested. Finally, the model pollutants degradation confirmed the great potential practical application for organic wastewater treatment by electro-Fenton.

Acknowledgments

This work was financially supported by National Key Research and Development Program (2016YFC0400706), Key Project of Natural Science Foundation of Tianjin (no. 16JCZDJC39300), Natural Science Foundation of China (no. 21273120 and 51178225), China National Water Project (no. 2015ZX07203-11), and Fundamental Research Funds for the Central Universities.

References

- [1] Campos-Martin J M, Blanco-Brieva G, Fierro J L, et al. Hydrogen peroxide synthesis: an outlook beyond the anthraquinone process[J]. *Angewandte Chemie International Edition*, 2006, 45: 6962-6984.
- [2] Biasi P, Menegazzo F, Canu P, et al. Role of a functionalized polymer (K2621) and an inorganic material (sulphated zirconia) as supports in hydrogen peroxide direct synthesis in a continuous reactor[J]. *Industrial & Engineering Chemistry Research*, 2013, 52: 15472-15480.
- [3] Huerta I, Biasi P, Garc ía-Serna J, et al. Effect of low hydrogen to palladium molar ratios in the direct synthesis of H₂O₂ in water in a trickle bed reactor[J]. *Catalysis Today*, 2015, 248: 91-100.
- [4] Johnke D, De Graaf S, Bathgate R, et al. Quercetin reduces the in vitro production of H₂O₂ during chilled storage of rabbit spermatozoa[J]. *Animal reproduction science*, 2014, 151: 208-219.
- [5] Zhao Z, Sun Y, Dong F, et al. Graphitic carbon nitride based nanocomposites: a review[J]. *Nanoscale*, 2015, 7: 15-37.
- [6] Pimentel M, Oturan N, Dezotti M, et al. Phenol degradation by advanced electrochemical oxidation process electro-Fenton using a carbon felt cathode[J]. *Applied Catalysis B: Environmental*, 2008, 83: 140-149.
- [7] zcan A, Şahin Y, Koparal A S, et al. Degradation of picloram by the electro-Fenton process[J]. *Journal of hazardous materials*, 2008, 153: 718-727.
- [8] Panizza M, Oturan M A, et al. Degradation of Alizarin Red by electro-Fenton process using a graphite-felt cathode[J]. *Electrochimica Acta*, 2011, 56: 7084-7087.
- [9] Liu J, Sun X, Song P, et al. High-Performance Oxygen Reduction Electrocatalysts based on Cheap Carbon Black, Nitrogen, and Trace Iron[J]. *Advanced materials*, 2013, 25: 6879-6883.
- [10] Thiam A, Zhou M, Brillas E, et al. Two-step mineralization of Tartrazine solutions: study of parameters and by-products during the coupling of electrocoagulation with electrochemical advanced oxidation processes[J]. *Applied Catalysis B: Environmental*, 2014, 150: 116-125.
- [11] Liu T, Wang K, Song S, et al. New electro-Fenton gas diffusion cathode based on nitrogen-doped graphene@ carbon nanotube composite materials[J]. *Electrochimica Acta*, 2016, 194:

228-238.

- [12] Carneiro J F, Paulo M J, Sijaj M, et al. Nb₂O₅ nanoparticles supported on reduced graphene oxide sheets as electrocatalyst for the H₂O₂ electrogeneration[J]. *Journal of catalysis*, 2015, 332: 51-61.
- [13] Yu F, Zhou M, Yu X, et al. Cost-effective electro-Fenton using modified graphite felt that dramatically enhanced on H₂O₂ electro-generation without external aeration[J]. *Electrochimica Acta*, 2015, 163: 182-189.
- [14] Chen X, Chen B, et al. Macroscopic and spectroscopic investigations of the adsorption of nitroaromatic compounds on graphene oxide, reduced graphene oxide, and graphene nanosheets[J]. *Environmental science & technology*, 2015, 49: 6181-6189.
- [15] Domínguez C, Perez-Alonso F, Salam M A, et al. Effect of the N content of Fe/N/graphene catalysts for the oxygen reduction reaction in alkaline media[J]. *Journal of Materials Chemistry A*, 2015, 3: 24487-24494.
- [16] Liu L, Liao L, Meng Q, et al. High performance graphene composite microsphere electrodes for capacitive deionisation[J]. *Carbon*, 2015, 90: 75-84.
- [17] Le T X H, Bechelany M, Champavert J, et al. A highly active based graphene cathode for the electro-Fenton reaction[J]. *RSC Advances*, 2015, 5: 42536-42539.
- [18] Mousset E, Wang Z, Hammaker J, et al. Physico-chemical properties of pristine graphene and its performance as electrode material for electro-Fenton treatment of wastewater[J]. *Electrochimica Acta*, 2016, 214: 217-230.
- [19] Chen C Y, Tang C, Wang H F, et al. Oxygen Reduction Reaction on Graphene in an Electro-Fenton System: In Situ Generation of H₂O₂ for the Oxidation of Organic Compounds[J]. *ChemSusChem*, 2016, 9: 1194-1199.
- [20] Leroux Y R, Bergamini J-F, Ababou S, et al. Synthesis of functionalized few-layer graphene through fast electrochemical expansion of graphite[J]. *Journal of Electroanalytical Chemistry*, 2015, 753: 42-46.
- [21] Lopes J H, Ye S, Gostick J T, et al. Electrocatalytic oxygen reduction performance of silver nanoparticle decorated electrochemically exfoliated graphene[J]. *Langmuir*, 2015, 31: 9718-9727.
- [22] Mousset E, Ko Z T, Syafiq M, et al. Electrocatalytic activity enhancement of a graphene ink-coated carbon cloth cathode for oxidative treatment[J]. *Electrochimica Acta*, 2016, 222: 1628-1641.
- [23] Qiang Z, Chang J-H, Huang C-P, et al. Electrochemical generation of hydrogen peroxide from dissolved oxygen in acidic solutions[J]. *Water Research*, 2002, 36: 85-94.
- [24] Yang J-F, Zhou S-B, Xiao A-G, et al. Chemical oxidation of sulfadiazine by the Fenton process: kinetics, pathways, toxicity evaluation[J]. *Journal of Environmental Science and Health, Part B*, 2014, 49: 909-916.
- [25] Yang W, Han H, Zhou M, et al. Simultaneous electricity generation and tetracycline removal in continuous flow electrosorption driven by microbial fuel cells[J]. *RSC Advances*, 2015, 5:

49513-49520.

[26] Duan W H, Gong K, Wang Q, et al. Controlling the formation of wrinkles in a single layer graphene sheet subjected to in-plane shear[J]. *Carbon*, 2011, 49: 3107-3112.

[27] Chen C-H, Yang S-W, Chuang M-C, et al. Towards the continuous production of high crystallinity graphene via electrochemical exfoliation with molecular in situ encapsulation[J]. *Nanoscale*, 2015, 7: 15362-15373.

[28] Mahato N, Parveen N, Cho M H, et al. Graphene nanodiscs from electrochemical assisted micromechanical exfoliation of graphite: Morphology and supramolecular behavior[J]. *Materials Express*, 2015, 5: 471-479.

[29] Guo J, Zhang T, Hu C, et al. A three-dimensional nitrogen-doped graphene structure: a highly efficient carrier of enzymes for biosensors[J]. *Nanoscale*, 2015, 7: 1290-1295.

[30] Munuera J, Paredes J, Villar-Rodil S, et al. High quality, low oxygen content and biocompatible graphene nanosheets obtained by anodic exfoliation of different graphite types[J]. *Carbon*, 2015, 94: 729-739.

[31] Yang S, Brüller S, Wu Z-S, et al. Organic radical-assisted electrochemical exfoliation for the scalable production of high-quality graphene[J]. *Journal of the American Chemical Society*, 2015, 137: 13927-13932.

[32] Xia G, Lu Y, Xu H, et al. Electrogeneration of hydrogen peroxide for electro-Fenton via oxygen reduction using polyacrylonitrile-based carbon fiber brush cathode[J]. *Electrochimica Acta*, 2015, 158: 390-396.

[33] Liu Y, Chen S, Quan X, et al. Efficient mineralization of perfluorooctanoate by electro-Fenton with H₂O₂ electro-generated on hierarchically porous carbon[J]. *Environmental science & technology*, 2015, 49: 13528-13533.

[34] Kwon B G, Lee D S, Kang N, et al. Characteristics of p-chlorophenol oxidation by Fenton's reagent[J]. *Water Research*, 1999, 33: 2110-2118.

[35] Panizza M, Cerisola G, et al. Electro-Fenton degradation of synthetic dyes[J]. *Water research*, 2009, 43: 339-344.

[36] Wang C-T, Hu J-L, Chou W-L, et al. Removal of color from real dyeing wastewater by Electro-Fenton technology using a three-dimensional graphite cathode[J]. *Journal of hazardous materials*, 2008, 152: 601-606.

[37] Zhou L, Zhou M, Zhang C, et al. Electro-Fenton degradation of p-nitrophenol using the anodized graphite felts[J]. *Chemical engineering journal*, 2013, 233: 185-192.

[38] Da Pozzo A, Di Palma L, Merli C, et al. An experimental comparison of a graphite electrode and a gas diffusion electrode for the cathodic production of hydrogen peroxide[J]. *Journal of Applied Electrochemistry*, 2005, 35: 413-419.

[39] Reis R M,

Beati A A, Rocha R S, et al. Use of gas diffusion electrode for the in situ generation of hydrogen peroxide in an electrochemical flow-by reactor[J]. *Industrial & Engineering Chemistry Research*, 2011, 51: 649-654.

[40] Yu X, Zhou M, Ren G, et al. A novel dual gas diffusion electrodes system for efficient hydrogen peroxide generation used in electro-Fenton[J]. *Chemical Engineering Journal*, 2015, 263: 92-100.

[41] Khamlich S, Khamliche T, Dhlamini M, et al. Rapid microwave-assisted growth of silver nanoparticles on 3D graphene networks for supercapacitor application[J]. *Journal of colloid and interface science*, 2017, 493: 130-137.

[42] Yang W, Fellingner T-P, Antonietti M, et al. Efficient metal-free oxygen reduction in alkaline medium on high-surface-area mesoporous nitrogen-doped carbons made from ionic liquids and nucleobases[J]. *Journal of the American Chemical Society*, 2010, 133: 206-209.

Chapter 3: Electrocatalytic destruction of pharmaceutical imatinib by electro-Fenton process with graphene-based cathode

Abstract

Electro-Fenton (EF) process is one of the most popular electrochemical advanced oxidation processes based on in-situ generation of H₂O₂ and continuous electrochemical regeneration of catalyst (generally Fe²⁺). The cathode material is a key factor for the high yield of H₂O₂ production which governs process efficiency. Therefore, in this study, the oxidative degradation and mineralization of imatinib (IMA), an antineoplastic drug for cancer treatment, were investigated by EF process using a graphene modified carbon felt cathode comparatively with raw carbon felt (CF) cathode. This is for the first time that the removal of IMA from water was investigated by EF process. Moreover, the absolute rate constant ($4.56 \times 10^9 \text{ M}^{-1} \text{ s}^{-1}$) for IMA oxidation by $\cdot\text{OH}$ was also determined for the first time. The effects of operating parameters including catalyst concentration and applied current on the process efficiency were considered. Complete mineralization of 34.5 mg L⁻¹ IMA was obtained at 8 h treatment with graphene modified CF cathode while only 75% TOC removal was attained with raw CF cathode under same operating conditions. Also, the formation and evolution of the carboxylic acids during oxidation process provided better performances with graphene-based CF cathode. N atoms presented in IMA were finally released to the solution as NH₄⁺ and NO₃⁻ ions. Besides, toxicity assessment with Microtox[®] method proved the formation of intermediates more toxic than IMA during mineralization process. However, solution toxicity was totally removed at the end of treatment with graphene-based CF cathode.

Keywords: Graphene modified carbon felt, Electro-Fenton, Imatinib, Electrocatalysis, Mineralization

3.1 Introduction

The presence and occurrence of pharmaceuticals in the environment has garnered increasing attention during the last decades. This pollution is sourced mainly by hospital effluents, industrial and domestic wastewaters, leading to long-term adverse impacts on human health and ecosystems^[1-3]. Conventional wastewater treatment plants are generally not capable of removing these emerging pollutants due to their high physical/chemical stability and non-biodegradable character, resulting in their discharge into the aquatic system^[4-6]. Therefore, pharmaceuticals have been frequently detected in groundwater, surface water and even drinking water^[7, 8]. Although the pharmaceuticals residues in the environment are at low concentration, they are believed to bring many negative impacts on water bodies and even the development of pathogen resistance and endocrine disruption^[9].

In contrast to the conventional wastewater treatment methods, electrochemical advanced oxidation processes (EAOPs) have been proved to be an alternative for efficient removal of persistent organic pollutants from wastewater^[10-13]. Among the most common EAOPs (anodic oxidation, photoelectrocatalysis and electro-Fenton)^[14-16], electro-Fenton (EF) process constitutes one of the most attractive technologies for effective destruction of organic contaminants [11, 17-18] in which H₂O₂ is in-situ generated via oxygen reduction reaction (ORR) on an appropriate cathode (Eq. (1)). H₂O₂ then reacts with externally added catalytic Fe²⁺ to produce hydroxyl radicals ([•]OH) according to the well-known Fenton's reaction (Eq. (2)). Fe³⁺ will be transformed to Fe²⁺ according to Eq. (3)^[17-20], which make EF electrocatalytic since Fe²⁺ is continuously regenerated.



Thus $\cdot\text{OH}$ is produced, which is a strong oxidizing agent ($E_{\cdot\text{OH}/\text{H}_2\text{O}} = 2.80 \text{ V/SHE}$) and reacts non-selectively with organic compounds leading to their mineralization^[17, 21].

The effectiveness of EF process depends on several parameters such as solution pH^[22, 23], applied current^[24], catalyst concentration^[1, 25], electrode materials^[26-28], etc. According to Eq. (1), cathode materials also play a key role in the ORR process for high yield of H_2O_2 whose concentration constitutes kinetically limiting parameter. Mostly, carbonaceous materials such as carbon nanotube^[29], activated carbon fiber^[30, 31], carbon felt (CF)^[32, 33], graphene^[34, 35] are regarded as the suitable cathodes. Especially, CF has been chosen as one of the most used cathodes for H_2O_2 generation because of its high specific surface and low cost.

Many attempts have been made to improve the yield of H_2O_2 on the cathode. Graphene, an allotrope of carbon, has many excellent properties such as high surface area, great electrical conductivity and high strength. In recent years, it has drawn much attention as a material capable of improving performances of EF process in many studies^[34, 36-38]. However, most of the studies were operated with the graphene bought or made by chemical oxidation processes, which are expensive and dangerous^[39, 40]. Given to the high cost and complicated process of preparation, our previous study has demonstrated a fast and effective method to produce graphene. Especially, CF modified with this electrochemically exfoliated graphene (EEGr) was proved capable of providing very high yield of H_2O_2 ($7.7 \text{ mg h}^{-1} \text{ cm}^{-2}$) compared with other cathodes^[41].

On the other hand, the pharmaceutical imatinib (IMA) constitutes an interesting target pollutant to be studied since it is one of largely used antineoplastic drugs for cancer treatments, with inhibition of cell growth or killing cancer cells via the interactions with DNA function and cell signaling^[42-45]. Though this anti-cancer drug are usually at trace concentration (ng L^{-1}), it drew our special attention to be selected for this study.

In this context, we used the CF modified with EEGr as cathode (EEGr-CF) for the electrochemical oxidation of IMA in EF process, and provided a thorough assessment of

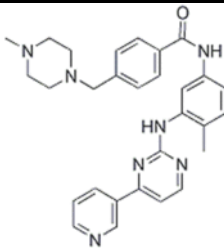
EEGr-CF for the degradation and mineralization of IMA by establishing the key operating parameters including concentration of Fe^{2+} and applied current. At the same time, a series of comparative researches with raw CF were presented. Additionally, formation and evolution of short-chain carboxylic acids as ultimate organic end-products before mineralization stage^[1] and inorganic ions as mineral end-products formed during EF process were investigated. Finally, the change in solution toxicity during EF treatment was assessed using Microtox[®] method.

3.2 Materials and methods

3.2.1 Chemicals

Analytical grade IMA ($\text{C}_{29}\text{H}_{31}\text{N}_7\text{O}$, CAS n^o: 152459-95-5, MW: 493.6 g mol⁻¹) with purity of 99.9% was purchased from Alfa and was used as target pollutant in the experiments without further purification. Anhydrous sodium sulfate (Na_2SO_4) was used as supporting electrolyte and iron (II) sulphate heptahydrate (99.5%) as source of the catalyst (Fe^{2+} ion) in EF experiments. H_2SO_4 (1 M) and NaOH (1M) were used to adjust solution pH. All solutions were prepared with ultrapure water from a Millipore Milli-Q system (Molsheim, France) with resistivity of 18 M Ω cm⁻¹. All experiments were performed in triplicate.

Table 1: Some physico-chemicals properties of IMA.

Chemical formula	Molecular structure	Molecular weight (g mol ⁻¹)	Solubility (mg L ⁻¹) in water at 20-25°C	CAS n ^o
$\text{C}_{29}\text{H}_{31}\text{N}_7\text{O}$		493.60	37.2	152459-95-5

3.2.2 Electrochemical cell

The experiments were operated in a 150 mL undivided cylindrical glass cell equipped with two electrodes and was stirred by magnetic bar. DSA (dimensionally stable anode) electrode ($3 \times 4 \text{ cm}^2$) was chosen as the anode while cathode was the developed EEGr-CF or the raw CF electrode with the same surface area. Compressed air was bubbled into the cell continuously, at the rate of 1 L min^{-1} to make sure an O_2 saturated solution. 150 mL aqueous solution of IMA (0.07 mM) containing 0.05 M Na_2SO_4 as electrolyte was adjusted to pH 3 and experiments were performed with applied current density ranging from 4.16 to 58.33 mA cm^{-2} . All of the experiments were conducted at room temperature.

3.2.3. Preparation and characterization of EEGr-CF cathode

The EEGr-CF cathode ($3 \times 4 \text{ cm}^2$) was prepared using raw CF as the base cathode modified with EEGr and carbon black^[41]. The powder was mixed with 0.14 mL PTFE, 3 mL ethanol and deionized water with quick shake for 10 s to form a kind of seriflux, which was homogeneously coated onto the two sides of the raw CF cathode and was annealed for 30 min at 360°C .

3.2.4 Instruments and analytical procedures

The decay kinetics of IMA was monitored by UPLC (Thermo Scientific, USA) equipped with diode array detector and a RP-18 Hypersil column ($1.9 \mu\text{m}$, $100 \text{ mm} \times 2.1 \text{ mm}$). The composition and flow rate of mobile phase were set as follow: water (1% acetic acid)-methanol (1% acetic acid) (70:30, v/v) and flow rate of 0.1 mL min^{-1} . The detector was set at 267 nm. Short-chain carboxylic acids generated during EF treatment of IMA were followed by ion-exclusion HPLC using a HPX-87H ion exclusion column

($\phi 7.8 \text{ mm} \times 300 \text{ mm}$) at 40°C at the wavelength of 220 nm using a L-2400 UV detector. $4 \text{ mM H}_2\text{SO}_4$ solution was chosen as eluent at 0.6 mL min^{-1} flow rate. Inorganic ions released into the solutions were detected using a Dionex ICS-1000 Ion Chromatograph equipped with a Dionex DS6 conductivity detector at 30°C . The concentration of NH_4^+ was measured by Dionex CS12A ($25 \text{ cm} \times 4 \text{ mm}$) cationic column with 1.0 mL min^{-1} mobile phase of $9 \text{ mM H}_2\text{SO}_4$, while the detection of anions (NO_3^- , NO_2^-) was operated with Dionex AS4A-SC ($25 \text{ cm} \times 4 \text{ mm}$) anionic column using the mobile phase composed of $1.8 \text{ mM Na}_2\text{CO}_3$ and 1.7 mM NaHCO_3 solution at flow rate of 2.0 mL min^{-1} .

The changes in solution TOC (total organic carbon) was measured by Shimadzu V_{CSH} TOC analyzer to assess the mineralization rate of IMA solution and determine the mineralization current efficiency (MCE) of the process which was calculated using the following equation (4) [46, 47].

$$MCE(\%) = \frac{nFV_s\Delta(\text{TOC})_{\text{exp}}}{4.32 \times 10^7 mIt} \times 100 \quad (3-4)$$

Where n represents the number of electrons consumed per IMA molecule during mineralization and was taken as 124 according to mineralization reaction given in Eq. (5) assuming that majority of the N contains in IMA was released as NH_4^+ [48], F is the Faraday constant (96485 C mol^{-1}), V_s is the volume of electrolyte solution (L), $\Delta(\text{TOC})_{\text{exp}}$ means the TOC decay at t time, 4.32×10^7 represents a conversion factor to homogenize units ($3600 \text{ s h}^{-1} \times 12000 \text{ mg of C mol}^{-1}$), m is the number of carbon atoms of IMA (29), I is the current applied (A) and t is the electrolysis time (h).



Energy consumption (EC) is another parameter studied to evaluate the performance

of cathode related to the cost effectiveness of the process. This parameter was calculated in the unit of kWh energy per g TOC removal during mineralization experiments and calculated as following [17]:

$$EC = \frac{UIt}{(\Delta TOC)_t V_s} \quad (3-6)$$

where U is the average cell voltage (V), I is the current (A) applied, t is the electrolysis time (h), $\Delta (TOC)_t$ represents the TOC decay at time t and V_s is the solution volume (L).

The absolute (second order) rate constant (k_{IMA}) for oxidation reaction of IMA by $\cdot OH$ was determined using competition kinetics method. The 4-hydroxybenzoic acid (4-HBA) was taken as competitor since the rate constant of the reaction between this compound and $\cdot OH$ is well known ($k_{4-HBA} = 2.19 \times 10^9 \text{ M}^{-1} \text{ s}^{-1}$) [16]. The method consists of the simultaneous degradation of pollutant under study and standard competitor (IMA and 4-HBA, respectively in this study) at equal concentration. The absolute rate constant of oxidative degradation of IMA with $\cdot OH$ was then calculated according to equation (7) [49]. It is noted here that the production of heterogeneous $\cdot OH$ generated on DSA anode is poor compared to $\cdot OH$ generated homogeneously in the bulk solution from Fenton's reaction and was neglected in this discussion.

$$k_{IMA} = k_{4-HBA} \frac{k_{app, IMA}}{k_{app, 4-HBA}} \quad (3-7)$$

Finally, the evolution of acute toxicity of the IMA solution during mineralization

experiments was monitored by Microtox[®] method^[11]. The toxicity was measured as inhibition percentage of bioluminescence of marine bacteria *Vibrio fischeri* after adjusting the pH of samples withdraw during treatment to 7.0-7.5 with 0.01-0.1 mM NaOH solution. Inhibition percentages were measured after 5 and 15 min of exposure to *Vibrio fischeri* bacteria.

3.3 Results and discussion

3.3.1 Effect of Fe²⁺ concentration and current on IMA oxidative degradation kinetics

It is well known that the concentration of catalyst (Fe²⁺) plays an important role in EF process according to Eqs. (2) and (3). The effect of Fe²⁺ concentration on the kinetics decay of IMA was explored. IMA solution (150 mL of 0.07 mM) was treated with raw CF cathode at a constant current density of 16.66 mA cm⁻² with catalyst concentrations of 0.05, 0.1 and 0.2 mM, respectively. In general this concentration depends on the chemical structure of the organic pollutants to be removed and the persistence of the intermediates formed. The results in Fig. 1(a) show that the degradation kinetics of IMA is accelerated with the increasing amount of Fe²⁺ due to the acceleration of Fenton's reaction rate improving ·OH generation via Eq. (2) and thus enhancing the degradation rate of IMA. However, there is not much difference on IMA removal for 0.1 and 0.2 mM catalyst concentration. This fact can be related to the acceleration of the rate of parasitic reaction (Eq. (8)) that have a relatively high reaction rate ($k = 3.2 \times 10^8 \text{ M}^{-1} \text{ s}^{-1}$) become competitive at high Fe²⁺ concentration to waste ·OH and thus diminishing the degradation rate of IMA^[17, 25]. Besides, as shown in the inset of the Fig. 1(a), the apparent rate constants for oxidative degradation of IMA, determined following a pseudo-first order kinetic model, were similar (0.10 and 0.11 min⁻¹) for 0.1 and 0.2 mM Fe²⁺ concentration respectively (Table 2). These findings are

in agreement with previous reports [17, 24]. From the analysis of these results one can notice that the value of 0.1 mM Fe²⁺ was optimal for EF degradation of IMA, and was selected as the catalyst concentration for the following experiments.



On the other hand, the degradation kinetics of organics pollutants in EF process is mainly dominated by the average generation rate of H₂O₂ on the cathode, which governs the rate of Fenton reaction and the production rate of homogeneous $\cdot\text{OH}$ in solution bulk. However, the optimal yield of H₂O₂ depends on the key parameters such as current applied and cathode materials [26, 27]. Therefore, the effect of current on the degradation efficiency of IMA was explored under 0.1 mM Fe²⁺ (as catalyst) with different current densities (4.16, 8.33, 16.66 and 33.33 mA cm⁻²), and the results were depicted in Fig. 1(b). The decay kinetics of IMA was enhanced with enhancement of current density until 16.66 mA cm⁻² due to the production of more H₂O₂ (Eq. (1)) and optimal concentration for catalyst (Fe²⁺) regeneration (Eq. (3)), resulting in a higher yield of homogeneous $\cdot\text{OH}$ in solution via reaction (2). However, the results of IMA decay decreased with the applied current density increasing from 16.66 to 33.33 mA cm⁻², in the same way as the rate constants in inset, diminishing from 0.14 min⁻¹ (16.66 mA cm⁻²) to 0.05 min⁻¹ (33.33 mA cm⁻²). This phenomenon can be explained that some side reactions Eq. (9-10) would be enhanced as the increase of current density, thus leading to the competition with IMA oxidative degradation [26]. Taken higher mineralization efficiency into consideration, the current density of 16.66 mA cm⁻² can be regarded as the optimal value for IMA degradation under the operating conditions selected.

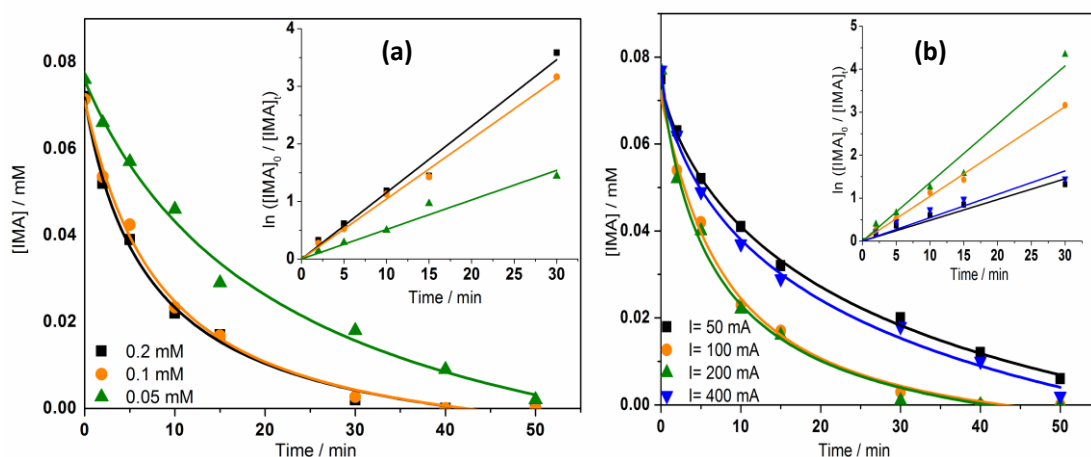


Fig. 1 Optimization of operating parameters for IMA degradation with raw CF cathode in EF process. Effect of catalyst $[\text{Fe}^{2+}]$ concentration at I : 16.66 mA cm^{-2} (a), and effect of current at $0.1 \text{ mM } [\text{Fe}^{2+}]$ (b) on IMA decay kinetics. $[\text{IMA}]$: 0.07 mM (34.5 mg L^{-1}), V : 150 mL , pH 3, $[\text{Na}_2\text{SO}_4]$: 50 mM .

Table 2: Values of the apparent rate constant (k_{app}) for the oxidation of IMA by $\bullet\text{OH}$ generated in EF process

Electrolytic cell	$[\text{Fe}^{2+}]$ (mM)	I (mA)	k_{app} (min^{-1})
DSA/CF	0.05	200	0.05
	0.1	200	0.10
	0.2	200	0.12
	0.1	50	0.05
	0.1	100	0.10
	0.1	200	0.14
	0.1	400	0.05
DSA/EEGr-CF	0.1	200	0.22
	0.2	200	0.23
	0.5	200	0.23

3.3.2 Comparative performance of raw CF and EEGr-CF cathodes in IMA degradation

The kinetics of oxidative degradation of IMA in EF process with raw CF and EEGr modified CF cathodes were comparatively carried out with the applied current density of 16.66 mA cm^{-2} . The results in Fig. 2(a) show that IMA could be completely degraded in both cases within 1 h electrolysis while a better performance was obtained with EEGr-CF cathode. For instance after 15 min electrolysis, IMA was completely

disappeared from the solution with EEGr-CF while only 82% of IMA was oxidized under same conditions with raw CF cathode. As well as the results in inset, the kinetics rate constant obtained with EEGr-CF was more than 2-fold of that with raw CF cathode, indicating that the graphene-based cathode owns much more potential for degradation of organics in water or wastewater.

The significantly high performance of EEGr-CF cathode in IMA degradation can be explained by its higher efficiency in H_2O_2 generation rate (Eq. (1)). As well, the yield of H_2O_2 generation controls the rate of Fenton reaction and consequently the formation rate of homogeneous $\cdot OH$ in the medium [26]. Therefore, the results of H_2O_2 generation on both cathodes were studied as comparison and showed in Fig. 2(b), providing that the yield of H_2O_2 generation could reach 400 mg L^{-1} at 120 min with EEGr-CF cathode, which was almost 4 times higher than that with raw CF cathode under the same operating conditions. What's more, the value of EC with EEGr-CF cathode for H_2O_2 generation was only half of the latter one as shown in the inset of Fig. 2(b), illustrating that graphene-based cathode could enhance the average generation rate of H_2O_2 in EF process. These results are in agreement with the performance of both cathodes for degradation kinetics of IMA depicted in Fig. 2(a).

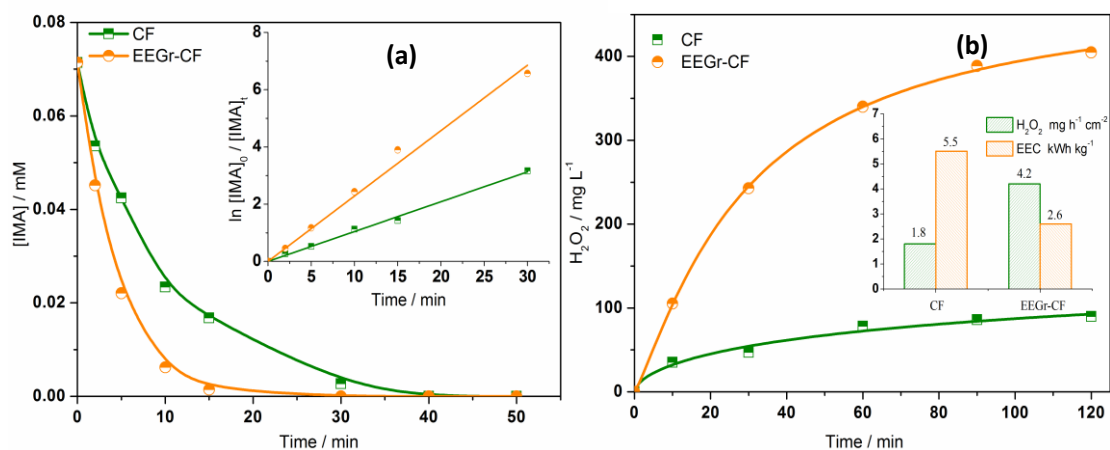


Fig. 2 Comparison of performance of raw CF and EEGr-CF cathodes in IMA degradation (a) and H_2O_2 generation (b). pH 3, 200 mA. [IMA]: 0.07 mM, $[Fe^{2+}]$: 0.1 mM, V: 150 mL, $[Na_2SO_4]$: 50

mM.

Further, the absolute rate constant of IMA degradation by $\cdot\text{OH}$ in EF process with EEGr-CF cathode was determined by using competition kinetics method [16, 50]. This experiment was operated at 5 mA cm^{-2} in order to avoid side reactions under high currents [26]. In this experiment, 4-hydroxybenzoic acid (4-HBA), with a well-known absolute rate constant ($k_{4\text{-HBA}} = 2.19 \times 10^9 \text{ M}^{-1} \text{ s}^{-1}$) [51], was regarded as standard competitor with IMA for reaction with $\cdot\text{OH}$. The concentration of 4-HBA and IMA (0.07 mM each) was followed by HPLC analysis during 30 min of treatment. The results in Fig. 3(a) present that the removal efficiency of 4-HBA and IMA was 45% and 73%, respectively. According to the slope of the curve of Fig. 3(b) and the Eq. (7), the absolute (second order) rate constant for oxidation of IMA by $\cdot\text{OH}$ was calculated to be $4.56 \times 10^9 \text{ M}^{-1} \text{ s}^{-1}$, showing that the degradation rate of IMA with EEGr-CF was quick and in agreement with the results of Fig. 2(a). To the best of our knowledge there is no k_{IMA} value already reported in the literature for comparison.

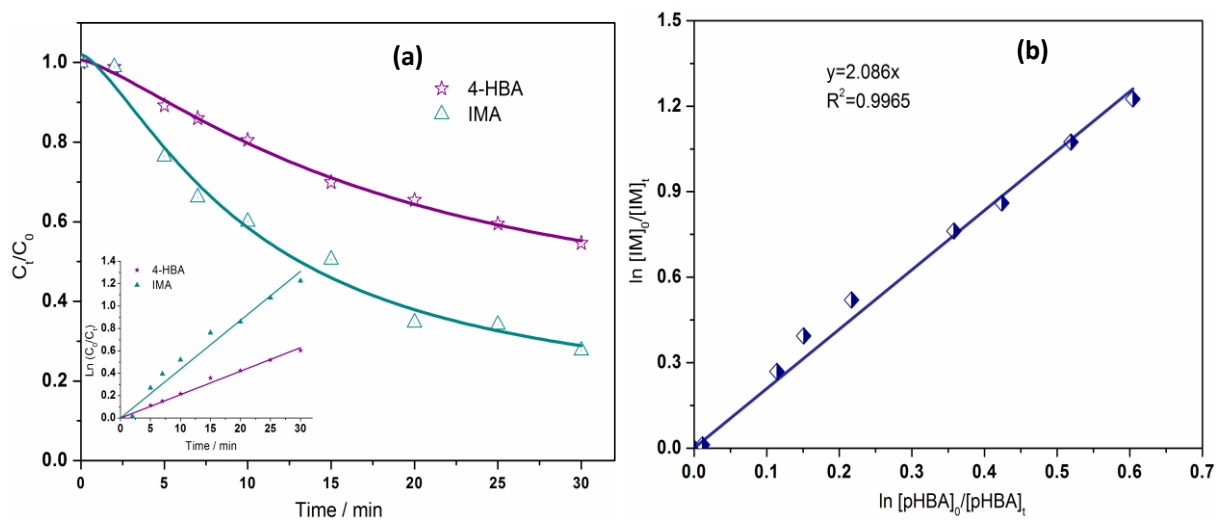


Fig. 3 Determination of absolute rate constant for IMA oxidation (k_{IMA}) by competition kinetics method using EEGr-CF cathode (a); Kinetic analysis for determination of k_{IMA} (b). [IMA]: 0.07 mM, [4-HBA]: 0.07 mM, V: 150 mL, pH: 3, $[\text{Fe}^{2+}]$: 0.1 mM, I: 60 mA, $[\text{Na}_2\text{SO}_4]$: 50 mM.

3.3.3 Comparison of the mineralization efficiency by EF process with raw CF and EEGr-CF cathode

It is well known that degradation of organic pollutants with AOPs can lead to the formation of intermediates even more toxic than the initial contaminants, thus leading to various environmental problems^[49, 52]. To avoid the presence of toxic intermediates in the solution, the treatment is extended until almost complete mineralization.

To clarify the efficiency of raw CF and EEGr-CF cathodes in mineralization of IMA, comparative experiments were performed under the same operating conditions (Fig. 4). In both cases, the mineralization of IMA enhanced with the increasing current densities, up to 16.66 mA cm⁻² with the maximum values of TOC removal. Subsequently, for currents higher than 33.33 mA cm⁻², in contrast, the TOC removal curves had much lower slope than the former one, with poorer mineralization efficiencies at the end of treatments. These phenomena were similar to the results of already published reports^[28]. The tendency of decreasing efficiency of TOC removal is due to the intensification of side reactions given in Eq. (11-12) under high current conditions, which competes with the formation of H₂O₂ generation (Eq. (1)) on the cathode. By comparison, Fig. 4(b) shows that the mineralization efficiency of IMA with EEGr-CF was significantly better than that obtained with raw CF cathode (Fig. 4(a)). The TOC of IMA solution can be almost completely removed under 16.66 mA cm⁻² current density at 480 min with EEGr-CF, whereas only 75% TOC removal could be achieved with raw CF under the same conditions. What's more, the curves in Fig. 4(b) have sharper slope than the ones in Fig. 4(a), especially with the current intensity of 8.33 and 16.66 mA cm⁻², which also illustrates that the decay rate of TOC with EEGr-CF is better than CF electrode.



The results of Fig. 4(c) and 4(d) depict the evolution of MCE for both cathodes. It can be observed that the values of MCE diminished in both cases with the increasing

currents, which can be attributed to the depletion of $\cdot\text{OH}$ consumed by a wasting reaction (Eq. (13)) and energy consumption by H_2 evolution reaction (Eq. (9)) [53, 54]. For comparison, the results highlights that MCE with EEGr-CF cathode was much higher than that of raw CF cathode. For instance, the MCE values for 33.33 and 58.33 mA cm^{-2} with EEGr-CF were two times of that with raw CF cathode, and in both cases, MCE curves increased to a maximum values at the beginning of the electrolysis, suggesting a quick degradation of intermediates by $\cdot\text{OH}$ generated in solution. Afterwards, the gradually decreasing MCE values were due to the formation of some recalcitrant by-products hardly oxidizable such as short chain carboxylic acids [25] and the increase of the amount of organic matters in the solution.

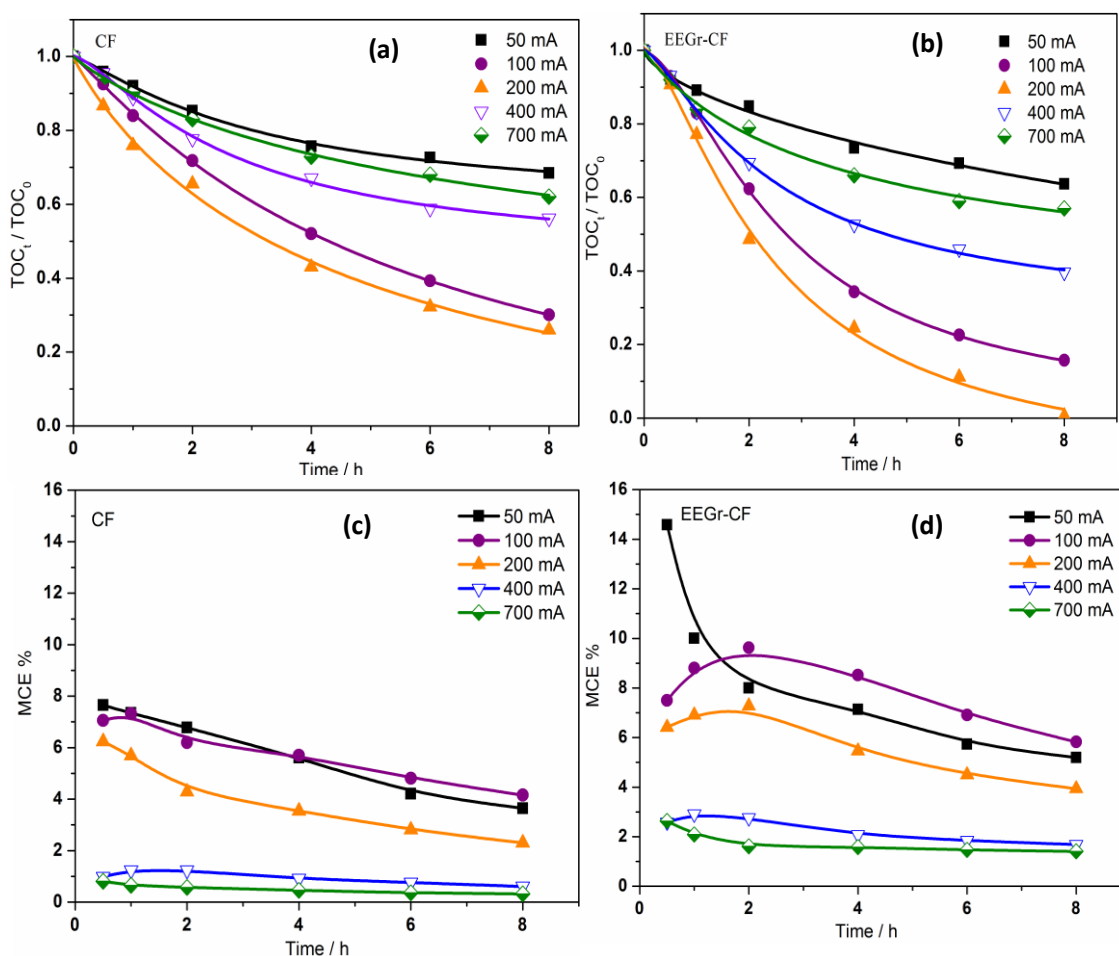


Fig. 4 Effect of current on TOC removal (a, b) and MCE (c, d) during mineralization of 0.07 mM (34.5 mg L⁻¹) IMA solution with raw CF (a, c) and EEGr-CF (b, d) cathodes V: 150 mL, pH: 3, [Fe²⁺]: 0.1 mM, [Na₂SO₄]: 50 mM.

Meanwhile, the value of EC calculated according to Eq. (6) and determined in unit of kWh energy per g TOC removed during EF process, is another important parameter. The results in Fig. 5 present the EC evolution during IMA degradation with different cathodes in this study. Obviously, during the mineralization process, the EC increased significantly with the higher currents along with the electrolysis time. At low current densities (4.16, 8.33 mA cm⁻²), EC values were pretty low (< 1.5 kWh (g TOC)⁻¹), however, they increased significantly for 16.66 and 33.33 mA cm⁻². For instance, the EC values of EF process with raw CF cathode were 8.1, 8.2, 11.0, 13.3 and 16.6 kWh (g TOC)⁻¹ at the electrolysis times of 1, 2, 4, 6 and 8 h, respectively, while they were lower for EEGr-CF cathode (4.3, 5.5, 9.3, 11.5 and 14.3 kWh (g TOC)⁻¹ for same treatment time).

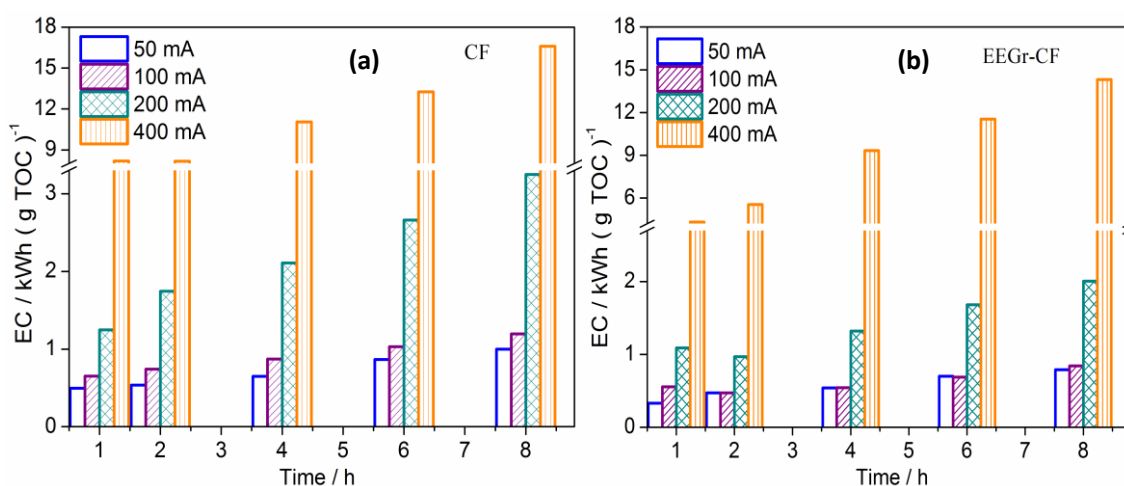


Fig. 5 Effect of applied current on EC evolution during IMA degradation by EF process with raw CF (a) and EEGr-CF (b) cathodes. V: 150 mL, pH: 3, [Fe²⁺]: 0.1 mM, [Na₂SO₄]: 50 mM.

According to the results above, the graphene-based cathode (EEGr-CF) provides a better performance in IMA degradation by EF process, as it is capable of remarkably accelerating the rate of organics mineralization due to the higher yield of H_2O_2 generation and consequently higher ability of producing $\cdot\text{OH}$ contributing thus to the quick destruction of organic pollutants ^[55].

3.3.4 Identification and evolution of carboxylic acids during EF treatment of IMA

During the oxidative degradation of organic pollutants by EAOPs, intermediate products formed are then generally converted to highly oxidized products that are not stable and leads to the formation of short-chain carboxylic acids under oxidative cleavage action of $\cdot\text{OH}$. These acids constitute the last organics before complete mineralization and react hardly with $\cdot\text{OH}$. The formation and evolution of the carboxylic acids was followed by ion-exclusion chromatography (as explained in sub-section of 2.4) and the results are depicted in Fig. 6. Seven carboxylic acids (oxalic, glycolic, maleic, acetic, pyruvic, oxamic and formic acids) were identified and quantified during EF process with two different cathodes (CF and EEGr-CF), glycolic and maleic acids were measured at trace levels and were not presented in the curves. As shown in Fig. 6, oxalic acid was the major carboxylic acid in both cases. Its concentration reached the maximum value of 0.07 mM at 120 min in DSA/CF cell and 0.1 mM at 100 min in DSA/EEGr-CF cell, respectively. It can be seen that these acids were generated from the beginning of oxidation process and accumulated with electrolysis time until reaching the maximum values, providing much differences with two different cathodes. The maximum values of formic, oxamic and pyruvic acids appeared early with EEGr-CF cathode than that with raw CF cathode. Subsequently, the following decrease rate of carboxylic acids were slow because that carboxylic acids are much less reactive with hydroxyl radicals compared to aromatics ^[11]. Finally, both acids were completely mineralized with EEGr-CF cathode, while which still remained obviously in solution with raw CF cathode at the end of the treatment time of 8 h. The

results of carboxylic acids were in agreement to the tendency of TOC removal depicted in Fig. 4. The higher values of TOC with raw CF cathode at 8 h were due to the certain amount of carboxylic acids remaining in solution. Besides, it can be observed that during the process of IMA mineralization, the degradation rates of carboxylic acids with EEGr-CF were higher compared to that with raw CF cathode. These results highlight again the greater ability of EEGr-CF cathode in mineralization of organic pollutants compared to the raw CF cathode in EF process.

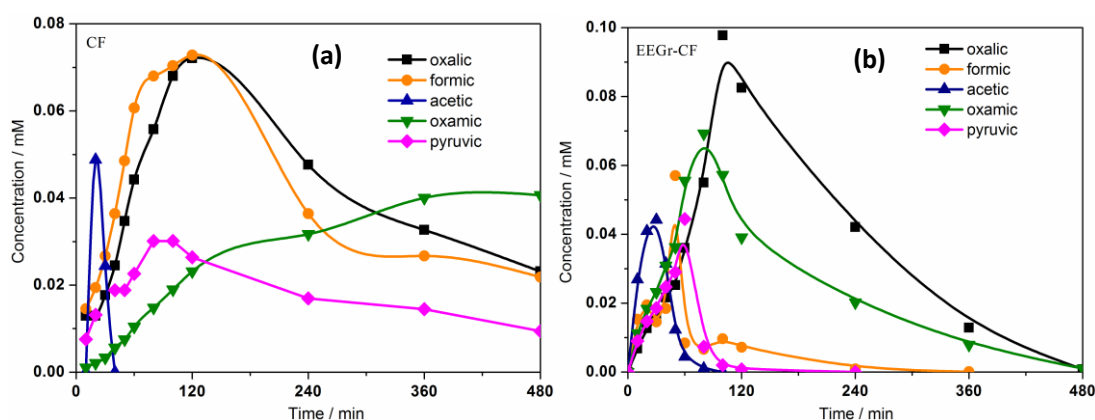


Fig. 6 Time-course of identified short-chain carboxylic acids during the electrooxidation of 0.07 mM (34.5 mg L^{-1}) IMA in EF process with raw CF (a) and EEGr-CF cathodes (b). V: 150 mL, pH: 3, $[\text{Fe}^{2+}]$: 0.1 mM, I : 200 mA, $[\text{Na}_2\text{SO}_4]$: 50 mM.

3.3.5 Evolution of inorganic ions during electro-oxidation of IMA

The identification of released inorganic ions is an important signal during the mineralization of organics^[56]. IMA contains N atoms that can be oxidized to inorganic ions such as NH_4^+ , NO_2^- and NO_3^- . The formation and evolution of the concentration of these ions were studied with cells having raw CF and EEGr-CF cathodes. NH_4^+ was the major inorganic ion in both cases compared to NO_3^- , whereas NO_2^- was not detected in this study. The maximum concentration of NH_4^+ and NO_3^- was 0.39 and 0.04 mM with EEGr-CF cathode at the end of treatment time (480 min). The sum of these two ions reached 88% of the total expected nitrogen concentration (0.49 mM), and remaining of the undetected nitrogen can be explained by the presence of other unidentified nitrogen

containing intermediates in the solution or lost in certain volatile nitrogen containing compounds [57]. As comparison, the concentration of nitrogen detected with raw CF cathode was 0.33 mM NH_4^+ , 0.02 mM NO_3^- and 0.04 mM oxamic acid; the total nitrogen detected being 80% of the theoretical nitrogen present in initial IMA solution. The results shown in Fig. 6(a) show that oxamic acid remains at a significant concentration at the end of electrolysis time, which proves the lower mineralization performance of the raw CF compared to EEGr-CF cathode. These results were in agreement with TOC removal efficiency of both cathodes in Fig. 4. The relatively higher residual TOC value of Fig. 4(b) at the end of electrolysis with raw CF cathode could be attributed to its relatively lower mineralization power in oxidation of short-chain carboxylic acids compared to EEGr-CF cathode, illustrating again the superior performance of the latest cathode in IMA degradation by EF process.

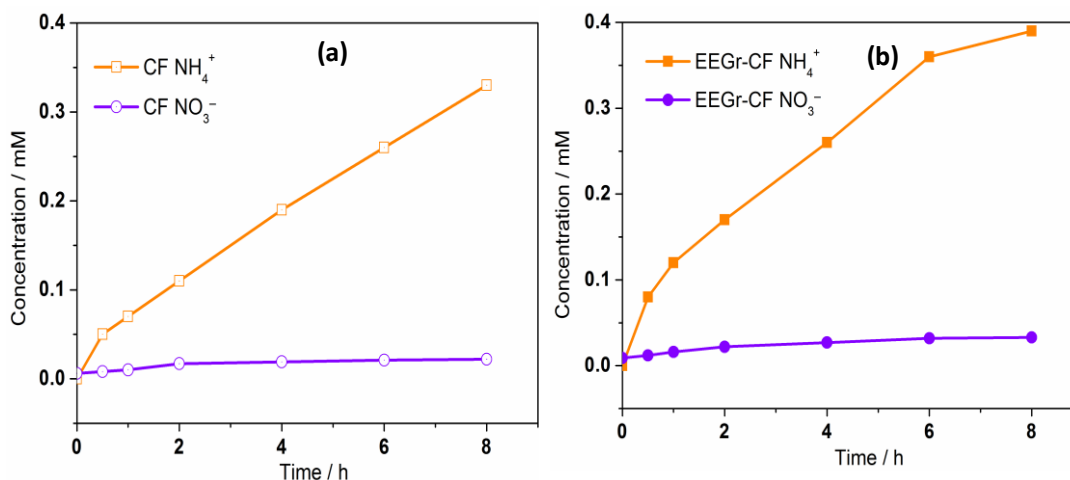


Fig. 7 Time-course of identified inorganic ions (NH_4^+ and NO_3^-) during electrooxidation of 0.07 mM (34.5 mg L^{-1}) IMA in EF process with raw CF (a) and EEGr-CF cathodes (b). V: 150 mL, pH: 3, $[\text{Fe}^{2+}]$: 0.1 mM, I : 200 mA, $[\text{Na}_2\text{SO}_4]$: 50 mM (for NO_3^-), $[\text{K}_2\text{SO}_4]$: 50 mM (for NH_4^+ since the presence of Na^+ ion hinders the detection of NH_4^+ in ion chromatography).

3.3.6 Assessment of toxicity during degradation of IMA with raw CF and EEGr-CF cathodes

During degradation of organic pollutants by AOPs/EAOPs, the toxicity of solution may be higher than that of initial solution due to the formation of toxic intermediates [58]. In this study, the change tendency of toxicity of 0.07 mM (34.5 mg L⁻¹) IMA solution during EF process with raw CF and EEGr-CF cathodes at 16.66 mA cm⁻² was monitored by Microtox[®] method by measuring the bioluminescence inhibition of marine bacteria *Vibrio fischeri*. The results presented in Fig. 8 show that the initial bioluminescence inhibition of IMA solution was about 60%, and significantly increased at the beginning of the electrolysis in both cases, illustrating that the formed aromatic intermediates are more toxic than initial IMA solution. In the case of EEGr-CF, the maximum inhibition value of 100% was obtained at 60 min, which was early than the one with raw CF (120 min) due to the quicker mineralization of formed intermediates. Subsequently, the toxicity of solution in both cases was decreased gradually along with degradation of intermediates. The bioluminescence inhibition dropped to minimum value of about 1% at 480 min with EEGr-CF, indicating the quasi-total mineralization of IMA solution and generating intermediates into non-toxic and biodegradable carboxylic acids, while there still existed certain level of bioluminescence inhibition (12% and 17% for 5 and 15 min exposition, respectively) at the end of electrolysis time with raw CF cathode because of remaining intermediates in the solution in agreement with TOC removal results presented in Fig. 4.

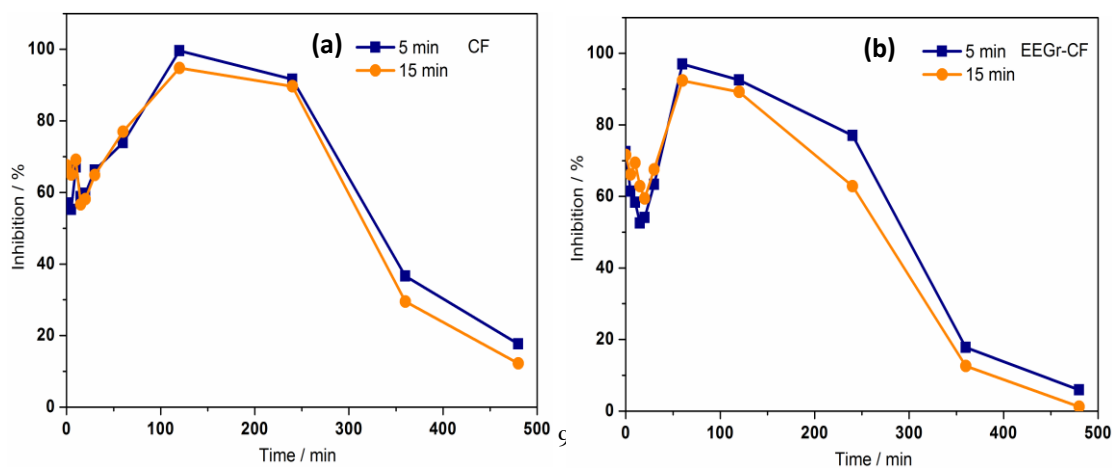


Fig. 8 Evolution of acute toxicity during EF treatment of 0.07 mM (34.5 mg L⁻¹) IMA solution with raw CF (a) and EGr-CF cathode (b) at 200 mA. The toxicity is expressed as the inhibition of the luminescence of *V. fischeri* bacteria after 5 min and 15 min exposure time. V: 150 mL, pH: 3, [Fe²⁺]: 0.1 mM, [Na₂SO₄]: 50 mM.

3.4 Conclusions

In this paper, the efficiency of EF process for the degradation and mineralization of IMA with graphene-based cathode (EGr-CF) was explored and compared with results of obtained with raw CF cathode. Kinetic decay of IMA obeyed a pseudo-first order reaction and a pretty high absolute rate constant value for oxidation reaction of IMA by $\bullet\text{OH}$ was obtained as $4.56 \times 10^9 \text{ M}^{-1} \text{ s}^{-1}$ with competitive kinetics method. The comparison performances of H₂O₂ generation, IMA kinetics decay and TOC removal efficiency demonstrated that EGr-CF was more remarkable for oxidative degradation and mineralization of IMA in EF process. Besides, the obtained results of short-chain carboxylic acids, inorganic ions (NH₄⁺ and NO₃⁻) and toxicity assessment during the mineralization of IMA solution highlighted again the greater advantages of EGr-CF in EF process for destruction of organics compared with raw CF cathode. These results proved that graphene-based cathode owns much more potential for the mineralization of IMA and shed new light on the EF process for pharmaceuticals removal in water or wastewater.

Acknowledgement

This work was financially supported by Key Project of Natural Science Foundation of Tianjin (no. 16JCZDJC39300), Natural Science Foundation of China (nos. 21773129, 21811530274, 91545126 and 21273120), National Key Research and Development Program (2016YFC0400706), China National Water Project (2017ZX07107002), 111 program, Ministry of Education, China (T2017002) and Fundamental Research Funds

for the Central Universities. This work was supported by the China Scholarship Council (CSC) [grant number 201706205095].

References

- [1] Barhoumi N, Olvera-Vargas H, Oturan N, et al. Kinetics of oxidative degradation/mineralization pathways of the antibiotic tetracycline by the novel heterogeneous electro-Fenton process with solid catalyst chalcopyrite[J]. *Applied Catalysis B: Environmental*, 2017, 209: 637-647.
- [2] Küster A, Adler N, et al. Pharmaceuticals in the environment: scientific evidence of risks and its regulation[J]. *Phil. Trans. R. Soc. B*, 2014, 369: 20130587.
- [3] Ribeiro A R, Nunes O C, Pereira M F, et al. An overview on the advanced oxidation processes applied for the treatment of water pollutants defined in the recently launched Directive 2013/39/EU[J]. *Environment International*, 2015, 75: 33-51.
- [4] Hernando M, Mezcua M, Fernández-Alba A, et al. Environmental risk assessment of pharmaceutical residues in wastewater effluents, surface waters and sediments[J]. *Talanta*, 2006, 69: 334-342.
- [5] Dong H, Yuan X, Wang W, et al. Occurrence and removal of antibiotics in ecological and conventional wastewater treatment processes: a field study[J]. *Journal of environmental management*, 2016, 178: 11-19.
- [6] Castiglioni S, Bagnati R, Fanelli R, et al. Removal of pharmaceuticals in sewage treatment plants in Italy[J]. *Environmental Science & Technology*, 2006, 40: 357-363.
- [7] Ternes T A, et al. Occurrence of drugs in German sewage treatment plants and rivers1[J]. *Water research*, 1998, 32: 3245-3260.
- [8] De García S A O, Pinto G P, García-Encina P A, et al. Ecotoxicity and environmental risk assessment of pharmaceuticals and personal care products in aquatic environments and wastewater treatment plants[J]. *Ecotoxicology*, 2014, 23: 1517-1533.
- [9] Rosal R, Rodríguez A, Perdigón-Melón J A, et al. Occurrence of emerging pollutants in urban wastewater and their removal through biological treatment followed by ozonation[J]. *Water research*, 2010, 44: 578-588.
- [10] Uribe I O, Mosquera-Corral A, Rodicio J L, et al. Advanced technologies for water treatment and reuse[J]. *AIChE Journal*, 2015, 61: 3146-3158.
- [11] Sirés I, Brillas E, Oturan M A, et al. Electrochemical advanced oxidation processes: today and tomorrow. A review[J]. *Environmental Science and Pollution Research*, 2014, 21: 8336-8367.
- [12] Ganzenko O, Huguenot D, Van Hullebusch E D, et al. Electrochemical advanced oxidation and biological processes for wastewater treatment: a review of the combined approaches[J]. *Environmental Science and Pollution Research*, 2014, 21: 8493-8524.
- [13] Moreira F C, Boaventura R A, Brillas E, et al. Electrochemical advanced oxidation processes: a

- review on their application to synthetic and real wastewaters[J]. *Applied Catalysis B: Environmental*, 2017, 202: 217-261.
- [14] Augugliaro V, Camera-Roda G, Loddo V, et al. Heterogeneous photocatalysis and photoelectrocatalysis: from unselective abatement of noxious species to selective production of high-value chemicals[J]. *The journal of physical chemistry letters*, 2015, 6: 1968-1981.
- [15] Pignatello J J, Oliveros E, Mackay A, et al. Advanced oxidation processes for organic contaminant destruction based on the Fenton reaction and related chemistry[J]. *Critical reviews in environmental science and technology*, 2006, 36: 1-84.
- [16] Oturan M A, Aaron J-J, et al. Advanced oxidation processes in water/wastewater treatment: principles and applications. A review[J]. *Critical Reviews in Environmental Science and Technology*, 2014, 44: 2577-2641.
- [17] Brillas E, Sirés I, Oturan M A, et al. Electro-Fenton process and related electrochemical technologies based on Fenton's reaction chemistry[J]. *Chemical reviews*, 2009, 109: 6570-6631.
- [18] Nidheesh P, Gandhimathi R, et al. Trends in electro-Fenton process for water and wastewater treatment: an overview[J]. *Desalination*, 2012, 299: 1-15.
- [19] Nidheesh P V, Gandhimathi R, Ramesh S T, et al. Degradation of dyes from aqueous solution by Fenton processes: a review[J]. *Environmental Science and Pollution Research*, 2013, 20: 2099-2132.
- [20] Nidheesh P, Zhou M, Oturan M A, et al. An overview on the removal of synthetic dyes from water by electrochemical advanced oxidation processes[J]. *Chemosphere*, 2018,
- [21] Mousset E, Oturan N, Oturan M A, et al. An unprecedented route of \bullet OH radical reactivity: ipso-substitution with perhalogenocarbon compounds[J]. *Applied Catalysis B: Environmental*, 2018, 226: 135-156.
- [22] Ren G, Zhou M, Su P, et al. Highly energy-efficient removal of acrylonitrile by peroxi-coagulation with modified graphite felt cathode: Influence factors, possible mechanism[J]. *Chemical Engineering Journal*, 2018, 343: 467-476.
- [23] Yu F, Zhou M, Yu X, et al. Cost-effective electro-Fenton using modified graphite felt that dramatically enhanced on H₂O₂ electro-generation without external aeration[J]. *Electrochimica Acta*, 2015, 163: 182-189.
- [24] Ganzenko O, Oturan N, Sirés I, et al. Fast and complete removal of the 5-fluorouracil drug from water by electro-Fenton oxidation[J]. *Environmental Chemistry Letters*, 2018, 16: 281-286.
- [25] Barhoumi N, Oturan N, Olvera-Vargas H, et al. Pyrite as a sustainable catalyst in electro-Fenton process for improving oxidation of sulfamethazine. Kinetics, mechanism and toxicity assessment[J]. *Water research*, 2016, 94: 52-61.
- [26] Sopaj F, Oturan N, Pinson J, et al. Effect of the anode materials on the efficiency of the electro-Fenton process for the mineralization of the antibiotic sulfamethazine[J]. *Applied Catalysis B: Environmental*, 2016, 199: 331-341.
- [27] Dominguez C M, Oturan N, Romero A, et al. Lindane degradation by electrooxidation process: Effect of electrode materials on oxidation and mineralization kinetics[J]. *Water research*, 2018, 135:

220-230.

- [28] Oturan N, Ganiyu S O, Raffy S, et al. Sub-stoichiometric titanium oxide as a new anode material for electro-Fenton process: application to electrocatalytic destruction of antibiotic amoxicillin[J]. *Applied Catalysis B: Environmental*, 2017, 217: 214-223.
- [29] Soltani R D C, Rezaee A, Khataee A, et al. Electrochemical generation of hydrogen peroxide using carbon black-, carbon nanotube-, and carbon black/carbon nanotube-coated gas-diffusion cathodes: effect of operational parameters and decolorization study[J]. *Research on Chemical Intermediates*, 2013, 39: 4277-4286.
- [30] Lan H, He W, Wang A, et al. An activated carbon fiber cathode for the degradation of glyphosate in aqueous solutions by the Electro-Fenton mode: Optimal operational conditions and the deposition of iron on cathode on electrode reusability[J]. *Water research*, 2016, 105: 575-582.
- [31] Trellu C, Oturan N, Keita F K, et al. Regeneration of Activated Carbon Fiber by Electro-Fenton Process[J]. *Environmental science & technology*, 2018,
- [32] zcan A, zcan A A, Demirci Y, et al. Evaluation of mineralization kinetics and pathway of norfloxacin removal from water by electro-Fenton treatment[J]. *Chemical Engineering Journal*, 2016, 304: 518-526.
- [33] Diaw P A, Oturan N, Seye M D G, et al. Oxidative degradation and mineralization of the phenylurea herbicide fluometuron in aqueous media by the electro-Fenton process[J]. *Separation and Purification Technology*, 2017, 186: 197-206.
- [34] Mousset E, Wang Z, Hammaker J, et al. Physico-chemical properties of pristine graphene and its performance as electrode material for electro-Fenton treatment of wastewater[J]. *Electrochimica Acta*, 2016, 214: 217-230.
- [35] Garcia-Rodriguez O, Lee Y Y, Olvera-Vargas H, et al. Mineralization of electronic wastewater by electro-Fenton with an enhanced graphene-based gas diffusion cathode[J]. *Electrochimica Acta*, 2018, 276: 12-20.
- [36] Mousset E, Ko Z T, Syafiq M, et al. Electrocatalytic activity enhancement of a graphene ink-coated carbon cloth cathode for oxidative treatment[J]. *Electrochimica Acta*, 2016, 222: 1628-1641.
- [37] Xu X, Chen J, Zhang G, et al. Homogeneous electro-Fenton oxidative degradation of reactive brilliant blue using a graphene doped gas-diffusion cathode[J]. *Int J Electrochem Sci*, 2014, 9: 569-579.
- [38] Le T X H, Bechelany M, Lacour S, et al. High removal efficiency of dye pollutants by electron-Fenton process using a graphene based cathode[J]. *Carbon*, 2015, 94: 1003-1011.
- [39] Chen J, Yao B, Li C, et al. An improved Hummers method for eco-friendly synthesis of graphene oxide[J]. *Carbon*, 2013, 64: 225-229.
- [40] Zhu Y, Murali S, Cai W, et al. Graphene and graphene oxide: synthesis, properties, and applications[J]. *Advanced materials*, 2010, 22: 3906-3924.
- [41] Yang W, Zhou M, Cai J, et al. Ultrahigh yield of hydrogen peroxide on graphite felt cathode

- modified with electrochemically exfoliated graphene[J]. *Journal of Materials Chemistry A*, 2017, 5: 8070-8080.
- [42] Nageswari A, Reddy K K, Mukkanti K, et al. Stability-indicating UPLC method for determination of Imatinib Mesylate and their degradation products in active pharmaceutical ingredient and pharmaceutical dosage forms[J]. *Journal of pharmaceutical and biomedical analysis*, 2012, 66: 109-115.
- [43] Elerseck T, Milavec S, Korošec M, et al. Toxicity of the mixture of selected antineoplastic drugs against aquatic primary producers[J]. *Environmental Science and Pollution Research*, 2016, 23: 14780-14790.
- [44] Lutterbeck C A, Kern D I, Machado L, et al. Evaluation of the toxic effects of four anti-cancer drugs in plant bioassays and its potency for screening in the context of waste water reuse for irrigation[J]. *Chemosphere*, 2015, 135: 403-410.
- [45] Mahnik S N, Rizovski B, Fuerhacker M, et al. Determination of 5-fluorouracil in hospital effluents[J]. *Analytical and bioanalytical chemistry*, 2004, 380: 31-35.
- [46] Panizza M, Dirany A, Sirés I, et al. Complete mineralization of the antibiotic amoxicillin by electro-Fenton with a BDD anode[J]. *Journal of applied electrochemistry*, 2014, 44: 1327-1335.
- [47] Lin H, Wu J, Oturan N, et al. Degradation of artificial sweetener saccharin in aqueous medium by electrochemically generated hydroxyl radicals[J]. *Environmental Science and Pollution Research*, 2016, 23: 4442-4453.
- [48] Chen T-S, Tsai R-W, Chen Y-S, et al. Electrochemical degradation of tetracycline on BDD in aqueous solutions[J]. *Int. J. Electrochem. Sci*, 2014, 9: e8434.
- [49] Dirany A, Sirés I, Oturan N, et al. Electrochemical treatment of the antibiotic sulfachloropyridazine: kinetics, reaction pathways, and toxicity evolution[J]. *Environmental science & technology*, 2012, 46: 4074-4082.
- [50] Oturan N, Zhou M, Oturan M A, et al. Metomyl degradation by electro-Fenton and electro-Fenton-like processes: a kinetics study of the effect of the nature and concentration of some transition metal ions as catalyst[J]. *The Journal of Physical Chemistry A*, 2010, 114: 10605-10611.
- [51] Beltran De Heredia J, Torregrosa J, Dominguez J R, et al. Kinetic model for phenolic compound oxidation by Fenton's reagent[J]. *Chemosphere*, 2001, 45: 85-90.
- [52] Dirany A, Aaron S E, Oturan N, et al. Study of the toxicity of sulfamethoxazole and its degradation products in water by a bioluminescence method during application of the electro-Fenton treatment[J]. *Analytical and bioanalytical chemistry*, 2011, 400: 353-360.
- [53] Panizza M, Oturan M A, et al. Degradation of Alizarin Red by electro-Fenton process using a graphite-felt cathode[J]. *Electrochimica Acta*, 2011, 56: 7084-7087.
- [54] Solano A M S, De Araújo C K C, De Melo J V, et al. Decontamination of real textile industrial effluent by strong oxidant species electrogenerated on diamond electrode: viability and disadvantages of this electrochemical technology[J]. *Applied Catalysis B: Environmental*, 2013, 130: 112-120.

- [55] Oturan N, Brillas E, Oturan M A, et al. Unprecedented total mineralization of atrazine and cyanuric acid by anodic oxidation and electro-Fenton with a boron-doped diamond anode[J]. *Environmental Chemistry Letters*, 2012, 10: 165-170.
- [56] Lin H, Niu J, Xu J, et al. Electrochemical mineralization of sulfamethoxazole by Ti/SnO₂-Sb/Ce-PbO₂ anode: kinetics, reaction pathways, and energy cost evolution[J]. *Electrochimica Acta*, 2013, 97: 167-174.
- [57] Brillas E, Garcia-Segura S, Skoumal M, et al. Electrochemical incineration of diclofenac in neutral aqueous medium by anodic oxidation using Pt and boron-doped diamond anodes[J]. *Chemosphere*, 2010, 79: 605-612.
- [58] Ganiyu S O, Oturan N, Raffy S, et al. Sub-stoichiometric titanium oxide (Ti₄O₇) as a suitable ceramic anode for electrooxidation of organic pollutants: A case study of kinetics, mineralization and toxicity assessment of amoxicillin[J]. *Water research*, 2016, 106: 171-182.

Chapter 4: Effect of anode materials on the performance of Electrocatalytic generation of homogeneous and heterogeneous hydroxyl radicals for cold mineralization of anti-cancer drug imatinib

Abstract

The effect of anode materials on the mineralization and electrochemical oxidation of pharmaceutical imatinib (IMA) was explored by electro-Fenton (EF) and anodic oxidation (AO) processes using four kinds of anode material: Pt, DSA (Ti/RuO₂-IrO₂), BDD and sub-stoichiometric titanium oxide (Ti₄O₇). A series of comparison experiments including oxidative degradation kinetics of IMA, total organic carbon (TOC) decay and mineralization efficiency were conducted at pH 3 and ambient temperature. In both cases, DSA and Pt was less effective anode for the anodic oxidation and mineralization of IMA solution compared with Ti₄O₇ and BDD anodes. Complete mineralization of 0.07 mM (corresponding to 24.11 mg L⁻¹ initial TOC) IMA solution was obtained both in EF and AO processes with BDD anode at 300 mA. The Ti₄O₇ anode exhibited better performances than DSA and Pt anode, reaching 84% TOC removal efficiency in EF and 73% in AO processes at 8 h electrolysis, providing much potent cathode material as the cost-effective candidate for wastewater treatment. Besides, the formation and evolution of five short-chain carboxylic acids (oxalic, pyruvic, oxamic, formic and acetic) and N-based inorganic ions (NH₄⁺, NO₃⁻) during mineralization of IMA solution were identified and followed by ion exclusion HPLC and ion chromatography, respectively. What's important is that the relative contribution of homogeneous (generated in the bulk) and heterogeneous (formed at anode surface) hydroxyl radicals on the oxidation kinetics of IMA and TOC removal efficiency during EF process with different anodes were explored. Finally, a plausible degradation pathway of IMA by [•]OH was proposed according to the intermediates detected by HPLC and GC-MS.

Keywords: Electro-Fenton; Imatinib; Ti₄O₇; Hydroxyl radical; Mineralization

4.1 Introduction

The environment pollution by pharmaceuticals was firstly brought to public's attention in 1990s when some pharmaceutical residues were detected in drinking water across Europe ^[1]. With the development of analytical methods, more and more kinds of pharmaceuticals have been discovered in the environmental samples of surface water, groundwater, urban wastewater and also tap water ^[2, 3], usually at pretty low levels of ng L^{-1} or $\mu\text{g L}^{-1}$ ^[4, 5]. The sources of pharmaceuticals in the aquatic water have been extensively reviewed ^[6, 7], including inappropriate disposal and leaching of medications by pharmaceutical industries, hospitals, households and animal farming fields ^[8, 9]. In general, many pharmaceuticals are not absolutely belong to the kind of persistent organic pollutants, most of which can be potentially degraded or bio-transformed ^[10-12], which are usually regarded to be the pseudo-persistent pollutants due to their continuous release into aquatic waters, which are not efficiently destroyed in many wastewater treatment plants (WWTPs) and therefore released to the natural water bodies ^[13-15]. Imatinib (IMA) as one of the major pharmaceutical used for treating leukemia, has caught attention due to the large consumption for increasing cancer cases ^[16]. Since it is designed to be relatively stable in biological environment and has a strong affinity to biological receptors, usually will be excreted within 24 h after usage, leading to high level of concentrations in municipal wastewater and then in natural water stream and therefore constitute a great threat to human beings and ecosystems ^[17, 18].

Due to the persistence of pharmaceuticals and lacking efficiency of conventional WWTPs ^[19, 20], many advanced treatment methods have been attempted to effectively degrade different kinds of pharmaceutical pollutants ^[21-25]. Among the technologies employed so far, advanced oxidation processes (AOPs) are considered to be great potential for the treatment of various emerging contaminants, involving in-situ generated highly reactive oxygen species with low selectivity such as hydroxyl radicals ^[26, 27]. However, when it comes to the practical application, complicated process control, long treatment time and high energy cost are usually the major hurdles faced ^[28]. As one of the AOPs, Fenton treatment has presented its proves for the quasi-complete

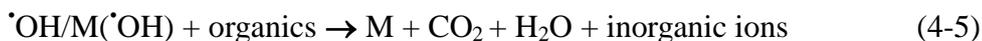
mineralization of trace-level pharmaceutical pollutants from water ^[29]. However, the large consumption of H₂O₂ along with generation of quantities of iron sludge during the process strongly restricted its successful implementation for practical applications. During the decades, new kinds of AOPs based on the electrochemical technology, namely electrochemical advanced oxidation processes (EAOPs) have been developed for remediation of environmental pollution ^[27, 30, 31]. Compared with AOPs, EAOPs provide some special advantages such as high efficiency, easy handling, safety and most importantly the use of electron used a clean reagent ^[32, 33] instead of chemicals.

Electro-Fenton (EF) and anodic oxidation (AO) are the most representative two EAOPs, where $\cdot\text{OH}$ is generated homogeneously in the bulk solution and heterogeneously at the anode surfaces ^[27, 34-42]. In the EF process, $\cdot\text{OH}$, the second most strong oxidant after flour ((E_{OH/H₂O} = 2.80 V/SHE), is produced electrocatalytically through the Fenton reaction (Eq.(1)), and reacts non-selectively with organics leading to their mineralization ^[27, 43]. In this process, the H₂O₂ is in-situ generated via oxygen reduction reaction (Eq. (2)) on the cathode, meanwhile, along with the regeneration of Fe²⁺ through electro-reduction of Fe³⁺ (Eq. (3)), which guarantees the electrocatalytically continuous generation of $\cdot\text{OH}$ during the process ^[27, 32].



AO is another EAOPs for degradation of organic pollutants in which heterogeneous hydroxyl radicals (M($\cdot\text{OH}$)) are generated from oxidation of water on the surface of anode (Eq. (4)) ^[34, 38]. This process has also been successfully applied to the treatment of pharmaceuticals wastewater ^[44, 45]. In the case of using an appropriate anode material (M) in EF process, homogeneous ($\cdot\text{OH}$) and heterogeneous (M($\cdot\text{OH}$)) are generated simultaneously enhancing oxidation power of the process according to the Eq. (5) ^[46].





Therefore, the anode material plays a significant role on the efficiencies of EAOPs (EF and AO). Various materials have been used as anodes for oxidative degradation of organic pollutants such as Pt, DSA (dimensionally stable anode), BDD (boron-doped diamond) [47], PbO_2 [48], graphite, TiO_2 , IrO_2 and others [23, 49]. Among those, the BDD was reported to be more potent anode for mineralization of organics because of its high O_2 evolution overpotential, high stability and availability of physisorbed $\text{M}(\cdot\text{OH})$ [50-52]. Though BDD anode can significantly enhance the efficiency of EAOPs, its highly expensive cost is a big drawback for large scale application. Recent years, another non-active anode, namely the sub-stoichiometric titanium oxides, Ti_4O_7 , has been investigated and proved to be a promising alternative to BDD for EAOPs due to the weak adsorption of generated $\text{Ti}_4\text{O}_7(\cdot\text{OH})$ on its surface, high electrical conductivity, chemical stability and lower cost [53, 54]. Some researchers, including our group, have explored the performance of this anode at low currents in EF and AO processes [55, 56]; however, there is no systematic works showing the comparative performance of Ti_4O_7 against other conventional anodes in oxidation of pharmaceuticals at high current conditions.

In this study, the treatment of solutions containing the pharmaceutical IMA by EF and AO processes was investigated with four different anodes (DSA, Pt, Ti_4O_7 , BDD). Carbon felt (CF) [57, 58], as one of the most popular electrodes, was used as cathode in all of the experiments. A series of comparative experiments were carried out to determine the efficiency of each anode on the basis of degradation kinetics of IMA, total organic carbon (TOC) removal of its aqueous solution and energy consumption related to each anode. Formation and evolution of short-chain carboxylic acids as end-products before complete mineralization and inorganic ions released to the solution during mineralization experiments were analyzed. What's more, the intermediates generated during mineralization of IMA were identified by gas chromatography-mass spectrometry (GC-MS) technique and a plausible degradation pathway of IMA by $\cdot\text{OH}$ was proposed. To our knowledge, the oxidative degradation mechanism of IMA by $\cdot\text{OH}$

generated in EAOPs was not already reported. Finally, the change in acute toxicity of IMA solution during EF treatment was assessed by using Microtox[®] method.

4.2 Materials and methods

4.2.1 Chemicals

Imatinib (IMA), $C_{29}H_{31}N_7O$, was analytical grade ($\geq 99\%$ purity) provided by Sigma-Aldrich and was used without further purification. Methanol and acetic acid used as HPLC eluent, anhydrous sodium sulfate ($Na_2SO_4 \geq 99\%$ purity) used as electrolyte and iron (II) sulphate heptahydrate (99.5%) used as source of the catalyst (Fe^{2+} ion) in EF experiments were provided by Sigma-Aldrich. H_2SO_4 (1M) and NaOH (1M) were prepared to adjust solution pH. All solutions were prepared with ultrapure water (resistivity of $18\text{ M}\Omega\text{ cm}^{-1}$) obtained from a Millipore Milli-Q system (Molsheim, France). Potassium hydrogen phthalate (99.5%) used for the calibration of TOC value was purchased from Shimadzu (France).

4.2.2 Electrolytic system

The experiments were operated in a 250 mL undivided electrolytic cell with four different anodes ($4\text{ cm} \times 6\text{ cm}$) and CF cathode ($14\text{ cm} \times 5\text{ cm} \times 0.5\text{ cm}$). The CF was obtained from MERSEN (France), and the anodes were purchased as: Pt from Goodfellow (Lille, France), DSA from GuangJiDian Liability Company (China), and BDD from CONDIAS GmbH (Germany). The sub-stoichiometric titanium oxide (Ti_4O_7) was provided by Saint-Gobain Research Provence (France). Anodes were centered in the electrolytic cell surrounded by CF cathode, which cover the inner wall of the cell. During the electrolysis, solutions were kept homogeneous with magnetic stirring.

Electrolysis of IMA (0.07 mM) in EF process was performed at pH 3 which is regarded as the optimal value^[25, 26]. The electrooxidation experiments were carried out with a series of current ranging from 100 to 500 mA at room temperature. Samples were

taken during electrolysis at pre-set intervals for kinetics decay of IMA TOC measurements, carboxylic acids and inorganic ions analyses. For AO process, all of the experimental conditions were same except without Fe^{2+} (catalyst of EF process). Experiments were carried out triplicate and the mean values are reported on the figures.

4.2.3 Electrochemical measurements and analysis

The decay in initial concentration of IMA (0.07 mM) during kinetic experiments was monitored by uHPLC (Ultimate 3000, Thermo Scientific) using a DAD detector and coupled with a RP-18 Hypersil column (1.9 μm , 10 cm \times 2.1 mm). The mobile phase was set as: water (1% acetic acid)-methanol (1% acetic acid) (70:30, v/v), with flow rate of 0.1 mL min^{-1} and the detection was made at 267 nm. Inorganic ions NH_4^+ and NO_3^- released in the treated solution during mineralization of IMA were analyzed by Dionex ICS-1000 Basic Ion Chromatography equipped with a Dionex DS6 conductivity detector at 35°C. This system is coupled with a cationic column (CS12A) for detection of NH_4^+ or anionic column (AS4A-SC) for detection of NO_3^- . The mobile phase for cations detection was 9 mM H_2SO_4 at flow rate of 1 mL min^{-1} , while for anions measurement, the mobile phase contained 1.8 mM Na_2CO_3 and 1.7 mM NaHCO_3 with flow rate of 2 mL min^{-1} . The applied current of suppressor SRS (Self Regenerating Suppressor) was 30 mA in both cases.

The TOC decay measurements were monitored by Shimadzu V_{CSH} TOC analyzer and the results obtained were used for the calculation of TOC removal efficiency (Eq. (6)), energy consumption (EC) (Eq. (7)) and mineralization current efficiency (MCE) (Eq. (8)):

$$TOC(\%) = \frac{\Delta(TOC)_{\text{exp}}}{TOC_0} \times 100 \quad (4-6)$$

$$EC = \frac{UIt}{(\Delta TOC)_t V_s} \quad (4-7)$$

$$MCE(\%) = \frac{nFV_s \Delta(TOC)_{\text{exp}}}{4.32 \times 10^7 mIt} \times 100 \quad (4-8)$$

where $\Delta (TOC)_{\text{exp}}$ is the experimental TOC decay at electrolysis time t (mg L^{-1}), and TOC_0 is the initial value of IMA solution. U , I , t are the voltage (V), current (A) applied and electrolysis time (h) of the experiments. V_s is the volume of the solution (L). For MCE calculation, the value of (number of electrons consumed per IMA molecule during the mineralization process) was taken as 124 according to the electrochemical mineralization reaction (Eq. (9)), F means the Faraday constant (96485 C mol^{-1}) and m represents the number of carbon atoms of IMA (29).



Intermediate organic products formed during the oxidative degradation of IMA were detected by HPLC and GC-MS: (i) the detection and evolution of carboxylic acids were identified and followed by ion exclusion chromatography using an HPLC equipped with a HPX-87H ion exclusion column ($\phi 7.8 \text{ mm} \times 300 \text{ mm}$) at 40°C coupled to a detector L-2400 UV, (ii) identification of cyclic/aromatic intermediates was operated, using Agilent (7890A/5975C, USA) GC-MS equipped with a HP-5MS column ($30 \text{ m}, 0.25 \text{ mm} \times 0.25 \mu\text{m}$). The operation condition was set as: 1.1 mL min^{-1} helium as the carrier gas, initial column temperature of 70°C for 3 min, subsequently increased to 150°C with $10^\circ\text{C min}^{-1}$ and held for 1 min at this temperature, and then continued rising to 280°C with $16^\circ\text{C min}^{-1}$ and kept for 5 min at this temperature. Both the injector and detector temperature were set at 280°C .

Besides, the evolution of the acute toxicity of IMA solution during the mineralization process was monitored and assessed by Microtox[®] method based on the measure of luminescence inhibition of bacteria *Vibrio fischeri*.

4.3 Results and discussion

4.3.1 Decay kinetics of IMA

The kinetics of oxidative degradation and mineralization of pollutants in EF and AO processes mainly dominated by the yield of in-situ generated H_2O_2 on the cathode

and the nature of anode, respectively. When using an appropriate (non-active) anode in EF process, the nature of both cathode and anode are important: The average generation rate of H_2O_2 on cathode (Eq. (2)) determines the rate of Fenton reaction (Eq. (1)) and therefore governs the amount of homogeneous $\cdot\text{OH}$ generated in solution while the anode material plays a significant role in the generation of heterogeneous hydroxyl radicals ($\text{M}(\cdot\text{OH})$) on the surface of anode (Eq. (4)). In spite of the prevailing effect of both electrodes on the performance of organics removal, current applied, concentration of catalyst (EF) and solution pH are also important parameters in EAOPs.

First, preliminary experiments were designed to find the optimized value of Fe^{2+} (as catalyst). All of the experiments were then conducted at proper pH 3 and a catalyst concentration fixed to 0.1 mM (only in EF process), focusing on the effects of current on the degradation of organics in EF and AO processes with different anodes. Fig. 1 (a, b) shows the comparative performances with DSA anode during EF (a) and AO (b) processes. A series of current ranging from 50 to 500 mA were explored in both cases. Results show that whatever the process (EF or AO), the decay of IMA concentration is enhanced when increasing the value of current due to higher H_2O_2 generation on the cathode (Eq. (2)) and regeneration rate of Fe^{2+} (Eq. (3)) resulting in higher concentration of homogeneous $\cdot\text{OH}$ in solution via Fenton reaction (Eq. (1)). In the case of AO, high currents promote the formation of $\text{M}(\cdot\text{OH})$. Besides, the performance of IMA removal in EF process was much better than that in AO process because of two sources of hydroxyl radical in the former case. It is noteworthy that IMA is completely disappeared from the solution within 40 min in EF process with DSA anode (Fig. 1(a)) while it still remained in AO process even after 120 min electrolysis with currents of 50, 100, and 200 mA (Fig. 1(b)). The kinetic decay rate of IMA was almost two times lower in AO than in EF under 50 and 100 mA (Table 1), thus illustrating that the homogeneous $\cdot\text{OH}$ in solution is remarkably efficient than the heterogeneous $\text{DSA}(\cdot\text{OH})$ for complete oxidation of IMA.

The performances relative to the oxidative degradation of IMA with Pt anode (Pt/CF cell) under the same experimental conditions are depicted on Figs. 1(c) and 1(d).

The decay rate of IMA concentration increased with the increasing current. Slightly higher efficiencies were obtained compared to the results of DSA/CF cell under the same currents (Fig. 1(a)). For instance, with the applied currents of 300 and 500 mA, the complete oxidative degradation of IMA was obtained at 20 min and 15 min, respectively, in Pt/CF cell (Fig. 1(c)), while it needed 35 min in DSA/CF cell (Fig. 1(a)). Similarly, the decay rate of IMA in Pt/CF cell during AO process was slightly higher than that of DSA/CF cell. This slight advantage is due to the different adsorption characteristics of anodes: The DSA is a slightly more active anode than Pt, resulting in more strongly adsorbed DSA(\cdot OH) on the surface of anode than Pt(\cdot OH).

The results obtained with Ti₄O₇/CF and BDD/CF cells show a different behavior compared to those of DSA/CF and Pt/CF cells discussed above. Fig. 1(e) depicts that the IMA kinetics decay was very fast in EF process with Ti₄O₇/CF cell, particularly under low currents, leading its complete removal within 35 min under 50, 100 and 200 mA. However, when the current was increased, lower IMA degradation efficiencies were obtained. The time needed for complete degradation of IMA was 30, 35 and 40 min under 200, 300 and 500 mA, respectively. This phenomenon is different with previous report ^[55] where the currents of significantly low range of 10-120 mA were tested. Under the condition of high current, the decline in degradation efficiency can be explained by two reasons: The first is the intensification of competitive side reactions (Eqs. (10) and (11)) competing with mineralization of IMA during the EF process ^[27]. The second one can be related to the surface modification of the Ti₄O₇ anode due to its oxidation to TiO₂ under high currents leading to the loss of process efficiency. The loss of efficiency with increasing current was also observed in AO with 200, 300, 500 mA for the same reasons.



Fig. 1(g) and 1(h) indicate the impact of different currents on the decay kinetics of IMA in BDD/CF cell during the EF and AO processes. The decay of IMA concentration

Chapter 4 Effect of anode materials on the performance of Electrocatalytic generation of homogeneous and heterogeneous hydroxyl radicals for cold mineralization of anti-cancer drug imatinib

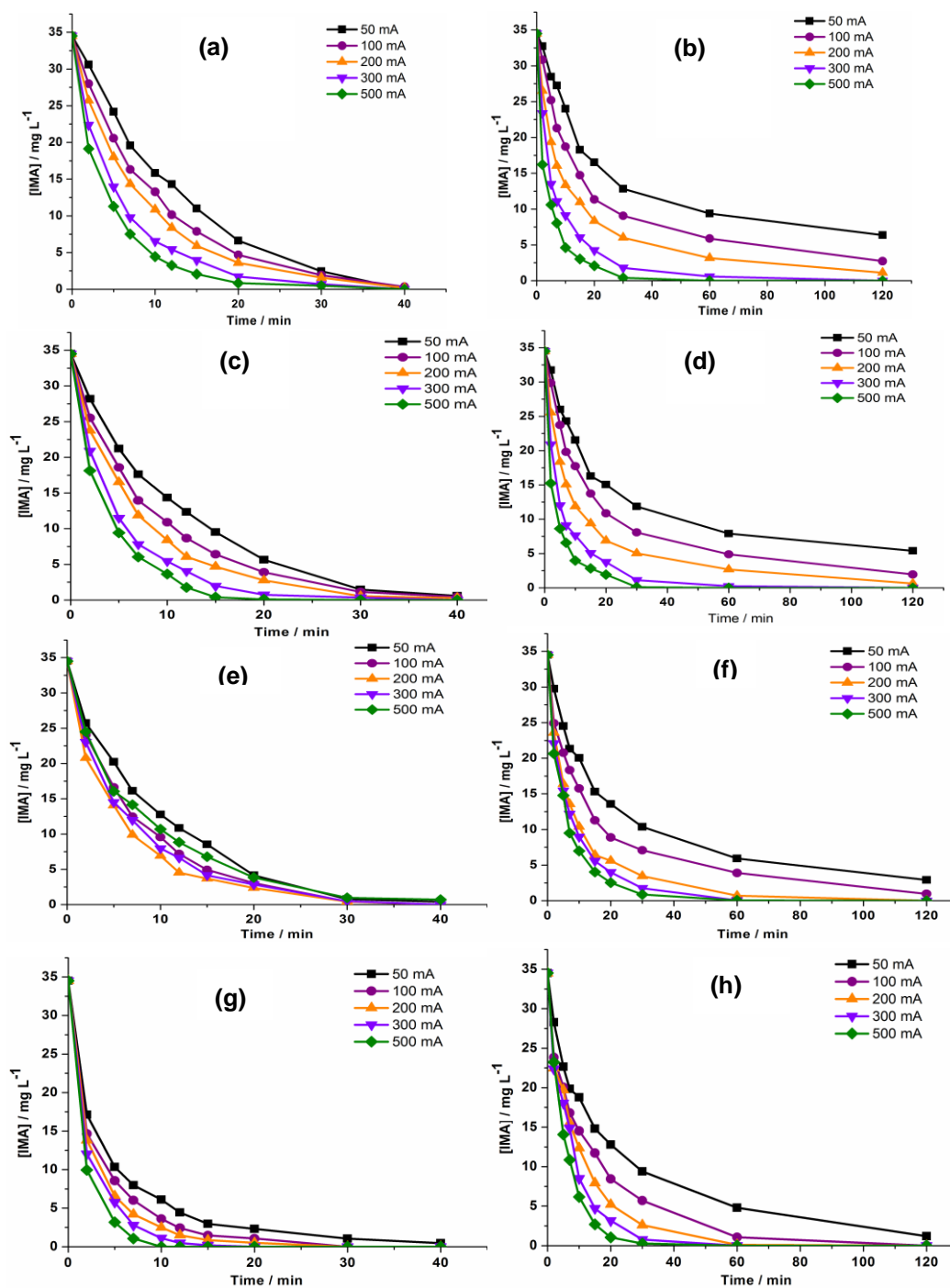


Fig. 1 Effect of applied current on the kinetics degradation of IMA in DSA/CF cell (a, b), Pt/CF cell (c, d), Ti₄O₇/CF cell (e, f) and BDD/CF cell (g, h): (a, c, e, g) EF, (b, d, f, h) AO process. [IMA]: 34.5 mg L⁻¹, V: 230 mL, [Fe²⁺]: 0.1 mM (only in EF process), pH 3, [Na₂SO₄]: 50 mM.

with electrolysis time follows pseudo-first order kinetics under the currents applied from 50 to 500 mA (Table 1). The results show clearly that the degradation kinetics is significantly higher in BDD/CF cell compared to the previous results. For instance, complete disappearance of IMA take place at 10 min in EF process which is strongly shorter than DSA/CF, Pt/CF and Ti₄O₇/CF cells. When comparing with Ti₄O₇/CF, the main difference is the continuous enhancement of degradation kinetics with rising applied current value. The greater performance of BDD anode in IMA degradation can be explained by the higher O₂ evolution overpotential allowing to generate high amounts of BDD([•]OH), which is weakly physisorbed and more available to react with organic compounds ^[46].

According to the analysis above, homogeneous [•]OHs generated in bulk solution play a dominant role in the degradation of organics during EF process compared to the limited contribution of heterogeneous M([•]OH). Especially, the performances of Ti₄O₇ and BDD anodes are much better than DSA and Pt anodes, due to the higher O₂ evolution overpotential and weaker ability of chemisorbed M([•]OH) of the formers anodes.

4.3.2 Comparison of the mineralization power of different anodes

The potential of anode materials for mineralization of 0.07 mM (corresponding to 24.1 mg L⁻¹ initial theoretical TOC) of IMA solutions was studied under a series of applied current from 50 to 500 mA. The complete mineralization of organics usually needs a significantly long electrolysis time along with a complicated process. Therefore all of the experiments for TOC removal of IMA solutions were kept for 8 h.

The results of TOC decay in DSA/CF cell (Fig. 2(a)) illustrate that the TOC removal rate is improved with the increasing applied current in the range of 50-300 mA in EF process with maximum TOC removal value of 61% obtained for 300 mA. Further increase in current to 500 mA was resulted in a very few enhancement in TOC removal efficiency. In spite of regular increase with rise of current, TOC removal rates obtained with AO process (Fig. 2(b)) are significantly lower than those obtained in EF process.

These results highlight that the homogeneous $\cdot\text{OH}$ generated in solution contributed to the relatively high results of TOC removal rates obtained in EF process. As can be seen in Figs. 2(c) and 2(d), the performances of IMA mineralization with Pt/CF cell revealed a better TOC removal efficiency compared to DSA/CF cell. Similar TOC decay kinetics was observed with optimal current value of 300 mA resulting in 78% TOC removal efficiency (Fig. 2(c)). Rising current to 500 mA gave a very few enhancement (80%) in TOC removal. AO process provided almost two times lower TOC decay efficiencies for all currents compared to EF process, reaching the maximum value of 45% with 500 mA after 8 h electrolysis.

Table 1: Apparent rate constants (k_{app}) as a function of anode materials and current applied for kinetics decay of IMA in EF and AO processes with CF cathode.

	Anode	DSA	Pt	Ti ₄ O ₇	BDD
	I (mA)	k_{app} (min ⁻¹)			
EF (k_1)	50	0.08	0.09	0.1	0.23
	100	0.10	0.12	0.17	0.27
	200	0.12	0.15	0.13	0.32
	300	0.15	0.19	0.15	0.37
	500	0.19	0.24	0.13	0.5
AO (k_2)	50	0.04	0.05	0.05	0.06
	100	0.06	0.07	0.07	0.08
	200	0.08	0.1	0.1	0.1
	300	0.12	0.15	0.12	0.13
	500	0.16	0.2	0.14	0.17

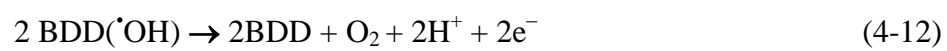
Results of mineralization of IMA solutions with Ti₄O₇ anode are depicted in Figs. 2(e) and 2(f). For the EF process (Fig. 2(e)), the mineralization degree improved with

the rising current and electrolysis time, obtaining the final TOC removal of 58%, 65%, 80%, 82% and 84% at 50, 100, 200, 300 and 500 mA, respectively. The mineralization efficiency was much higher than those with DSA and Pt anodes, as well as the significant performances in AO (Fig. 2(f)) process, demonstrating the higher mineralization power and effectiveness of Ti_4O_7 anode for removal of organics from aqueous solution. This behavior is consistent with the kinetics decay of IMA (Fig. 1) due to the generation of high quantity and more powerful $Ti_4O_7(\cdot OH)$ on the anode surface, leading to a quick oxidation and mineralization of IMA and its oxidation intermediates.

Highest mineralization efficiencies were obtained with BDD anode in both EF and AO processes (Figs. 2(g), 2(h)). Mineralization kinetics curves exhibited a different trends compared to other anodes: TOC removal efficiency increased regularly with increasing applied current, reaching to complete mineralization of IMA solution after 4 h electrolysis in EF (Fig. 2(g)) and 6 h in AO (Fig. 2(h)) at 500 mA. This results can be explained by generation of a great amount of BDD($\cdot OH$) with outstanding oxidation on the BDD anode due to its high O_2 overpotential and weak sorption of formed radicals [26]. The remarkable performances of TOC removal with BDD in both processes were in agreement with the results of kinetics experiments (Figs. 1(g) and 1(h)).

The evolution of MCE% corresponding to mineralization experiments was explored in Fig. 3. In DSA/CF cell, the MCE% values for EF and AO processes (Figs. 3(a) and 3(b)) show regular trends, with maximum values obtained for the lower currents of 50 mA. The MCE values for EF (Fig. 3(c)) and AO (Fig. 3(d)) processes with Pt anode were both higher compared with those obtained with DSA anode. These results are in agreement with the literature [46] reporting the TOC removal efficiency with Pt anode at the same condition. The MCE% values both in EF and AO processes with Ti_4O_7 anode (Figs. 3(e) and 3(f)) were more than two times of those obtained with DSA anode. With BDD anode, the trend of MCE curves was similar to TOC removal, as well as decreasing with the high currents due to the gradual enhancement of side reactions (Eqs. (12) and (13)) consuming the generated $\cdot OH$ [55].

Chapter 4 Effect of anode materials on the performance of Electrocatalytic generation of homogeneous and heterogeneous hydroxyl radicals for cold mineralization of anti-cancer drug imatinib



Chapter 4 Effect of anode materials on the performance of Electrocatalytic generation of homogeneous and heterogeneous hydroxyl radicals for cold mineralization of anti-cancer drug imatinib

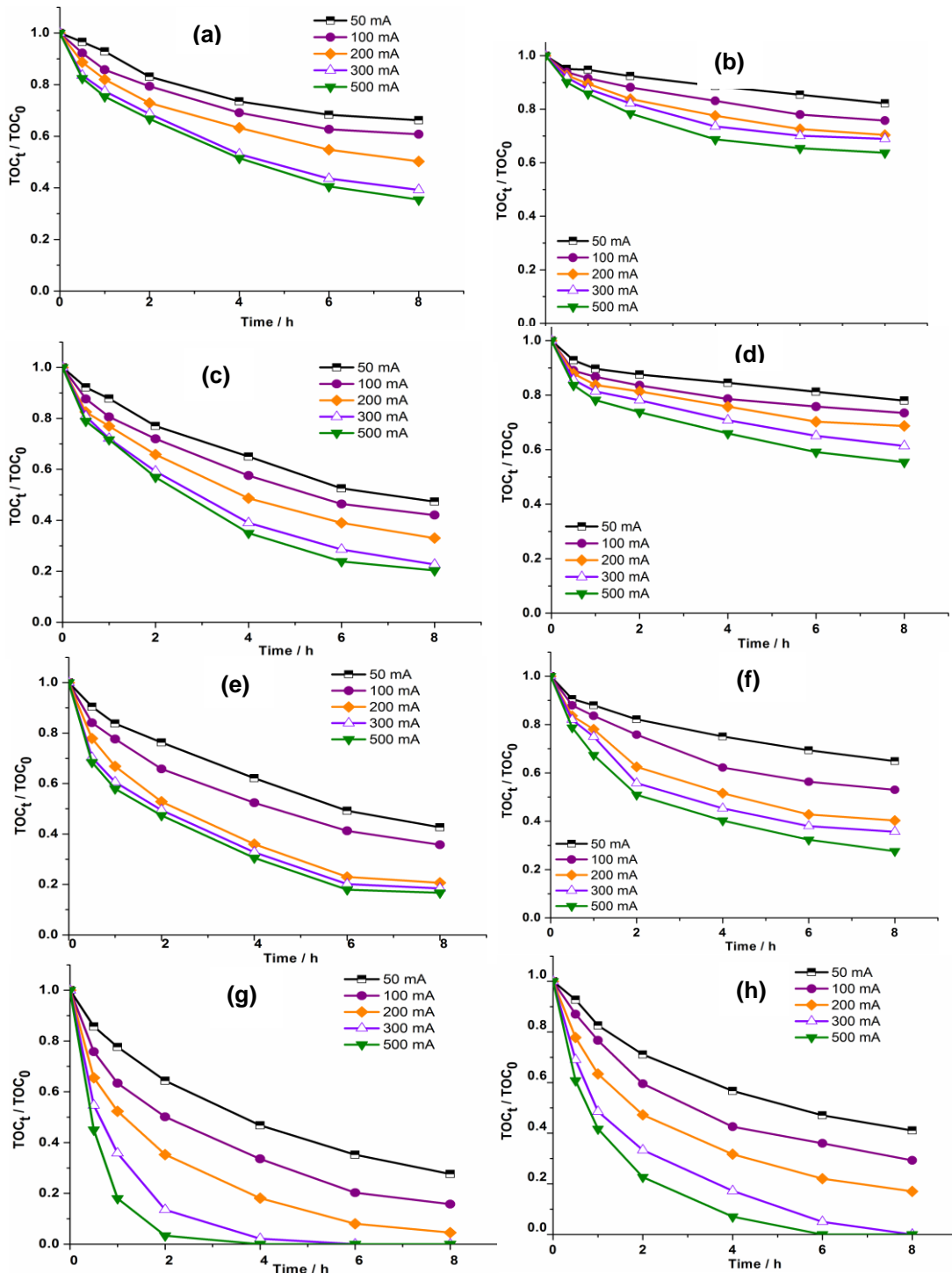


Fig. 2 Effect of current on the TOC removal of 0.07 mM IMA solution (corresponding to 24.1 mg L⁻¹ initial TOC) in EF (a, c, e, h) and AO (b, d, f, g) with DSA/CF (a, b), Pt/CF (c, d), Ti₄O₇/CF (e, f) and BDD/CF (g, h) cells. V: 230 mL, [Fe²⁺]: 0.1 mM (only in EF), pH 3, [Na₂SO₄]: 50 mM.

Chapter 4 Effect of anode materials on the performance of Electrocatalytic generation of homogeneous and heterogeneous hydroxyl radicals for cold mineralization of anti-cancer drug imatinib

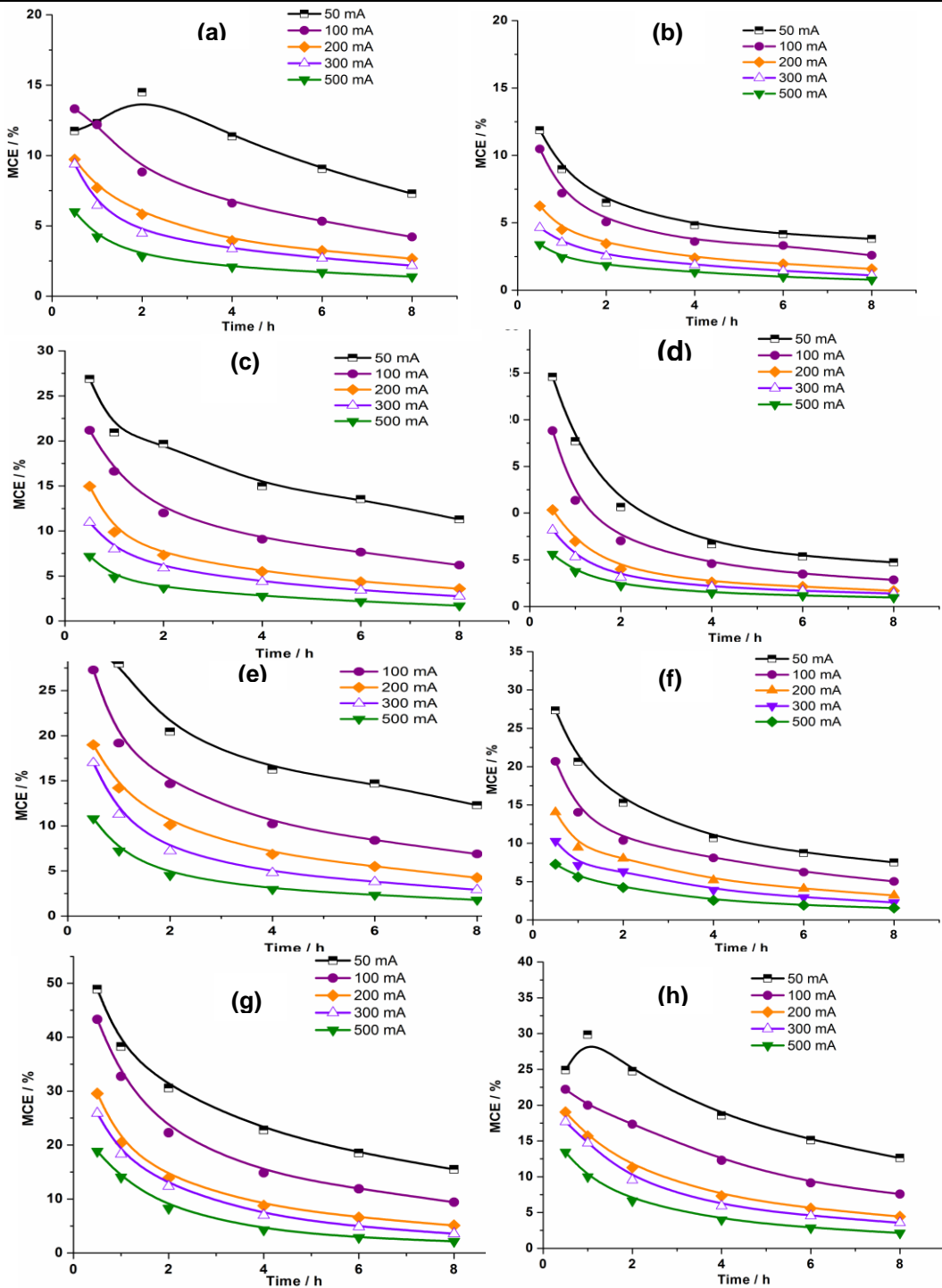


Fig. 3 Effect of applied current on the evolution of MCE with different anodes in EF (a, c, e, h) and AO (b, d, f, g) with DSA/CF (a, b), Pt/CF (c, d), Ti4O7/CF (e, f) and BDD/CF (g, h) cells [IMA]₀: 0.07 mM (34.5 mg L⁻¹), V: 230 mL, [Fe²⁺]: 0.1 mM (only in EF), pH 3, [Na₂SO₄]: 50 mM.

Based on the analysis of TOC removal percentages and MCE values, the potential of anodes under study for oxidation/mineralization of IMA was ranked as BDD > Ti₄O₇ > Pt > DSA. Especially, high current (300 and 500 mA) are not beneficial to the performances of pollutants removal with Ti₄O₇ anode. The results reveal the less contribution of AO to IMA mineralization compared with EF process (except BDD anode), evidencing the dominant role of homogeneous $\cdot\text{OH}$ generated in bulk solution.

However, the TOC removal efficiency in AO process shows that Ti₄O₇ and BDD anodes provide prominent performances for mineralization of IMA solutions due to Ti₄O₇($\cdot\text{OH}$) and BDD($\cdot\text{OH}$) with relative strong oxidation power.

Generally, it can be regarded that, in EF process, the organics are degraded and mineralized via the combined effect of homogeneous $\cdot\text{OH}$ in solution and heterogeneous M($\cdot\text{OH}$) on the anode surface. In order to further explore the effect of anode materials on the contribution of heterogeneous and homogeneous radicals to kinetics decay of IMA and TOC degradation, the corresponding apparent rate constants (k_{app} in min⁻¹) with four kinds of anodes were calculated assuming first-order reaction kinetics and presented in Tables 1 and 2.

Table 2: Apparent rate constants (k_{app}) as a function of anode materials and current applied for TOC degradation in EF and AO processes with CF cathode.

Anode	DSA	Pt	Ti ₄ O ₇	BDD	
	k_{app} (min ⁻¹)				
EF (k_1)	50	0.07	0.11	0.12	0.18
	100	0.09	0.14	0.16	0.28
	200	0.11	0.17	0.26	0.44
	300	0.15	0.22	0.28	0.97
	500	0.16	0.25	0.3	1.7
AO (k_2)	50	0.03	0.04	0.07	0.13
	100	0.05	0.06	0.11	0.19
	200	0.06	0.07	0.16	0.28
	300	0.07	0.08	0.18	0.49
	500	0.08	0.1	0.21	0.69

Here we chose α as the value of $(k_1 - k_2)/k_2$, assuming that there is no other reactions in the process to sketchily reflect the function of $\cdot\text{OH}$ and $\text{M}(\cdot\text{OH})$ with current for kinetics decay of IMA and TOC removal, where k_1 and k_2 represents the apparent rate (k_{app}) in EF and AO process, respectively. Fig. 4(a) shows that generally the value of α decreased with the rising current, suggesting that the effect of heterogeneous $\cdot\text{OH}$ for IMA removal was enhanced with the increasing currents. The results depicted in Fig. 4(b) also illustrate that high applied currents are beneficial to the function of $\cdot\text{OH}$ for removal of IMA. What's more, it can be seen that the function of heterogeneous $\cdot\text{OH}$ for kinetics decay of IMA with Ti_4O_7 anode is better than others. The ability of making contribution to kinetics decay of IMA via heterogeneous $\text{M}(\cdot\text{OH})$ can be ranked as $\text{Pt} > \text{DSA} > \text{Ti}_4\text{O}_7 > \text{BDD}$ under condition of low currents (50 and 100 mA), while with high currents (200, 300 and 500 mA), it would be ranked as $\text{Ti}_4\text{O}_7 > \text{Pt} > \text{DSA} > \text{BDD}$. Fig. 4c shows that for DSA, Pt and Ti_4O_7 anodes, the contribution made by homogeneous $\cdot\text{OH}$ for TOC degradation was the lowest under 100 mA, while its contribution was continuously enhanced with the increasing currents for BDD anode (Fig. 4(c), (d)), which was in agreement with the results presented in Fig. 2. The plots of Fig. 4(d) illustrate that the effect of homogeneous $\cdot\text{OH}$ for TOC removal was the highest with Pt anode under the same condition of current. The analysis of α value provides more information about the contribution made by homogeneous or heterogeneous hydroxyl radicals to oxidation kinetics of IMA and TOC removal of its solution in EF process.

In the EAOPs, high applied currents could generally improve the mineralization efficiency but also at the same time usually lead to the decrease in MCE% because of the intensification of side/wasting reactions and also formation of intermediates hardly oxidizable such as carboxylic acids ^[59]. Therefore, another important parameter is the electrical energy consumption (EC) that will be taken into consideration in comparison of mineralization performance according to the (Eq. (7)). As depicted in Fig. 5, the trend in evolution of EC as a function of time clearly shows that the applied current affects significantly this parameter; it is mostly enhanced as the current increasing from 50 to

500 mA regardless of anode material. The EC values for 500 mA are generally several times higher than that of 50 mA, particularly in the case of DSA and Pt anodes. Ti_4O_7 exhibits a different behavior; although EC curves have similar values for low currents, energy consumption becomes very high at high currents due to the efficiency loss as explained above. As expected from TOC removal effectiveness, the BDD anode consumed the lowest electrical energy per mass unit (g) TOC removal during mineralization of IMA solution.

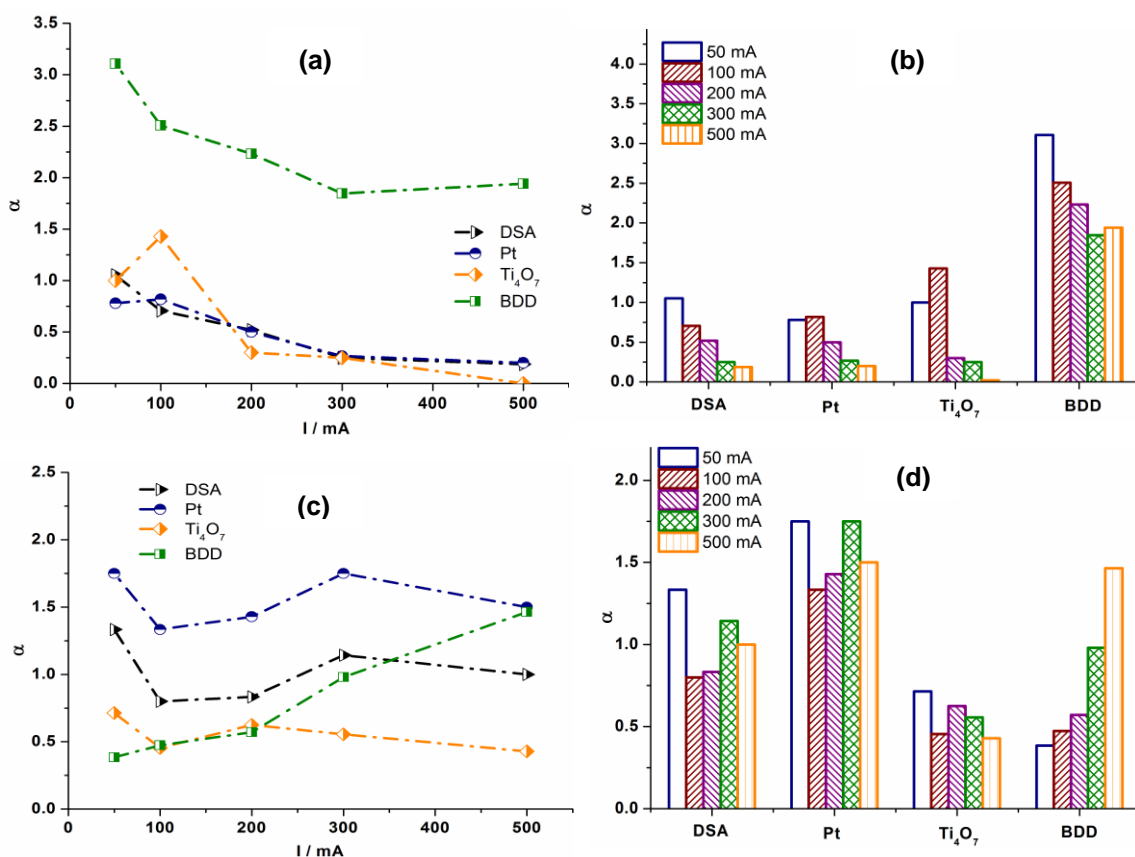


Fig. 4 The function ($\alpha: (k_{EF}-k_{AO})/k_{AO}$) of homogeneous $\cdot OH$ and heterogeneous $\cdot OH$ with current applied for kinetics decay of IMA (a, b) and TOC degradation (c, d) with different anodes.

4.3.3 Identification and evolution of inorganic ions and carboxylic acids during EF degradation of IMA

The complete mineralization of organics in EAOPs is accompanied by the formation of aromatic intermediates, inorganic ions and short chain aliphatic carboxylic acids [60]. During the electrochemical oxidation, the N atoms contained in IMA molecule would be released into the solution as inorganic ions NH_4^+ , NO_3^- and NO_2^- via cleavage of covalent bonds, which can be regarded as an important signal of IMA mineralization.

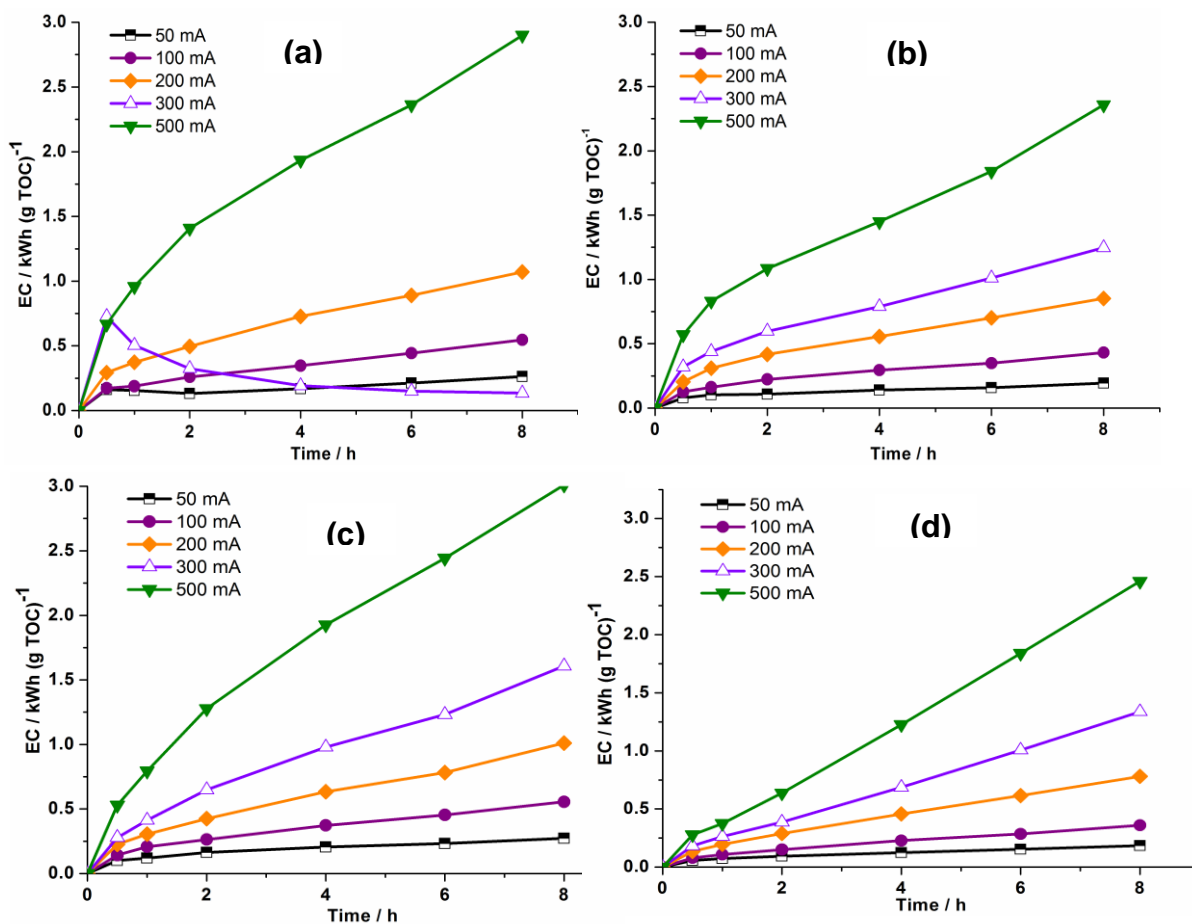


Fig. 5 Effect of applied current on the EC of IMA degradation in EF process with DSA (a), Pt (b), Ti_4O_7 (c) and BDD (d) anode. [IMA]: 0.1 mM, V: 230 mL, $[\text{Fe}^{2+}]$: 0.1 mM, pH 3, $[\text{Na}_2\text{SO}_4]$: 50 mM

The concentration of nitrogen ions evolved with BDD anode was presented in Fig. 6. NO_2^- ion was not detected in the solution. It can be observed that the concentration of NH_4^+ released to the solution is much higher than that of NO_3^- in solution along with the electrolysis time. At the early stage of the experiment, concentration of NH_4^+ and NO_3^- increased quickly and gradually reached to a plateau, with generation of 0.58 mM NH_4^+ and 0.09 mM NO_3^- in the solution. The sum of NH_4^+ and NO_3^- represents 95% of the nitrogen expected for the theoretically complete mineralization of IMA. The little loss in mass balance could be explained with the formation of gaseous nitrogen compounds such as N_2 and N_2O_5 [46]. The relatively high concentration of the NH_4^+ can be related to the progressive cathodic reduction of formed NO_3^- .

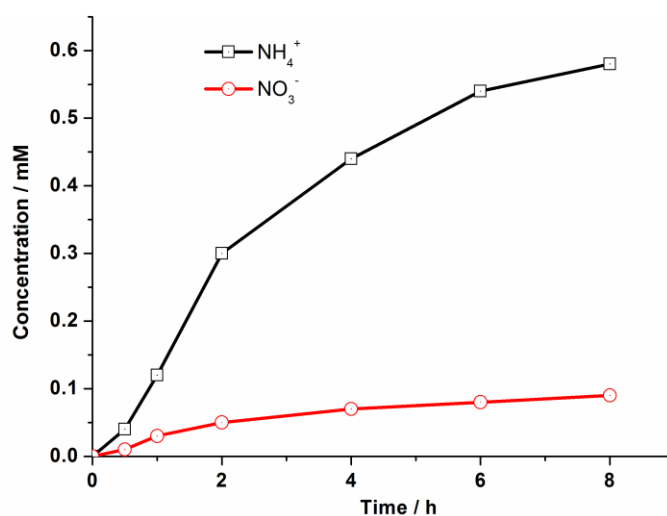


Fig. 6 Time-course of identified inorganic ions (NH_4^+ and NO_3^-) during electrooxidation of 0.1 mM IMA in EF process with BDD anode. V: 230 mL, $[\text{Fe}^{2+}]$: 0.1 mM, pH 3, I: 300 mA, $[\text{Na}_2\text{SO}_4]$: 50 mM (for NO_3^-), $[\text{K}_2\text{SO}_4]$: 50 mM (for NH_4^+ since the presence of Na^+ ion hinders the detection of NH_4^+ in ion chromatography).

The identification and evolution of carboxylic acids during the mineralization of IMA solution with BDD anode in EF process was shown as Fig. 7. The plots illustrate

that five kinds of carboxylic acids were identified and followed with the ion-exclusion chromatography. The well-defined peaks corresponding to oxalic, pyruvic, oxamic, formic and acetic acids were detected at the retention time of 7.0, 8.6, 10.7, 12.4 and 14.9 min, respectively. The concentration of these carboxylic acids accumulated quickly at the early stage of the electrochemical oxidation (60-120 min), and gradually decreased with the electrolysis time. Among which, oxalic acid, the ultimate product of the oxidation of aromatic intermediates [61, 62], was obtained at a maximum concentration during the EF process for IMA mineralization. Also, formic, acetic and oxamic acids reached maximum values at 40, 120 and 60 min, respectively. It is noted that the concentration of formic and oxamic acids were detected as trace level in the EF process with BDD anode at treatment time of 8 h demonstrating high performance of BDD anode in the mineralization of IMA in agreement with the results of TOC removal kinetics (Fig. 7).

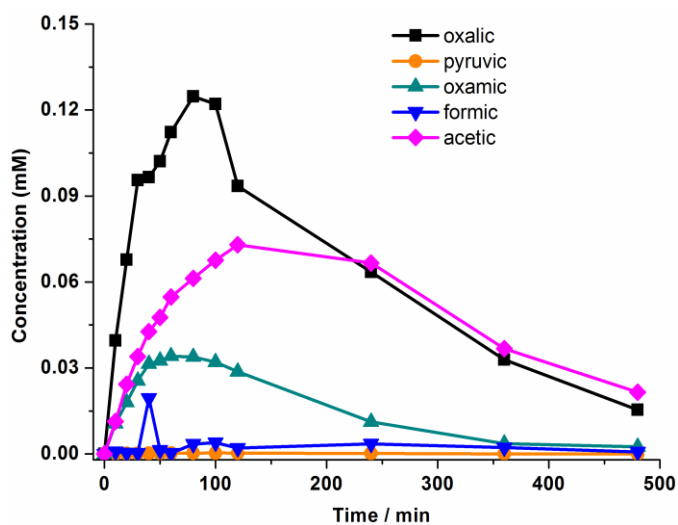
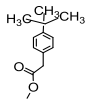
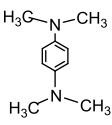
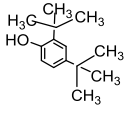


Fig. 7 Identification and evolution of carboxylic acids generated during the process of IMA degradation in EF system with BDD anode. [IMA]: 0.1 mM, V: 230 mL, [Fe²⁺]: 0.1 mM, pH 3, I: 300 mA, [Na₂SO₄]: 50 mM.

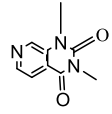
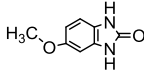
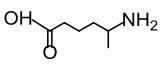
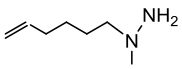
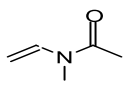
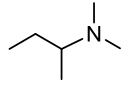
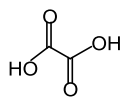
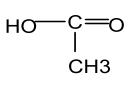
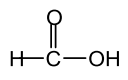
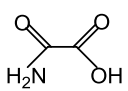
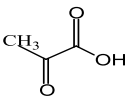
4.3.4. Identification of aromatic intermediates and proposed reaction pathway

The intermediate products formed during mineralization of IMA were detected and identified with GC-MS and HPLC (Table 3) analyses. Based on identified intermediates, a plausible scheme of IMA degradation by hydroxyl radicals generated in EF process with BDD anode has been established (Fig. 8), assuming that the detected products are representative of the complicated mixture of the degradation intermediates. In this way and according to the analysis of detected intermediates, compound (I) was formed from demethylation of the methylamine group of IMA in agreement with the literature [63]. Further attack of $\cdot\text{OH}$ to C-N bond leads to the formation of compounds (II) and (III). These two identified intermediate products are the same as the results reported by Turkay et al. [64]. Subsequent progressive oxidative breaking of aromatic rings generates aliphatic compounds (IV) - (VIII) which then oxidized by $\cdot\text{OH}/\text{M}(\cdot\text{OH})$ to short-chain carboxylic acids [65], which are finally mineralized into CO_2 and water.

Table3: Intermediate products identified using HPLC and GC-MS during the mineralization of IMA with BDD anode in EF process

Compound	Chemical	Molecular mass (g mol^{-1})	Molecular structure	Analytical technique
I	piperazine	86		GC-MS
II	Methyl p-tert-butylphenylacetate	206		GC-MS
III	N,N,N',N'-Tetramethyl-1,4-phenylenediamine	62		GC-MS
IV	2,4-Di-tert-butylphenol	206		GC-MS

Chapter 4 Effect of anode materials on the performance of Electrocatalytic generation of homogeneous and heterogeneous hydroxyl radicals for cold mineralization of anti-cancer drug imatinib

V	Pyrido[3,4-d]pyrimidine-2,4(1H,3H)-dione,1,3-dimethyl-	191		GC-MS
VI	5-methoxy-1,3-dihydrobenzimidazo-1,2-one	164		GC-MS
VII	5-Aminohexanoic acid	131		GC-MS
VIII	1-(5-Hexenyl)-1-methylhydrazine	128		GC-MS
IX	N-ethenyl-N-methylacetamide	99		GC-MS
X	N,N-dimethylbutan-2-amine	101		GC-MS
XI	Oxalic acid	90		HPLC
XII	Acetic acid	60		HPLC
XIII	Formic acid	46		HPLC
XIV	Oxamic acid	89		HPLC
XV	Pyruvic acid	88		HPLC

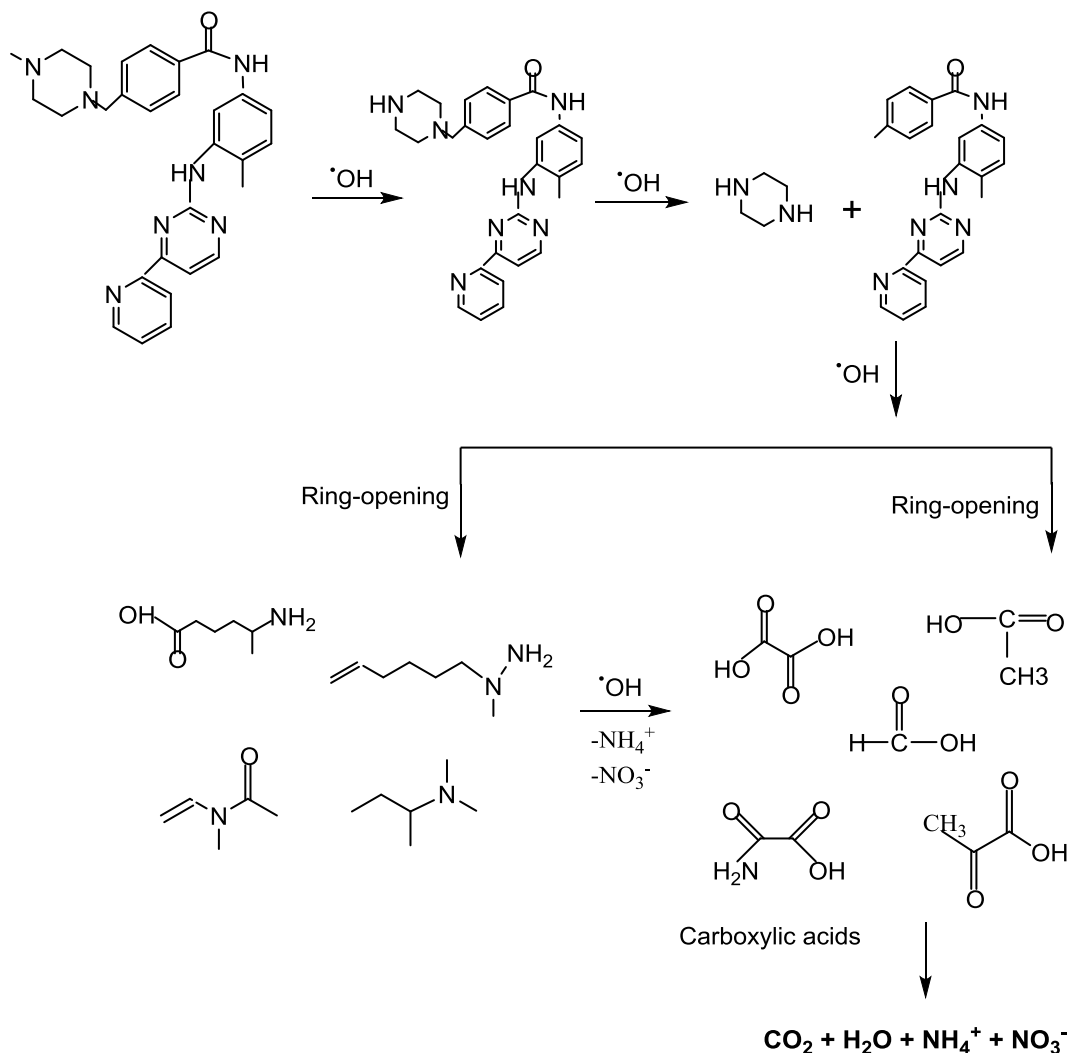


Fig. 8 Proposed degradation pathway for IMA degradation by $\cdot\text{OH}$ radicals generated in EF process with BDD anode.

4.3.5 Assessment of acute toxicity during EF degradation of IMA solution

The evolution of acute toxicity of 0.07 mM (34.5 mg L^{-1}) IMA solution over electrolysis time during EF process with BDD anode at 300 mA was investigated via monitoring the bioluminescence inhibition of *V. fischeri* bacteria using Microtox[®] method. As depicted in Fig. 9, the inhibition percentage increased to a maximum values

at the early electrolysis stages (60-120 min), illustrating the formation of intermediates more toxic than IMA [25]. The bioluminescence inhibition percentage increased up to 100% at 60 min, whereafter, it decreased with the electrolysis time. The inhibition profile in Fig. 9 shows that the maximum inhibition value was followed by a sharp decrease, with obtaining minimum value of 3.6% (after 15 min exposition) after 120 min of the electrolysis time. The drastic decay in toxicity was owing to the further mineralization of toxic intermediates into the non-toxic compounds in agreement with the TOC decay results depicted in Fig. 9. The data of toxicity evolution of IMA solution with BDD anode demonstrates again the high oxidation and mineralization performance of BDD anode for wastewater treatment.

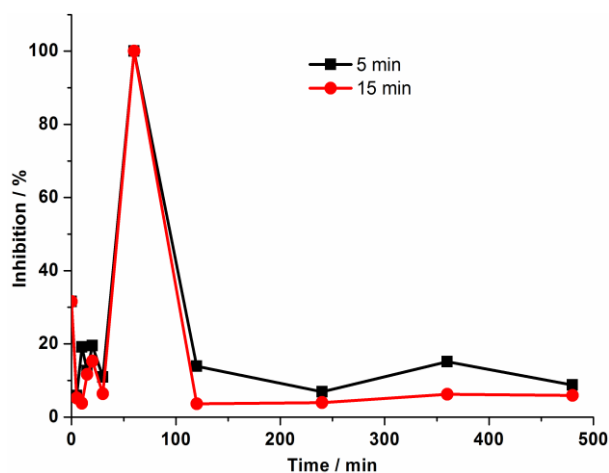


Fig. 9 Evolution of acute toxicity of IMA solution during EF treatment with BDD anode at 300 mA. The toxicity is expressed as the inhibition of luminescence of *V. fischeri* bacteria after 5 min and 15 min exposure time. V: 230 mL, $[\text{Fe}^{2+}]$: 0.1 mM, pH 7, I: 300 mA, $[\text{Na}_2\text{SO}_4]$: 50 mM.

4.4 Conclusions

The comparative efficiency of different anode materials, i.e., DSA, Pt, Ti_4O_7 and BDD, for advanced oxidation processes EF and AO were systematically investigated taking the anti-cancer drug IMA as target pollutant. The kinetics decay of IMA

illustrated a little difference with four anodes; however high currents (300 mA and 500 mA) were not advantageous to oxidation efficiency with Ti_4O_7 anode. Significantly better mineralization efficiencies (in terms of TOC removal percentage) were observed with BDD anode attaining complete TOC removal at 4 h (EF process) and 6 h (AO process) under 500 mA. The analysis of $\alpha ((k_{EF}-k_{AO})/k_{AO})$ value indicated that Ti_4O_7 is a potential anode for generating heterogeneous $\text{Ti}_4\text{O}_7(\cdot\text{OH})$ in AO process under low current. The homogeneous $\cdot\text{OH}$ plays the major role for TOC degradation with Pt anode. Formation and evolution of carboxylic acids and aromatic intermediates during electrolysis were assessed. Almost complete release of organic N as inorganic ions (NH_4^+ and NO_3^-) into solution and removal of acute toxicity also confirmed the outstanding behavior of BDD anode for effective treatment of wastewater contaminated by persistent organic pollutants.

Acknowledgement

This work was financially supported by Key Project of Natural Science Foundation of Tianjin (no. 16JCZDJC39300), Natural Science Foundation of China (nos. 21773129, 21811530274, 91545126 and 21273120), National Key Research and Development Program of China (2016YFC0400706), 111 program, Ministry of Education, China (T2017002) and Fundamental Research Funds for the Central Universities. This work was supported by the China Scholarship Council (CSC) [grant number 201706205095].

References

- [1] Hester R E, Harrison R M, Pharmaceuticals in the Environment, Royal Society of Chemistry 2015.
- [2] Huerta-Fontela M, Galceran M T, Ventura F, et al. Occurrence and removal of pharmaceuticals and hormones through drinking water treatment[J]. Water research, 2011, 45: 1432-1442.
- [3] Jelic A, Gros M, Ginebreda A, et al. Occurrence, partition and removal of pharmaceuticals in sewage water and sludge during wastewater treatment[J]. Water research, 2011, 45: 1165-1176.
- [4] Richardson S D, et al. Water analysis: emerging contaminants and current issues[J]. Analytical chemistry, 2009, 81: 4645-4677.

- [5] Sangion A, Gramatica P, et al. Hazard of pharmaceuticals for aquatic environment: prioritization by structural approaches and prediction of ecotoxicity[J]. *Environment international*, 2016, 95: 131-143.
- [6] Kaur A, Umar A, Kansal S K, et al. Heterogeneous photocatalytic studies of analgesic and non-steroidal anti-inflammatory drugs[J]. *Applied Catalysis A: General*, 2016, 510: 134-155.
- [7] Kanakaraju D, Glass B D, Oelgemöller M, et al. Titanium dioxide photocatalysis for pharmaceutical wastewater treatment[J]. *Environmental Chemistry Letters*, 2014, 12: 27-47.
- [8] Khetan S K, Collins T J, et al. Human pharmaceuticals in the aquatic environment: a challenge to green chemistry[J]. *Chemical reviews*, 2007, 107: 2319-2364.
- [9] Kanakaraju D, Glass B D, Oelgemöller M, et al. Advanced oxidation process-mediated removal of pharmaceuticals from water: A review[J]. *Journal of environmental management*, 2018, 219: 189-207.
- [10] Villar-Navarro E, Baena-Nogueras R M, Paniw M, et al. Removal of pharmaceuticals in urban wastewater: High rate algae pond (HRAP) based technologies as an alternative to activated sludge based processes[J]. *Water research*, 2018, 139: 19-29.
- [11] Brodin T, Fick J, Jonsson M, et al. Dilute concentrations of a psychiatric drug alter behavior of fish from natural populations[J]. *Science*, 2013, 339: 814-815.
- [12] Guo C, Zhang T, Hou S, et al. Investigation and application of a new passive sampling technique for in situ monitoring of illicit drugs in waste waters and rivers[J]. *Environmental science & technology*, 2017, 51: 9101-9108.
- [13] Caracciolo A B, Topp E, Grenni P, et al. Pharmaceuticals in the environment: biodegradation and effects on natural microbial communities. A review[J]. *Journal of pharmaceutical and biomedical analysis*, 2015, 106: 25-36.
- [14] Verlicchi P, Al Aukidy M, Zambello E, et al. Occurrence of pharmaceutical compounds in urban wastewater: removal, mass load and environmental risk after a secondary treatment—a review[J]. *Science of the total environment*, 2012, 429: 123-155.
- [15] Rivera-Utrilla J, Sánchez-Polo M, Ferro-García M, et al. Pharmaceuticals as emerging contaminants and their removal from water. A review[J]. *Chemosphere*, 2013, 93: 1268-1287.
- [16] Pala L, Bergamini C, Imbimbo M, et al. Safety of combination treatment with imatinib mesylate, carboplatin, and cetuximab in a patient with multiple cancers: a case report[J]. *Tumori Journal*, 2016, 102: S1-S2.
- [17] Klančar A, Trontelj J, Kristl A, et al. An advanced oxidation process for wastewater treatment to reduce the ecological burden from pharmacotherapy and the agricultural use of pesticides[J]. *Ecological Engineering*, 2016, 97: 186-195.
- [18] Castiglioni S, Bagnati R, Calamari D, et al. A multiresidue analytical method using solid-phase extraction and high-pressure liquid chromatography tandem mass spectrometry to measure pharmaceuticals of different therapeutic classes in urban wastewaters[J]. *Journal of Chromatography*

Chapter 4 Effect of anode materials on the performance of Electrocatalytic generation of homogeneous and heterogeneous hydroxyl radicals for cold mineralization of anti-cancer drug imatinib

A, 2005, 1092: 206-215.

[19] Westerhoff P, Yoon Y, Snyder S, et al. Fate of endocrine-disruptor, pharmaceutical, and personal care product chemicals during simulated drinking water treatment processes[J]. *Environmental science & technology*, 2005, 39: 6649-6663.

[20] Bolong N, Ismail A, Salim M R, et al. A review of the effects of emerging contaminants in wastewater and options for their removal[J]. *Desalination*, 2009, 239: 229-246.

[21] Kyzas G Z, Deliyanni E A, Matis K A, et al. Graphene oxide and its application as an adsorbent for wastewater treatment[J]. *Journal of Chemical Technology & Biotechnology*, 2014, 89: 196-205.

[22] Paranj S, Rajasekaran M, Ganesan S, et al. Biodegradation of the endocrine disrupting chemical o-phenylenediamine using intracellular enzymes from *Citrobacter freundii* and its kinetic studies[J]. *Journal of Chemical Technology & Biotechnology*, 2016, 91: 171-183.

[23] Sopaj F, Rodrigo M A, Oturan N, et al. Influence of the anode materials on the electrochemical oxidation efficiency. Application to oxidative degradation of the pharmaceutical amoxicillin[J]. *Chemical Engineering Journal*, 2015, 262: 286-294.

[24] Sirés I, Brillas E, et al. Remediation of water pollution caused by pharmaceutical residues based on electrochemical separation and degradation technologies: A review[J]. *Environment International*, 2012, 40: 212-229.

[25] Dirany A, Sirés I, Oturan N, et al. Electrochemical treatment of the antibiotic sulfachloropyridazine: kinetics, reaction pathways, and toxicity evolution[J]. *Environmental science & technology*, 2012, 46: 4074-4082.

[26] Oturan M A, Aaron J-J, et al. Advanced oxidation processes in water/wastewater treatment: principles and applications. A review[J]. *Critical Reviews in Environmental Science and Technology*, 2014, 44: 2577-2641.

[27] Brillas E, Sirés I, Oturan M A, et al. Electro-Fenton process and related electrochemical technologies based on Fenton's reaction chemistry[J]. *Chemical reviews*, 2009, 109: 6570-6631.

[28] Esplugas S, Gimenez J, Contreras S, et al. Comparison of different advanced oxidation processes for phenol degradation[J]. *Water research*, 2002, 36: 1034-1042.

[29] Mousset E, Weiqi V H, Kai B F Y, et al. A new 3D-printed photoelectrocatalytic reactor combining the benefits of a transparent electrode and the Fenton reaction for advanced wastewater treatment[J]. *Journal of Materials Chemistry A*, 2017, 5: 24951-24964.

[30] Martinez-Huitle C A, Ferro S, et al. Electrochemical oxidation of organic pollutants for the wastewater treatment: direct and indirect processes[J]. *Chemical Society*

Reviews, 2006, 35: 1324-1340.

- [31] Ganiyu S O, Zhou M, Martínez-Huitle C A, et al. Heterogeneous electro-Fenton and photoelectro-Fenton processes: A critical review of fundamental principles and application for water/wastewater treatment[J]. Applied Catalysis B Environmental, 2018,
- [32] Sirés I, Brillas E, Oturan M A, et al. Electrochemical advanced oxidation processes: today and tomorrow. A review[J]. Environmental Science and Pollution Research, 2014, 21: 8336-8367.
- [33] Ganiyu S O, Dos Santos E V, De Araújo Costa E C T, et al. Electrochemical advanced oxidation processes (EAOPs) as alternative treatment techniques for carwash wastewater reclamation[J]. Chemosphere, 2018, 211: 998-1006.
- [34] Panizza M, Cerisola G, et al. Direct and mediated anodic oxidation of organic pollutants[J]. Chemical reviews, 2009, 109: 6541-6569.
- [35] Panizza M, Cerisola G, et al. Application of diamond electrodes to electrochemical processes[J]. Electrochimica Acta, 2005, 51: 191-199.
- [36] Panizza M, Michaud P, Cerisola G, et al. Anodic oxidation of 2-naphthol at boron-doped diamond electrodes[J]. Journal of Electroanalytical Chemistry, 2001, 507: 206-214.
- [37] Zhou M, Oturan M A, Sirés I, Electro-Fenton Process: New Trends and Scale-Up, Springer 2017.
- [38] Sáez C, López-Vizcaíno R, Cañizares P, et al. Conductive-diamond electrochemical oxidation of surfactant-aided soil-washing effluents[J]. Industrial & Engineering Chemistry Research, 2010, 49: 9631-9635.
- [39] Nidheesh P, Gandhimathi R, et al. Electro Fenton oxidation for the removal of Rhodamine B from aqueous solution in a bubble column reactor under continuous mode[J]. Desalination and Water Treatment, 2015, 55: 263-271.
- [40] Mousset E, Wang Z, Lefebvre O, et al. Electro-Fenton for control and removal of micropollutants—process optimization and energy efficiency[J]. Water Science and Technology, 2016, wst2016353.
- [41] Olvera-Vargas H, Wee Yong Han V, Garcia-Rodriguez O, et al. Near-neutral electro-Fenton treatment of pharmaceutical pollutants: the effect of triphosphate ligand and BDD electrode[J]. ChemElectroChem,
- [42] Olvera-Vargas H, Rouch J-C, Coetsier C, et al. Dynamic cross-flow electro-Fenton process coupled to anodic oxidation for wastewater treatment: Application to the degradation of acetaminophen[J]. Separation and Purification Technology, 2018, 203: 143-151.
- [43] Mousset E, Oturan N, Oturan M A, et al. An unprecedented route of \bullet OH radical reactivity: ipso-substitution with perhalogenocarbon compounds[J]. Applied Catalysis B: Environmental, 2018, 226: 135-156.
- [44] Feng L, Van Hullebusch E D, Rodrigo M A, et al. Removal of residual anti-inflammatory and analgesic pharmaceuticals from aqueous systems by electrochemical advanced oxidation processes.

Chapter 4 Effect of anode materials on the performance of Electrocatalytic generation of homogeneous and heterogeneous hydroxyl radicals for cold mineralization of anti-cancer drug imatinib

- A review[J]. *Chemical Engineering Journal*, 2013, 228: 944-964.
- [45] Altun Y, Dogan-Topal B, Uslu B, et al. Anodic behavior of sertindole and its voltammetric determination in pharmaceuticals and human serum using glassy carbon and boron-doped diamond electrodes[J]. *Electrochimica Acta*, 2009, 54: 1893-1903.
- [46] Sopaj F, Oturan N, Pinson J, et al. Effect of the anode materials on the efficiency of the electro-Fenton process for the mineralization of the antibiotic sulfamethazine[J]. *Applied Catalysis B: Environmental*, 2016, 199: 331-341.
- [47] Rodrigo M, Michaud P, Duo I, et al. Oxidation of 4-chlorophenol at boron-doped diamond electrode for wastewater treatment[J]. *Journal of the Electrochemical Society*, 2001, 148: D60-D64.
- [48] Santos J E L, De Moura D C, Da Silva D R, et al. Application of TiO₂-nanotubes/PbO₂ as an anode for the electrochemical elimination of acid red 1 dye[J]. *Journal of Solid State Electrochemistry*, 2018, 1-10.
- [49] Zaky A M, Chaplin B P, et al. Mechanism of p-substituted phenol oxidation at a TiO₂ reactive electrochemical membrane[J]. *Environmental science & technology*, 2014, 48: 5857-5867.
- [50] zcan A, Şahin Y, Koparal A S, et al. Protham mineralization in aqueous medium by anodic oxidation using boron-doped diamond anode: Influence of experimental parameters on degradation kinetics and mineralization efficiency[J]. *Water Research*, 2008, 42: 2889-2898.
- [51] Chen X, Chen G, et al. Anodic oxidation of Orange II on Ti/BDD electrode: Variable effects[J]. *Separation and Purification Technology*, 2006, 48: 45-49.
- [52] Escalona-Durán F, Villegas-Guzman P, Dos Santos E V, et al. Intensification of petroleum elimination in the presence of a surfactant using anodic electrochemical treatment with BDD anode[J]. *Journal of Electroanalytical Chemistry*, 2019, 832: 453-458.
- [53] Geng P, Su J, Miles C, et al. Highly-Ordered Magn₂TiO₇ Nanotube Arrays as Effective Anodic Material for Electro-oxidation[J]. *Electrochimica Acta*, 2015, 153: 316-324.
- [54] Bejan D, Guinea E, Bunce N J, et al. On the nature of the hydroxyl radicals produced at boron-doped diamond and Ebonex® anodes[J]. *Electrochimica Acta*, 2012, 69: 275-281.
- [55] Ganiyu S O, Oturan N, Raffy S, et al. Sub-stoichiometric titanium oxide (TiO₂) as a suitable ceramic anode for electrooxidation of organic pollutants: A case study of kinetics, mineralization and toxicity assessment of amoxicillin[J]. *Water research*, 2016, 106: 171-182.
- [56] Ganiyu S O, Oturan N, Raffy S, et al. Use of sub-stoichiometric titanium oxide as a ceramic electrode in anodic oxidation and electro-Fenton degradation of the beta-blocker propranolol: degradation kinetics and mineralization pathway[J]. *Electrochimica Acta*, 2017, 242: 344-354.
- [57] Yang W, Zhou M, Liang L, et al. Highly efficient in-situ metal-free electrochemical advanced oxidation process using graphite felt modified with N-doped graphene[J]. *Chemical Engineering Journal*, 2018, 338: 700-708.
- [58] Yang W, Zhou M, Cai J, et al. Ultrahigh yield of hydrogen peroxide on graphite felt cathode modified with electrochemically exfoliated graphene[J]. *Journal of Materials Chemistry A*, 2017, 5:

8070-8080.

- [59] Oturan N, Ganiyu S O, Raffy S, et al. Sub-stoichiometric titanium oxide as a new anode material for electro-Fenton process: application to electrocatalytic destruction of antibiotic amoxicillin[J]. *Applied Catalysis B: Environmental*, 2017, 217: 214-223.
- [60] Diagne M, Oturan N, Oturan M A, et al. Removal of methyl parathion from water by electrochemically generated Fenton's reagent[J]. *Chemosphere*, 2007, 66: 841-848.
- [61] Oturan M A, Pimentel M, Oturan N, et al. Reaction sequence for the mineralization of the short-chain carboxylic acids usually formed upon cleavage of aromatics during electrochemical Fenton treatment[J]. *Electrochimica Acta*, 2008, 54: 173-182.
- [62] Brillas E, Garcia-Segura S, Skoumal M, et al. Electrochemical incineration of diclofenac in neutral aqueous medium by anodic oxidation using Pt and boron-doped diamond anodes[J]. *Chemosphere*, 2010, 79: 605-612.
- [63] Barhoumi N, Olvera-Vargas H, Oturan N, et al. Kinetics of oxidative degradation/mineralization pathways of the antibiotic tetracycline by the novel heterogeneous electro-Fenton process with solid catalyst chalcopyrite[J]. *Applied Catalysis B: Environmental*, 2017, 209: 637-647.
- [64] Turkay O, Barışçı S, Ulusoy E, et al. Anodic oxidation of anti-cancer drug Imatinib on different electrodes: Kinetics, transformation by-products and toxicity assessment[J]. *Electrochimica Acta*, 2018, 263: 400-408.
- [65] Almeida L C, Garcia-Segura S, Bocchi N, et al. Solar photoelectro-Fenton degradation of paracetamol using a flow plant with a Pt/air-diffusion cell coupled with a compound parabolic collector: process optimization by response surface methodology[J]. *Applied Catalysis B: Environmental*, 2011, 103: 21-30.

Chapter 5: Highly efficient in-situ metal-free electrochemical advanced oxidation process using graphite felt modified with N-doped graphene

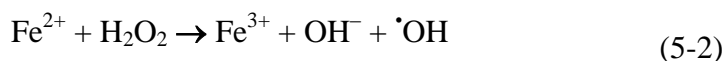
Abstract:

Developing highly efficient carbon based catalyst for electrochemical advanced oxidation processes (EAOPs) application is significant for environmental remediation. Herein, for the first time, the in-situ metal-free EAOPs with graphite felt cathode modified by N-doped graphene (N-EEGr) was established and demonstrated a superior and reusable catalytic activity for activation of H_2O_2 to $\cdot\text{OH}$. N-EEGr-GF was systematically characterized, and its electrocatalytic behavior for oxygen reduction reaction as well as the degradation performance were investigated. N-doping was found not changing the electrochemical generation of H_2O_2 , but increasing the catalytic decomposition with a doubled phenol degradation rate. ESR spectra, methanol and benzoquinone capture confirmed the existence of $\cdot\text{OH}$ and $\cdot\text{O}_2$ in EAOPs, while the former played the dominant role. Compared with traditional electro-Fenton (EF), this in-situ metal-free EAOP demonstrated 4-times higher efficiencies with a more broad suitability upon pH. In view of its competitive advantage in reusability and environmental friendliness without catalysts addition and second pollution, this process can be regarded as the competent substitution of traditional EF for wastewater treatment. This study illustrated insights into the versatile N-EEGr for sustainable activation of H_2O_2 to $\cdot\text{OH}$ and may shed light on the development of remarkable catalyst for highly efficient metal-free EAOPs.

Keywords: N-doped graphene; catalytic activity; metal-free electrochemical advanced oxidation processes; in-situ activation; graphite felt modification

5.1 Introduction

Numerous innovative and comprehensive researches provide an extensive understanding on traditional and advanced techniques used for water and wastewater treatment [1-5]. Among these methods, advanced oxidation processes (AOPs) are usually applied to remove refractory organic pollutants whenever conventional oxidation techniques are inefficient and insufficient, thereby requiring the consumption of excessive reactants that makes the treatment far less cost-affordable [4, 6-8]. Thanks to the in-situ electrochemical generation of reactants including powerful hydroxyl radicals ($\cdot\text{OH}$), electrochemical advanced oxidation processes (EAOPs) have attracted ever-increasing attention because of their advantages of high-efficiency, environmental friendliness and economic feasibility [9]. In particular, electro-Fenton (EF) has been one of the most popular EAOPs, in which H_2O_2 generated by oxygen cathodic reduction (eq. 1) reacts with the added Fe^{2+} to form powerful $\cdot\text{OH}$ (eq. 2) [4, 10, 11].



Over the past decades, EF has demonstrated remarkable potential for the decontamination of organic pollutants such as toxic and persistent pesticides, synthetic dyes, pharmaceuticals and personal care products (PPCPs) and various industrial pollutants [6, 12-16]. Cathode material is confirmed to be one of the most important parameters affecting EF performance since it determines the electrochemical generation of H_2O_2 through oxygen reduction reaction (ORR) [17, 18]. Besides air diffusion cathodes with high yield of H_2O_2 [19, 20], graphite felt is perhaps one of the most widely studied carbonaceous cathodes due to the special advantages such as high H_2 evolution over-potential, low cost and non-toxicity [6]. Though great efforts have been devoted to improve cathode efficiency by electrochemical/chemical modification or nano-structured doping [21-25], there are still two intrinsic drawbacks seemed unavoidable for EF.

One is the optimal pH range for EF is very limited as narrow as 2.5-3.5 (probably near 3), avoiding the formation of coagulation at high pH condition and some side effects in strong acid medium [26-30]. This would increase the treatment cost.

Secondly, the production of iron sludge is another big issue as second pollution, though many attempts have been made to solve this practical problem [22, 30, 31]. Heterogeneous catalyst such as iron minerals or transition metal ions on solid supports usually suffer from catalyst falling off or dissolution, leading to the cathode activity inactivation and metal ions pollution [10]. Recently, it has been reported that carbon material could be efficient catalyst for decomposition of the added H₂O₂ toward [•]OH [32]. Therefore, to overcome the aforementioned two drawbacks existing in traditional EF and improve the eco-friendliness of EAOPs, developing highly efficient metal-free carbon based catalyst for the in-situ generation of free radicals from the decomposition of electrochemical generated H₂O₂ would be more promising for application, though still is a big challenge.

Herein, for the first time, an efficient in-situ metal-free EAOPs for organic pollutant degradation was established based on the graphite felt cathode modified with N-doped graphene (N-EEGr-GF), which provided ultrahigh yield of H₂O₂ (6.2 mg h⁻¹ cm⁻²) in ORR. The N-EEGr was synthesized via calcination of ammonium nitrate and graphene (EEGr) derived from electrochemical exfoliation of graphite foil. Such in-situ metal-free EAOPs exhibited a more wide suitability on pH, and higher efficiency compared with traditional EF, while without iron sludge production and additional catalysts except for cheap air, therefore N-EEGr-GF should be a promising cathode material in the development of metal-free EAOPs for environmental remediation.

5.2 Experimental

5.2.1 Synthesis of N-EEGr

Ammonium nitrate was selected as nitrogen resource for N-EEGr. The EEGr was derived from electrochemical exfoliation of graphite foil [21], and was mixed with ammonium nitrate (mass ratio 1:1) in ethanol solution, stirring for 30 min and then was heated at 55 °C to evaporate ethanol. Finally, the dried mixed powder was calcinated at 360 °C for 1 h in a furnace under nitrogen atmosphere. The obtained N-EEGr was used to modify GF cathode for high yield of in-situ H₂O₂ generation in EAOPs. Details about the preparation of EEGr-GF, N-EEGr-GF electrodes and electrochemical detections are presented in supporting information.

5.2.2 Physical Characterization

The morphology of N-EEGr was analyzed by scanning electron microscopy (SEM) (LEO-1530VP, Germany). Raman spectra were determined with a Renish Modular Raman spectrometer equipped with a Stellar Pro Argon-ion laser at 514 nm (50 mW). X ray diffraction (XRD) (XRD-7000, Shimadzu) and X-ray photoelectron spectroscopy (XPS) (Krato-ultra DLD, Shimadzu) using Mono Al Ka radiation ($h\nu = 1486.7$ eV) were used to detect the crystalline structure of N-EEGr.

5.2.3 Electrochemical Measurements

Rotating disk electrode (RDE) was used to detect the oxygen reduction activity of N-EEGr in saturated O₂ solution at a scan rate of 20 mV s⁻¹ by AUTOLAB (PGSTAT100) with saturated calomel reference electrode (SCE). Electron transfer numbers were calculated according to the slopes of the Koutecky-Levich plots to determine the selectivity for H₂O₂ production.^[33]

$$\frac{1}{J} = \frac{1}{J_k} + \frac{1}{Bw^{\frac{1}{2}}} \quad (5-3)$$

$$B = 0.62nFA\nu^{\frac{1}{6}}C_{O_2}D_{O_2}^{\frac{2}{3}} \quad (5-4)$$

Where J and J_k are the detected current density and kinetic current density, respectively (mA cm⁻²), w is the angular velocity (rad s⁻¹), n is the electron transfer numbers, F represents the Faraday constant (96485 C mol⁻¹), C_{O_2} is the bulk concentration of O₂ (1.2×10⁻⁶ mol cm⁻³), D_{O_2} is the diffusion coefficient of O₂ in the electrolyte solution (1.9×10⁻⁵ cm² s⁻¹) and ν is the kinematic viscosity (0.01 cm² s⁻¹).

5.2.4 Catalytic Activity Measurements

The performance of N-EEGr-GF was tested in a 100 mL reactor containing 50 mg L⁻¹ phenol. The anode and cathode were DSA (2.5×5 cm²) and N-EEGr-GF electrode (2.5×4 cm²), with a distance of 1 cm. The concentration of phenol was analyzed by HPLC (U3000, Thermo Scientific, USA, C18 column, 5 μm, φ4.6×250 mm) with diode array detector (wavelengths at 270 nm). The analytical conditions were as follows: the mobile-phase was 60% methanol and 40% water with a flow rate of 0.3 mL min⁻¹. The degradation of phenol with different electrode was also

evaluated by the pseudo-first-order reaction rate constant (k).

Besides, electron spin resonance (ESR) was used to detect the existence of free radicals with 5,5-dimethyl-1-pyrroline N-oxide (DMPO) as trapping agent [32]. The sample of 0.32 mL was mixed with 0.08 mL DMPO (4:1) thoroughly for 30 s and then transferred to a capillary tube for detection. For quantitative calculating of $\cdot\text{OH}$ produced by electrodes, dimethyl sulfoxide (DMSO) trapping and 2,4-dinitrophenylhydrazine (DNPH) were used to form a kind of corresponding hydrazone (HCHO-DNPH) and detected by HPLC (U3000, Thermo Scientific, USA, C18 column, 5 μm , $\phi 4.6 \times 250$ mm) with a diode array detector (wavelengths at 355 nm) [34, 35]. Methanol and water (60:40, v/v) was selected as the mobile phase with a flow rate of 0.3 mL min^{-1} .

5.3 Results and discussion

5.3.1. Material characterization

Figure 1a presents the SEM images of EEGr (inset) and N-EEGr, both are thin sheet with several crumpled layers. The surface of N-EEGr was a little flat and smooth than that of EEGr, which was due to the reduction of some oxygen functional groups in EEGr during calcination under nitrogen atmosphere [36]. The XRD characterization showed that EEGr was oxidized during electrochemical exfoliation because of the presence of peak at $2\theta = 12.3^\circ$ (Figure 1b). Conversely, it was disappeared in N-EEGr, indicating that EEGr was further reduced due to the calcination under nitrogen atmosphere [36, 37]. Raman spectrum of the samples revealed two peaks at around 1350 (D band) and 1582 cm^{-1} (G band), which are typical characteristics of graphene (Figure 1c). Moreover, the I_D/I_G ratios of EEGr and N-EEGr were detected to be 0.52 and 0.67, respectively, showing that I_D/I_G increased due to the reduction and nitrogen doping [38], which was similar to the results in literature [37]. Therefore the defective degree of N-EEGr was higher than EEGr, possibly because of the interruption caused by nitrogen doping on the well-ordered sp^2 -hybridized graphene [39].

Figure 1d shows the XPS spectrum of EEGr and N-EEGr samples, with C/O ratios of 20.6 and 35.4, respectively. N 1s peaks around the binding energy of 400 eV were detected for the two samples, presenting 0.42 and 1.49 at% N doping, which was

similar to NG-20 (0.5-1.8 at%) in report [39]. It should be noted that the N content in EEGr was derived from raw graphite foil. Figure 1e and f indicate the fitted three types of N doping including graphitic N, pyrrolic N and pyridinic N [36]. It could be seen that after N-doping pyridinic N increased but graphitic N decreased in N-EEGr, which indicated that the calcination at low temperature is not able to incorporate N into the graphitic carbon frameworks and change the bulk structure of EEGr, so more portion of the N located at defective sites with only surface modification [40]. The much higher content of pyridinic N and pyrrolic N in N-EEGr at defective sites were attributed to the remarkable activity [41, 42]. This result was consistent with the literature reported, in which a 7.8-fold of activity was achieved with only 0.88 at% N doping level [43].

5.3.2. Activity towards ORR

CV measurement was performed to analyze the electrocatalytic activity of EEGr and N-EEGr under constant potential reduction. The characteristic reduction peaks current at - 0.27 V ~ - 0.32 V changed little after N-doping, confirming that the rate of electrochemical reduction of N-EEGr was close to that of EEGr [44]. Typical LSV curves of EEGr and N-EEGr in an oxygen-saturated 0.05 M Na₂SO₄ electrolyte are shown in Figure 2b and 2c. The current curves presented a typical increase with the rotation rate due to the shortened diffusion layer [33]. Analysis of the inset Koutecky-Levich plots indicated two-electron process of the ORR on EEGr (n=2.6) and N-EEGr (n=2.7), with H₂O₂ as the main product, proving that N-doping did not change the electron transfer routes of ORR.

5.3.3. Characterization of modified electrode

Composite electrodes (EEGr-GF and N-EEGr-GF) were further prepared as cathodes in EAOPs, using the developed EEGr and N-EEGr above. Compared with GF (Figure S2), the clean fiber structure was coated with a large number of particles on the two electrodes (Figure 3a and 3b), and the particles on N-EEGr-GF (insert figure in Figure 3b) were much uniform than the ones on EEGr-GF (insert figure in Figure 3a). As shown in nitrogen adsorption isotherms in Figure 1c, the hysteresis loop on N-EEGr-GF was a little narrower than the EEGr-GF electrode, indicating a lower surface area and pore volume obtained after N doping on EEGr. The BET surface area and pore volume of N-EEGr-GF electrode were 8.51 m² g⁻¹ and 0.028

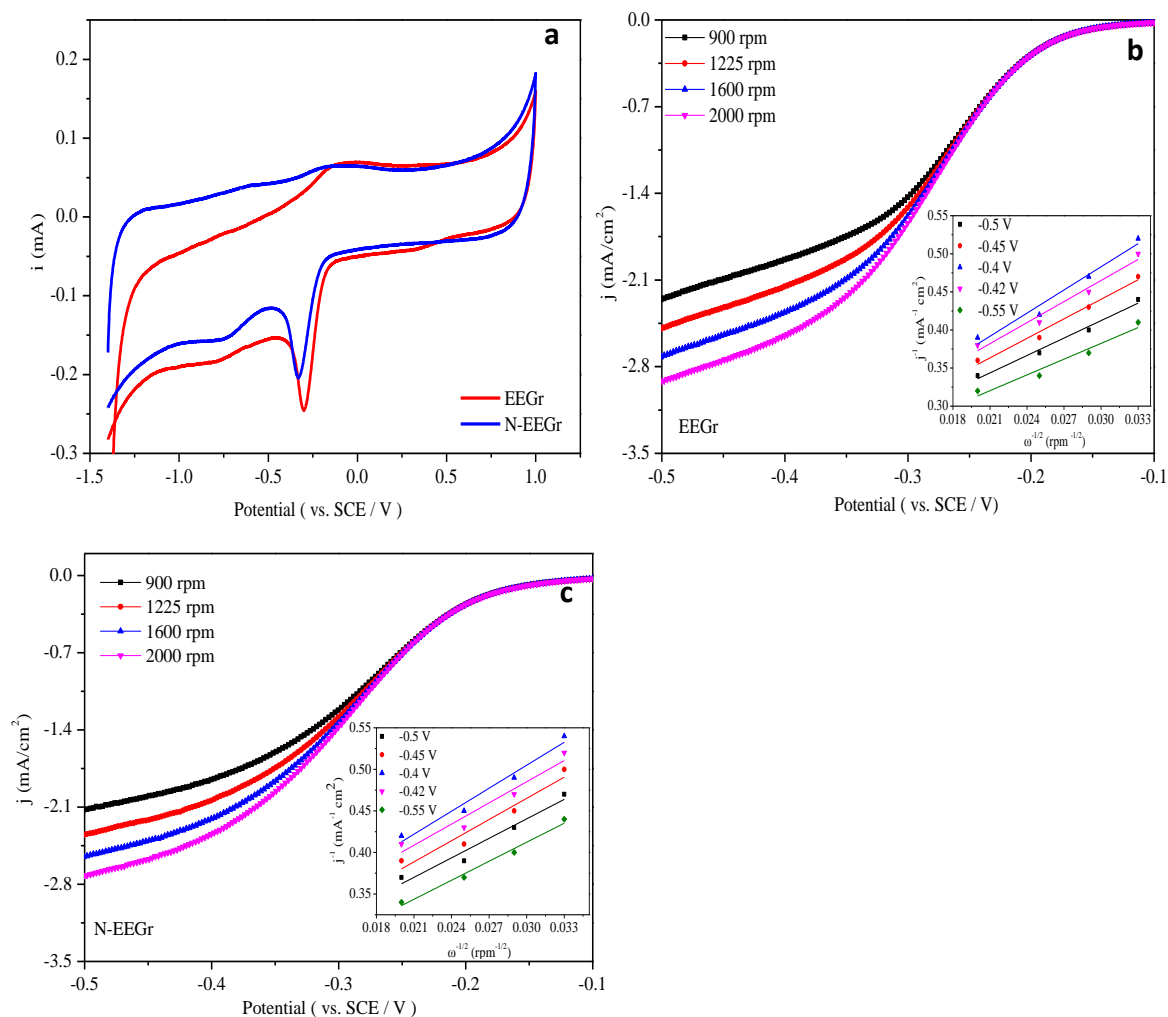


Fig. 2 Cyclic voltammograms of EEGr and N-EEGr (a); The Linear sweep voltammetry of EEGr (b) and N-EEGr (c) in O_2 saturated Na_2SO_4 solution at a scan rate of 20 mV s^{-1} with RDE. Inset: K-L plots at different potentials.

Electroactive surface area is directly correlated to the surface chemistry of carbon-based electrodes^[45, 46]. Figure 3d shows that the peak current of EEGr-GF was a little higher than N-EEGr-GF. According to eq. S1, the electroactive surface area of EEGr-GF was calculated to be 90 cm^2 , which was 1.3-fold of N-EEGr-GF, thus leading to a higher rate of electrochemical reactions on the cathode.

In order to explore the effect of N-doping on the conductivity of N-EEGr-GF, electrochemical impedance spectroscopy (EIS) of EEGr-GF and N-EEGr-GF are shown in Figure 3e, the intercepts of the semicircle with X-axis indicate the resistance

of the two electrodes were similar, which equaled 5.0 (N-EEGr-GF) and 6.7 Ω (EEGr-GF), respectively. The curves showed that EEGr-GF had a smaller semicircle than N-EEGr-GF in the high frequency region and a more vertical line in the range of low frequency, indicating that N-EEGr-GF had a little higher charge transfer resistance and lower ion diffusion rate than EEGr-GF [17, 21, 47].

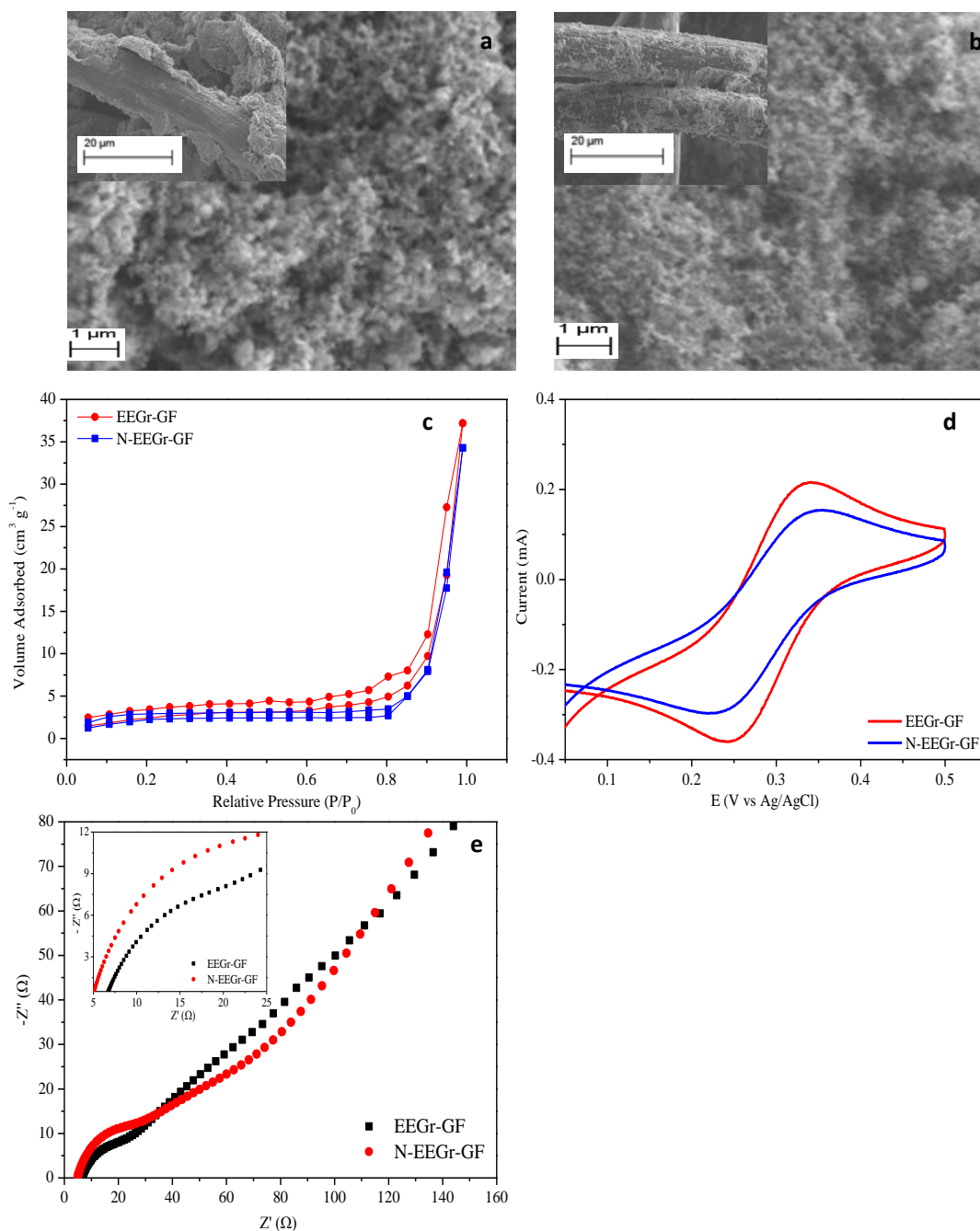


Fig. 3 SEM images of EEGr-GF (a) and N-EEGr-GF (b); N_2 adsorption/desorption isotherms of the EEGr-GF and N-EEGr-GF electrodes (c); Electroactive surface area of EEGr-GF and N-EEGr-GF detection (d); Nyquist plot of the two electrodes (EEGr-GF and N-EEGr-GF) (e).

5.3.4. Catalytic performances of in-situ metal-free EAOPs with modified electrode

The catalytic performances of EAOPs on EEGr-GF and N-EEGr-GF cathodes were evaluated using the extensively studied phenol^[40, 48-51] as the model pollutant (Figure 4a), observing a complete phenol removal ratio within 50 min on N-EEGr-GF. The pseudo-first-order reaction rate constant (k) of N-EEGr-GF was calculated to be 2-fold of EEGr-GF. To illustrate the roles of free radicals in the degradation of phenol in EAOPs, methanol was added into solution as the scavenger of $\cdot\text{OH}$ ^[52-55]. It was observed obviously that the phenol removal ratio decreased dramatically on both EEGr-GF and N-EEGr-GF, remaining at 17.1% and 8.9% within 50 min respectively, which proved the contributory role of $\cdot\text{OH}$ in EAOPs. These facts also indicated that some other radicals contributed the degradation. Consequently, benzoquinone (BQ), the scavenger of $\cdot\text{O}_2$ ^[56-59] was added into the solution, observing a slight decrease in phenol removal ratio on two cathodes. The phenomena denoted that $\cdot\text{O}_2$ was generated during EAOPs but was not the major role for phenol removal. Additionally, anodic oxidation might also contribute to the phenol removal. To confirm this, these cathodes were replaced by Pt sheet, while the anode remained unchanged. It proved the minor role of anodic oxidation for phenol degradation account for the low removal ratio of phenol (only 7.2% within 50 min).

Based on the analysis above, it might be reasonable to deduce that in the in-situ metal-free EAOPs, the better performance of EAOPs with N-EEGr-GF was due to the higher concentration of $\cdot\text{OH}$ produced via the activation of in-situ generated H_2O_2 on cathode. However, the concentration of H_2O_2 generated was found very close under the same experimental conditions (Figure 4b). The yield of H_2O_2 on the two cathodes were both pretty high at pH 7, with an average generation rate of 6.5 (EEGr-GF) and 6.2 (N-EEGr-GF) $\text{mg h}^{-1} \text{cm}^{-2}$, and the electric energy consumption (EEC) was 9.5 and 10.3 kWh kg^{-1} (Figure S3), respectively. This ultrahigh yield of H_2O_2 would give rise to an efficient activation to generate $\cdot\text{OH}$ on the cathode^[10]:



Strictly, a little depressed H_2O_2 generation was obtained on N-EEGr-GF when compared with EEGr-GF cathode, which might be due to the decrease of electron transfer rate and electroactive surface area as shown in Figure 3d. These results

seemed to be inconsistent with the performance of phenol removal with the two cathodes. A possible assumption would be that the activation of H_2O_2 for $\cdot OH$ generation on N-EEGr-GF was much more efficient than the one on EEGr-GF.

To approve this hypothesis, the existence of $\cdot OH$ on two cathodes were detected via DMPO spin-trapped ESR spectroscopy^[30]. As shown in Figure 4c, both of the two electrodes gave rise to exclusively 1:2:2:1 quartet signal in the ESR spectra, which are characteristic of DMPO- $\cdot OH$ adducts via trapping of $\cdot OH$ radicals by DMPO reagent^[60], indicating that $\cdot OH$ was the active specie for the two cathodes. Clearly, the concentration of $\cdot OH$ in the two systems increased with the time, which was in agreement with literature^[34, 60], and the signal on N-EEGr-GF was much stronger than that on EEGr-GF. Therefore it could be concluded that the catalytic decomposition of H_2O_2 to $\cdot OH$ on N-EEGr-GF was more efficient than that on EEGr-GF, resulting in the enhancement of phenol removal ratios in EAOPs. bThe significant strong activation of H_2O_2 to $\cdot OH$ on N-EEGr-GF might be related with the N-doping on EEGr, which disrupt sp^2 hybridized carbon structure because certain species of N-doping could be regarded as the metal-free active sites [47], thus creating new “activated regions” on N-EEGr and improved the activation of free radicals^[61-64].

To further evaluate the activation of in-situ generated H_2O_2 to $\cdot OH$ in EAOPs, the concentrations of $\cdot OH$ generated on two cathodes were detected (Figure 4d). On N-EEGr-GF, the $\cdot OH$ concentration reached 88 μM at 5 min, which was more than 2 times of that on EEGr-GF (43 μM). At 40 min, the concentration of $\cdot OH$ arrived at 172 μM in EAOPs on N-EEGr-GF. The difference on the generated $\cdot OH$ concentration on the two cathodes was consistent with the results of ESR (Figure 4c) and the removal ratio of phenol in Figure 4a, presenting that N-doping on EEGr could effectively accelerate the rate of in-situ activation of H_2O_2 to $\cdot OH$ in EAOPs.

5.3.5. Possible mechanism of in-situ metal-free EAOPs with N-doped graphene

It has been suggested that N-doping can significantly enhance the catalytic performance of carbon materials^[37, 48], and the introduction of N atom into EEGr layer would disrupt sp^2 -hybridized configuration and create new active sites for activation reactions^[61, 62, 65]. According to the analysis above, the mechanism of EAOPs for organics removal on the N-EEGr-GF can be depicted in Figure 5. The

migrated oxygen electrochemically reacted with electrons via two routes. Most of the oxygen performed in a two-electron ORR approach with H_2O_2 generation, and then the delocalized electrons from zigzag edges of EEGr would be transferred to activate the in-situ generated H_2O_2 to form $\cdot\text{OH}$ for organics degradation [58, 66]. At the same time, another small part of the migrated oxygen was connected with one electron to generate $\cdot\text{O}_2$. N-doping on the EEGr can break the chemical inertness of sp^2 carbon layer and catalytic activity of EEGr, thus increasing new active regions, stimulating the activation rate of H_2O_2 to $\cdot\text{OH}$ and improving the removal ratio of organics.

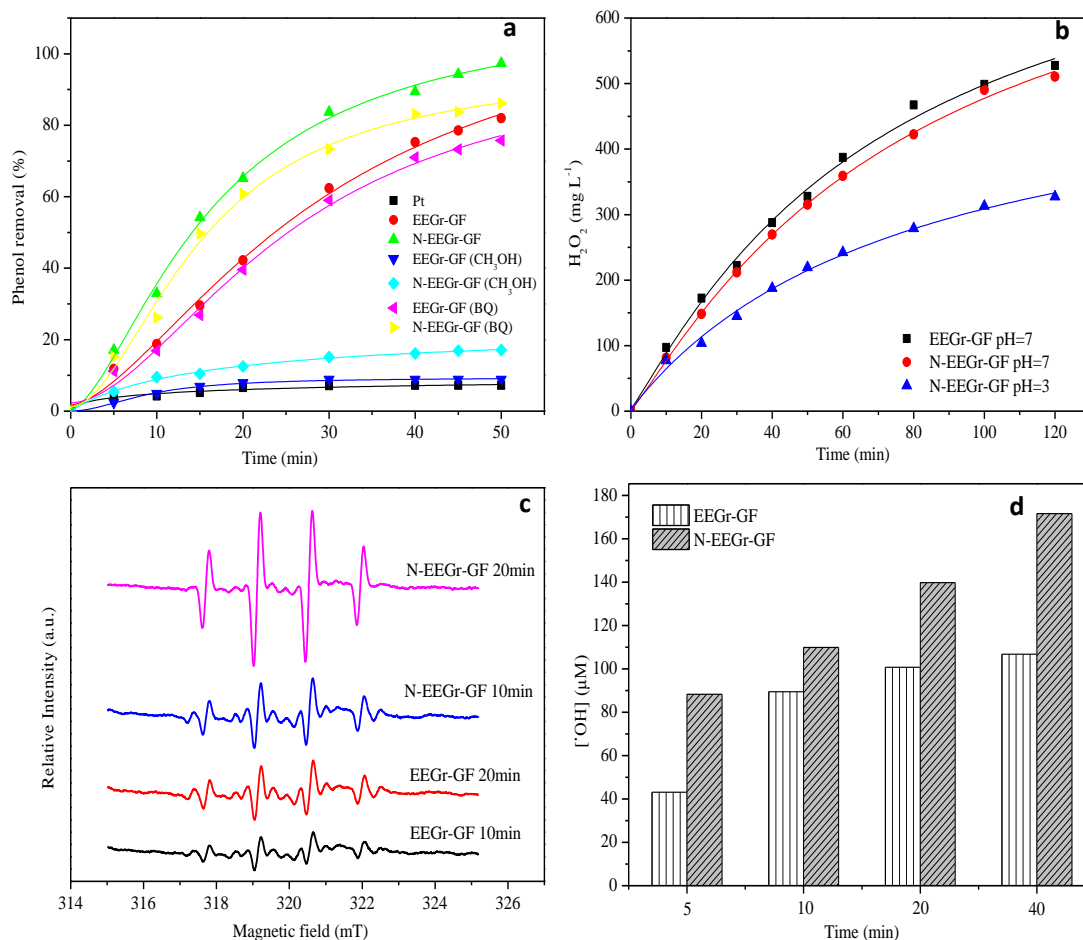


Fig. 4 The degradation of phenol in the EAOPs at different experiment conditions, methanol 20 mL and benzoquinone 5 mM; $V=100$ mL; $\text{pH}=3$; Na_2SO_4 : 50 mM; Potential: -0.9 V (a); The performance of H_2O_2 generation with EEGr-GF and N-EEGr-GF (b); ESR spectrum in EAOPs with two different modified cathode electrodes (c); The concentration of $\cdot\text{OH}$ on the two electrodes in EAOPs (d).

5.3.6. Performance comparison with traditional EF process

The efficiencies of in-situ metal-free EAOPs on N-EEGr-GF were compared with EF process on EEGr-GF cathode for phenol removal at pH 3 and 7. As shown in Figure 6a, the removal ratios of phenol on N-EEGr-GF in metal-free EAOPs kept stably at pH 3 and 7, reaching 97% and 92% in 50 min, respectively, comparable to that of EF process at pH=3 (99%). It is generally acknowledged that one big drawback of EF is the narrow suitability at around pH 3. In agreement with this conclusion, the phenol removal ratio of EF at pH 7 dramatically decreased to 42%. Though a higher Fe^{2+} addition of 0.8 and 1.2 mM could help to increase the phenol removal ratio and reaction rate constant, it would lead to a second pollution with a higher iron sludge production. Additionally, the k value of EAOPs on N-EEGr-GF was also 5-fold of the one in EF on EEGr-GF at pH 7. Accordingly, such in-situ metal-free EAOPs could overcome the two disadvantages of conventional EF.

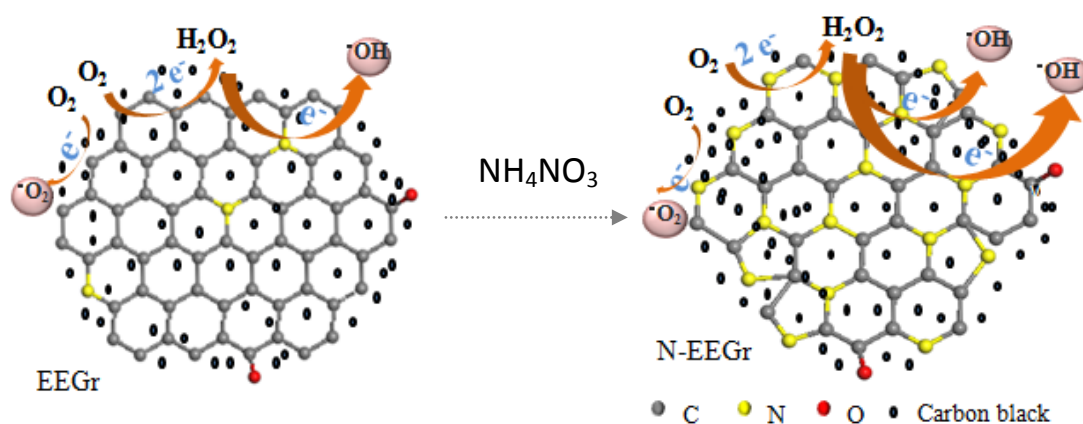


Fig. 5 Schematic illustration of the in-situ metal-free EAOPs with EEGr-GF and N-EEGr-GF electrode.

The degradation performance of this metal-free EAOP was further compared with other results for phenols in literature. The most significant characteristic of these metal-free EAOPs was that it performed stably at pH 3 and 7 (k value of 0.063 and 0.052 min^{-1}) with comparable or even more efficient performance than other AOPs (e.g., EF) at pH 3. Therefore the in-situ metal-free EAOP on N-EEGr-GF electrode exhibited a broader suitable pH value and without iron sludge generation, which was more effective and eco-friendly for contaminants removal.

For EF process, as an indispensable reagent, Fe^{2+} in solution cannot be cost-effectively reused for organics degradation, increasing the treatment cost and the remaining iron sludge disposal. To check whether this drawback could be overcome, the reusability of N-EEGr-GF was carried out in five runs for phenol removal, using simple ethanol regeneration after every run (Figure 6b). The fresh electrode (first run) was able to remove phenol completely within 50 min, and obtained 94%, 94%, 92% and 89% at 50 min for the second, third, fourth and fifth runs, respectively. Sun et al. reported that the N-doped graphene could obtain 56% removal ratio in the second run, which was only half of the first run for phenol degradation,³² also, 58%, 31% of phenol were removed in the second, third runs and with a removal ratio of 85% in 180 min after heat treatment^[45]. The outstanding performance of stability in the present work proved that the in-situ metal-free EAOPs on N-EEGr-GF could be a sustainable system for pollutants removal without additional catalysts and iron sludge generation.

A further exploration indicated that without ethanol regeneration the phenol removal ratio dramatically decreased from 100% in the first run to about 20% in second cycle, though there was only a slight fluctuation of H_2O_2 generation during the five runs. To explain this, the concentrations of $\cdot\text{OH}$ generation on N-EEGr-GF with and without ethanol treatment were compared, observing that the $\cdot\text{OH}$ concentration after ethanol regeneration was about three times of the one without ethanol treatment. These facts supported that the degradation intermediates covered on the active sites would hinder the formation of hydroxyl radical from the generated hydrogen peroxide, while ethanol treatment could effectively recovery these active sites by dissolving degradation intermediates, through which the potential for the activation of in-situ H_2O_2 to $\cdot\text{OH}$ generation was regenerated.

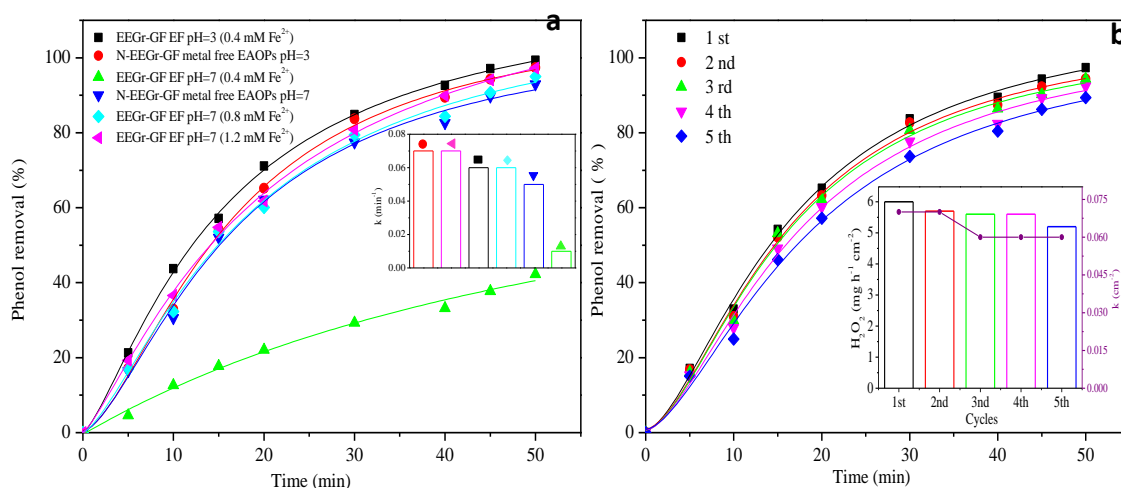


Fig. 6 Comparison with traditional EF process and in-situ metal-free EAOPs (a); The stability of N-EEGr-GF electrode in EAOPs (b).

In summary, N-EEGr has a superior catalytic activity for activation of H_2O_2 to $\cdot\text{OH}$, which fulfill N-EEGr-GF as cost-effective and reusable cathode for metal-free EAOPs for organics degradation. In view of its competitive advantage in stable performance under wider pH conditions and environmental friendliness without second pollution and catalysts addition except for cheap air, this process can be regarded as the competent substitution of traditional EF process for organic wastewater treatment.

5.4 Conclusions

Synthesized via calcination at low temperature with NH_4NO_3 as nitrogen resource, the prepared N-EEGr demonstrated a superior catalytic activity for activation of H_2O_2 to $\cdot\text{OH}$ for organics degradation. The in-situ metal-free EAOPs on N-EEGr-GF exhibited a more broad suitability upon pH, remarkable performance and excellent stability for phenol degradation. ESR spectra, methanol and benzoquinone capture confirmed $\cdot\text{OH}$ played the dominant role in the degradation. At the same time, without catalysts addition and iron sludge generation compared with traditional EF process, such a process can be regarded as a potential candidate for wastewater treatment. This study provided an insight into the in-situ metal-free EAOPs for sustainable environmental remediation by activation of in-situ generated H_2O_2 to $\cdot\text{OH}$.

Acknowledgement

This work was financially supported by Natural Science Foundation of China (nos. 21773129, 91545126 and 21273120), Key Project of Natural Science Foundation of Tianjin (no. 16JCZDJC39300), National Key Research and Development Program (2016YFC0400706), China National Water Project (nos. 2015ZX07203-11), and Fundamental Research Funds for the Central Universities.

References

- [1] Barhoumi N, Olvera-Vargas H, Oturan N, et al. Kinetics of oxidative degradation/mineralization pathways of the antibiotic tetracycline by the novel heterogeneous

- electro-Fenton process with solid catalyst chalcopyrite[J]. *Applied Catalysis B: Environmental*, 2017, 209: 637-647.
- [2] Küster A, Adler N, et al. Pharmaceuticals in the environment: scientific evidence of risks and its regulation[J]. *Phil. Trans. R. Soc. B*, 2014, 369: 20130587.
- [3] Gogate P R, Pandit A B, et al. A review of imperative technologies for wastewater treatment I: oxidation technologies at ambient conditions[J]. *Advances in Environmental Research*, 2004, 8: 501-551.
- [4] Hernando M, Mezcuca M, Fernández-Alba A, et al. Environmental risk assessment of pharmaceutical residues in wastewater effluents, surface waters and sediments[J]. *Talanta*, 2006, 69: 334-342.
- [5] Dong H, Yuan X, Wang W, et al. Occurrence and removal of antibiotics in ecological and conventional wastewater treatment processes: a field study[J]. *Journal of environmental management*, 2016, 178: 11-19.
- [6] Castiglioni S, Bagnati R, Fanelli R, et al. Removal of pharmaceuticals in sewage treatment plants in Italy[J]. *Environmental Science & Technology*, 2006, 40: 357-363.
- [7] Shannon M A, Bohn P W, Elimelech M, et al. Science and technology for water purification in the coming decades[J]. *Nature*, 2008, 452: 301-310.
- [8] De García S a O, Pinto G P, García-Encina P A, et al., et al. Ecotoxicity and environmental risk assessment of pharmaceuticals and personal care products in aquatic environments and wastewater treatment plants[J]. *Ecotoxicology*, 2014, 23: 1517-1533.
- [9] Liu W, Ai Z, Zhang L, et al. Design of a neutral three-dimensional electro-Fenton system with foam nickel as particle electrodes for wastewater treatment[J]. *J Hazard Mater*, 2012, 243: 257-264.
- [10] Sires I, Brillas E, Oturan M A, et al. Electrochemical advanced oxidation processes: today and tomorrow. A review[J]. *Environ Sci Pollut Res Int*, 2014, 21: 8336-8367.
- [11] Augugliaro V, Camera-Roda G, Loddo V, et al. Heterogeneous photocatalysis and photoelectrocatalysis: from unselective abatement of noxious species to selective production of high-value chemicals[J]. *The journal of physical chemistry letters*, 2015, 6: 1968-1981.
- [12] Barhoumi N, Olvera-Vargas H, Oturan N, et al. Kinetics of oxidative degradation/mineralization pathways of the antibiotic tetracycline by the novel heterogeneous electro-Fenton process with solid catalyst chalcopyrite[J]. *Applied Catalysis B: Environmental*, 2017, 209: 637-647.
- [13] Murati M, Oturan N, Aaron J J, et al. Degradation and mineralization of sulcotrione and mesotrione in aqueous medium by the electro-Fenton process: a kinetic study[J]. *Environ Sci Pollut Res Int*, 2012, 19: 1563-1573.
- [14] Li X, Jin X, Zhao N, et al. Novel bio-electro-Fenton technology for azo dye wastewater treatment using microbial reverse-electrodialysis electrolysis cell[J]. *Bioresour Technol*, 2017, 228: 322-329.
- [15] Gong Y, Li J, Zhang Y, et al. Partial degradation of levofloxacin for biodegradability improvement by electro-Fenton process using an activated carbon fiber felt cathode[J]. *J Hazard Mater*, 2016, 304: 320-328.
- [16] Mousset E, Ko Z T, Syafiq M, et al. Electrocatalytic activity enhancement of a graphene ink-coated carbon cloth cathode for oxidative treatment[J]. *Electrochimica Acta*, 2016, 222:

1628-1641.

- [17] Mousset E, Wang Z, Hammaker J, et al. Physico-chemical properties of pristine graphene and its performance as electrode material for electro-Fenton treatment of wastewater[J]. *Electrochimica Acta*, 2016, 214: 217-230.
- [18] Rodrigo M A, Oturan N, Oturan M A, et al. Electrochemically assisted remediation of pesticides in soils and water: a review[J]. *Chem Rev*, 2014, 114: 8720-8745.
- [19] Dos Santos A J, De Lima M D, Da Silva D R, et al. Influence of the water hardness on the performance of electro-Fenton approach: Decolorization and mineralization of Eriochrome Black T[J]. *Electrochimica Acta*, 2016, 208: 156-163.
- [20] Garcia-Segura S, Brillas E, et al. Combustion of textile monoazo, diazo and triazo dyes by solar photoelectro-Fenton: Decolorization, kinetics and degradation routes[J]. *Applied Catalysis B: Environmental*, 2016, 181: 681-691.
- [21] Oturan M A, Aaron J-J, et al. Advanced oxidation processes in water/wastewater treatment: principles and applications. A review[J]. *Critical Reviews in Environmental Science and Technology*, 2014, 44: 2577-2641.
- [22] Yu F, Zhou M, Yu X, et al. Cost-effective electro-Fenton using modified graphite felt that dramatically enhanced on H₂O₂ electro-generation without external aeration[J]. *Electrochimica Acta*, 2015, 163: 182-189.
- [23] Sirés I, Garrido J A, Rodríguez R M, et al. Catalytic behavior of the Fe³⁺/Fe²⁺ system in the electro-Fenton degradation of the antimicrobial chlorophene[J]. *Applied Catalysis B: Environmental*, 2007, 72: 382-394.
- [24] Miao J, Zhu H, Tang Y, et al. Graphite felt electrochemically modified in H₂SO₄ solution used as a cathode to produce H₂O₂ for pre-oxidation of drinking water[J]. *Chemical Engineering Journal*, 2014, 250: 312-318.
- [25] Zhou L, Zhou M, Hu Z, et al. Chemically modified graphite felt as an efficient cathode in electro-Fenton for p-nitrophenol degradation[J]. *Electrochimica Acta*, 2014, 140: 376-383.
- [26] Ren G, Zhou M, Liu M, et al. A novel vertical-flow electro-Fenton reactor for organic wastewater treatment[J]. *Chemical Engineering Journal*, 2016, 298: 55-67.
- [27] Cheng M, Zeng G, Huang D, et al. Hydroxyl radicals based advanced oxidation processes (AOPs) for remediation of soils contaminated with organic compounds: A review[J]. *Chemical Engineering Journal*, 2016, 284: 582-598.
- [28] Cheng T-H, Huang C-P, Huang Y-H, et al. Kinetic study and optimization of electro-Fenton process for dissolution and mineralization of ion exchange resins[J]. *Chemical Engineering Journal*, 2017, 308: 954-962.
- [29] Trellu C, Mousset E, Pechaud Y, et al. Removal of hydrophobic organic pollutants from soil washing/flushing solutions: A critical review[J]. *J Hazard Mater*, 2016, 306: 149-174.
- [30] Dong H, Su H, Chen Z, et al. Fabrication of Electrochemically Reduced Graphene Oxide Modified Gas Diffusion Electrode for In-situ Electrochemical Advanced Oxidation Process under Mild Conditions[J]. *Electrochimica Acta*, 2016, 222: 1501-1509.
- [31] Bokare A D, Choi W, et al. Review of iron-free Fenton-like systems for activating H₂O₂ in advanced oxidation processes[J]. *J Hazard Mater*, 2014, 275: 121-135.
- [32] Saputra E, Muhammad S, Sun H, et al. Activated carbons as green and effective catalysts for generation of reactive radicals in degradation of aqueous phenol[J]. *RSC Advances*, 2013, 3:

21905.

- [33] Sun X, Song P, Zhang Y, et al. A class of high performance metal-free oxygen reduction electrocatalysts based on cheap carbon blacks[J]. *Sci Rep*, 2013, 3: 2505.
- [34] Pignatello J J, Oliveros E, Mackay A, et al. Advanced oxidation processes for organic contaminant destruction based on the Fenton reaction and related chemistry[J]. *Critical reviews in environmental science and technology*, 2006, 36: 1-84.
- [35] Brillas E, Sirés I, Oturan M A, et al. Electro-Fenton process and related electrochemical technologies based on Fenton's reaction chemistry[J]. *Chemical reviews*, 2009, 109: 6570-6631.
- [36] Zhou Y, Bao Q, Tang L a L, et al. Hydrothermal Dehydration for the "Green" Reduction of Exfoliated Graphene Oxide to Graphene and Demonstration of Tunable Optical Limiting Properties[J]. *Chemistry of Materials*, 2009, 21: 2950-2956.
- [37] Sun H, Wang Y, Liu S, et al. Facile synthesis of nitrogen doped reduced graphene oxide as a superior metal-free catalyst for oxidation[J]. *Chem Commun (Camb)*, 2013, 49: 9914-9916.
- [38] Ferrari A C, Meyer J C, Scardaci V, et al. Raman spectrum of graphene and graphene layers[J]. *Phys Rev Lett*, 2006, 97: 187401.
- [39] Duan X, Sun H, Wang Y, et al. N-Doping-Induced Nonradical Reaction on Single-Walled Carbon Nanotubes for Catalytic Phenol Oxidation[J]. *ACS Catalysis*, 2014, 5: 553-559.
- [40] Wang C, Kang J, Sun H, et al., et al. One-pot synthesis of N-doped graphene for metal-free advanced oxidation processes[J]. *Carbon*, 2016, 102: 279-287.
- [41] Yang W, Li J, Fu Q, et al., et al. A simple method for preparing a binder-free paper-based air cathode for microbial fuel cells[J]. *Bioresour Technol*, 2017, 241: 325-331.
- [42] Soares O S G P, Rocha R P, Gonçalves A G, et al., et al. Easy method to prepare N-doped carbon nanotubes by ball milling[J]. *Carbon*, 2015, 91: 114-121.
- [43] Sun H, Kwan C, Suvorova A, et al. Catalytic oxidation of organic pollutants on pristine and surface nitrogen-modified carbon nanotubes with sulfate radicals[J]. *Applied Catalysis B: Environmental*, 2014, 154-155: 134-141.
- [44] Le T X H, Bechelany M, Lacour S, et al. High removal efficiency of dye pollutants by electron-Fenton process using a graphene based cathode[J]. *Carbon*, 2015, 94: 1003-1011.
- [45] Chen W, Yang X, Huang J, et al. Iron oxide containing graphene/carbon nanotube based carbon aerogel as an efficient E-Fenton cathode for the degradation of methyl blue[J]. *Electrochimica Acta*, 2016, 200: 75-83.
- [46] Grewal Y S, Shiddiky M J, Gray S A, et al. Label-free electrochemical detection of an *Entamoeba histolytica* antigen using cell-free yeast-scFv probes[J]. *Chem Commun (Camb)*, 2013, 49: 1551-1553.
- [47] Soltani R D C, Rezaee A, Khataee A, et al. Electrochemical generation of hydrogen peroxide using carbon black-, carbon nanotube-, and carbon black/carbon nanotube-coated gas-diffusion cathodes: effect of operational parameters and decolorization study[J]. *Research on Chemical Intermediates*, 2013, 39: 4277-4286.
- [48] Duan X, Ao Z, Sun H, et al. Nitrogen-doped graphene for generation and evolution of reactive radicals by metal-free catalysis[J]. *ACS Appl Mater Interfaces*, 2015, 7: 4169-4178.
- [49] Garcia-Rodriguez O, Lee Y Y, Olvera-Vargas H, et al. Mineralization of electronic wastewater by electro-Fenton with an enhanced graphene-based gas diffusion cathode[J]. *Electrochimica Acta*, 2018, 276: 12-20.

- [50] Dai C, Zhang A, Liu M, et al. Hollow Alveolus-Like Nanovesicle Assembly with Metal-Encapsulated Hollow Zeolite Nanocrystals[J]. ACS Nano, 2016, 10: 7401-7408.
- [51] Zhu Y, Murali S, Cai W, et al. Graphene and graphene oxide: synthesis, properties, and applications[J]. Advanced materials, 2010, 22: 3906-3924.
- [52] Miao Z, Gu X, Lu S, et al. Enhancement effects of reducing agents on the degradation of tetrachloroethene in the Fe(II)/Fe(III) catalyzed percarbonate system[J]. J Hazard Mater, 2015, 300: 530-537.
- [53] Pelaez M, Falaras P, Likodimos V, et al. Use of selected scavengers for the determination of NF-TiO₂ reactive oxygen species during the degradation of microcystin-LR under visible light irradiation[J]. Journal of Molecular Catalysis A: Chemical, 2016, 425: 183-189.
- [54] Ling L, Wang C, Ni M, et al. Enhanced photocatalytic activity of TiO₂/single-walled carbon nanotube (SWCNT) composites under UV-A irradiation[J]. Separation and Purification Technology, 2016, 169: 273-278.
- [55] Fan J-H, Liu X, Ma L-M, et al. EDTA enhanced degradation of 4-bromophenol by Al₂O₃-Fe₃O₄-O₂ system[J]. Chemical Engineering Journal, 2015, 263: 71-82.
- [56] Xiao J, Xie Y, Han Q, et al. Superoxide radical-mediated photocatalytic oxidation of phenolic compounds over Ag(+)/TiO₂: Influence of electron donating and withdrawing substituents[J]. J Hazard Mater, 2016, 304: 126-133.
- [57] Wang Y, Xie Y, Sun H, et al., et al. 2D/2D nano-hybrids of gamma-MnO(2) on reduced graphene oxide for catalytic ozonation and coupling peroxydisulfate activation[J]. J Hazard Mater, 2016, 301: 56-64.
- [58] Enoki T, Fujii S, Takai K, et al. Zigzag and armchair edges in graphene[J]. Carbon, 2012, 50: 3141-3145.
- [59] Chen X J, Dai Y Z, Wang X Y, et al. Synthesis and characterization of Ag₃PO₄ immobilized with graphene oxide (GO) for enhanced photocatalytic activity and stability over 2,4-dichlorophenol under visible light irradiation[J]. J Hazard Mater, 2015, 292: 9-18.
- [60] Yan S C, Li Z S, Zou Z G, et al. Photodegradation of rhodamine B and methyl orange over boron-doped g-C₃N₄ under visible light irradiation[J]. Langmuir, 2010, 26: 3894-3901.
- [61] Liu H, Liu Y, Zhu D, et al. Chemical doping of graphene[J]. J. Mater. Chem., 2011, 21: 3335-3345.
- [62] Su D S, Perathoner S, Centi G, et al. Nanocarbons for the development of advanced catalysts[J]. Chem Rev, 2013, 113: 5782-5816.
- [63] Liu Y, Yu L, Ong C N, et al. Nitrogen-doped graphene nanosheets as reactive water purification membranes[J]. Nano Research, 2016, 9: 1983-1993.
- [64] Wang H, Maiyalagan T, Wang X, et al. Review on Recent Progress in Nitrogen-Doped Graphene: Synthesis, Characterization, and Its Potential Applications[J]. ACS Catalysis, 2012, 2: 781-794.
- [65] Su D S, Zhang J, Frank B, et al. Metal-free heterogeneous catalysis for sustainable chemistry[J]. ChemSusChem, 2010, 3: 169-180.
- [66] Jiang D E, Sumpter B G, Dai S, et al. Unique chemical reactivity of a graphene nanoribbon's zigzag edge[J]. J Chem Phys, 2007, 126: 134701.

Chapter 6: Enhanced activation of hydrogen peroxide using nitrogen doped graphene for effective removal of herbicide 2,4-D from water by iron-free electrochemical advanced oxidation

Abstract

Degradation of the herbicide 2,4-dichlorophenoxyacetic acid (2,4-D) in aqueous solutions has been studied by electrochemical oxidation process using N-doped graphene modified graphite felt cathode with ammonium nitrate as nitrogen source. The graphene was obtained via electrochemically exfoliated method (EEGr). Different ratios of EEGr/ammonium nitrate (1:0, 1:1, 1:3, 1:7) modified cathodes (N0-EEGr-GF, N1-EEGr-GF, N3-EEGr-GF, N7-EEGr-GF) were explored with electrochemical characterizations, and it was verified that N1-EEGr had the most significant catalytic performance for accelerating the activation of in-situ generated H_2O_2 into hydroxyl radicals. The effects of operating parameters such as applied potential, solution pH and initial concentration of 2,4-D on the degradation efficiency with N1-EEGr-GF were investigated. A fairly high mineralization rate (88%) was attained at pH 7 after 480 min electrolysis of 20 mg L^{-1} 2,4-D solution. The N-doped graphene as catalyst was found to be more efficient in degradation performance compared with the unmodified graphite felt cathode. The electrochemical advanced oxidation process using this modified cathode allows extension of the working pH range compared to electro-Fenton process which is optimal at pH 3. Finally, a plausible pathway for 2,4-D mineralization was proposed according to the identified intermediated products.

Keywords: N-doped graphene, Iron-free, electrochemical advanced oxidation, Cost-effective, 2,4-D

6.1 Introduction

During the last decades, herbicides are constantly released into aquatic environments mainly from the agricultural sector, individual usages and public authorities to maintain the public domains (roads, highways, railways, etc.) leading their occurrence nowadays in surface water, groundwater and even in drinking water due to their persistency for long periods ^[1]. Most of them have been shown toxic to natural organisms and human beings ^[2-5] because of their bioaccumulative character and thus easily transfer to the food chain. As one of the most widely used herbicides, 2,4-dichlorophenoxyacetic acid (2,4-D), a versatile agrochemical to manage various types of weeds thanks to its low cost, easy availability and high functions, has been classified as an endocrine disruptor for human ^[6, 7] and with moderate potential of lixiviation in soils ^[7]. Due to toxic properties of this herbicide and its persistence to biodegradation, the classical water treatment processes such as adsorption ^[8, 9], biodegradation ^[10] and electrocatalytic dechlorination ^[11] remain ineffective to remove it efficiently from water ^[12, 13].

On the other hand, the technologies so-called advanced oxidation processes (AOPs), based on the in-situ generation and action of strongly reactive oxidants, mainly hydroxyl radical ($\cdot\text{OH}$) constitute promising technologies for the treatment of wastewater containing persistent/toxic organic pollutants ^[14-18]. Among the AOPs, Fenton's reaction ^[19] constitutes a simple way to produce $\cdot\text{OH}$ from decomposition of H_2O_2 with ferrous iron (Fe^{2+}) (Eq. 1).



To get rid of the high cost and risks of provision, storage and transport of H_2O_2 , electro-Fenton (EF) process is regarded as one of the most popular electrochemical advanced oxidation processes (EAOPs) with formation of $\cdot\text{OH}$ in aqueous medium via in-situ electrochemical generation of H_2O_2 (Eq. 2). However, EF process has to be performed better at pretty acidic pH (~ 3.0) since at $\text{pH} > 4$, insoluble iron species, especially ferric hydroxide sludge, are formed ^[20], leading to the catalyst loss and decrease of process efficiency.



To address this challenge, heterogeneous EF containing iron species catalysts

have been developed as potential alternatives to traditional homogeneous EF process [21-23]. For example, a composite nickel-iron-foam (Ni-Fe-F) cathode with providing Fe^{2+} ions necessary for Fenton's reaction was used as cathode in the EF, which was proved to enhance the efficiency of EF at near neutral pH [24]. Pyrite as source of Fe^{2+} was used as a sustainable catalyst in EF process for improving the oxidation of sulfamethazine, with parallel regulation of pH of the solution to about 3 [25]. Besides, Iron oxychloride (FeOCl) was studied as an efficient Fenton-like catalyst for removal of organics [26]. Olmos et al. (2012) used Fe-zeolites as catalysts in the photo-Fenton like reactions [27], and iron-doped mesoporous silica was studied as a heterogeneous catalyst in EF process for rhodamine B removal [28]. However, very few of these catalysts could exhibit significant performances at neutral pH with satisfied catalytic efficiency [29]. Besides, these catalysts usually suffer from dropping off, agglomeration, dissolution and decreasing catalyst activity in the process of wastewater treatment [30].

Hence, it is an interesting challenge to solve the issues in order to perform EF process at neutral or near neutral pH conditions without adjusting the initial effluent pH. As evidenced in Eq. 2, cathode materials play a crucial role in the generation of H_2O_2 via 2-electron oxygen reduction reaction (ORR). Carbon material is nontoxic and exhibits relative good stability, conductivity and high over-potential for H_2 evolution, favoring H_2O_2 formation [31]. Graphite [32], gas diffusion electrode [33], graphene [34], activated carbon fiber [35, 36], carbon nanotubes [37] and graphite felt [38] have been reported to be suitable cathode materials for H_2O_2 generation. In this context, a previous work, the graphite felt cathode modified with electrochemically exfoliated graphene (EEGr-GF) has been shown to be able to provide ultrahigh yield of H_2O_2 generation [38], which was in agreement with the results already reported [39]. Additionally, it was noted that some of the carbon-based materials are supposed to have the ability of activating H_2O_2 to $\cdot\text{OH}$ for organics degradation [40, 41], inspiring the development of in-situ iron-free EAOPs for contaminants removal from wastewater.

Therefore, this study focused on the degradation/mineralization of the widely used herbicide 2,4-dichlorophenoxyacetic acid (2,4-D) aqueous solution [42] with an in-situ iron-free EAOP for which performance was regulated by different N species on the cathode. Different ratios of EEGr/ammonium nitrate (1:0, 1:1, 1:3, 1:7) in graphite

felt (GF) cathode modification (N0-EEGr-GF, N1-EEGr-GF, N3-EEGr-GF, N7-EEGr-GF) were explored, and N1-EEGr-GF demonstrated the great performance in oxidative degradation of 2,4-D. What's more, process optimization, catalyst reusability as well as the possible mechanism for 2,4-D degradation in iron-free EAOP process were investigated to gain insight into the application of this promising in-situ iron-free EAOP process. This in-situ iron-free EAOP could effectively avoid the usage of chemicals (hydrogen peroxide and iron salts) and extended the suitable range of pH value compared with traditional EF process.

6.2 Materials and methods

6.2.1 Chemical reagents

The graphite felts (Shanghai Qijie Carbon Material Co., Ltd.), carbon black, ethanol and polytetrafluoroethylene (PTFE) (Shanghai Hesun Electric Co., Ltd.) were used for cathode preparation. The EEGr was achieved via electrochemical exfoliation of graphite foil^[38], and ammonium nitrate was chosen as nitrogen source for preparation of N-EEGr. 2,4-D (Beijing, Lideshi chemical technology Co., Ltd) was used as the target pollutant. H₂SO₄ and NaOH were purchased from Tianjin Kemiou Chemical Reagent Co., Ltd and used to adjust the pH of solution. Na₂SO₄ and FeSO₄ were purchased from Tianjin Yongda chemical reagents development center. All experiments were operated at room temperature.

6.2.2 Preparation of N-EEGr and N-EEGr-GF

The EEGr and ammonium nitrate were mixed at different mass ratio (EEGr : ammonium nitrate = 1:1, 1:3, 1:7) in ethanol solution under stirring and heated at 50°C until ethanol evaporated completely, and then the mixed powder was calcinated at 360°C in furnace under nitrogen atmosphere for 30 min to fabricate the N1-EEGr, N3-EEGr and N7-EEGr^[43]. These three kinds of N-EEGr were mixed with carbon black at the ratio of N-EEGr : carbon black = 1 : 4, PTFE (0.5 mL), deionized water and ethanol, and were shaken to be a mash, then was coated on the two sides of the graphite felt, calcinated at 360°C for 30 min under nitrogen atmosphere. The N-EEGr-GF was used as cathode for high yield of in-situ H₂O₂ in EAOP.

6.2.3 Characterizations and electrochemical measurements

The structures of the synthesized N1-EEGr, N3-EEGr, and N7-EEGr were analyzed by X-ray photoelectron spectroscopy (XPS) (Krato-ultra DLD, Shimadzu) using Mono Al K α radiation ($h\nu = 1486.7$ eV).

The cyclic voltammetry (CV) of N0-EEGr-GF (without nitrogen doping) and N-EEGr-GF (N1, N3, N7) were measured in Na₂SO₄ solution (0.05 M) with a three-electrode system, in which the modified graphite felt cathode (3×4 cm²) was used as the working electrode, Pt sheet (2×2 cm²) and saturated calomel electrode (Hg₂Cl₂ (s)/Hg (l) in saturated KCl solution) were used as counter and reference electrode, respectively.

The electroactive surface area of these cathodes (N0, N1, N3, N7) were calculated referencing the following Randles-Sevcik equation^[34, 44]:

$$I_p = 2.69 \times 10^5 \times AD^{1/2} n^{3/2} \nu^{1/2} C \quad (6-3)$$

where I_p , is the current peak, A is the area of the electrode (cm²), D is the diffusion coefficient of the molecular under study (7.6×10⁻⁶ cm² s⁻¹), n is the number of electrons exchange in redox reaction ($n=1$) by the probe molecule, ν is the scan rate (0.01 V s⁻¹) in CV experiment and C is the concentration of probe molecular in the bulk solution (1×10⁻⁵ mol cm⁻³), respectively.

Additionally, the concentration of H₂O₂ generated on N-EEGr-GF (N0, N1, N3, N7) electrodes were detected by UV-Vis spectrophotometer (UV835, Shanghai Instrument Analysis Co., Ltd) with the potassium titanium (IV) oxalate method at $\lambda = 400$ nm.

6.2.4 Degradation of 2,4-D with in-situ EAOP

The in-situ EAOP was then applied to the degradation of 2,4-D in an electrochemical cell of 150 mL capacity equipped with dimensionally stable anode (DSA, 3×4 cm²) anode composed of following metal oxides on Ti substrate (Ti/RuO₂-IrO₂) and N-EEGr-GF (N0, N1, N3, N7) (3×4 cm²) cathode under potential controlled electrolysis. Na₂SO₄ (50 mM) was used as the electrolyte solution. Compressed air was continuously bubbled into the solution at a constant flow rate of 1 L min⁻¹ starting 10 min before the beginning of the electrolysis. The concentration of 2,4-D was monitored by HPLC (Ultimate 3000, Thermo Scientific, USA) with an

Acclaim™ 120 C18 column (3 μm, 3.0×100 mm) with the mobile phase of methanol-water-acetic acid (60:38:2 v/v/v) at flow rate of 0.3 mL min⁻¹. The detection was carried out using a diode array detector at wavelength of 280 nm. The degradation efficiency (R) was calculated according to Eq. 4 [31] :

$$R(\%) = \frac{(C_0 - C_t)}{C_0} \times 100 \quad (6-4)$$

and the pseudo-first-order rate constant (k_{app}) for the oxidation of 2,4-D by $\cdot\text{OH}$ was determined according to the Eq. 5, suggesting that it follows a pseudo first order reaction kinetics.

$$\ln\left(\frac{C_0}{C_t}\right) = -kt \quad (6-5)$$

$$MCE(\%) = \frac{nFV_s \Delta(\text{TOC})_{\text{exp}}}{4.32 \times 10^7 mIt} \times 100 \quad (6-6)$$

n is the number of electrons consumed per 2,4-D molecule during its electrochemical mineralization reaction and was taken as 30 referring to the reaction (7), F is the Faraday constant (96487 C mol⁻¹), V_s is the solution volume (0.15 L), $\Delta(\text{TOC})_{\text{exp}}$ is the TOC decay (mg L⁻¹) at time t , 4.32×10^7 is the conversion factor to homogenize units (3600 s h⁻¹ × 1200 mg C mol⁻¹), m represents the number of carbon atoms of 2,4-D (8), I is electrolysis current (A) and t is the electrolysis time (h).



The intermediate products were detected by HPLC (Thermo Scientific, USA) with the mobile phase of methanol (1% acetic acid)/H₂O (1% acetic acid) (72:28, v/v) at flow rate of 0.05 mL min⁻¹ under an diode array detector at wavelength of 280 nm, and GC-MS (Agilent 7890A/5975C, USA) equipped with a HP-5MS column (30 m, 0.25 mm × 0.25 μm). The operation condition of GC-MS was set as: 1.0 mL min⁻¹ helium as the carrier gas, initial column temperature was set at 35°C for 1 min, and then increased to 300°C with 10°C min⁻¹ and held for 1 min at this temperature. Both the injector and detector temperature were set at 280°C. Carboxylic acids were analyzed by ion-exclusion HPLC using a HPX-87H ion exclusion column (300×7.8 mm) at 40°C, and coupled with UV detector set at wavelength of 220 nm, using the mobile phase of 4 mM H₂SO₄ at 0.6 mL min⁻¹.

6.3 Results and discussion

6.3.1 Characterization of different N-EEGr

The data depicted in Fig. 1 and Table 1 present the results of XPS analysis which provides insight into the chemical composition of the synthesized N-EEGr (N0, N1, N3, N7) with O/C ratios and the contents of three types of N, including pyrrolic N, graphitic N and pyridinic N^[43]. The molar ratio of O/C for N0-EEGr was 0.049, and oxygen existed at a pretty low ratio of 4.62%, suggesting that the EEGr was obtained with high quality and low oxidation state. The 0.42% nitrogen detected in N0-EEGr would come from the process of graphene preparation with raw material (graphite foil). The oxygen level was subsequently decreased to 2.7% for N1-EEGr after nitrogen doping, which was consistent with the results of a previous report^[45]. For N3-EEGr and N7-EEGr, the oxygen level increased to 12.28% and 20.35% with a nitrogen content of 0.5% and 0.38%, respectively. This can be explained that the N level detected by XPS was the relative content not the absolute amount of N in N3-EEGr and N7-EEGr. The contents of the three species of N were presented in Fig. 1c. It could be seen that pyridinic N content in N1-EEGr was the highest (0.66%), which was generally regarded as the active sites for ORR^[46].

6.3.2 Electrocatalytic activity of N-EEGr by CV

The results of CV measurements of N-EEGr (N0, N1, N3, N7) were presented in Fig. 2a, current intensity and potential (-0.37 V ~ -0.39 V/(Saturated calomel reference electrode)) of the reduction peak of N-EEGr changed in function of nitrogen doping compared with N0-EEGr. The current intensity of the peak of N1-EEGr was much higher than the others (N3-EEGr, N7-EEGr) with higher content of graphite N, providing more potential for H₂O₂ generation in ORR, which will be explained in details below.

In order to further investigate the performances of N-EEGr, the yield of H₂O₂ with modified cathodes N-EEGr-GF (N0, N1, N3, N7) were determined under voltage of 4 V and at pH 7 with DSA anode. Results showed that the H₂O₂ generation with N0-EEGr-GF was the highest, with the average H₂O₂ generation rate of 4.3 mg h⁻¹ cm⁻², being slightly better than that of N1-EEGr-GF (4.0 mg h⁻¹ cm⁻²) due to the

higher current response as shown in Fig. 2a [38]. These results allowed exploring the relationship between N doping degree (%) and H₂O₂ generation rate as shown in Fig. 2b. The current intensity of the electrochemical process diminished with the increasing graphite nitrogen, while at the same time, with a rising tendency of the average generation rate of H₂O₂, which can be explained that the doping of graphite N on N-EEGr could accelerate H₂O₂ generation rate with a higher current response in the process of ORR.

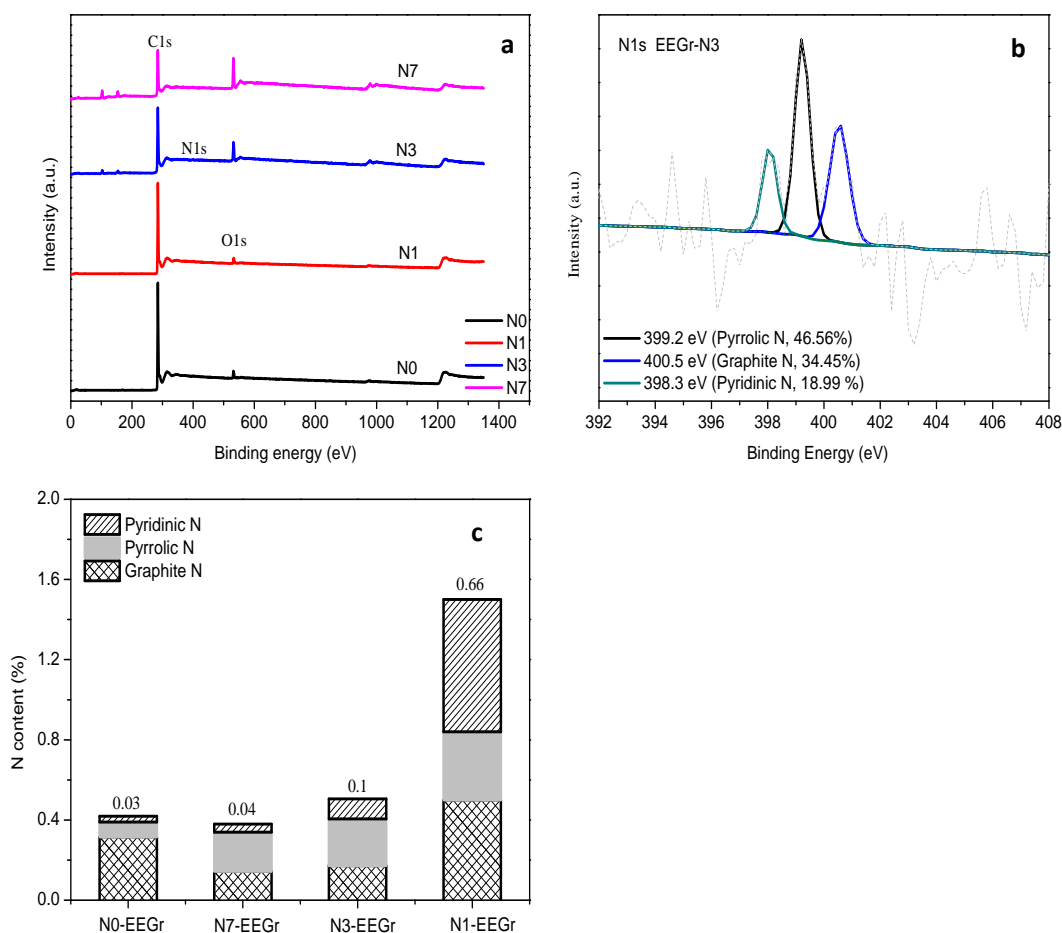


Fig. 1 XPS spectra of N-EEGr (N0, N1, N3, N7) (a); high-resolution N 1s spectrum of N3-EEGr (b) and three kinds of N content in N-EEGr (N0, N1, N3, N7) (c).

Thereafter, the electroactive surface area of N-EEGr-GF (N0, N1, N3, N7), which is closely correlated to the surface chemistry of the electrode materials [44], was measured by CV in 10 mM K₃[Fe(CN)₆] solution via the redox reactions of the couple Fe^{III}/Fe^{II} at the electrode surface. According to Eq. 3, the electroactive surface area of N-EEGr-GF (N0, N1, N3, N7) was calculated as 57, 72, 37 and 18 cm², respectively.

Table 1 Atomic percentage in the samples

Sample	C1s	O1s	O/C	N1s	
N0-EEGr	94.95	4.62	0.049	0.42	Pyrrolic N: 27.5
					Graphite N: 65.2
					Pyridinic N: 7.14
N1-EEGr	95.68	2.7	0.028	1.49	Pyrrolic N: 12.53
					Graphite N: 43.42
					Pyridinic N: 44.0
N3-EEGr	83.51	12.28	0.147	0.5	Pyrrolic N: 46.56
					Graphite N: 34.45
					Pyridinic N: 18.99
N7-EEGr	70.46	20.35	0.289	0.38	Pyrrolic N: 51.41
					Graphite N: 37.69
					Pyridinic N: 10.90

It can be noted that the electroactive surface area of N1-EEGr-GF is significantly higher than others, and that of N3-EEGr-GF is obviously higher than N7-EEGr-GF, thus showing a much higher rate of catalytic performance of the former one as cathode.

Moreover the effect of N doping on catalytic performance was presented in Fig. 3. The electroactive surface area increased with the level of pyridinic N on the N-EEGr-GF, which demonstrates that the contents of pyridinic N dominated the catalytic performances of the cathode. For comparison of N3-EEGr-GF and N7-EEGr-GF, the current response and H₂O₂ generation on N7-EEGr-GF was slightly better than the former one as shown in Fig. 2, while a lower electroactive surface area was achieved due to the lower content of pyridinic N, demonstrating the significant role of the pyridinic N doping on N-EEGr for enhancing the rate of activating in-situ

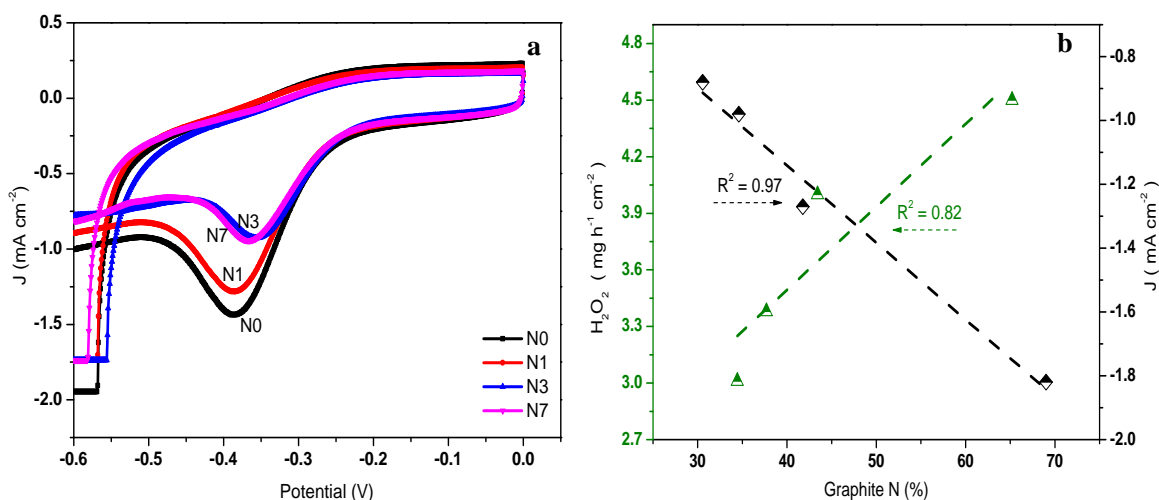


Fig. 2 Cyclic voltammograms of N-EEGr (N0, N1, N3, N7) (a); The relationship between graphite N and H₂O₂ generation rate (b).

generated H₂O₂ to [•]OH according to Eq. 8 [19], thus leading to the decrease of H₂O₂ generation detected (Fig. 2) while increasing the degradation efficiency of contaminants.



According to the analysis above, N1-EEGr-GF, which was proved to be most effective for H₂O₂ activation to [•]OH due to the good current response rate and the highest content of pyridinic N doping, was chosen as the cathode in the EAOP for 2,4-D degradation.

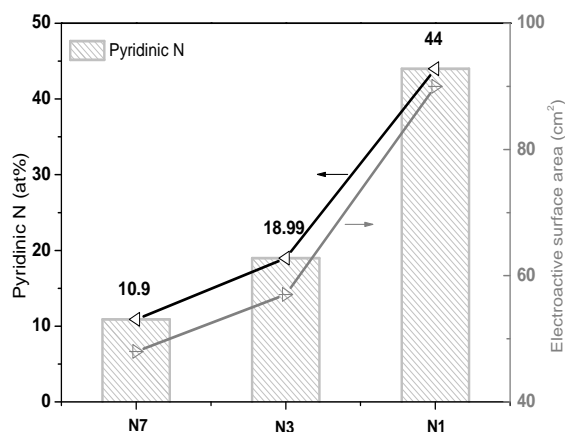


Fig. 3 Relationship between the content of pyridinic N and catalytic performance of EAOP.

Aiming to explore 2,4-D degradation in electrochemical advanced oxidation under the most favorable conditions, the effects of operating parameters including initial concentration of pollutant, solution pH and voltage on degradation efficiency were investigated.

Different initial concentrations (10, 20, 50, 100 mg L⁻¹) of 2,4-D were treated with N1-EEGr-GF cathode. As shown in Fig. 4a, 10 mg L⁻¹ 2,4-D could be degraded completely within 5 min at pH 3 with the cell voltage of 4.0 V. The time required for complete disappearance of higher concentration was longer, as expected, since a higher amount of 2,4-D molecules have to be oxidized for the same production rate of [•]OH. For instance, the complete oxidation of 100 mg L⁻¹ 2,4-D necessitated 40 min electrolysis. The inset of the Fig. 4a also illustrated that the apparent rate constant of 10 mg L⁻¹ concentration was much higher than others. Taken the decay rate of 2,4-D and degradation efficiency into consideration, the average level of 20 mg L⁻¹ 2,4-D was chosen in the following study.

It is well known that pH value plays a dominant role in the traditional EF process [20, 21]. Therefore, the effect of initial pH on the degradation efficiency of 2,4-D in EAOP was studied and results were depicted in Fig. 4b. The degradation performances at pH 3 was significantly better than others, obtaining the complete removal of 2,4-D at 20 min. At pH 5 and 7, 2,4-D could also be degraded but in a longer time (1 h). For the conventional EF process, generally, the degradation efficiency is significantly impaired when pH is around 4 or higher due to the formation of ferric hydroxide precipitate [47, 48] as well as the decreasing H₂O₂ generation rate at neutral or basic solution, and the pH 3 is acknowledged to be the optimized condition for contaminants degradation [49, 50]. As contrast, this EAOP could also obtain satisfactory performance for 2,4-D degradation at pH 7, resulting in extending the suitable pH range compared to traditional EF processes.

As shown in Fig. 4c, the degradation of 2,4-D performed the best with applied cell voltages of 4 V at pH 7, while a further increase to 5 V led to the decrease of the 2,4-D degradation efficiency. This was probably due to the enhancement of wasting reactions (Eq. 9 and 10) under high voltage (5 V), consuming the [•]OH generated on the cathode [51]. Besides, the energy consumption (EC) during the EAOP treatment was 0.09, 0.12 and 0.32 kWh g⁻¹ (2,4-D) for 3.5, 4 and 5 V applied voltage, respectively [31, 52, 53]. The corresponding values of *k_{app}* were 0.03, 0.04 and 0.03 min⁻¹ for 3, 4 and 5 V (Table 2), demonstrating again that the decay rate of 2,4-D in the EAOP was best at 4 V.



Also, the stability of N1-EEGr-GF electrode was explored at the proper conditions for 5 runs (Fig. 4d). All of the degradation efficiencies reached above 90%, only with a slight fluctuation for the 5th cycles. It was worth noting that, after each time the electrode used, a simple regeneration with ethanol was operated, which was proved to be a sustainable cathode and could provide great potential for the practical application in future.

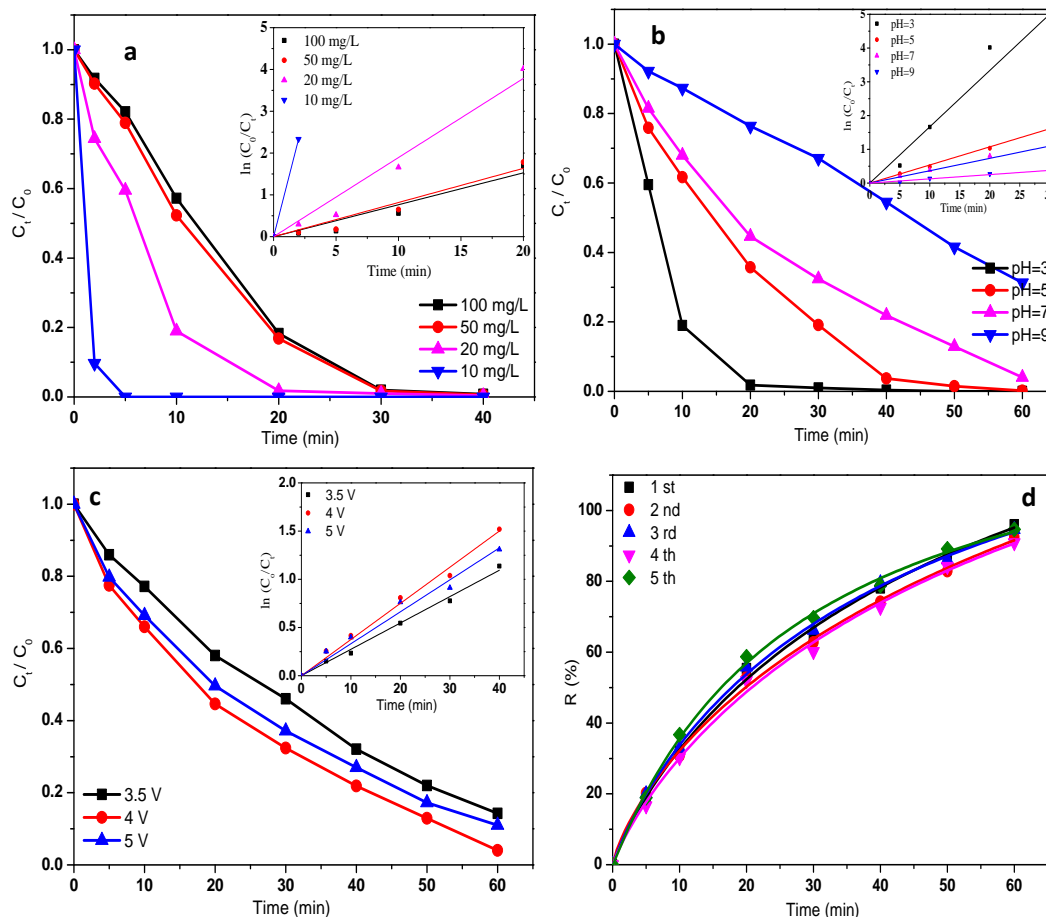


Fig. 4 Effect of initial concentration of 2,4-D, pH 3, applied voltage: 4 V (a), pH (b) and applied voltage (c) on the degradation of 2,4-D and stability of N1-EEGr-GF cathode for 2,4-D degradation (d). [2,4-D]: 20 mg L⁻¹ (for Figures 4b-4c), pH 7, applied voltage: 4 V, volume: 100 mL, [Na₂SO₄]: 50 mM.

6.3.3 Mineralization of 2,4-D using N-EEGr-GF cathode in EAOP

To evidence the effect of N-doping on N-EEGr-GF cathode in mineralization

Table 2 The values of k_{app} of 2,4-D degradation with in-situ EAOPs

Conditions		k_{app} (min ⁻¹)
2,4-D (mg L ⁻¹)	10	1.17
	20	0.20
	50	0.08
	100	0.08
pH	3	0.19
	5	0.05
	7	0.04
	9	0.01
Voltage (V)	3.5	0.03
	4	0.04
	5	0.03

efficiency of 2,4-D, comparative experiments were carried out. It can be seen in Fig. 5 that during the first 2 h, solution TOC was reduced by 35% with N0-EEGr-GF, while it was remarkably increased to 53% with N1-EEGr-GF cathode, which presented a better performance with N-doped graphene as catalyst for the in-situ EAOP. Besides, it was noted that at the early stage of treatment with N1-EEGr-GF cathode, the value of MCE increased to the maximum peak, suggesting a rapid mineralization of 2,4-D (and its first oxidation intermediates) (insert of Fig. 5). The TOC removal rate and MCE decreased on longer treatment time probably due to the formation of hardly oxidizable intermediates such as short-chain carboxylic acids. Obviously, higher MCE values were observed with N1-EEGr-GF, which was consistent with the results of better mineralization rate reaching 88% TOC removal value after 8 h treatment. At this mineralization stage, the solution does not contain toxic intermediates; the residual TOC is mainly formed of short-chain carboxylic acids which are biodegradable and non-toxic^[31]. Higher TOC removal efficiency can be obtained by different ways by i) increasing the applied current (until an optimal value), ii) extending the electrolysis time, iii) increasing the ratio volume/electrode surface. In this study, TOC removal efficiency was enhanced by increasing applied current and keeping longer electrolysis time of 2,4-D solution.

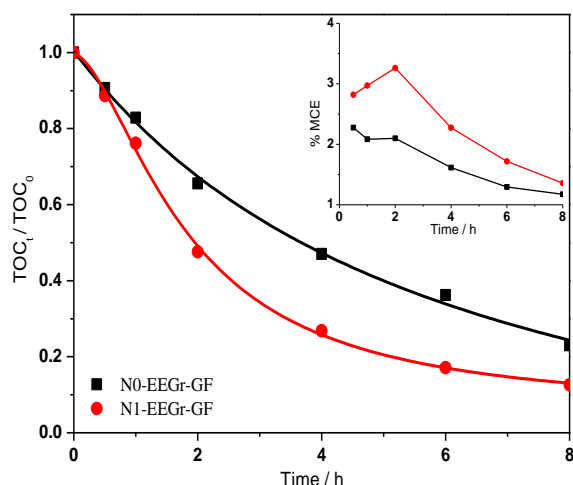


Fig. 5 Evolution of TOC and MCE during EAOP with N0-EEGr-GF and N1-EEGr-GF cathodes. [2,4-D]: 20 mg L⁻¹, volume: 100 mL, pH 7, applied voltage : 4 V, [Na₂SO₄]: 50 mM.

6.3.4 Performances of the iron-free EAOP compared with literatures

Performances of 2,4-D degradation with the EAOP were compared with literatures. The results in Table 3 show that in the photo-Fenton process, 2,4-D can be degraded completely in 1 h with solar irradiation [20], heterogeneous Fenton-like process (FeS/H₂O₂) obtained 90% percent of the 2,4-D removal at 50 min [54], 40% of the TOC was degraded at 360 min in the combination of anodic oxidation and electro-Fenton process with O₂-diffusion cathode [51] at pH 3. It was reported that the degradation efficiency of 2,4-D at pH 6.5 decreased to 45% compared with 90% for pH 3 at 50 min [54].

In contrast, in the present study, the degradation efficiency of 2,4-D reached 100% within 20 min at pH 3, which was significantly better than others. Moreover, at the pH 7, considerable performance was obtained (100% removal at 60 min) compared with other EAOPs, while without the addition of Fe²⁺ or UV/solar irradiation, which can effectively decrease the treatment cost, and energy consumption illustrated this conclusion as well. In this present study, the EC for the degradation of 2,4-D was 0.04 kWh g⁻¹ at pH 3, which was two times lesser than that obtained in EF process with Fe²⁺ at pH 3 (0.104 kWh g⁻¹) [51]. Besides, 0.12 kWh g⁻¹ was consumed for the mineralization of 2,4-D at pH 7, which also demonstrated the cost effectiveness of the EAOP. The performances of 2,4-D removal obtained in this

study show that the EAOP with N1-EEGr-GF could overcome two big drawbacks of traditional EF with extending the range of pH suitability at around pH 7 and getting rid of the usage of an iron salt.

Table 3 Performances of 2,4-D degradation comparison with literature

$C_{0(2,4-D)}$	Process	Conditions	Performance	EC (kWh g ⁻¹ 2,4-D)	Reference
20 mg L ⁻¹	Ozone/peroxymono-sulfate (PMS)	PMS: 2 mM, ozone: 16 mg L ⁻¹ , MCFN: 0.2 g L ⁻¹ , pH 6	40 min: R:100%, R _{TOC} :67.3%	/	[7]
10 mg L ⁻¹	Plasma treatment	Voltage: 15-25 kV	14 min: R:100%	3.50	[6]
24.3 mg L ⁻¹	Photo-Fenton	H ₂ O ₂ : 10 mg L ⁻¹ , solar irradiation, pH 2.8	60 min: R:100%	/	[20]
10 mg L ⁻¹	Heterogeneous Fenton-like catalytic degradation (FeS/H ₂ O ₂)	H ₂ O ₂ : 340 mg L ⁻¹ , FeS: 0.5 g L ⁻¹ ,	50 min: R:90%, (pH 3) R:45% (pH 6.5)	/	[54]
92 mg L ⁻¹	Electrochemical oxidation/ (BDD) electro-Fenton (Pt/air-diffusion)	Air flow: 10 L min ⁻¹ , I: 1.0 A, Fe ²⁺ : 0.5 mM pH 3	300 min: R:100%, R _{TOC} :66%	0.056	[55]
100 mg L ⁻¹	Photo-electro-Fenton (H ₂ O ₂ /UV/Fe ²⁺) rotating cylinder electrode	I: 0.18 A, U: 2.5 V, pH 3.5	60 min: R:90%, R _{TOC} :67%	0.05	[56]
230 mg L ⁻¹	Anodic oxidation/electro-Fenton (Pt/O ₂ -diffusion cathode)	I: 0.1 A, Fe ²⁺ : 1 mM pH 3	360 min: R:99%, R _{TOC} :40%	0.104	[51]
20 mg L ⁻¹	In-situ metal-free advanced oxidation process (EAOP)	I: 0.1 A, pH 7	60 min: R:100%, 120 min R _{TOC} :45%	0.12	Present study
20 mg L ⁻¹	In-situ metal-free advanced oxidation process (EAOP)	I: 0.1 A, pH 3	20 min: R:100%, 120 min R _{TOC} :65%	0.04	

6.3.5 Identification of aromatic intermediates and carboxylic acids

The formation of aromatic intermediate products during oxidation of 2,4-D were identified by HPLC and GC-MS (Table 4) as explained in sub-section 2.4. Whereafter, aiming to further identify the effective formation of [•]OH radicals being responsible for

organics degradation, methanol (1 mM) was used as the scavenger of $\cdot\text{OH}$ in the EAOP. As shown in Fig. 6a, the degradation efficiencies of 2,4-D decreased significantly from 96% to 24% with the addition of methanol, demonstrating that $\cdot\text{OH}$ played the contributory role for degradation of 2,4-D. Besides, the experiment with DSA anode and Pt cathode to explore the impact of DSA and active chlorine on the efficiency of 2,4-D degradation in iron-free EAOP was conducted. The results showed that 12% of 2,4-D removal efficiency was obtained under this condition.

During the treatment of organics by AOPs, ultimate end-products before mineralization are the short-chain carboxylic acids [31]. Carboxylic acids formed during oxidation of 2,4-D were analyzed by ion-exclusion HPLC, aiming to identify and quantify their generation and evolution. Five well-defined peaks were detected with the retention time (t_R) of 6.8, 7.8, 11.0, 14.3 and 14.6 min corresponding to oxalic, maleic, glycolic, fumaric and acetic acids, respectively. As shown in Fig. 6b, oxalic and acetic acids were formed in large amount and these two acids are usually regarded as the end-products before complete mineralization. All the carboxylic acids formed during oxidation process were then gradually destroyed by EAOP with N1-EEGr-GF until a non-significant value at the end of 480 min electrolysis.

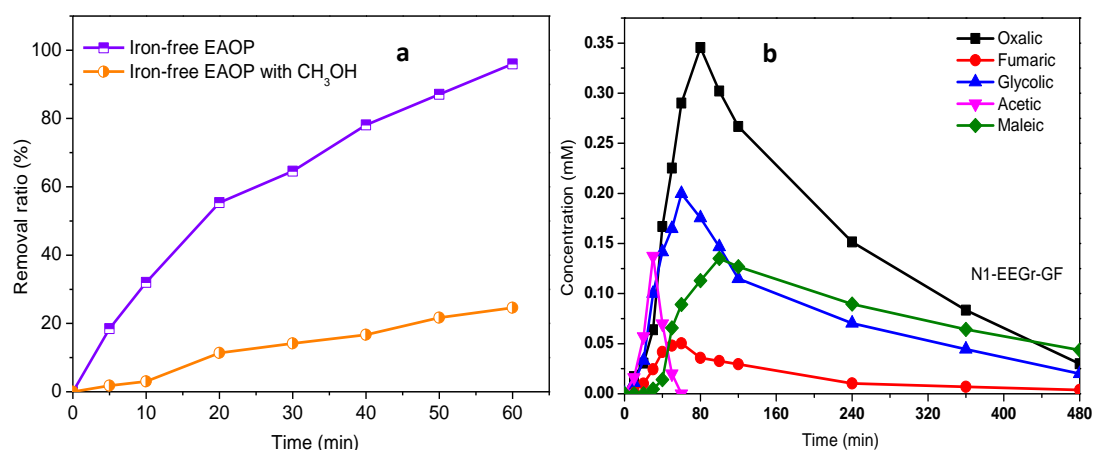
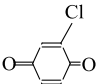
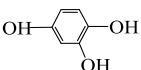
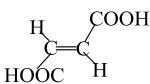


Fig. 6 The degradation of 2,4-D with scavengers of $\cdot\text{OH}$ (methanol) in the EAOP (a); Time-course of the identified short-chain carboxylic acids with N1-EEGr-GF electrode in EAOP (b). [2,4-D]: 20 mg L⁻¹, volume : 100 mL, pH: 7, applied voltage : 4 V, [Na₂SO₄]: 50 mM.

Table 4 Intermediate products detected by HPLC and GC-MS.

Compound No	Chemical	Chemical structure	M	Retention time/min	Detected method
I	2,4-DCP		163.00	9.1	HPLC, GC-MS
II	Hydroquinone		110.11	5.6	HPLC
III	1,4-Benzoquinone		108.09	5.9	HPLC
IV	2-Chloro-1,4-benzoquinone		142.54	7.1	HPLC
V	1,2,4-Benzotriol		126.11	5.8	HPLC
VI	4,6-Dichlororesorcinol		179.00	6.7	HPLC
VII	Oxalic acid		90.03	10.7	HPLC, GC-MS
VIII	Maleic acid		116.07	11.2	HPLC, GC-MS
IX	Glycolic acid		76.05	12.3	HPLC, GC-MS
X	Acetic acid		60.05	14.9	HPLC, GC-MS
XI	Fumaric acid		116.07	18.9	HPLC, GC-MS

Based on identified aromatic intermediates and short-chain carboxylic acids, a plausible degradation pathway was proposed (Fig. 7). Firstly, the $\cdot\text{OH}$ attacked C-O bond on the phenoxy group of 2,4-D with the generation of 2,4-DCP and glycolic acid. This statement is in agreement with the literature ^[57]. Then, 2,4-DCP would be further converted to 2,5-dihydroxychlorobenzene by dechlorination (following ipso addition of $\cdot\text{OH}$) of C1 atom on C5 to form the 2-chlorohydroquinone, which was not identified by HPLC and GC-MS in this study, while this way has been evidenced from other reports ^[6, 57, 58] and was deduced with dotted line in Fig. 7.

Dechlorination/dehydrogenization of this product led to the formation of hydroquinone and benzoquinone that were generally detected during oxidation of aromatic compounds. On the other hand, 2,4-DCP was oxidized by $\cdot\text{OH}$ addition reaction to generate the 4,6-dichlororesorcinol. Further oxidation by $\cdot\text{OH}$ leads to the

formation of polyhydroxylated products. Polyhydroxylated benzenes and quinones are not stable and then easily converted to carboxylic acids through oxidative ring opening reactions promoted by $\cdot\text{OH}$. The last step is the conversion of carboxylic acids to CO_2 . The mechanism is in agreement with the one proposed by Chen et al. using electrochemically generated hydroxyl radicals for the treatment of 2,4-D^[54], in which several of the detected intermediates coincides with the ones found in this study. However, as a significant difference, in the present study, the $\cdot\text{OH}$ for the mineralization of 2,4-D was formed by the activation of in-situ generated H_2O_2 via nitrogen-doped graphene (N1-EEGr-GF), without other chemicals (iron salts) in the EAOP. To the best of our knowledge, the mineralization pathway of 2,4-D by in-situ EAOP has not been already reported.

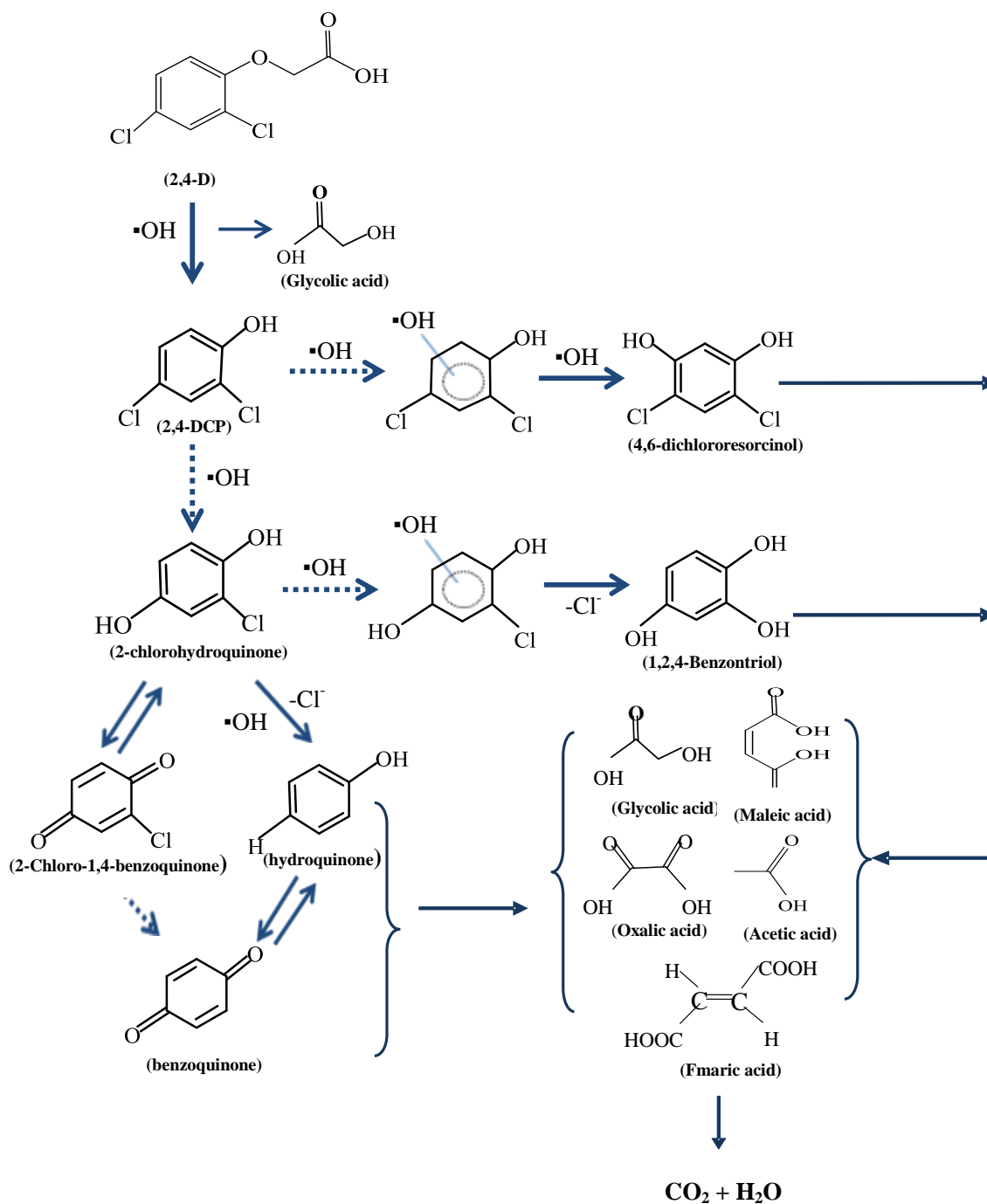


Fig. 7 Reaction pathway proposed for degradation of 2,4-D by the EAOP.

6.4 Conclusions

An EAOP for in-situ generation of $\cdot\text{OH}$ using N-doped graphene modified cathode was optimized with different mass of nitrogen sources and successfully applied for the degradation and mineralization of 2,4-D aqueous solution. This process provides three important advantages: i) the N-doped graphene could accelerate the rate of activation H_2O_2 to $\cdot\text{OH}$, thus enhancing the mineralization efficiency to 88% with N1-EEGr-GF, ii) the EAOP effectively get rid of the usage of chemicals (hydrogen peroxide and iron salts), and iii) extend the suitable range of pH value in traditional EF process. The performances of 2,4-D degradation with N1-EEGr-GF at pH 7 were significant, obtaining complete degradation of 20 mg L^{-1} 2,4-D at 60 min and TOC removal efficiency of 45% at 120 min. The study showed that electrooxidation using N-doped EEGr-GF can be successfully used to remove efficiently the herbicide 2,4-D from water even at neutral pH values. The process can be extended to the treatment of wastewater polluted with other persistent organic pollutants.

Acknowledgement

This work was financially supported by Key Project of Natural Science Foundation of Tianjin (no. 16JCZDJC39300), Natural Science Foundation of China (nos. 21773129, 91545126 and 21811530274), National Key Research and Development Program (2016YFC0400706), China National Water Project (2017ZX07107002), 111 program, Ministry of Education, China (T2017002) and Fundamental Research Funds for the Central Universitie.

References

- [1] Rodrigo M A, Oturan N, Oturan M A, et al. Electrochemically assisted remediation of pesticides in soils and water: a review[J]. *Chem Rev*, 2014, 114: 8720-8745.
- [2] Pastrana-Martínez L M, Faria J L, Doña-Rodríguez J M, et al. Degradation of diphenhydramine pharmaceutical in aqueous solutions by using two highly active TiO₂ photocatalysts: Operating parameters and photocatalytic mechanism[J]. *Applied Catalysis B: Environmental*, 2012, 113-114: 221-227.
- [3] Radjenovic J, Petrovic M, Ventura F, et al. Rejection of pharmaceuticals in nanofiltration and reverse osmosis membrane drinking water treatment[J]. *Water Res*, 2008, 42: 3601-3610.
- [4] Kumar A, Xagorarakis I, et al. Pharmaceuticals, personal care products and endocrine-disrupting chemicals in U.S. surface and finished drinking waters: a proposed ranking system[J]. *Sci Total Environ*, 2010, 408: 5972-5989.
- [5] Focazio M J, Kolpin D W, Barnes K K, et al. A national reconnaissance for pharmaceuticals and other organic wastewater contaminants in the United States--II) untreated drinking water sources[J]. *Sci Total Environ*, 2008, 402: 201-216.
- [6] Singh R K, Philip L, Ramanujam S, et al. Removal of 2,4-dichlorophenoxyacetic acid in aqueous solution by pulsed corona discharge treatment: Effect of different water constituents, degradation pathway and toxicity assay[J]. *Chemosphere*, 2017, 184: 207-214.
- [7] Jaafarzadeh N, Ghanbari F, Ahmadi M, et al. Efficient degradation of 2,4-dichlorophenoxyacetic acid by peroxymonosulfate/magnetic copper ferrite nanoparticles/ozone: A novel combination of advanced oxidation processes[J]. *Chemical Engineering Journal*, 2017, 320: 436-447.
- [8] Kearns J P, Wellborn L S, Summers R S, et al. 2,4-D adsorption to biochars: effect of preparation conditions on equilibrium adsorption capacity and comparison with commercial activated carbon literature data[J]. *Water Res*, 2014, 62: 20-28.
- [9] Jung B K, Hasan Z, Jung S H, et al. Adsorptive removal of 2,4-dichlorophenoxyacetic acid (2,4-D) from water with a metal-organic framework[J]. *Chemical Engineering Journal*, 2013, 234: 99-105.
- [10] Ma J-Y, Quan X-C, Yang Z-F, et al. Biodegradation of a mixture of 2,4-dichlorophenoxyacetic acid and multiple chlorophenols by aerobic granules cultivated through plasmid pJP4 mediated bioaugmentation[J]. *Chemical Engineering Journal*, 2012, 181-182: 144-151.
- [11] Sun C, Baig S A, Lou Z, et al. Electrocatalytic dechlorination of 2,4-dichlorophenoxyacetic acid using nanosized titanium nitride doped palladium/nickel foam electrodes in aqueous solutions[J]. *Applied Catalysis B: Environmental*, 2014, 158-159: 38-47.
- [12] Chair K, Bedoui A, Bensalah N, et al. Combining bioadsorption and photoelectrochemical oxidation for the treatment of soil-washing effluents polluted with herbicide 2,4-D[J]. *Journal of Chemical Technology & Biotechnology*, 2017, 92: 83-89.
- [13] Chen H, Zhang Z, Feng M, et al. Degradation of 2,4-dichlorophenoxyacetic acid in water by persulfate activated with FeS (mackinawite)[J]. *Chemical Engineering Journal*, 2017, 313: 498-507.

- [14] Duan X, Sun H, Wang Y, et al. N-Doping-Induced Nonradical Reaction on Single-Walled Carbon Nanotubes for Catalytic Phenol Oxidation[J]. *ACS Catalysis*, 2014, 5: 553-559.
- [15] Rosario-Ortiz F L, Wert E C, Snyder S A, et al. Evaluation of UV/H₂O₂ treatment for the oxidation of pharmaceuticals in wastewater[J]. *Water Res*, 2010, 44: 1440-1448.
- [16] Ziylan A, Ince N H, et al. The occurrence and fate of anti-inflammatory and analgesic pharmaceuticals in sewage and fresh water: treatability by conventional and non-conventional processes[J]. *J Hazard Mater*, 2011, 187: 24-36.
- [17] Mendez-Arriaga F, Otsu T, Oyama T, et al. Photooxidation of the antidepressant drug Fluoxetine (Prozac(R)) in aqueous media by hybrid catalytic/ozonation processes[J]. *Water Res*, 2011, 45: 2782-2794.
- [18] Oturan M A, Aaron J-J, et al. Advanced Oxidation Processes in Water/Wastewater Treatment: Principles and Applications. A Review[J]. *Critical Reviews in Environmental Science and Technology*, 2014, 44: 2577-2641.
- [19] Sires I, Brillas E, Oturan M A, et al. Electrochemical advanced oxidation processes: today and tomorrow. A review[J]. *Environ Sci Pollut Res Int*, 2014, 21: 8336-8367.
- [20] Gutiérrez-Zapata H M, Rojas K L, Sanabria J, et al. 2, 4-D abatement from groundwater samples by photo-Fenton processes at circumneutral pH using naturally iron present. Effect of inorganic ions[J]. *Environmental Science and Pollution Research*, 2017, 24: 6213-6221.
- [21] Bokare A D, Choi W, et al. Review of iron-free Fenton-like systems for activating H₂O₂ in advanced oxidation processes[J]. *J Hazard Mater*, 2014, 275: 121-135.
- [22] Barhoumi N, Olvera-Vargas H, Oturan N, et al. Kinetics of oxidative degradation/mineralization pathways of the antibiotic tetracycline by the novel heterogeneous electro-Fenton process with solid catalyst chalcopyrite[J]. *Applied Catalysis B: Environmental*, 2017, 209: 637-647.
- [23] Nidheesh P, Olvera-Vargas H, Oturan N, et al., *Heterogeneous Electro-Fenton Process: Principles and Applications*, Electro-Fenton Process, Springer 2017, pp. 85-110.
- [24] Deng F, Olvera-Vargas H, Garcia-Rodriguez O, et al. The synergistic effect of nickel-iron-foam and tripolyphosphate for enhancing the electro-Fenton process at circum-neutral pH[J]. *Chemosphere*, 2018, 201: 687-696.
- [25] Barhoumi N, Oturan N, Olvera-Vargas H, et al. Pyrite as a sustainable catalyst in electro-Fenton process for improving oxidation of sulfamethazine. Kinetics, mechanism and toxicity assessment[J]. *Water Research*, 2016, 94: 52-61.
- [26] Yang X J, Xu X M, Xu J, et al. Iron oxychloride (FeOCl): an efficient Fenton-like catalyst for producing hydroxyl radicals in degradation of organic contaminants[J]. *J Am Chem Soc*, 2013, 135: 16058-16061.
- [27] Gonzalez-Olmos R, Martin M J, Georgi A, et al. Fe-zeolites as heterogeneous catalysts in solar Fenton-like reactions at neutral pH[J]. *Applied Catalysis B: Environmental*, 2012, 125: 51-58.
- [28] Jinisha R, Gandhimathi R, Ramesh S T, et al. Removal of rhodamine B dye from aqueous solution by electro-Fenton process using iron-doped mesoporous silica as a heterogeneous catalyst[J]. *Chemosphere*, 2018, 200: 446-454.
- [29] Lyu L, Zhang L, Wang Q, et al. Enhanced Fenton Catalytic Efficiency of γ -Cu-Al₂O₃ by σ -Cu²⁺-Ligand Complexes from Aromatic Pollutant Degradation[J]. *Environmental Science &*

Technology, 2015, 49: 8639-8647.

[30] Dong H, Su H, Chen Z, et al. Fabrication of Electrochemically Reduced Graphene Oxide Modified Gas Diffusion Electrode for In-situ Electrochemical Advanced Oxidation Process under Mild Conditions[J]. *Electrochimica Acta*, 2016, 222: 1501-1509.

[31] Enric B, Ignasi S, Oturan M A, et al. Electro-Fenton process and related electrochemical technologies based on Fenton's reaction chemistry[J]. *Chemical Reviews*, 2009, 109: 6570.

[32] Wang Q, Li Y, Liao N, et al. Synthesis of boron and nitrogen-doped expanded graphite as efficient reinforcement for Al₂O₃-C refractories[J]. *Ceramics International*, 2017, 43: 16710-16721.

[33] So K, Ozawa H, Onizuka M, et al. Highly Permeable Gas Diffusion Electrodes with Hollow Carbon Nanotubes for Bilirubin Oxidase-Catalyzed Dioxygen Reduction[J]. *Electrochimica Acta*, 2017, 246: 794-799.

[34] Le T X H, Bechelany M, Lacour S, et al. High removal efficiency of dye pollutants by electron-Fenton process using a graphene based cathode[J]. *Carbon*, 2015, 94: 1003-1011.

[35] Gong Y, Li J, Zhang Y, et al. Partial degradation of levofloxacin for biodegradability improvement by electro-Fenton process using an activated carbon fiber felt cathode[J]. *J Hazard Mater*, 2016, 304: 320-328.

[36] Trellu C, Oturan N, Keita F K, et al. Regeneration of Activated Carbon Fiber by Electro-Fenton Process[J]. *Environmental science & technology*, 2018,

[37] Zuo K, Liu H, Zhang Q, et al. Enhanced performance of nitrogen-doped carbon nanotube membrane-based filtration cathode microbial fuel cell[J]. *Electrochimica Acta*, 2016, 211: 199-206.

[38] Yang W, Zhou M, Cai J, et al. Ultrahigh yield of hydrogen peroxide on graphite felt cathode modified with electrochemically exfoliated graphene[J]. *Journal of Materials Chemistry A*, 2017, 5: 8070-8080.

[39] Garcia-Rodriguez O, Lee Y Y, Olvera-Vargas H, et al. Mineralization of electronic wastewater by electro-Fenton with an enhanced graphene-based gas diffusion cathode[J]. *Electrochimica Acta*, 2018, 276: 12-20.

[40] Saputra E, Muhammad S, Sun H, et al. Activated carbons as green and effective catalysts for generation of reactive radicals in degradation of aqueous phenol[J]. *RSC Advances*, 2013, 3: 21905.

[41] Yang W, Zhou M, Liang L, et al. Highly efficient in-situ metal-free electrochemical advanced oxidation process using graphite felt modified with N-doped graphene[J]. *Chemical Engineering Journal*, 2018, 338: 700-708.

[42] Cai J, Zhou M, Yang W, et al. Degradation and mechanism of 2, 4-dichlorophenoxyacetic acid (2, 4-D) by thermally activated persulfate oxidation[J]. *Chemosphere*, 2018,

[43] Sun H, Wang Y, Liu S, et al., et al. Facile synthesis of nitrogen doped reduced graphene oxide as a superior metal-free catalyst for oxidation[J]. *Chemical Communications*, 2013, 49: 9914-9916.

[44] Grewal Y S, Shiddiky M J, Gray S A, et al. Label-free electrochemical detection of an *Entamoeba histolytica* antigen using cell-free yeast-scFv probes[J]. *Chem Commun (Camb)*, 2013, 49: 1551-1553.

[45] Duan X, Sun H, Wang Y, et al. N-Doping-Induced Nonradical Reaction on Single-Walled

- Carbon Nanotubes for Catalytic Phenol Oxidation[J]. ACS Catalysis, 2014, 5: 553-559.
- [46] Wang C, Kang J, Sun H, et al. One-pot synthesis of N-doped graphene for metal-free advanced oxidation processes[J]. Carbon, 2016, 102: 279-287.
- [47] Moreira F C, Soler J, Alpendurada M F, et al. Tertiary treatment of a municipal wastewater toward pharmaceuticals removal by chemical and electrochemical advanced oxidation processes[J]. Water Res, 2016, 105: 251-263.
- [48] Wang Q, Shao Y, Gao N, et al. Degradation kinetics and mechanism of 2,4-Di-tert-butylphenol with UV/persulfate[J]. Chemical Engineering Journal, 2016, 304: 201-208.
- [49] He Z, Chen J, Chen Y, et al. An activated carbon fiber-supported graphite carbon nitride for effective electro-Fenton process[J]. Electrochimica Acta, 2018, 276: 377-388.
- [50] Ren G, Zhou M, Liu M, et al. A novel vertical-flow electro-Fenton reactor for organic wastewater treatment[J]. Chemical Engineering Journal, 2016, 298: 55-67.
- [51] Brillas E, Boye B, Sires I, et al. Electrochemical destruction of chlorophenoxy herbicides by anodic oxidation and electro-Fenton using a boron-doped diamond electrode[J]. Electrochimica Acta, 2004, 49: 4487-4496.
- [52] Oturan N, Ganiyu S O, Raffy S, et al. Sub-stoichiometric titanium oxide as a new anode material for electro-Fenton process: application to electrocatalytic destruction of antibiotic amoxicillin[J]. Applied Catalysis B: Environmental, 2017, 217: 214-223.
- [53] Sopaj F, Oturan N, Pinson J, et al. Effect of the anode materials on the efficiency of the electro-Fenton process for the mineralization of the antibiotic sulfamethazine[J]. Applied Catalysis B: Environmental, 2016, 199: 331-341.
- [54] Chen H, Zhang Z, Yang Z, et al. Heterogeneous fenton-like catalytic degradation of 2, 4-dichlorophenoxyacetic acid in water with FeS[J]. Chemical Engineering Journal, 2015, 273: 481-489.
- [55] Garc á O, Isarain-Ch ávez E, El-Ghenymy A, et al. Degradation of 2,4-D herbicide in a recirculation flow plant with a Pt/air-diffusion and a BDD/BDD cell by electrochemical oxidation and electro-Fenton process[J]. Journal of Electroanalytical Chemistry, 2014, 728: 1-9.
- [56] Badellino C, Rodrigues C A, Bertazzoli R, et al. Oxidation of pesticides by in situ electrogenerated hydrogen peroxide: Study for the degradation of 2, 4-dichlorophenoxyacetic acid[J]. Journal of hazardous materials, 2006, 137: 856-864.
- [57] Oturan M A, et al. An ecologically effective water treatment technique using electrochemically generated hydroxyl radicals for in situ destruction of organic pollutants: Application to herbicide 2,4-D[J]. Journal of Applied Electrochemistry, 2000, 30: 475-482.
- [58] Brillas E, Calpe J C, Casado J, et al. Mineralization of 2,4-D by advanced electrochemical oxidation processes[J]. Water Research, 2000, 34: 2253-2262.

Chapter 7 Conclusions and Prospects

7.1 Main conclusions

Advanced oxidation technology, as an efficient pollutant treatment technology, is widely used in the treatment of refractory organic pollutants such as emerging organic pollutants in water because of its strong oxidation ability, which can effectively degrade pollutants in mineralized water. Electro-Fenton (EF) process is one of the most widely used advanced electrochemical oxidation technologies. By the combination of electric field and Fenton reaction, in-situ hydrogen peroxide and iron ion cycling reactions produce strong oxidative hydroxyl radicals, which have strong mineralization ability for organic matter. However, conventional EF technology has two obvious bottlenecks: narrow application range of pH and limited degradation efficiency of pollutants. Graphene is a new type of carbon material. Because of its excellent conductivity and high specific surface area, graphene can be used in EF cathode to promote oxygen reduction reaction, increase hydrogen peroxide production and enhance the degradation efficiency of EF. In this paper, the role of graphene modified electrode in electrochemical advanced oxidation technology was studied in detail from the aspects of preparation of graphene via electrochemical exfoliation, electrodes modified with graphene, construction of in situ non-metallic advanced oxidation technology by nitrogen doping graphene to treat new organic pollutants and so on, and the high-efficiency catalysis of graphene modified electrode in electrochemical advanced oxidation technology was clarified. The main conclusions are as follows:

(1) Platinum sheet and graphite foil were used as cathode and anode respectively. Deionized water containing concentrated sulfuric acid and potassium hydroxide was used as electrolyte to prepare graphene by electrochemical stripping. It was characterized by scanning electron microscopy (SEM), transmission electron microscopy (TEM), atomic force microscopy (AFM), Raman spectroscopy (Raman spectroscopy), X-ray diffraction (XRD) and energy dispersive X-ray spectroscopy (EDX), and proved to be a 3-4 layer thin film with low defects. Carbon felt cathode was prepared by blending graphene and carbon black. The results show that the yield of hydrogen peroxide is very high, reaching 7.7 mg H₂O₂ cm⁻², while the energy

consumption is relatively low (9.7 kWh kg⁻¹). Under the optimized cathodic potential of - 0.9 V and pH 7, the modified cathode maintained a stable hydrogen peroxide yield, which was twice as high as that of graphene-free cathode. Further studies on cyclic voltammetry, rotating disc electrode (RDE) and contact angle show that the presence of EEGr is beneficial to accelerating electron transfer rate and promoting oxygen reduction reaction, but does not change the two-electron number transfer mechanism, which is helpful to improve the cathode hydrogen peroxide yield. The electrochemical degradation of four typical pollutants (orange II, methylene blue, phenol, sulfadiazine) by graphene modified carbon felt cathode has proved that it has great potential in wastewater treatment. The oxidative degradation and mineralization of imatinib (IMA), an anticancer drug, were studied using this electrode as an EF cathode. The absolute rate constant of OH oxidation of IMA ($4.56 \times 10^9 \text{ M}^{-1} \text{ s}^{-1}$) was determined. Under the same operating conditions, after 8 hours of cathodic treatment of graphene modified carbon fibers, 34.5 mg L⁻¹ IMA can be completely mineralized, while the unmodified carbon felt cathode can only remove 75% of the total organic carbon. At the same time, toxicity assessment results of short-chain carboxylic acid, inorganic ions (NH₄⁺ and NO₃⁻) and IMA solution during mineralization showed that graphene modified electrode had more advantages than untreated carbon felt cathode in the destruction of organic matter in the process of electro-Fenton. These results indicate that graphene-based cathodes have greater IMA mineralization potential, which provides a new idea for the EF process to remove organic pollutants from wastewater or water. The new graphene modified carbon felt electrode is conducive to the development of high efficiency oxygen reduction reaction cathode in the field of electrochemical technology, and is of great significance to the chemical industry and the application of environmental remediation.

(2) The effects of different anode materials (DSA, Pt, Ti₄O₇, BDD) on the mineralization and electrochemical oxidation of imatinib (IMA) were studied by comparing EF with AO. Compared with Ti₄O₇ and BDD anodes, DSA and Pt anodes have less effect on the oxidation and mineralization of IMA solution. The complete mineralization of 0.1 mM (equivalent to 34.8 mg L⁻¹ initial TOC) IMA solution can be achieved by using BDD anode in both EF and AO processes at 300 mA. Ti₄O₇ anode has better performance than DSA and Pt anode. In the 8 h electrolysis process, the removal rates of TOC in EF and AO processes reach 84% and 73%, respectively. Different anode materials have BDD > Ti₄O₇ > Pt > DSA on IMA

oxidation/mineralization performance. High current (300 and 500 mA) is not conducive to Ti_4O_7 anode removal of pollutants. AO contributes less to IMA mineralization than EF process (except BDD anode), which proves the dominant role of homogeneous OH in the mineralization process. The relative contribution of homogeneous (formed in aqueous solution) and heterogeneous (formed on the surface of the anode) hydroxyl radicals to the dynamic attenuation and mineralization of IMA was systematically studied by using a $((k_{\text{EF}}-k_{\text{AO}})/k_{\text{AO}})$ value. Under low current (50 and 100 mA), the ability of inhomogeneous M (OH) to influence the dynamic attenuation of IMA can be ranked as $\text{Pt} > \text{DSA} > \text{Ti}_4\text{O}_7 > \text{BDD}$, while at high current (200, 300 and 500 mA), it can be ranked as $\text{Ti}_4\text{O}_7 > \text{Pt} > \text{DSA} > \text{BDD}$.

(3) N-doped graphene (N-EEGr) was synthesized by low temperature calcination using ammonium nitrate as nitrogen source. Graphene is further reduced by calcination in nitrogen atmosphere. Nitrogen doping can cause disorder of ordered SP^2 hybridization on graphene. Compared with graphene (EEGr), N-doped graphene (N-EEGr) has higher pyridine nitrogen content, but lower graphite nitrogen content, which indicates that low-temperature calcination can not incorporate N into the graphite-carbon framework, change the volume structure of EGr, but mostly be doped in the defect location for surface modification. Phenol was degraded by in situ non-metallic EAOPS system of carbon felt cathode modified by N-EEGr. The first order reaction rate constant (k) of N-EEGr-GF is twice as much as that of EGr-GF. At pH 7, the average hydrogen peroxide yield of the two cathodes is 6.5 (EEGr-GF) and 6.2 (N-EEGr-GF) $\text{mg H}_2\text{O}_2 \text{ cm}^{-2} \text{ h}^{-1}$, and the energy consumption (EEC) is 9.5 and 10.3 kWh kg^{-1} , respectively. When using N-EEGr-GF cathode, the concentration of $\cdot\text{OH}$ reaches 88 micrometers in 5 minutes, which is more than twice the concentration of free radicals (43 microns) produced by EGr-GF cathode. At 40 minutes, the concentration of $\cdot\text{OH}$ produced by N-EEGr-GF cathode reached 172 μM . Using N1-EEGr-GF cathode EAOP system to degrade 2,4-D, the TOC of solution decreased by 53% in 2 hours, which was 1.5 times as much as that of EGr-GF cathode EAOP system. Compared with the traditional EF technology, this in-situ non-metallic EAOP has four times higher degradation efficiency, wider applicability to pH, better reusability and environmental friendliness without adding catalyst and secondary pollution. It can be regarded as an emerging organic pollutant treatment technology with potential for development.

7.2 Prospects and suggestions

Through this study, it is preliminarily proved that nitrogen-doped graphene-based in-situ advanced non-metallic oxidation technology has unique advantages in the treatment of emerging organic compounds, but there are still some shortcomings in depth and breadth. Therefore, based on the research in this paper, the following aspects can be studied in depth:

(1) Graphene was modified by doping other non-metallic heteroatoms to explore its catalytic properties.

(2) It is possible to explore the preparation of iron oxide and graphene composite materials, their catalytic properties, and the preparation of composite electrodes by using this material, and to explore its application in heterogeneous EF as a cathode for the degradation of emerging organic pollutants.

(3) This study is limited to the laboratory synthetic wastewater. Because the pollutant composition in the actual wastewater is very complex, the treatment result of the actual wastewater is still unclear. To explore the effect of graphene-based in-situ advanced non-metallic oxidation technology on the treatment of actual wastewater so that the technology can be applied to the treatment of actual wastewater as soon as possible.

Publications

1. **W.L. Yang**, M.H. Zhou, N. Oturan, Y.W. Li, M.A. Oturan, Electrocatalytic destruction of pharmaceutical imatinib by electro-Fenton process with graphene-based cathode, *Electrochim. Acta.* 305 (2019) 285-294. (IF: 5.11)
2. **W.L. Yang**, M.H. Zhou, N. Oturan, Y.W. Li, P. Su, M.A. Oturan, Enhanced activation of hydrogen peroxide using nitrogen doped graphene for effective removal of herbicide 2,4-D from water by iron-free electrochemical advanced oxidation, *Electrochim. Acta.* 297 (2019) 582-592. (IF: 5.11)
3. **W.L. Yang**, M.H. Zhou, L. Liang, Highly efficient in-situ metal-free electrochemical advanced oxidation process using graphite felt modified with N-doped graphene, *Chem. Eng. J.* 338 (2018) 700-708. (IF: 6.73)
4. **W.L. Yang**, M.H. Zhou, J.J. Cai, L. Liang, G.B. Ren, L.L. Jiang, Ultrahigh yield of hydrogen peroxide on graphite felt cathode modified with electrochemically exfoliated graphene, *J. Mater. Chem. A.* 5 (2017) 8070-8080. (IF: 9.93)
5. **W.L. Yang**, H.X. Han, M.H. Zhou, J. Yang. Simultaneous electricity generation and tetracycline removal in continuous electrosorption driven by microbial fuel cells, *RSC Adv.* 5 (2015) 49513-49520. (IF: 2.94)
6. **W.L. Yang**, N. Oturan, M.H. Zhou, M.A. Oturan, Effect of anode materials on the efficiency of electrochemical advanced oxidation process for the mineralization of pharmaceutical imatinib. (in revision)
7. **W.L. Yang**, M.H. Zhou, L. Ma, Novel flow-through electrosorption for cost-effective removal of organic pollutants. (in revision)
8. **W.L. Yang**, M.H. Zhou, L. Liang, S.J. Zuo. Modified cathode with graphene for high yield of hydrogen peroxide. *15th National organic electrochemical Conference*, 2016, 7.23-7.25.
9. J.J. Cai, M.H. Zhou, **W.L. Yang**, Y.W. Pan, X.Y. Lu, K.G. Serrano. Degradation and mechanism of 2,4-dichlorophenoxyacetic acid (2,4-D) by thermally activated persulfate oxidation. *Chemosphere* 212 (2018) 784-793.
10. L. Liang, M.H. Zhou, **W.L. Yang**, L.L. Jiang. Enhanced activation of persulfate by carbohydrate-derived carbon cryogels for effective removal of organic pollutants. *Chem. Eng. J.* 352 (2018) 673-681.
11. H.J. Yang, M.H. Zhou, **W.L. Yang**, G.B. Ren, L. Ma. Rolling-made gas diffusion electrode with carbon nanotube for electro-Fenton degradation of acetylsalicylic acid.

Chemosphere 206 (2018) 439-446.

12. G.B. Ren, M.H. Zhou, P. Su, L. Liang, **W.L. Yang**, E. Mousset. Highly energy-efficient removal of acrylonitrile by peroxi-coagulation with modified graphite felt cathode: Influence factors, possible mechanism. *Chem. Eng. J.* 343 (2018) 467-476.

13. L. Ma, M.H. Zhou, G.B. Ren, **W.L. Yang**, L. Liang. A highly energy-efficient flow-through electro-Fenton process for organic pollutants degradation. *Electrochim. Acta.* 200 (2016) 222-230.

14. J. Yang, M.H. Zhou, Y.S. Hu, **W.L. Yang**. Cost-effective copper removal by electrosorption powered by microbial fuel cells. *Bioproc. Biosyst. Eng.* 39 (2016) 511-519.

15. H.J. Yang, M.H. Zhou, M.M. Liu, **W.L. Yang**, T.Y. Gu. Cost-effective Microbial fuel cells for biosensor applications. *Biotechnol. Lett.* 37 (2015) 2357-2364.